A PREDICTIVE OUT-OF-STEP PROTECTION SCHEME BASED ON PMU ENABLED DISTRIBUTED DYNAMIC STATE ESTIMATION

A Dissertation
Presented to
The Academic Faculty

by

Evangelos Farantatos

In Partial Fulfillment
of the Requirements for the Degree
Doctor of Philosophy in the
School of Electrical and Computer Engineering

Georgia Institute of Technology
December 2012

A PREDICTIVE OUT-OF-STEP PROTECTION SCHEME BASED ON PMU ENABLED DISTRIBUTED DYNAMIC STATE ESTIMATION

Approved by:

Dr. A. P. Sakis Meliopoulos, Advisor
School of Electrical and Computer Engineering
Georgia Institute of Technology

Dr. Fumin Zhang
School of Electrical and Computer Engineering
Georgia Institute of Technology

Dr. Ronald G. Harley
School of Electrical and Computer Engineering
Georgia Institute of Technology

Dr. Shijie Deng
School of Industrial and Systems Engineering
Georgia Institute of Technology

Dr. Santiago Grijalva
School of Electrical and Computer Engineering
Georgia Institute of Technology

Date Approved: October 17, 2012

To my beloved parents Dimitra and Maximos and my brother Yannis.

ACKNOWLEDGEMENTS

This dissertation would not have been completed without the various kinds of support from many people. First and foremost, I would like to express my deepest gratitude to my advisor Professor Sakis Meliopoulos for the guidance and support during my studies at Georgia Tech. It was a great honor for me to have him as a teacher academically but also lifewise. Apart from his expertise on the field which has contributed to making me a better power systems engineer, his character and his personality have extremely influenced me. There is a Greek proverb that describes perfectly my feelings: "*με όποιον δάσκαλο καθίσεις, τέτοια γράμματα θα μάθεις*" ("Your level of knowledge depends on the teacher who will seat next to you").

I would also like to thank the reading members of my committee Professor Santiago Grijalva and Professor Ronald Harley for their valuable feedback on my thesis, and Professor Fumin Zhang and Professor Shijie Deng for serving as members in my Ph.D. committee. I am also grateful to Professor Costas Vournas, my advisor during my undergraduate studies at National Technical University of Athens. He was a great motivation for me, he strongly encouraged and supported my enrollment at Georgia Tech, and he is still doing so for my future steps. I would like also to acknowledge the collaboration I had with Professor George Cokkinides for the completion of this work.

Special thanks to all my labmates, Yongnam Cho, Dr. Curtis Roe, Sungyun Choi, Yonghee Lee, Stephan Ntwoku, Dr. Tao Ye, Jongkook Park, and the girl of the group, Xuebei Yu, first of all for the excellent collaboration we had, but most importantly for the extremely friendly lab environment we have all created. Especially, I would like to thank Renke Huang for the excellent collaboration we had in parts of this work but also in other projects. His help and contributions were crucial in the completion of this thesis. I could not have asked for a better partner and friend in the lab. Of course I cannot forget the help and support from a special member of the lab, especially during my first years in Atlanta and at Georgia Tech, my great Greek friend Dr. George Stefopoulos. His help and his friendship are invaluable. I am also thankful to Dr. Salman Mohagheghi and Dr. Binh Dam for their friendship. Furthermore, I want to wish good luck to the new members of the lab, Evangelos Polymeneas, Liangyi Sun, Zhenyu Tan, Rui Fan, Dongbo Zhao and Aniemi Umana. Finally, I would also like to thank the rest of the students of the power group at Georgia Tech, and especially Dr. Rohit Moghe, Dustin Howard, Diogenes Molina, Jorge Hernandez, Prasad Kandula, Frank Kreikebaum, Dr. Stefan Grubic, Dr. Jiaqi Liang, Dr. Anish Prasai, Dr. Harjeet Johal and Dr. Debrup Das, for their friendship and the great moments we had in Atlanta.

In addition, I would like to express my gratitude to all my Greek friends for the great moments we had in Atlanta. First and foremost, I want to thank my roommate these five years and great friend, Vasilis Lakafosis. His support in many aspects of the everyday life was invaluable. I was very lucky to have him walk in parallel with me our routes towards the Ph.D degree. Special thanks also to Dr. Yannis Doudalis, Dr. George Georgoulas, Dr. Yannis Raptis, Dr. Michael Balchanos, Dr. Nikos Vasiloglou and Spyros Pavlidis.

Last but not least I would like to thank my parents Dimitra and Maximos, and my brother Yannis to whom this dissertation is dedicated to. I know it is painful for all of us to be thousands of miles away from each other.

TABLE OF CONTENTS

LIST OF FIGURES

LIST OF TABLES

SUMMARY

Recent widespread blackouts that have taken place in many countries throughout the world, have indicated the need for more efficient and accurate power system monitoring, control and protection tools. Power system state estimation, which is the major tool that is used nowadays for providing the real-time model of the system, has significant biases resulting mainly from the complexity and geographic spread and separation of an electric power system. It is based on a centralized architecture, where simplified models are utilized, and as a result the short-term dynamics of the system cannot be captured. These restrictions limit the control actions that can be taken on the system in order to protect it from major disturbances.

Synchrophasor technology is a promising technology that has numerous advantages compared to conventional metering devices. PMUs provide synchronized measurements, where synchronization is achieved via a GPS clock which provides the synchronizing signal with accuracy of 1 μsec. As a result, the computed phasors have a common reference (UTC time) and can be used in local computations, thus distributing the state estimation process. The distributed state estimation architecture that synchrophasor technology enables, along with the fast sampling rate and the accuracy of the measurements that PMUs provide, enable the computation of the real-time dynamic model of the system and the development of numerous power system applications for more efficient control and protection of the system.

Towards these goals, the main objectives of this work are (a) to develop a distributed dynamic state estimator that is performed at the substation level based on synchronized (available from PMUs) and non-synchronized (available from relays and meters) measurements, captures with high fidelity the dynamics of the system and extracts in real time the dynamic model of the system and (b) to develop a transient stability monitoring scheme that utilizes the information given by the dynamic state estimation, achieves real-time monitoring of the transient swings of the system, characterizes in real time the stability of the system and enables a novel, predictive, generator out-of-step protection

scheme capable of detecting potential generator loss of synchronism after a system disturbance.

The theoretical background and the mathematical formulation of a PMU based distributed dynamic state estimator (DSE) is presented. Two formulations of the DSE are developed. The first one, referred to as DSE-Q, is used to capture with high fidelity the electromechanical dynamics of the system. The second one, referred to as DSE-T, is used to capture both electromechanical and electrical transients. The approach utilizes quadratic power system component modeling which converts the problem in quadratic without any approximation, and improves the convergence characteristics of the algorithm. The solution is further simplified if only synchronized measurements are used and the associated devices are linear, in which case the state estimation becomes linear and has a direct solution. Moreover, it uses a three-phase, asymmetric and breaker oriented power system model in order to account for system imbalances, asymmetries and topology changes. DSE is implemented based on object-oriented and sparcity techniques. In addition, the decentralized architecture of the proposed DSE is also emphasized. In particular, DSE is performed at the substation level by utilizing only local measurements available from PMUs, meters, FDRs etc in the substation only, thus avoiding all issues associated with transmission of data and associated time latencies. This approach enables very fast DSE update rate which can go up to more than 60 executions per second. The developed DSE has been tested on actual substation models, the LongBay and RHPP substations of US Virgin Islands power system and the Gilboa-Blenheim substation of New York Power Authority's power system.

A novel, predictive, transient stability monitoring scheme with an application to generator out-of-step protection is also presented. In particular, the real-time dynamic model of the system, as given by the DSE, is utilized to evaluate the system's energy function based on Lyapunov's direct method and monitor the energy of the generator continuously and in real time, in order to characterize the stability of the system. The two major components of the scheme are a) the calculation of the center of oscillations of the system and b) the derivation of an equivalent, reduced sized model which is used for the calculation of the potential and kinetic energy of the system based on which the stability

of the system is determined. Finally an application of this scheme, which is a novel predictive generator out-of-step protection scheme is described, in which the energy of the generator is continuously monitored and if it exceeds a predefined threshold then instability is asserted and a trip signal can be sent to the generator. The developed scheme is compared with the state-of-the art technology for generator out-of-step protection, which is based on impedance relays that monitor the impedance trajectory at the terminals of the generator. The major advantage of the proposed scheme is that the out-of-step condition is predicted before its occurrence and therefore relays can act much faster than today's technology.

1 INTRODUCTION

1.1 Problem Statement

The major cause of one of the most widespread blackouts in history, the August 2003 Northeastern United States and Canada blackout, was identified to be lack of system's situational awareness [1]. This conclusion has demonstrated the need for more efficient, accurate, and reliable tools to monitor the power system in real time. The major tool that is presently used to achieve this functionality in modern energy management systems (EMS) is power systems state estimation (SE).

In particular, SE is performed in a centralized manner based on asynchronous measurements that are collected in the control center where the SE is performed every few minutes [2]-[3]. Steady-state system models are used, while measurements of various electrical quantities (including voltage and current magnitudes, active and reactive power flows and injections) are available via a supervisory control and data acquisition (SCADA) system. However, the complexity, the large dimensionality, and the geographic extent of the modern power systems impose significant biases in the formulation and execution of SE [4].

The introduction and the continuously growing installation of phasor measurement units (PMUs), which provide highly accurate synchronized measurements, have opened up the possibility for more efficient and accurate monitoring of the power system. SE is one of the major power system monitoring functions that can be modernized based on synchronized measurements technology and advances in substation automation. Biases in existing state estimators can be eliminated using PMU measurements in combination with highly accurate, three-phase and asymmetric power system models. In addition, PMUs provide phasor measurements that are GPS-synchronized to a common reference (UTC time reference), and thus are globally valid and can be used in local computations. As a result, PMUs allow for the implementation of SE in a distributed and decentralized architecture that eliminates the biases resulting from a centralized architecture.

PMU technology enables also the development and advancement of numerous power system applications and especially of advanced protection schemes that will improve the robustness and the security of power systems. A representative example of these applications is an on-line transient stability assessment tool that will efficiently and accurately characterize in real time the stability of the system and indicate the remedial actions that are required to prevent instability of the system or protect individual components of the system such as generators. The accuracy, the fast sampling rate, but most importantly the synchronized on a common reference (UTC time) measurements that PMUs provide, can be used to design on-line transient stability tools that will be able to evaluate in real time the dynamic model of the power system, monitor the transient swings of the system upon a disturbance, characterize its stability and indicate whether a generator has to be tripped before it goes into out-of-step operating condition. As a result, synchrophasor technology opens up the capability of the development of such tools and as a result overcome the disadvantages of currently available technology that is used for transient stability analysis which is based on computationally intense off-line studies.

Given the identified need for more efficient tools for monitoring and protection of the power system, and given the characteristics of the PMU technology that can enable the development of such tools, the objectives of this work are given next.

1.2 Research Objectives

The dissertation objectives are (a) to develop a distributed dynamic state estimator that is performed at the substation level based on synchronized (available from PMUs) and non-synchronized (available from relays and meters) measurements, captures with high fidelity the dynamics of the system and extracts in real time the dynamic model of the system and (b) to develop a transient stability monitoring scheme that utilizes the information given by the dynamic state estimation, achieves real-time monitoring of the transient swings of the system, characterizes in real time the stability of the system and enables a novel, predictive, generator out-of-step protection scheme capable of detecting potential generator loss of synchronism after a system disturbance.

In particular, initially the dissertation presents a distributed dynamic state estimator, which is performed at the substation level by utilizing only local measurements available from PMUs, meters, FDRs etc in the substation only, thus avoiding all issues associated with transmission of data and associated time latencies. This approach enables very fast DSE update rate which can go up to more than 60 executions per second. Two formulations of the proposed DSE are presented. The first one, referred to as DSE-Q, is used to capture with high fidelity the electromechanical dynamics of the system. The second one, referred to as DSE-T, is used to capture both electromechanical and electrical transients. The approach utilizes quadratic power system component modeling in order to improve the convergence of the algorithm. If only synchronized measurements are used and the associated devices in the substation are linear, the solution is further simplified since the state estimation becomes linear and has a direct solution. Moreover, it uses a three-phase, asymmetric and breaker oriented power system model in order to account for system imbalances, asymmetries and topology changes. The object-oriented formulation of the DSE is emphasized which is one of the key characteristics in the implementation of the DSE towards its very fast execution rates.

Towards the second objective of the work, a transient stability monitoring scheme is presented that utilizes the information given by the dynamic state estimation and enables real-time monitoring of the transient swings of the system and characterizes the stability of the system in real time. In particular, the real-time dynamic model of the system, as given by the DSE, is utilized to evaluate the system's energy function based on Lyapunov's direct method and extract stability properties from the energy function. The two major components of the scheme are a) the calculation of the center of oscillations of the system and b) the derivation of an equivalent, reduced sized model which is used for the calculation of the potential and kinetic energy of the system based on which the stability of the system is determined. An application of the transient stability monitoring scheme is an energy based, generator out-of-step protection scheme that is also presented. The energy of the generator is continuously monitored and if it exceeds a predefined threshold then instability is asserted and a trip signal can be sent to the generator. The major advantage of the proposed scheme is that the out-of-step condition is predicted before its occurrence and therefore relays can act much faster than today's technology.

1.3 Thesis Outline

The outline of the remaining parts of this document is as follows:

In Chapter 2, background information is provided on the origin of the topic along with presently available technologies that are being used. In addition, a thorough literature survey is presented that summarizes related research work efforts. In particular, the presently utilized technology for state estimation along with its biases and limitations are presented. Synchrophasor technology and how it can be utilized for the development of advanced state estimators is also presented. A literature review on the real-time transient stability assessment methodologies, describing the advantages and disadvantages of the existing methods that have been proposed and developed follows. Finally, present state-of-the-art protection schemes that are used for generator out-of-step protection are presented.

Chapter 3 presents in detail the mathematical formulation and the solution methodology of the developed distributed dynamic state estimator. More specifically, the object-oriented device modeling that is used for the two DSE formulations (DSE-Q and DSE-T) is presented in detail. The mathematical model and the categorization of the DSE measurements are also presented. The DSE solution algorithm and performance evaluation, along with bad data detection, identification and rejection methodology follow. Finally, the overall algorithm of the DSE with emphasis on the object-oriented implementation is described.

Chapter 4 presents the developed transient stability monitoring scheme. In particular, the utilization of the information on the real-time dynamic model of the system provided by the DSE, combined with Lyapunov's direct method for transient stability analysis is described. The major components of the algorithm which are a) the calculation of the center of oscillations of the system and b) the derivation of an equivalent, reduced sized model which is used for the calculation of the potential and kinetic energy of the system based on which the stability of the system is characterized, are described, along with the overall algorithm of the proposed scheme. Finally, a novel, generator out-of-step protection scheme that has been developed as an application of the transient stability monitoring scheme is also described.

Chapter 5 presents demonstrating examples on the DSE. In particular, the DSE has been tested on NYPA's Blenheim-Gilboa substation and on two substations (Longbay and RHPP) of USVI's power system.

Chapter 6 presents demonstrating examples of the developed transient stability monitoring and generator out-of-step protection schemes. The schemes are presented on multiple substation systems and in NYPA's Blenheim-Gilboa generating substation. The developed generator out-of-step scheme is compared to presently available state-of-the-art out-of-step protection schemes in order to verify its superiority.

Finally, Chapter 7 summarizes the research work and outlines the results and contributions of this dissertation.

There are also four appendices in this dissertation. In Appendix A the quadratic integration method is summarized. Appendix B describes the mathematical procedure for the calculation of the potential energy function of the generators in a multi-machine power system. Finally Appendices C and D describe the NYPA and USVI power system respectively, that were used as testbeds in the demonstrating examples.

2 LITERATURE REVIEW AND BACKGROUND INFORMATION

2.1 Overview

This chapter provides the background information of currently available technologies related to the research along with a literature review of the research efforts on these topics. In particular, the first section summarizes the currently utilized technology in state estimation and the biases and limitations of it. Then a short introduction is given on PMUs, in order to emphasize on the characteristics of this technology and how it can be utilized for the development of advanced state estimators, such as the proposed one.

The second section provides a literature review on the real-time transient stability assessment methodologies that have been proposed and developed. The requirements for a reliable and accurate online transient stability monitoring tool are discussed along with the advantages and disadvantages of the existing methods.

Finally, the third section summarizes present state-of-the-art protection schemes that are used for generator out-of-step protection. This information is given as background material since a comparison of the existing schemes with the developed scheme is performed.

2.2 Conventional and PMU-Based State Estimation

Control and operation of electric power systems is based on the ability to determine the system's state in real time. A reliable and accurate real time model of a power system is of paramount importance for is effective control and operation. Historically, the importance of this issue was recognized immediately after the 1965 blackout. Power system state estimation (SE) was introduced in the late 60s in order to achieve this objective [5]-[7] and has traditionally been treated as a static state estimation problem. It is based on a centralized approach that makes use of a steady state system model and of measurements of various electrical quantities (voltage and current magnitudes, active and reactive power flows and injections, etc) available via a SCADA system [2]-[3]. All the

measurements are sent from local remote terminal units (RTUs) to a central control center that monitors the entire system under control. The resulting real-time model of the system is of key importance for system monitoring and control. In fact, all the additional applications that may run in a power system control center, like contingency analysis, unit commitment, economic dispatch, etc use the results of state estimation as their input and perform their analysis based on these results. Therefore, state estimation is currently the cornerstone of control center real-time applications.

The complexity and geographic spread and separation of an electric power system have imposed significant restrictions in the implementation of power system state estimation. Contrary to other plants that are locally monitored and controlled, or that are remotely monitored and controlled but all measurements come from a specific location, an electric power system is widely spread. This means that measurements originating from multiple different locations (substations) have to travel significant distances to the data collection and processing center, usually referred to as energy management system (EMS). Thus, communication issues and latencies become an important problem [8]. Furthermore, if measurements are not accurately time-stamped, in a unified way, independent of the measurement location and thus are not synchronized, they can introduce significant biases in the estimation, and may even be practically useless in a dynamic estimation framework. The current centralized state estimation is also characterized by biases which arise from system asymmetries (not taken into account in the current system modeling), imbalanced operation and instrumentation errors [4],[9]. Additional disadvantages of centralized state estimation are (a) long execution time that is needed for the state estimation due to the large number of data and the model size and complexity, (b) bad data detection and identification becomes more complex and less sharp and (c) excessive communication requirements, since all SCADA data must be sent to a central location.

Such implementation issues have limited the power system state estimation to only basic, static, least squares-based algorithms. The process is executed relatively infrequent and is thus not suitable for dynamic monitoring of the system. The available measurements are limited to slow varying quantities, like power flows, voltage and

current magnitudes (not phase angles or instantaneous values) or discrete measurements of breaker status (that determine the system configuration). Such measurements are fitted to a steady state system model. The estimation algorithm is executed at a frequency of every several minutes. No dynamics are included in the models, since most of even the slower system dynamics have time scales of the order of milliseconds or at most seconds, and usually a very limited amount of system dynamic data have been available by the electric utilities. Most of such data are also of low accuracy, contrary to simple steady state models, for which utilities usually have precise information.

In summary, power system state estimation, in its current status, is not capable of capturing the system dynamic behavior. It only provides monitoring information in the form of a sequence of steady states. This also limits the wide area control actions on the system to very slow steady state control that is usually manually executed by the system operators. Such control application can be, e.g. economic generation dispatch among units, power flow redirection, reactive power and voltage profile control, static security assessment and control, load forecasting. Fast automatic control during faults and transients in general is provided only locally, on a component basis, not taking thus into consideration the wide area system behavior.

Recent major power system outages such as the 2003 U.S.-Canada black-out emerged the need for more efficient methods of monitoring the state of power systems. A promising technology that can revolutionize state estimation is phasor measurement units (PMUs) [10]-[16]. PMUs provide synchronized measurements where synchronization is achieved via a GPS (Global Positioning System) clock which provides the synchronizing signal with accuracy of 1 μsec. This time precision is translated into a precision of 0.02 degrees of the US power frequency (60 Hz). Therefore, the technology has the potential to measure the phase angles with a precision of 0.02 degrees. This means that measurements taken, or phasors computed via a time reference, at one location, are globally valid and can be used in local computations (making their results also globally valid) or along with data collected or computed at different locations. So, this eliminates problems originating from the wide geographic separation of a power system by making local measurements or computed quantities globally valid. The detailed definition of a

time synchronized phasor can be found in IEEE C37.118 Standard [17] and is illustrated in Figure 2.1.

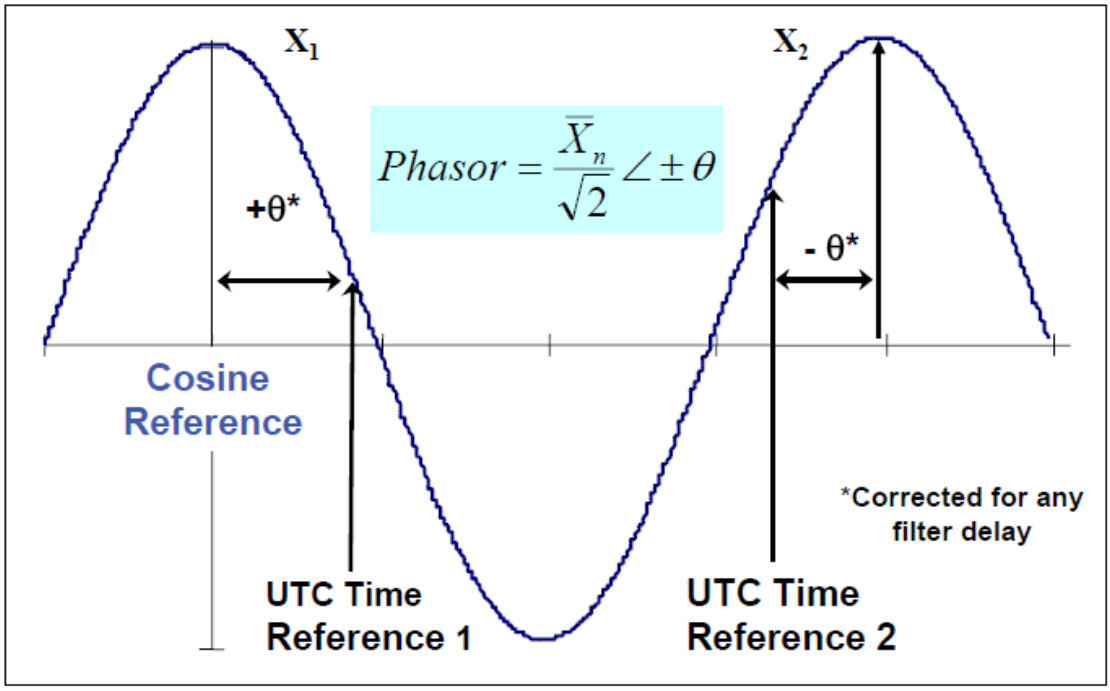

Figure 2.1. Synchrophasor definition [18].

The advantages from the integration of synchronized measurements into an existing nonlinear estimator have been addressed in several publications [19]-[20]. Moreover, state estimators that utilize only PMU measurements, thus resulting in linear estimators, have been also proposed. The first linear estimator using PMU technology was introduced in 1994 [10]. Multi-level linear estimators have also been proposed in [21]-[22]. Another advantage is that the introduction of PMUs has made it possible to locally measure both magnitude and phase of electrical quantities and distribute the state estimation procedure. Therefore, PMU technology opens-up the possibility of developing distributed state estimation approaches, which has been an active research topic for the past few years [23]-[28]. This is the basic idea of SuperCalibrator concept [29]-[32]. The technology is based on a flexible hybrid state estimation formulation. This is a combination of the traditional state estimation formulation and the GPS-synchronized measurement formulation, which uses an augmented set of available data. The basic idea is to provide a model based correction of the errors from all known sources of errors.

Specifically, the basic idea is to utilize a detailed model of the substation, (three-phase, breaker oriented model and instrumentation channel inclusive model) to perform the distributed state estimation that will provide a validated and high fidelity model of the system. The set of measurements comprises of:

- Traditional, non-synchronized measurements (voltage magnitude, active and reactive line flows and bus injections, and other standard SCADA data),
- GPS-synchronized measurements of voltage and current phasors for each phase,
- GPS synchronized measurements of frequency and rate of frequency change,
- Appropriate virtual-measurements and pseudo-measurements.

The measurements obtained from any device, PMU, relay, SCADA etc are utilized in an estimation method that statistically fits the data to the detailed model. This approach leads to a distributed state estimation procedure performed at the substation level. The functional description of the distributed state estimation is illustrated in Figure 2.2 and consists of the following procedures:

1. Perform state estimation on each substation using all available data and a three-phase, breaker oriented, instrumentation inclusive model,
2. Perform bad-data identification and correction (or rejection) as well as topology error identification on each substation,
3. Collect the results from all substations at a central location (control center) to construct the system-wide operating state of the system.

The advantages of SuperCalibrator compared to conventional state estimators are the following:

a. Utilization of a high fidelity model (three-phase, breaker-oriented and instrumentation channel inclusive model).

b. Utilization of all available data at the substation level, i.e. SCADA, relays, meters, PMUs, DFRs, etc.

c. State estimation accuracy quantification and bad data detection, identification, and removal.

d. Distributed processing of data at each substation (this requires that there is at least one GPS synchronized measurement at each substation) and subsequent transfer of the substation estimation results to the control center for synthesis of the system wide state estimate.

A conceptual illustration of SuperCalibrator is illustrated in Figure 2.3.

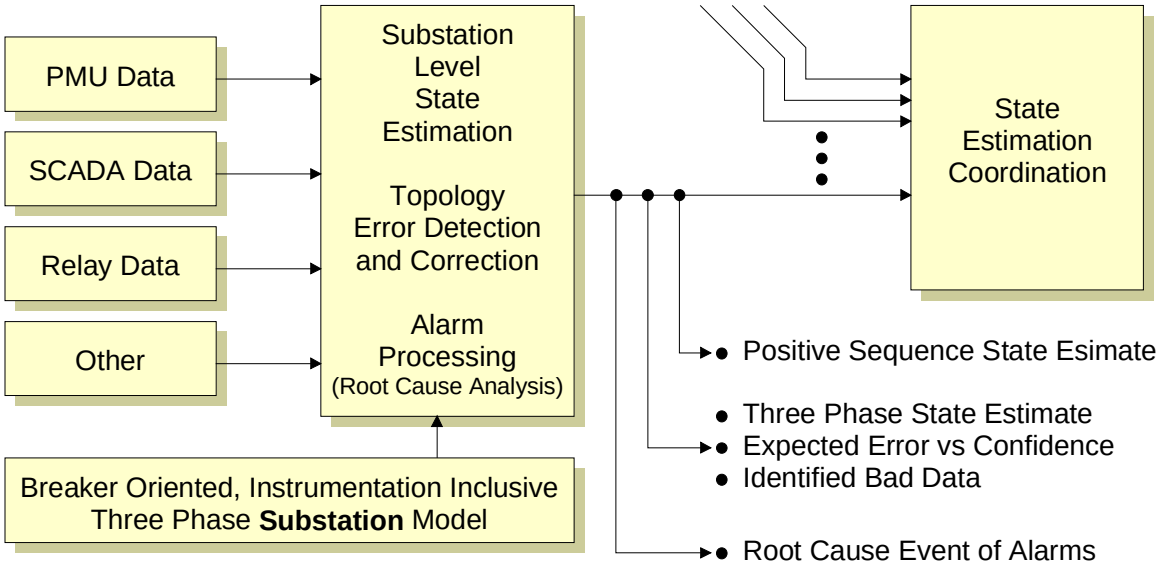

Figure 2.2. Functional description of the distributed state estimator (SuperCalibrator) [27].

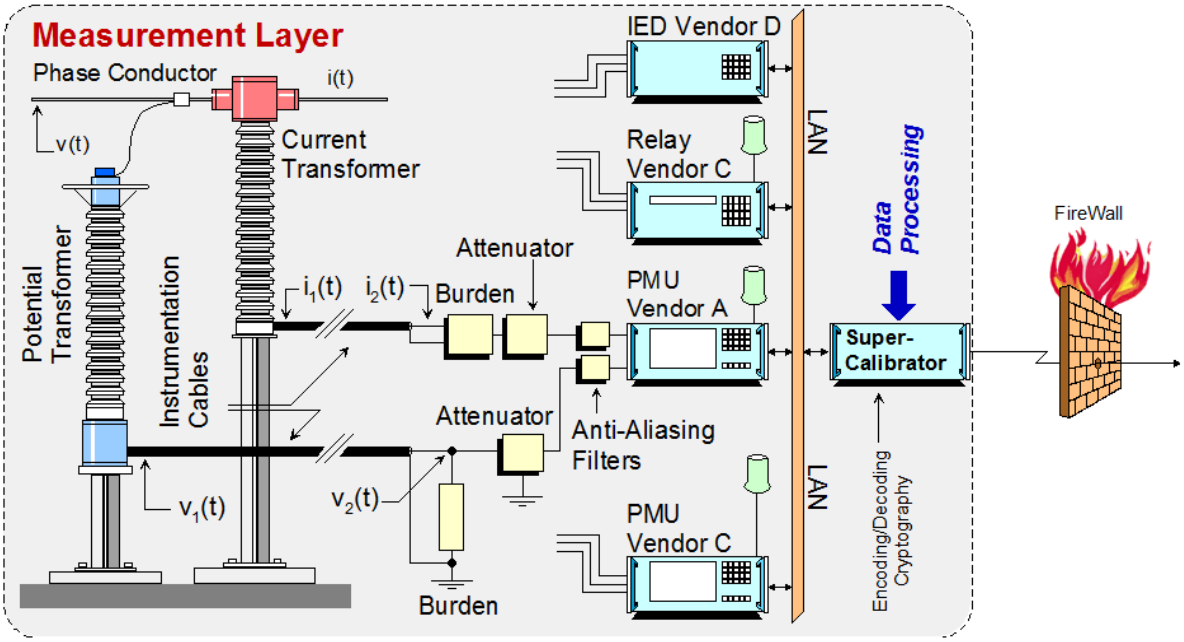

Figure 2.3. Conceptual illustration of the SuperCalibrator concept [27].

Inclusion of the dynamic behavior of the system into the state estimation algorithm results in a dynamic state estimator (DSE). DSE has been introduced, to some basic level, for power system applications in the past [33]-[35]. However, it has not been widely spread, let alone implemented, due to the fact that implementation of such concepts could not be possible without the phasor measurement units with GPS-synchronization and a distributed state estimation architecture. The majority of the related publications are based on simplified power system dynamic models, they utilize Kalman filter algorithms for the estimation procedure [35]-[37] and are practically unsuitable for large scale and real time implementations. Research attempts have been also made for DSE using computational intelligence techniques such as artificial neural networks [38].

Apart from state estimation, PMUs open up the possibility for the development and advancement of numerous other power system applications. A list of potential applications follows next [39]-[54]:

- Model Benchmarking and Parameter Identification
- Voltage Stability
- Angle/Frequency Stability

- Power System Protection
- Thermal Overload Monitoring
- Distributed Generation Integration
- Wide Area Monitoring Protection and Control Schemes

The benefits from such PMU based applications have recently been recognized by the power systems community and as a result PMU installation is rapidly growing in the developing countries. Figure 2.4 illustrates the currently existing PMUs in the North American Power Grid.

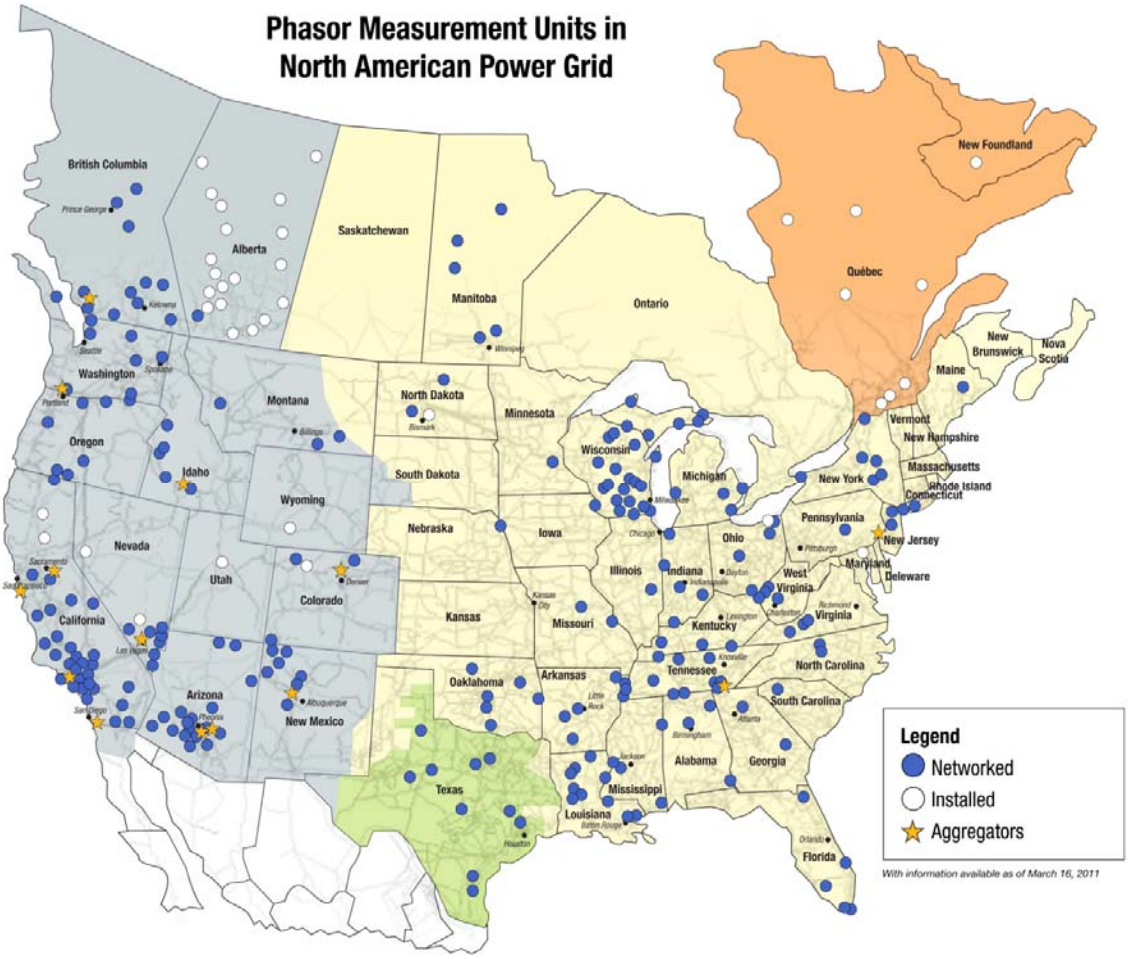

Figure 2.4. Phasor measurement units in North American power grid [55].

2.3 Real-Time Transient Stability Assessment

This section presents a brief literature survey on the state-of-the-art on real-time transient stability assessment (TSA) methodologies. More details on the fundamentals of power systems transient stability and TSA algorithms can be found in [56]-[61].

The major challenge in the topic of online transient stability assessment is the requirement for real-time operation with fast and highly precise calculations, without reducing the complexity or the large dimensionality of the power system dynamic models. Several approaches have been proposed and used to deal with this problem efficiently, without compromising the accuracy of the results.

The most commonly used tool for transient stability analysis is time domain dynamic simulations. The power system is modeled as a set of nonlinear differential-algebraic equations and the equations are solved using a numerical integration method. The major advantage of this method is the accuracy of the results since very detailed dynamic models of power system components can be used without the need for modeling simplifications. However, the major disadvantage is the fact that it requires a huge computational effort, which makes it intractable and unsuitable for online applications. That is the reason why this method is mainly used for offline transient stability studies. Another disadvantage is that time domain simulation method does not provide any guidelines for control actions that could prevent system instability [60].

The most popular and widely used approach for online stability analysis is direct methods [61]. A direct method for transient stability analysis is defined as a method that is able to determine stability without explicitly integrating the differential equations that describe the post-fault system. Their major advantage is that the computational effort that they require is dramatically reduced compared to time domain simulations and result in straightforward computations of transient stability limits. As a result they are more suitable for real-time applications. In addition, they can provide stability regions around an operating point and enable sensitivity analysis [61].

Among this class of direct methods, Lyapunov's based direct method for stability analysis is mostly used. The use of Lyapunov's method in power system has been

proposed since the late 40's and 50's [62]-[63]. The application of Lyapunov's direct method to power systems is referred to as the transient energy function method (TEF) because it requires the evaluation of a Lyapunov-type function, called TEF, in order to compute the region of stability around the post disturbance equilibrium point of the system. The boundary of the region of stability allows the assessment of the stability of an equilibrium point qualitatively as well as quantitatively via the computation of critical clearing times or critical energies. The main disadvantage of these methods is the difficulty in determining a suitable Lyapunov function. Several different functions, either simplified or complex, have been proposed as candidate Lyapunov functions [64]-[74]. The major limitations in determining an accurate Lyapunov function relate to the fact that a very accurate model of the system that is studied is needed, which in general is difficult to have. Despite the ongoing efforts in the power systems community for creating and using common models for the Eastern Interconnection or the WECC (Western Electricity Coordinating Council) systems, such models are not available yet. Note that the Lyapunov function is a system level function that represents the energy of the whole system. As a result, given the inaccuracy of the existing power system models, the construction of an accurate Lyapunov function is challenging. The other major challenge is that the Lyapunov energy function has to be constructed for the post-fault system configuration. This inherently means that in real time, the post fault system has to be identified, along with initial conditions on the post fault system that can be only obtained accurately by time-domain approaches [75]. This task is very challenging to be achieved for large realistic systems, given the time limitations within which these computations have to be performed. Finally another disadvantage is that the function based direct methods are only applicable for first swing transient stability analysis. In addition, the application of the TEF methods also involves the simulation of the system, at least during the fault period, so combinations of TEF methods with time domain analysis are very common in literature. Another challenging and computationally intensive part of the TEF methods is the calculation of the post-fault system equilibrium points. However, despite their disadvantages, these methods are by far more efficient and suitable for real-time application compared to full time domain analysis.

Another TSA method is the extended equal area criterion method (EEAC). The basic principle of the EEAC method is the separation of the system machines in two subsets, the critical and the non critical machines. These two machine groups are transformed into two equivalent machines and then the system is reduced to an equivalent single machine infinite bus system (SMIB) where the equal area criterion is applied to [76]-[79]. EEAC can be also combined with time domain simulations for more accurate results.

The majority of currently existing commercial programs for online transient stability assessment use one of the above mentioned methods, or combinations of them. In addition, several techniques have been investigated to improve the performance of online TSA algorithms. These techniques include advanced numerical integration algorithms for more efficient time domain simulation. Parallel processing implementations have been also proposed and investigated [80]-[84], that suggest distributed computing or parallel processor architectures in order to reduce the computational time of the TSA.

Finally, apart from the analytical methods described so far, some attempts have been made for completely "non-conventional" approaches to the issue of power system transient stability by using computational intelligence methods. In particular, decision trees (DTs) based methods have been developed [60],[85]-[87]. DTs are used as classifiers to perform a filtering screening to possible contingencies and select the ones to be further analyzed. Artificial neural networks (ANN) are also a very popular computational-intelligence technique and significant research has been published in this area [88]-[92]. However, ANNs act as a "black box" and do not allow a thorough investigation on the phenomena that might lead to system instability. In general, despite the research efforts on this area, presently there is no commercially based application that is using ANN or some other computational intelligence based technique, since these techniques do not meet the efficiency, accuracy and robustness requirements that are necessary for the assessment of the stability of an actual system in real time.

2.4 Generator Out-of-Step Protection

Generator protection from out-of-step conditions is mainly performed by distance relays that monitor the impedance trajectory. An overview of the out-of-step protection schemes that are presently used for generator protection is summarized next [93]-[95].

Consider the two source equivalent as illustrated in Figure 2.5.

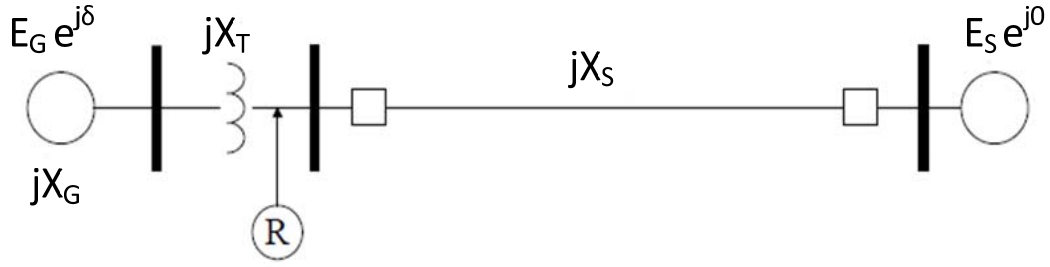

Figure 2.5. A two-source system.

The impedance as seen by the relay is:

$$Z = \frac{V}{I} = \frac{E_G\angle\delta - I\cdot j\cdot(x_G + x_T)}{\dfrac{E_G\angle\delta - E_S}{j\cdot(x_G + x_T + x_s)}} = -j\cdot(x_G + x_T) + j\cdot(x_G + x_T + x_s)\cdot\frac{E_G\angle\delta}{E_G\angle\delta - E_S} \tag{2.1}$$
$$= j\cdot\frac{(x_G + x_T + x_s)\cdot n\cdot(n - \cos\delta - j\cdot\sin\delta)}{(n-\cos\delta)^2 + \sin^2\delta} - j\cdot(x_G + x_T)$$

where $n = \dfrac{E_G}{E_S}$

The impedance locus represented by equation (2.1) is illustrated in Figure 2.6. For $n = 1$ the impedance trajectory is a straight line that is perpendicular and is crossing the middle point of the total impedance $x_G + x_T + x_s$. For $n \neq 1$ the trajectory is a circle.

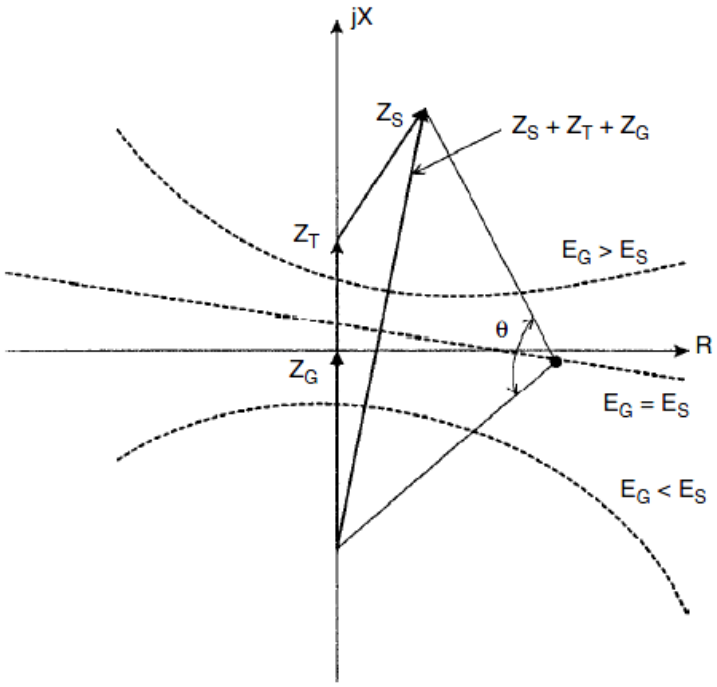

Figure 2.6. Impedance trajectory during a power swing [93].

The most common out-of-step protection scheme is a mho relay with single blinders as illustrated in Figure 2.7 [94]. Out-of-step condition is detected if the impedance trajectory remains within the two blinders for a time greater than a specified duration, or if it crosses both the two blinders. For example, scenarios "a" and "b" are considered stable scenarios while scenario "c" is an unstable scenario, as illustrated in Figure 2.7. An advantage of the blinder scheme is that it can be used independently of the distance protection functions of the mho relay. However the major disadvantage is that if an unstable swing is detected, tripping is usually delayed to avoid overstresses on the opened breaker. Another disadvantage of this scheme is that determination of the settings for the mho relay usually requires numerous stability simulations [94].

Double blinder schemes have also been proposed and implemented as illustrated in Figure 2.8 [94]. In these schemes the time that is needed for the impedance to cross both the outer blinder (RRO) and the inner blinder (RRI) is measured, and if it is greater than the setting time, a swing is detected.

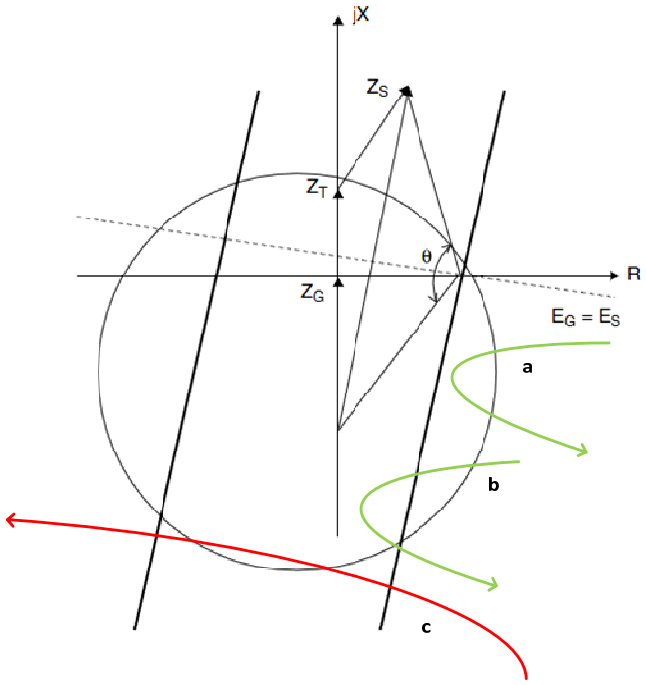

Figure 2.7. Single blinder out-of-step protection scheme [94].

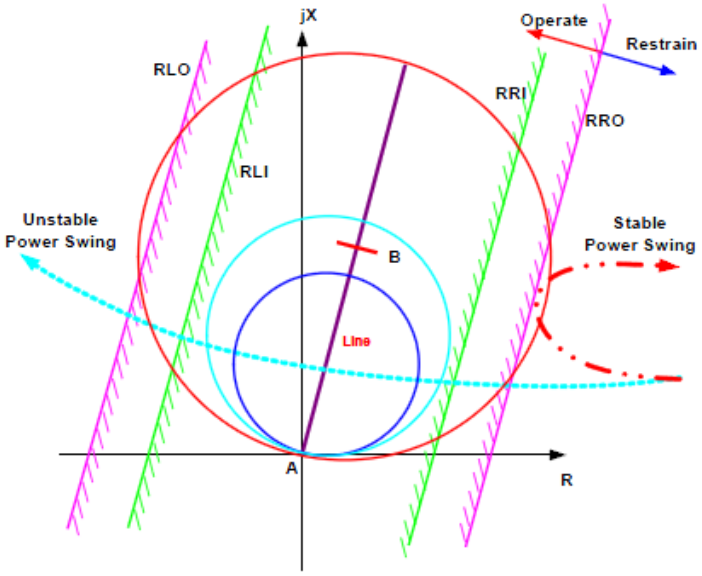

Figure 2.8. Double blinder out-of-step protection scheme [94].

Concentric characteristic schemes have been also used for out-of-step protection. The operating principle is to measure the rate of change of the impedance using two impedance characteristics and a timing device. If the impedance stays between the inner

and outer zone for more than a specified time then a signal is issued to block the distance relay operation. The inner zone has to be placed outside the largest distance protection region. The main disadvantage of this method is that it is sensitive to load encroachment. Several types of concentric characteristics have been used and are illustrated in Figure 2.9 [94].

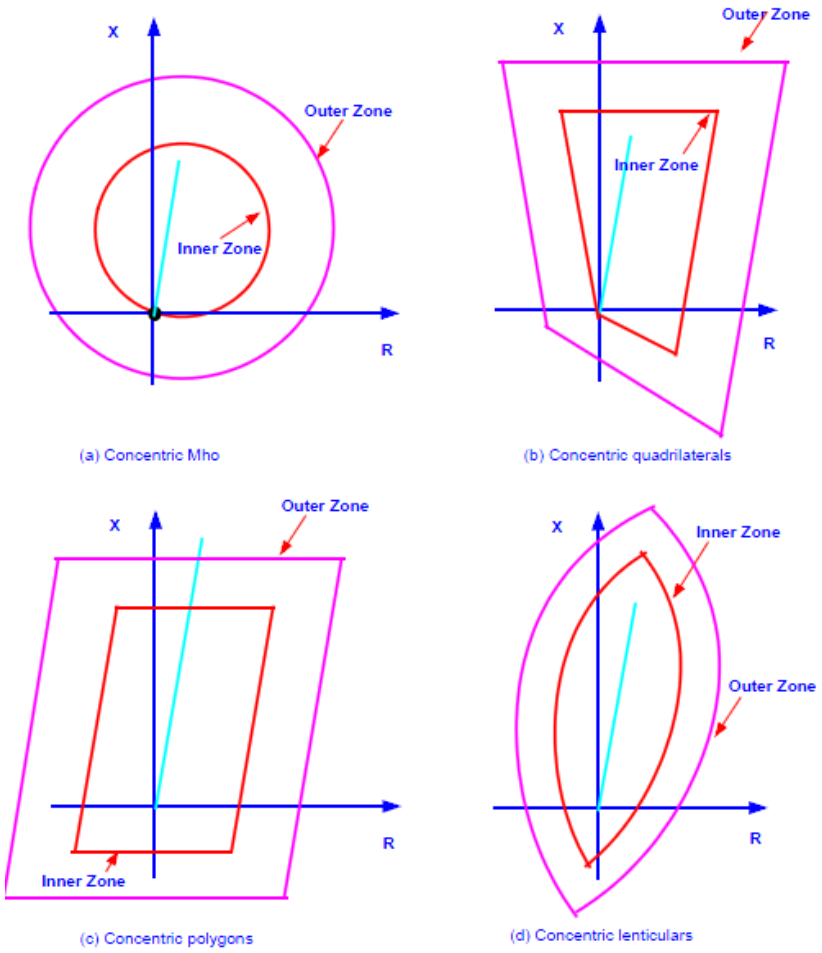

Figure 2.9. Out-of-step concentric distance relay characteristics [94].

Finally, additional out-of-step protection schemes that are based on wavelet transforms [96], fuzzy logic [97] and neural networks [98] have been also proposed in the literature but there is no actual implementation of them.

2.5 Summary

This chapter presented an overall description and related work on the research topics of this dissertation. In particular, the first section summarizes the present practices on state estimation and its limitations. The synchrophasor technology is also introduced and it is discussed how it can contribute to the reformulation of state estimation and the elimination of its biases.

The next section provides a literature review of the methods that have been used and proposed for transient stability assessment. The advantages and disadvantages of each method are discussed. Finally, in the next section, the present state-of-the-art technology on generator out-of-step protection is summarized.

3 PMU-BASED DISTRIBUTED DYNAMIC STATE ESTIMATION

3.1 Overview

A PMU-based distributed dynamic state estimator is described in this chapter. DSE is performed at the substation level by utilizing only local measurements available from PMUs, meters, FDRs etc in the substation only, thus avoiding all issues associated with transmission of data and associated time latencies. This approach enables very fast DSE update rate which can go up to more than 60 executions per second.

In sections 3.3 and 3.4 two formulations of the proposed DSE are presented. The first one, referred to as DSE-Q, is used to capture with high fidelity the electromechanical dynamics of the system. The second one, referred to as DSE-T, is used to capture both electromechanical and electrical transients. The object-oriented mathematical model of the devices, which is enabled by quadratic power system component modeling, is given for each formulation of the DSE.

The object-oriented DSE measurement model is described in section 3.5. The different types of measurements that are used in the DSE process are explained in detail. The DSE solution algorithm is given in section 3.6. Sections 3.7 and 3.8 describe the procedures for evaluating the quality of the results of the state estimator and the bad data detection, identification and rejection method in case of existing bad data.

The overall DSE algorithm is summarized in section 3.9. Finally, section 3.10 describes the distributed architecture of the DSE and how it can be used as the major component of a PMU-based wide area monitoring system.

3.2 DSE Introduction

In general, dynamic state estimation extends the concept of static state estimation by using the dynamic states of the power system, such as the generator speed or the generator acceleration. The generic dynamic state estimation model is described by a set

of differential and algebraic equations (DAEs), which express the dynamics of the system as follows:

$$\frac{dx(t)}{dt} = f(x(t), y(t), t), \qquad 0 = g(x(t), y(t), t), \tag{3.1}$$

where x and y are the dynamic and algebraic states of the system respectively. The system measurements z are related to the states through the following equations:

$$z = h(x(t), y(t), t) + \eta, \tag{3.2}$$

where η represents the measurement error, which is often described as random variable with Gaussian probability distribution. The measurement error is directly related to the accuracy of the data acquisition system.

The overall approach is illustrated in Figure 3.1. The set of physical measurements z_a are obtained from PMUs, relays, and other metering devices at the substation level. These values are then compared with the "model" values, which are obtained from the dynamic model of the power system, i.e., z_m , forming a measurement error e. Additional relations that hold based on the system model (3.1) are also included in the measurement set and are referred to as virtual measurements. Such equations are also of the form (3.2), with a measurement value of 0 and a very small measurement error. A standard least squares estimation is performed, which minimizes the sum of the errors squared and provides the best estimate of the system state. If the dynamic state estimator results are not satisfactory, this might indicate the presence of bad data. Statistical hypothesis methods are used, based on the chi-square criterion to check the presence of bad data. The bad data are identified, based on their normalized residual values, removed from the measurement set and the procedure is repeated. Otherwise, the best estimates of the system states and measurements denoted by $\hat{x}_e$, $\hat{y}_e$, and $\hat{z}_e$ are calculated and can be used as an input for numerous power systems applications such as stability monitoring etc.

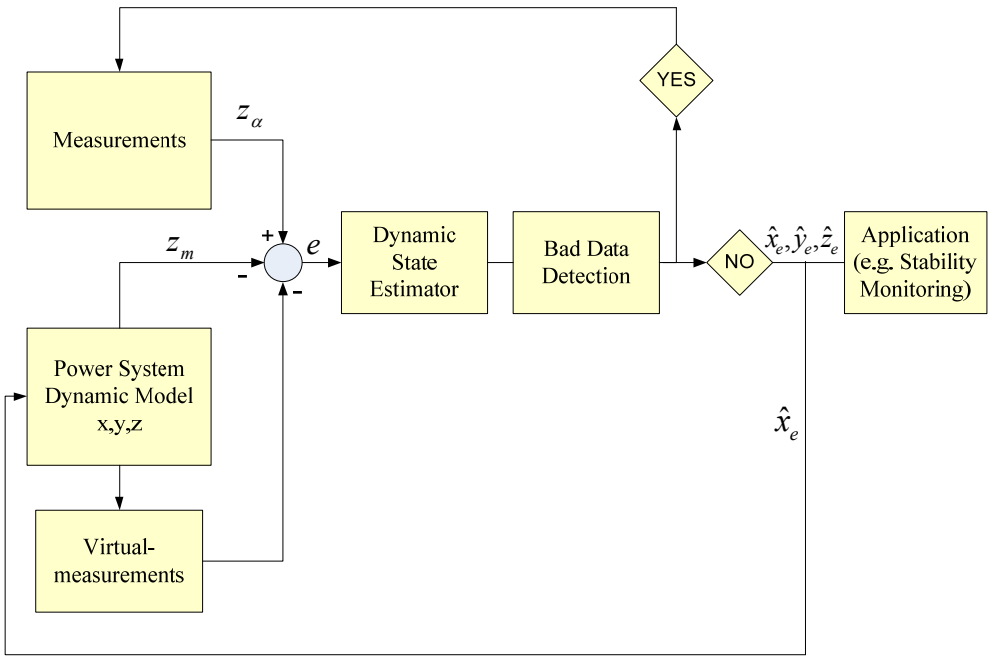

Figure 3.1. Schematic diagram of dynamic state estimator [99].

The dynamic state estimation can be formulated in two ways. A first approach is to use quasi-static models for modeling the power system. Thus, in this approach the electromechanical dynamics of the system are modeled but the electrical transients are neglected. This formulation of the dynamic state estimator will be referred to as DSE-Q. In the second approach, full transient models are used for the power system modeling. Thus, in this approach both the electromechanical and the electrical transients can be captured. This formulation of the dynamic state estimator will be referred to as DSE-T. In the following sections a detailed description of DSE-Q and DSE-T follows.

3.3 DSE-Q Formulation

3.3.1 Definition of States

The state is defined as the collection of the voltage phasors for each phase at each bus of the substation. So for every bus i of the substation the voltage state is defined as:

$$\widetilde{V}_i = \left[\widetilde{V}_{i,A} \quad \widetilde{V}_{i,B} \quad \widetilde{V}_{i,C} \quad \widetilde{V}_{i,N}\right]^T$$

Note that in a rectangular coordinates formulation there are two states for each phasor voltage, the real and the imaginary part. So the actual states are:

$$V_i = \begin{bmatrix} V_{i,A,R} & V_{i,A,I} & V_{i,B,R} & V_{i,B,I} & V_{i,C,R} & V_{i,C,I} & V_{i,N,R} & V_{i,N,I} \end{bmatrix}^T$$

where subscripts R and I denote real and imaginary part.

The state is extended to include internal states (algebraic or dynamic) of the devices, for example the torque angle and the rotor speed of a generator or the magnetic flux linkage of a transformer. The system state also includes the states of the buses at the other ends of the lines/circuits connected to the substation. The conceptual illustration of the dynamic state estimator and the state definition is shown in Figure 3.2.

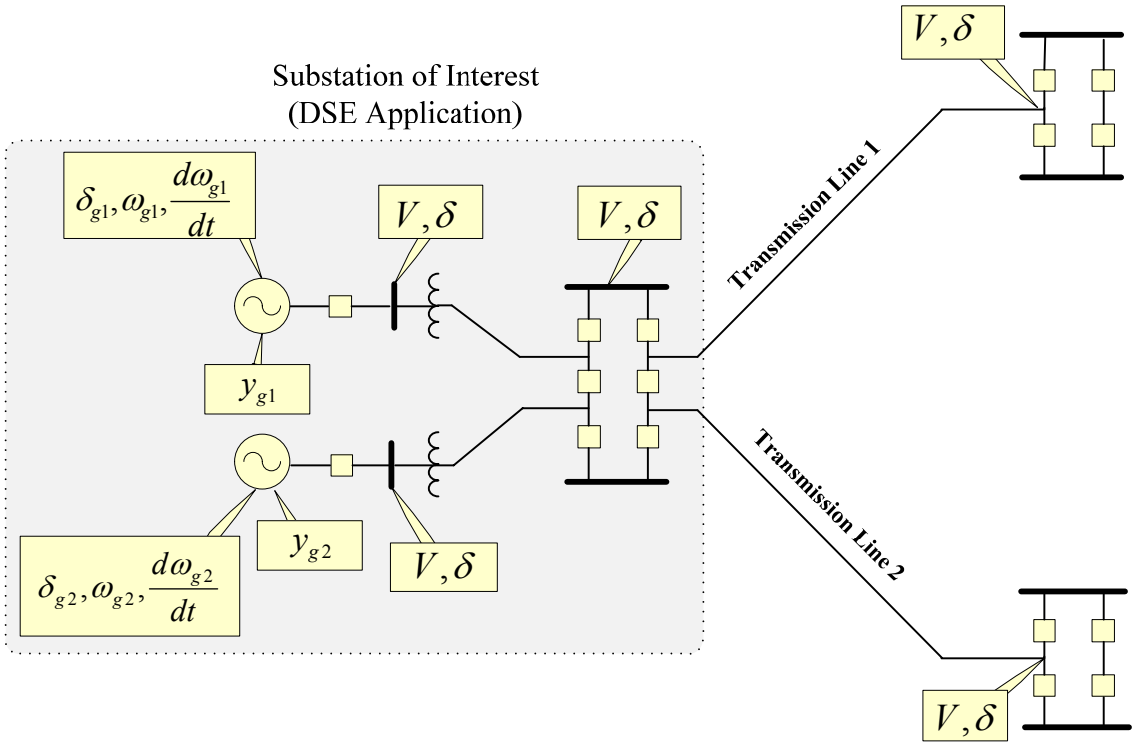

Figure 3.2. DSE-Q state definition [100].

3.3.2 Device Modeling

Each device that participates in the DSE algorithm is modeled based on a standard form that captures the dynamic behavior of the device. In this work the Algebraic Companion Form (ACF) is used to describe the model of a device in standard form. This form contains the equations for the through variables (or external equations) of the model

along with the additional internal model equations. This standardization enables object-oriented implementation of the DSE because each physical measurement can be formulated with the aid of the ACF as it will be explained in detail in section 3.5. The ACF model of each device has the following format:

$$\begin{bmatrix} \widetilde{I}(t) \\ 0 \\ \widetilde{I}(t_m) \\ 0 \end{bmatrix} = Y_{eq} \cdot \begin{bmatrix} \widetilde{V}(t) \\ y(t) \\ \widetilde{V}(t_m) \\ y(t_m) \end{bmatrix} + \begin{bmatrix} \begin{bmatrix} \widetilde{V}(t) & y(t) & \widetilde{V}(t_m) & y(t_m) \end{bmatrix} \cdot F_{eq,1} \cdot \begin{bmatrix} \widetilde{V}(t) \\ y(t) \\ \widetilde{V}(t_m) \\ y(t_m) \end{bmatrix} \\ \vdots \\ \begin{bmatrix} \widetilde{V}(t) & y(t) & \widetilde{V}(t_m) & y(t_m) \end{bmatrix} \cdot F_{eq,n} \cdot \begin{bmatrix} \widetilde{V}(t) \\ y(t) \\ \widetilde{V}(t_m) \\ y(t_m) \end{bmatrix} \end{bmatrix} - b_{eq} \qquad (3.3)$$

where

$$b_{eq} = N_{eq} \cdot \begin{bmatrix} \widetilde{V}(t-h) \\ y(t-h) \end{bmatrix} + M_{eq} \cdot \begin{bmatrix} \widetilde{I}(t-h) \\ 0 \end{bmatrix} + K_{eq} \qquad (3.4)$$

$\widetilde{I}$: the through variables of the device model.

$\widetilde{V}$: the external states of the device model.

$y(t)$: the internal states of the device model.

Y_{eq} : matrix defining the linear part of the device model.

$F_{eq,i}$: matrices defining the quadratic part of the device model.

N_{eq} : constant matrix defining the contribution of the states of previous time steps

M_{eq} : constant matrix defining the contribution of the through variables of previous time steps

K_{eq} : constant vector defining the constant part of the device model

The steps for deriving the ACF for each device and the syntax of the standard form are explained next.

In general the dynamic model of a device is described by a set of DAEs. Given the set of DAEs a quadratization procedure is applied. This can be achieved without any approximations by introducing additional state variables and their defining algebraic equations (for each additional state variable one more equation is added). Note that the number of the new state variables equals the number of the new defined equations. In addition, in the proposed formulation, there are no nonlinearities in the dynamic part of the model. That is, all nonlinearities are moved to the algebraic part of the model by the introduction of additional appropriate state variables. The resulting set of equations are linear or quadratic in terms of the state variables. This quadratization methodology improves the performance characteristics of DSE because it improves the convergence of the state estimation algorithm since application of Newton's iterative method for the solution (described in section 3.6) is ideally suited. Upon the quadratization procedure the device model can be cast in the following form:

$$A_{10}\frac{dp(t)}{dt} = A_{11}\cdot p(t) + A_{12}\cdot q(t) + A_{13}\cdot r(t) + A_{14} \qquad \text{(linear differential equations)}$$

$$0 = \begin{bmatrix} B_{11} & B_{12} & B_{13} \end{bmatrix} \cdot \begin{bmatrix} p(t) \\ q(t) \\ r(t) \end{bmatrix} + B_{10} \qquad \text{(linear algebraic equations)} \quad (3.5)$$

$$0 = \begin{bmatrix} B_{21} & B_{22} & B_{23} \end{bmatrix} \cdot \begin{bmatrix} p(t) \\ q(t) \\ r(t) \end{bmatrix} + \begin{bmatrix} s^T(t)\cdot F_1 \cdot s(t) \\ \vdots \\ s^T(t)\cdot F_2 \cdot s(t) \end{bmatrix} + B_{20} \qquad \text{(quadratic algebraic equations)}$$

where

$p(t)$: the dynamic states of the device model.

$q(t)$: the algebraic states of the device model.

$r(t)$: additional algebraic (internal) states introduced for the quadratization of the device model.

$s(t) = \begin{bmatrix} p(t) & q(t) & r(t) \end{bmatrix}$: the state vector

In order to bring the model (3.5) in the ACF form, the variables are categorized into through variables, external state variables and internal state variables. The model equations are rearranged such that external equations (equations that relate the through variables to the state variables) are given first, followed by the internal equations which are either differential or algebraic equations of order no more than two. As a result, the device model can be written in the following form:

$$A \cdot \widetilde{I}(t) = B_1 \cdot \widetilde{V}(t) + B_2 \cdot y(t) + B_3 \qquad \text{(external equations)}$$

$$0 = \frac{dy(t)}{dt} + C_2 \cdot \widetilde{V}(t) + C_3 \cdot y(t) + C_4 \qquad \text{(internal differential equations)} \quad (3.6)$$

$$0 = \begin{bmatrix} D_1 & D_2 \end{bmatrix} \cdot \begin{bmatrix} \widetilde{V}(t) \\ y(t) \end{bmatrix} + \begin{bmatrix} \begin{bmatrix} \widetilde{V}(t) & y(t) \end{bmatrix}^T \cdot F_1 \cdot \begin{bmatrix} \widetilde{V}(t) & y(t) \end{bmatrix} \\ \vdots \\ \begin{bmatrix} \widetilde{V}(t) & y(t) \end{bmatrix}^T \cdot F_n \cdot \begin{bmatrix} \widetilde{V}(t) & y(t) \end{bmatrix} \end{bmatrix} + E_0 \qquad \text{(internal quadratic algebraic}$$

equations)

where:

$\widetilde{I}$: are the through variables of the model.

$\widetilde{V}$: are the external states of the system.

$y(t)$: are the internal states of the system.

Quadratic integration [101]-[105] (see Appendix A) is used to integrate the dynamic model of the device (3.6). The result is the following algebraic form:

$$A \cdot \widetilde{I}(t) = B_1 \cdot \widetilde{V}(t) + B_2 \cdot y(t) + B_3$$

$$A \cdot \widetilde{I}(t_m) = B_1 \cdot \widetilde{V}(t_m) + B_2 \cdot y(t_m) + B_3$$

$$0 = y(t) - y(t-h) + C_2 \cdot \left(\frac{h}{6} \cdot \widetilde{V}(t) + \frac{2h}{3} \cdot \widetilde{V}(t_m) + \frac{h}{6} \cdot \widetilde{V}(t-h)\right)$$

$$+ C_3 \cdot \left(\frac{h}{6} \cdot y(t) + \frac{2h}{3} \cdot y(t_m) + \frac{h}{6} \cdot y(t-h)\right) + h \cdot C_4$$

$$
\begin{aligned}
0 &= y(t_m) - y(t-h) + C_2 \cdot (-\frac{h}{24} \cdot \widetilde{V}(t) + \frac{h}{3} \cdot \widetilde{V}(t_m) + \frac{5h}{24} \cdot \widetilde{V}(t-h)) \\
&+ C_3 \cdot (-\frac{h}{24} \cdot y(t) + \frac{h}{3} \cdot y(t_m) + \frac{5h}{24} \cdot y(t-h)) + \frac{h}{2} \cdot C_4
\end{aligned}
\tag{3.7}
$$

$$
0 = \begin{bmatrix} D_1 & D_2 \end{bmatrix} \cdot \begin{bmatrix} \widetilde{V}(t) \\ y(t) \end{bmatrix} + \begin{bmatrix} \begin{bmatrix} \widetilde{V}(t) & y(t) \end{bmatrix}^T \cdot F_1 \cdot \begin{bmatrix} \widetilde{V}(t) & y(t) \end{bmatrix} \\ \vdots \\ \begin{bmatrix} \widetilde{V}(t) & y(t) \end{bmatrix}^T \cdot F_n \cdot \begin{bmatrix} \widetilde{V}(t) & y(t) \end{bmatrix} \end{bmatrix} + E_0
$$

$$
0 = \begin{bmatrix} D_1 & D_2 \end{bmatrix} \cdot \begin{bmatrix} \widetilde{V}(t_m) \\ y(t_m) \end{bmatrix} + \begin{bmatrix} \begin{bmatrix} \widetilde{V}(t_m) & y(t_m) \end{bmatrix}^T \cdot F_1 \cdot \begin{bmatrix} \widetilde{V}(t_m) & y(t_m) \end{bmatrix} \\ \vdots \\ \begin{bmatrix} \widetilde{V}(t_m) & y(t_m) \end{bmatrix}^T \cdot F_n \cdot \begin{bmatrix} \widetilde{V}(t_m) & y(t_m) \end{bmatrix} \end{bmatrix} + E_0
$$

Upon manipulations of equations (3.7) the integrated Algebraic Companion Form (ACF) device model can be cast in the standard form provided earlier and repeated here for convenience:

$$
\begin{bmatrix} \widetilde{I}(t) \\ 0 \\ \widetilde{I}(t_m) \\ 0 \end{bmatrix} = Y_{eq} \cdot \begin{bmatrix} \widetilde{V}(t) \\ y(t) \\ \widetilde{V}(t_m) \\ y(t_m) \end{bmatrix} + \begin{bmatrix} \begin{bmatrix} \widetilde{V}(t) & y(t) & \widetilde{V}(t_m) & y(t_m) \end{bmatrix} \cdot F_{eq,1} \cdot \begin{bmatrix} \widetilde{V}(t) \\ y(t) \\ \widetilde{V}(t_m) \\ y(t_m) \end{bmatrix} \\ \vdots \\ \begin{bmatrix} \widetilde{V}(t) & y(t) & \widetilde{V}(t_m) & y(t_m) \end{bmatrix} \cdot F_{eq,n} \cdot \begin{bmatrix} \widetilde{V}(t) \\ y(t) \\ \widetilde{V}(t_m) \\ y(t_m) \end{bmatrix} \end{bmatrix} - b_{eq} \tag{3.8}
$$

3.4 DSE-T Formulation

3.4.1 Definition of States

The dynamic state of the substation is defined as the voltage magnitude, phase angle, angular speed (frequency), and rate of change of frequency at each bus of the substation as well as at the buses at the other ends of the lines/circuits connected to the substation. The state is extended to include internal states (algebraic or dynamic) of the devices, for example the torque angle and the rotor speed of a generator or the magnetic flux linkage

of a transformer. The definition of the dynamic state of the substation is illustrated in Figure 3.3.

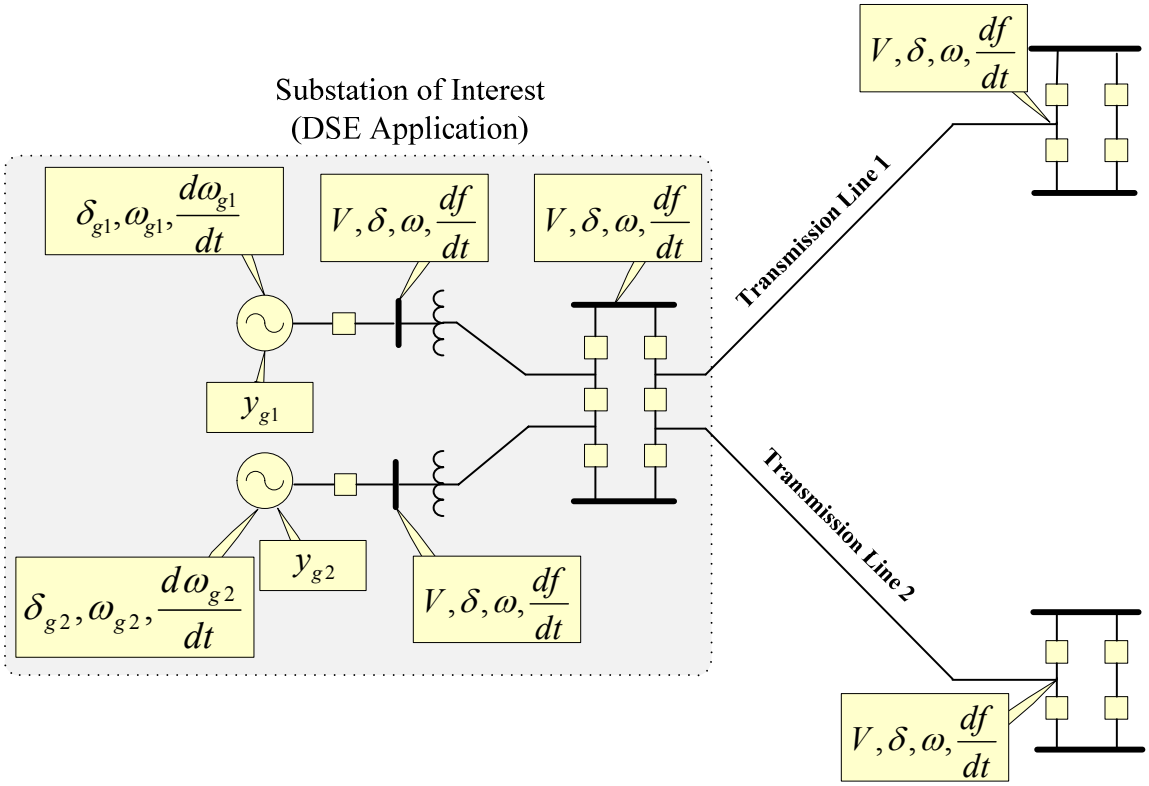

Figure 3.3. DSE-T state definition [100].

3.4.2 Device Modeling

The Algebraic Companion Form (ACF) is used to describe the model of a device in standard form. As mentioned before, this standardization enables object-oriented implementation of the DSE because each physical measurement can be formulated with the aid of the ACF as it will be explained in detail in section 3.5. The ACF model of each device is given next. The details on the derivation of the ACF device model (quadratization, quadratic integration etc) are omitted since the procedure is very similar to the one described in section 3.3.2.

$$\begin{bmatrix} i(t) \\ 0 \\ i(t_m) \\ 0 \end{bmatrix} = Y_{eq} \begin{bmatrix} v(t) \\ y(t) \\ v(t_m) \\ y(t_m) \end{bmatrix} + \begin{bmatrix} \begin{bmatrix} v^T(t) & y^T(t) & v^T(t_m) & y^T(t_m) \end{bmatrix} \cdot F_{eq,1} \cdot \begin{bmatrix} v(t) \\ y(t) \\ v(t_m) \\ y(t_m) \end{bmatrix} \\ \vdots \\ \begin{bmatrix} v^T(t) & y^T(t) & v^T(t_m) & y^T(t_m) \end{bmatrix} \cdot F_{eq,n} \cdot \begin{bmatrix} v(t) \\ y(t) \\ v(t_m) \\ y(t_m) \end{bmatrix} \end{bmatrix} - b_{eq} \tag{3.9}$$

where

$$b_{eq} = N_{eq} \cdot \begin{bmatrix} v(t-h) \\ y(t-h) \end{bmatrix} + M_{eq} \cdot \begin{bmatrix} i(t-h) \\ 0 \end{bmatrix} + K_{eq} \tag{3.10}$$

$i(t)$: the through variables of the device model.

$v(t)$: the external states of the device model.

$y(t)$: the internal states of the device model.

Y_{eq}: matrix defining the linear part of the device model.

$F_{eq,i}$: matrices defining the quadratic part of the device model.

N_{eq}: constant matrix defining the contribution of the states of previous time steps

M_{eq}: constant matrix defining the contribution of the through variables of previous time steps

K_{eq}: constant vector defining the constant part of the device model

3.5 Measurement Model and Object-Oriented Measurement Processing

The system measurements z are in general related to the states through the following equations:

$$z = h(x(t)) + \eta, \tag{3.11}$$

where η represents the measurement error, which is often described as random variables with Gaussian probability distribution and $x(t)$ is the system state vector. Due to the existence of a variety of measurements and models (GPS synchronized, non synchronized, nonlinear models, etc.) the relationship between the states and the measurements is not necessarily linear. However due to the quadratic modeling that is followed in the described formulation, a physical measurement or a virtual-measurement is at most quadratic in terms of the states and will have the following generic formulation:

$$z_k = c_k + \sum_i a_{k,i} \cdot x_i + \sum_{i,j} b_{k,i,j} \cdot x_i \cdot x_j + \eta_k \,, \tag{3.12}$$

where

z_k : is the measured value

c_k : is the constant term

$a_{k,i}$: are the linear coefficients

$b_{k,i,j}$: are the nonlinear coefficients

η_k : is the error term

Note that the measurements are related to the states with a degree of at most quadratic. The set of physical measurements z are obtained from PMUs, relays, and other metering devices at the substation level. Additional relations that hold based on the system model are also included in the measurement set and are referred to as virtual measurements. Such equations are also of the form (3.12), with a measurement value of 0 and a very small measurement error.

The measurements are classified in seven categories:

1. Actual Across Measurement:

This type of measurement is a real measurement that can be obtained by available metering devices. It is a direct state measurement so it is not related to a device. Typical measurements that belong in this category are voltage phasor measurements.

2. Pseudo Across Measurement:

This type of measurement is not a real measurement. The pseudo across measurement is also not related to a device. For example if only the voltage phasor measurement for phase A, is available, the voltage phasor measurements for phase B and C can be added as pseudo across measurements in the estimation algorithm with the same magnitude and a phase difference of +/- 120 accordingly.

3. Actual Through Measurement:

This type of measurement is a real measurement that can also be obtained by available metering devices. Typical measurements that belong in this category are current phasor measurements or real power measurements. Actual through measurements are related to a specific device of the system. Thus, for creating the model of an actual through measurement, the device (distribution line, transformer, etc.) that this measurement refers to, has to be known. Then the measurement formula is derived as a function of the states of the device.

As discussed in section 3.3.2, each device is represented by an ACF. The model of the actual through measurement can be easily derived from the ACF of the corresponding device. For example the model of a synchronized current phasor measurement that is taken from phase k of a device is expressed as:

$$i_k^m = \sum_i Y_{eq,i}^k \cdot x_i + \sum_{i,j} F_{eqi,j}^{\ k} \cdot x_i \cdot x_j - b_{eq}^k + \eta_k \qquad (3.13)$$

where:

Y_{eq}^k are the elements of the kth row of the Yeq matrix of the corresponding device ACF.

F_{eq}^k are the elements of the kth Feq matrix that corresponds to the kth equation of the device ACF.

b_{eq}^k is the kth element of the beq vector of the corresponding device ACF.

4. Virtual (noiseless) Through Measurement:

This type of measurement is not a real measurement and it is also derived from the ACF of the device. Virtual through measurements are related to the internal equations of the ACF of the device. Note that as explained in section 3.3.2, due to the quadratization procedure, additional internal states and equations may be created for a specific model. Inclusion of these measurements in the state estimation procedure, achieves observability of the internal states of the devices and increases the measurement redundancy.

The models of the virtual through measurements of a device are created upon reading of the first actual through measurement that is related to this device. The measurement value of the virtual through measurement is 0 (noiseless), because it is created from the internal equations of the device ACF. For example the model of a virtual measurement is:

$$0 = \sum_{i} Y_{eq,i}^{k} \cdot x_i + \sum_{i,j} F_{eq\,i,j}^{\;k} \cdot x_i \cdot x_j - b_{eq}^{k} + \eta_k \tag{3.14}$$

where k is the corresponding row of the virtual measurement to the ACF model of the device.

5. Pseudo Through Measurement:

This type of measurement is not a real measurement. Typical measurements that belong in this category are derived from the network topology such as Kirchhoff's current law, neutral/shield wire current etc. [27], [29]-[32]. For example, if only the current phasor measurement of phase A is available, the current phasor measurements for phases B and C can be added as pseudo across measurements in the estimation algorithm with the same magnitude and a phase difference of +/- 120 accordingly.

6. Derived Through Measurement:

A derived measurement is a through measurement (measurement related to a device) that is included in the measurement set and increases the observability and the measurement redundancy of the system. For example, assume a phasor current measurement that is taken at Node1 of a single phase capacitor as is shown in Figure 3.4. Then a derived current measurement for Node2 with the opposite value compared to the original measurement can be created and used in the estimation, that is:

$$i_2(t) = -i_1(t) \tag{3.15}$$

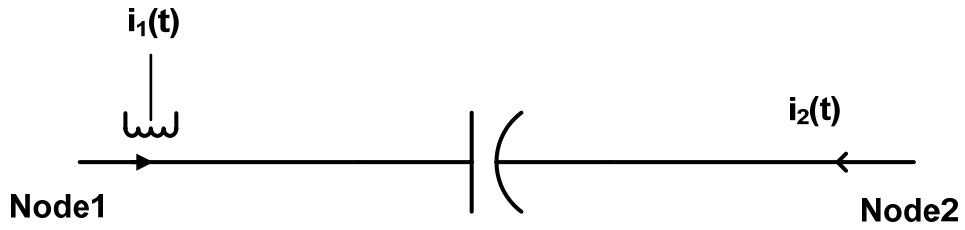

Figure 3.4. Derived measurement on a device.

Another example of a derived measurement is given next. Assume a node where three branches are connected and GPS synchronized current measurements are available for two of the devices, as shown in Figure 3.5. Then a derived measurement can be created for the current in the third device with the value of the measurement being the negative of the sum of the two original measurements that is :

$$i_3(t) = -i_1(t) - i_2(t) \tag{3.16}$$

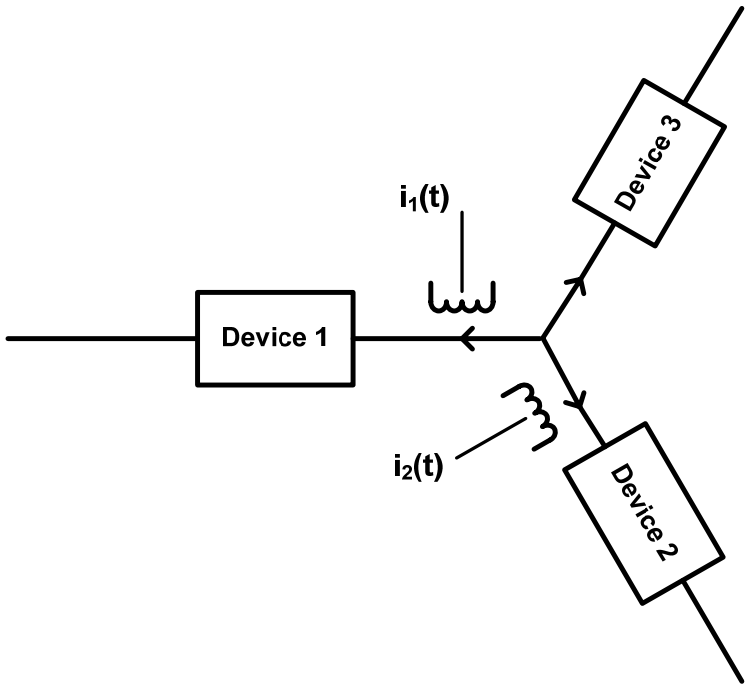

Figure 3.5. Derived measurement on a node.

7. KCL Virtual Measurement:

Another type of measurement that can be added in the estimation procedure is the KCL virtual measurement. Assume for example the case with the three branches as in Figure 3.5 but with one GPS-synchronized and one non-synchronized measurement. Then a derived measurement cannot be introduced since the value of the current at the third device cannot be computed, however a KCL virtual measurement can be added, with the measurement formula being:

$$0 = i_1(t) + i_2(t) + i_3(t) \tag{3.17}$$

Note that the value of the measurement is 0 and there is no error in this measurement since it is derived by a physical law, so a very small standard deviation is given for this measurement.

The block diagram of the algorithm for the inclusion of the derived measurements and the KCL virtual measurements is shown in Figure 3.6. Initially the derived measurements that result from devices that have the same current at a terminal pair are included. Once this is defined for each device (only during initialization), and there is a through measurement in such a node, then a derived measurement is added for the other corresponding node. Then the derived measurements for a node where a measurement is missing from a link are introduced. In particular, for each node, the number of links and the corresponding devices that are connected are defined. If all these devices are modeled and if there is at least one missing measurement then, the number of missing measurements has to be found. If there are more than one missing measurements then a flag is set for this node for introducing a KCL virtual measurement. For the case that only one measurement is missing, if at least one of the available measurements is non-GPS synchronized then the flag for introducing a KCL virtual measurement is also set. Otherwise, if only one measurement is missing and all the available measurements are GPS synchronized then a derived measurement can be added and there is no need for a KCL virtual measurement to be added for this node. Note that the whole procedure is repeated until there is no added derived measurement after scanning all the devices and all the nodes. Finally, after including all the derived measurements, the KCL virtual measurements are included for the nodes for which the corresponding flag is set.

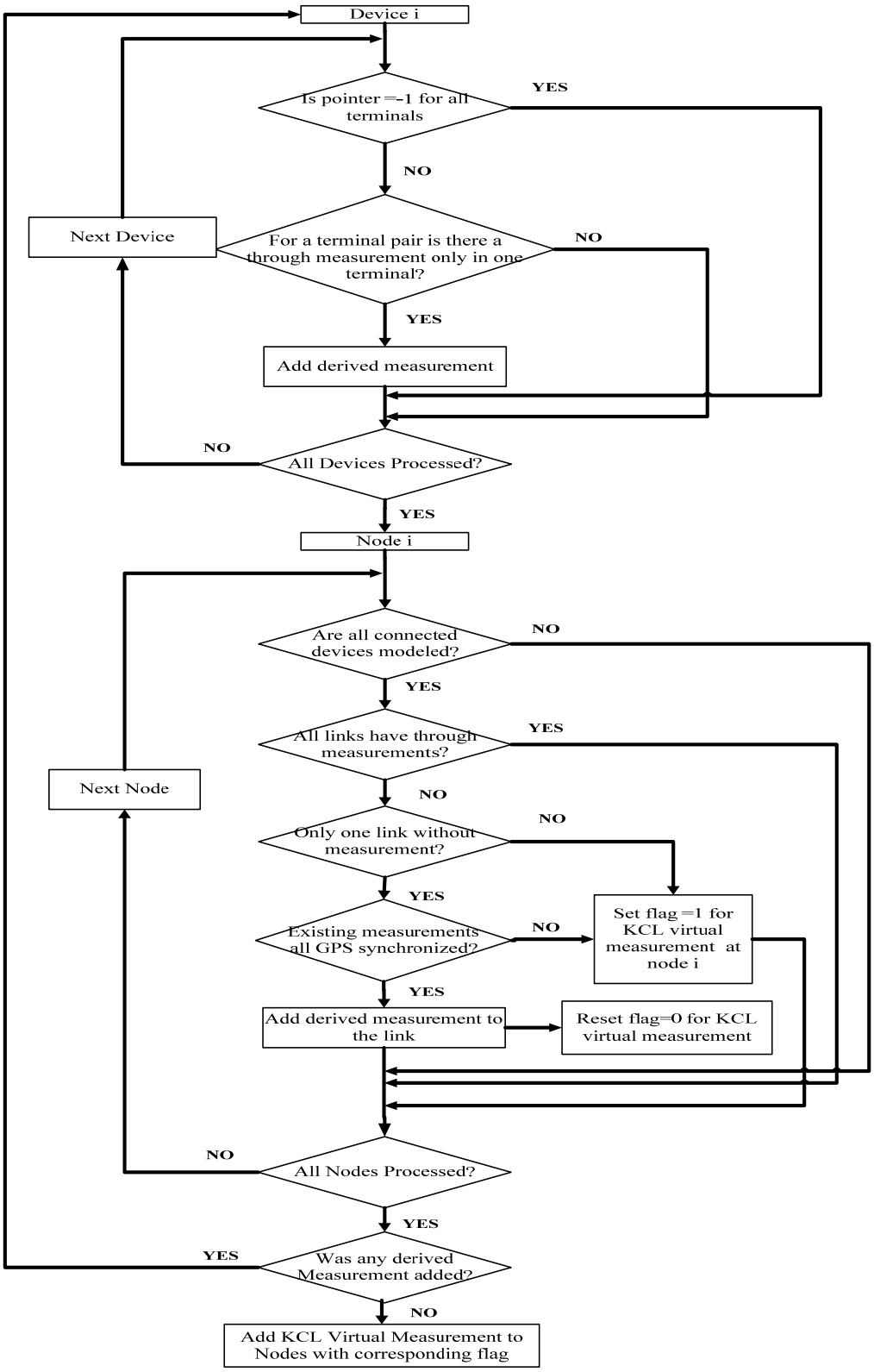

Figure 3.6. Block diagram for derived measurements and KCL virtual measurements.

Another key issue in the proposed formulation of the state estimator is the processing of non-synchronized phasor measurements. If a metering device does not have a GPS clock, the phasor measurements are not synchronized to the global time reference that the GPS clock offers. Data from metering devices that are not GPS synchronized are referenced to the phase A voltage. The "actual" phase angle of the phase A voltage is introduced as an “unknown state” that is estimated by the state estimation as follows:

$$\widetilde{A}_{non-synch} = \widetilde{A}_{synch} \cdot e^{ja} \tag{3.18}$$

where: $e^{ja} = \cos(\alpha) + j\sin(\alpha) = x_{NS,R} + j \cdot x_{NS,I}$ (3.19)

The introduced "unknown state" is a complex variable with the restriction that its magnitude is 1 and its phase angle is α. As a result the following virtual measurement can also be added.

$$0 = x_{NS,R}{}^2 + x_{NS,I}{}^2 - 1 \tag{3.20}$$

Note that there is one α variable for each non-synchronized metering device.

3.6 DSE Solution Algorithm

The problem is defined, at each time step, as a static estimation problem. The objective is to estimate the state vector x which in general includes both dynamic and algebraic states. The least squares approach is used and the problem is formulated as follows:

$$Minimize \qquad J(x,y) = \eta^T W \eta\,, \tag{3.21}$$

where

$$\eta = z - h(x)\,, \tag{3.22}$$

and W is a diagonal matrix, the non-zero entries of which are equal to the inverse of the variance of the measurement errors:

$$W = diag\left[\frac{1}{\sigma_v^2}\right]. \tag{3.23}$$

The best estimate of the system state is obtained from the Gauss-Newton iterative algorithm:

$$\hat{x}^{\nu+1} = \hat{x}^{\nu} - (H^T W H)^{-1} H^T W (h(\hat{x}^{\nu}) - z) \ , \tag{3.24}$$

where $\hat{x}$ refers to the best estimate of the state vector x, and H is the Jacobian matrix of the measurement equations.

The derivation of the information matrix $H^T W H$ and the vector $H^T W (h(\hat{x}^{\nu}) - z)$ from the measurement data is performed using sparcity techniques and a suitable sparse matrix library. In particular, at each time step of the estimation algorithm, the contributions of each measurement to the information matrix $H^T W H$ and the vector $H^T W (h(\hat{x}^{\nu}) - z)$ are computed based on the object-oriented measurement model described in section 3.5. For example assuming that the i[th] measurement has the following generic form:

$$z_i = c_i + a_{i1} \cdot x_{i1} + a_{i2} \cdot x_{i2} \cdot x_{i3} + \eta_i \tag{3.25}$$

Then the Jacobian matrix's i[th] row will be:

$$\begin{bmatrix} 0 & \cdots & a_{i1} & \cdots & a_{i2} \cdot x_{i2} & \cdots & a_{i2} \cdot x_{i3} & \cdots & 0 \end{bmatrix} \tag{3.26}$$

The contribution of this row to the information matrix is the following:

$$\begin{bmatrix} 0 & \cdots & 0 & \cdots & 0 & \cdots & 0 & \cdots & 0 \\ \vdots & & \vdots & & \vdots & & \vdots & & \vdots \\ 0 & \cdots & w_i a_{i1} a_{i1} & \cdots & w_i a_{i1} a_{i2} x_{i2} & \cdots & w_i a_{i1} a_{i2} \cdot x_{i3} & \cdots & 0 \\ \vdots & & \vdots & & \vdots & & \vdots & & \vdots \\ 0 & \cdots & w_i a_{i1} a_{i2} \cdot x_{i2} & \cdots & w_i \left(a_{i2} \cdot x_{i2}\right)^2 & \cdots & w_i a_{i2}^2 \cdot x_{i2} x_{i3} & \cdots & 0 \\ \vdots & & \vdots & & \vdots & & \vdots & & \vdots \\ 0 & \cdots & w_i a_{i1} a_{i2} \cdot x_{i3} & \cdots & w_i a_{i2}^2 \cdot x_{i2} x_{i3} & \cdots & w_i \left(a_{i2} \cdot x_{i3}\right)^2 & \cdots & 0 \\ \vdots & & \vdots & & \vdots & & \vdots & & \vdots \\ 0 & \cdots & 0 & \cdots & 0 & \cdots & 0 & \cdots & 0 \end{bmatrix} \tag{3.27}$$

The contribution of the measurement to the vector $H^T W (h(\hat{x}^{\nu}) - z)$ is the following:

$$\begin{bmatrix} 0 \\ \vdots \\ w_i a_{i1} b_i \\ \vdots \\ w_i a_{i2} \cdot x_{i2} b_i \\ \vdots \\ w_i a_{i2} \cdot x_{i3} b_i \\ \vdots \\ 0 \end{bmatrix}, \quad where \quad b_i = c_i + a_{i1} \cdot x_{i1} + a_{i2} \cdot x_{i2} \cdot x_{i3} - z_i \tag{3.28}$$

Based on the above formulas, the non-zero contributions of each measurement formula are computed and the contributions are inserted to the information matrix $H^T WH$ and the vector $H^T W(h(\hat{x}^\nu) - z)$. Once the reading of all the measurements is completed and their contribution is added to the corresponding matrix and vector, the formation of the information matrix $H^T WH$ and the vector $H^T W(h(\hat{x}^\nu) - z)$ is completed and stored in sparse form using a suitable sparse library.

3.7 State Estimation Performance Metrics

The accuracy of the state estimate and the estimation confidence levels are obtained via a standard, chi-square-based analysis. The normalized residual (or error) for each measurement i is defined as

$$s_i = \frac{\eta_i}{\sigma_i} \tag{3.29}$$

and thus the vector of normalized residuals is

$$s = \sqrt{W} \cdot \eta \tag{3.30}$$

It is assumed that the normalized errors are Gaussian-distributed with standard deviation 1.0 and zero cross-correlation. The variable

$$\chi^2 = s^T s \tag{3.31}$$

is a random variable and it is chi-square distributed with $v = m - n$ degrees of freedom, where m is the total number of measurements, including virtual measurements and pseudo measurements, and n is the number of state variables that are estimated. Defining

$$\zeta = \hat{s}^T \hat{s} \,, \tag{3.32}$$

where the "hat" symbol indicates quantities computed at the estimate $\hat{x}$, the estimation confidence level at each step is given by the probability:

$$\Pr\left[\chi^2 \geq \zeta\right] = 1.0 - \Pr\left[\chi^2 \leq \zeta\right] = 1.0 - \Pr(\zeta, v) \ . \tag{3.33}$$

The chi-square test is utilized to provide the probability that the expected error of the estimated state values will be within a specific range. Because there are many data acquisition devices in any substation with different accuracy, a normalization constant k has been introduced. The variable k is defined as follows: if it is 1.0 then the standard deviation of each measurement is equal to the accuracy of the meter with which this measurement was obtained. If different than 1.0 then the standard deviation of the measurement error equal the accuracy of the meter times k. The introduction of the variable k allows us to characterize the accuracy of the estimated state with only one variable. This is equivalent of providing the expected error (which equals the variable k times the standard deviation of the measurement error) versus probability (confidence level). Figure 3.7 illustrates the K-factor curve, that is the parameter k versus confidence level.

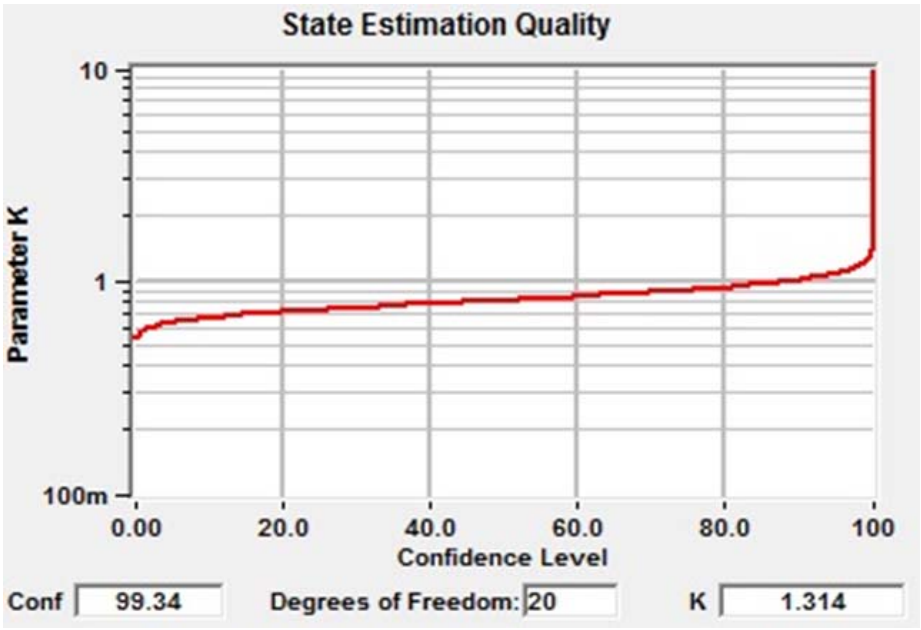

Figure 3.7. State estimation quality - Chi Square test.

For an acceptable confidence level, the accuracy of the solution, at each time step, is computed via the covariance (or information) matrix. The covariance matrix of the state is defined as

$$C_x = E\left[(\hat{x} - \bar{x})(\hat{x} - \bar{x})^T\right], \tag{3.34}$$

where $\bar{x}$ denotes the true state value, and computed as

$$C_x = \left(H^T W H\right)^{-1}. \tag{3.35}$$

Once the information matrix of the solution has been computed, the standard deviation of a component of the solution vector is given by

$$\sigma_{x_i} = \sqrt{C_x(i,i)}, \tag{3.36}$$

where $C_x(i,i)$ is the ith diagonal entry of the C_x. The expected value of is

$$E[\hat{x}] = \bar{x} \ . \tag{3.37}$$

The estimates of the measurements are defined as

$$\hat{b} = h(\hat{x}, \hat{y}). \tag{3.38}$$

Their expected value is

$$E[\hat{b}] = h(\bar{x}, \bar{y}) , \tag{3.39}$$

and their covariance matrix

$$Cov(\hat{b}) = H\left(H^T W H\right)^{-1} H^T \ . \tag{3.40}$$

3.8 Bad Data Detection Identification and Removal

Detection of the existence of bad data can be achieved with the chi-square test, i.e. by computing the confidence level. If the system measurement equations are free of bad data, the confidence level will be high. In the presence of one or more bad data, the confidence level will decrease. Figure 3.8 gives an example of the chi-square test which shows a very low confidence level due to the effect of some bad data. Note that the chi-square test does not indicate which datum or data is bad. The identification of the bad data is described next.

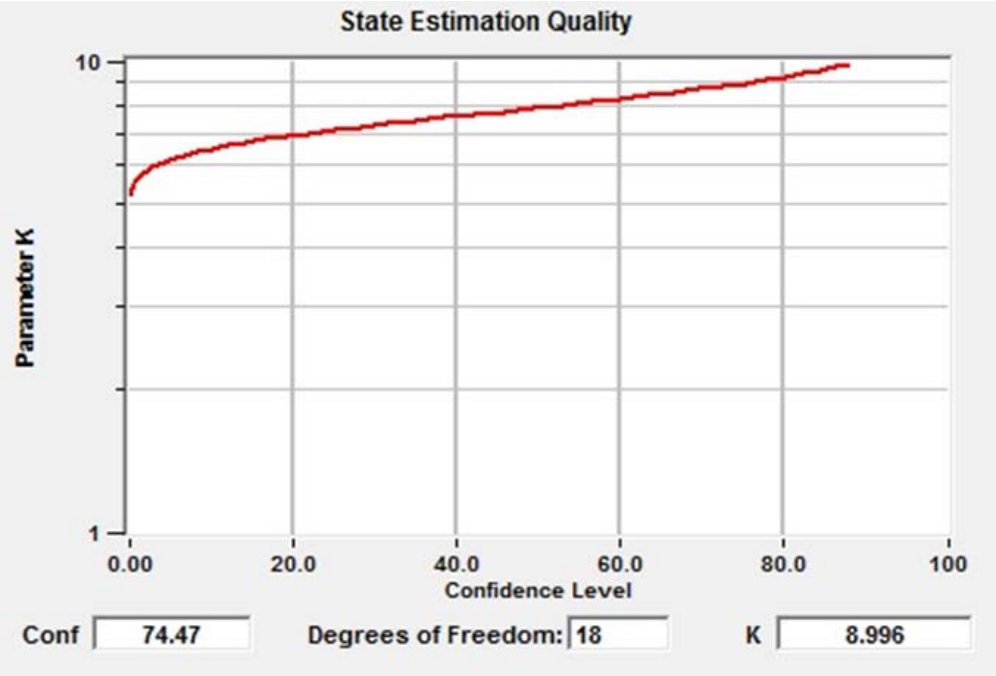

Figure 3.8. Low confidence level due to the effect of bad data.

Bad data can be classified into the following types:

1) Measurement Bad Data, which means that the measurement may contain a significant error comparing with its actual value.

2) Status/Topology Bad Data, which means that the bad data is related with the breaker or switch's open/close status or in other words, the topology of the system.

The methodology of the identification of bad data normally consists of two steps. In the first step, bad data may be identified by inspection or simple consistency rules. This step identifies the obviously bad data and it is very much system dependent. As an example, in power system state estimation, measurements of voltages, power flow, etc., are known to have specific ranges. If a measurement is out of this range, it will be classified as a bad measurement or at least as a measurement suspected of being bad (suspect measurement). In the second step, bad data are identified with statistical analysis of the residuals and/or its effects on confidence level. This analysis depends on the selected method for the solution of the estimation problem. In the case of least square solution, the possible bad data are identified with their large residuals. However, it is known that it is possible that: (a) a measurement with a large residual may not be always a bad measurement and (b) a bad measurement may have a very small residual (outliers). A rather secure, but computationally demanding, way to identify a bad datum is by means of hypothesis testing. Specifically, assume that a measurement (or a group of measurements) has been identified as suspect (this characterization may be due to a large normalized residual or because of failure to pass a consistency check, etc.). For this purpose, the suspect datum is removed, i.e. the corresponding equation $b_i = h_i(\mathbf{x})$ is removed from measurement equations set and the least square solution is computed again. Subsequently, the confidence level is computed. A drastic improvement in the confidence level indicates that the data under consideration is bad [110].

3.9 Object-Oriented Dynamic State Estimation Algorithm

The block diagram describing the steps for the execution of the DSE is shown in Figure 3.9. In the initialization procedure, all the devices that are in the substation along

with the lines that connect the substation to the neighboring substations are identified and are added in the device database. Based on the connectivity of these devices, the network configurator is executed and defines the states in the substation.

At each time step, once the data packet with a specific time stamp is read, the status measurements are initially processed. The status measurements define the connectivity of the devices in the substation. If there is a change in the configuration then the network configurator is executed in order to update the connectivity of the devices and the states of the system.

The analog measurements are processed next. Based on the set of the available measurements and the connectivity of the devices, a set of derived measurements is defined. The detailed algorithm for the creation of derived measurements is given in section 3.5. Then the mathematical model for all the measurements (actual, derived, virtual, pseudo) that are used for the execution of the state estimation algorithm, for the specific time step is created. Finally, the state estimation algorithm is executed, along with a bad data detection, identification procedure and metrics computations.

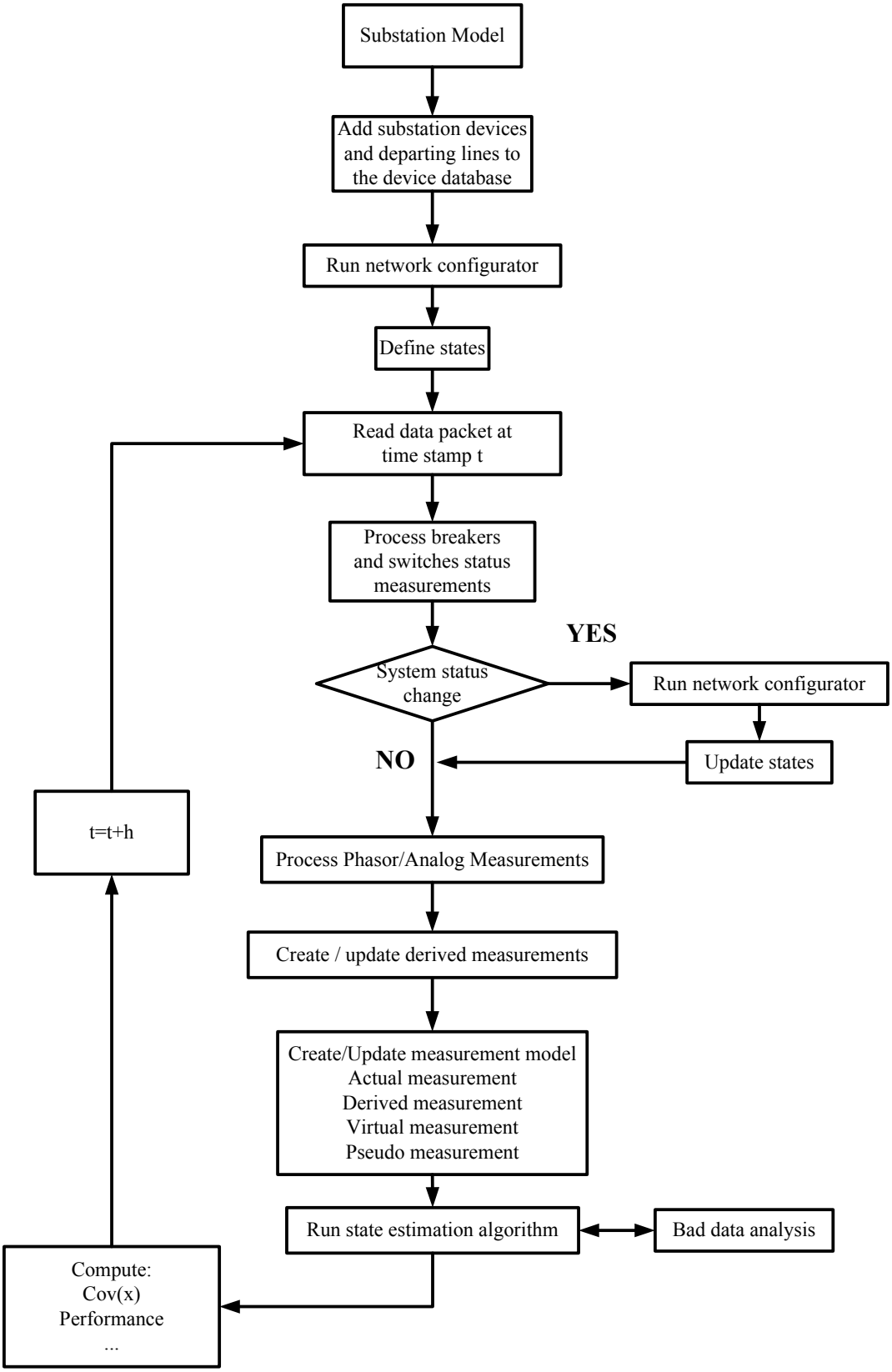

Figure 3.9. Flow chart of the implementation of dynamic state estimation.

3.10 DSE Distributed Architecture

The dynamic state estimator is implemented in a distributed architecture, at the substation level. This is a novel approach compared to presently available state estimation applications that are based on a centralized architecture and are executed in the control center. The distributed application of the state estimation is enabled by the availability of synchronized measurements that are referenced to the GPS clock signal. As a result, these measurements are globally valid and enable a distributed approach for the implementation of state estimation.

Local (substation) measurements are used to estimate the states of the substation but also the states of the buses at the other ends of the lines/circuits that connect the substation of interest with the neighboring substations. The substation based dynamic state estimation uses data from relays, PMUs, meters, FDRs etc in the substation only, thus avoiding all issues associated with transmission of data and associated time latencies. It runs at rates comparable to the suggested rates in the synchrophasors standard C37.118. Presently it has been implemented to execute with rate at 60 times per second thus providing the dynamic state of the substation more than 60 times per second. The data flow is illustrated in Figure 3.10.

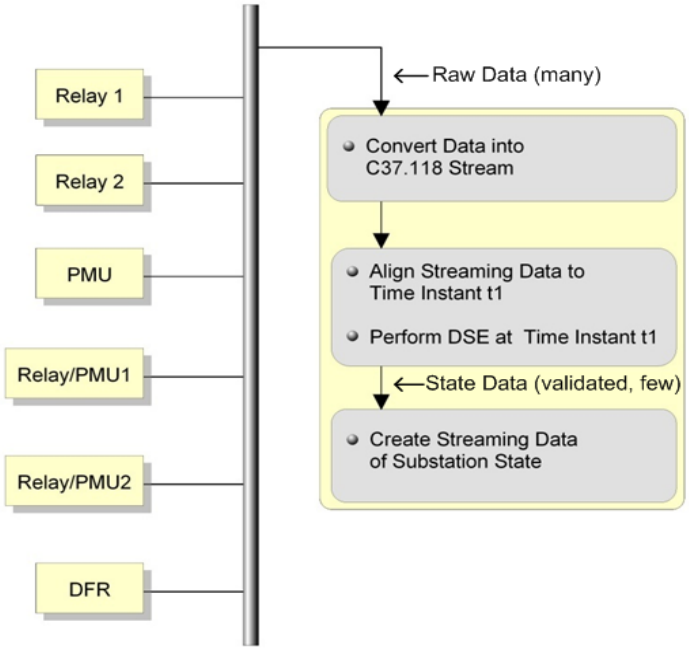

Figure 3.10. Data flow in dynamic state estimation [100].

The advantages of the distributed architecture are numerous. First of all, the state estimation algorithm is implemented using only local measurements to estimate only the states of the substation and of the neighboring buses. As a result the dimensionality of the problem is significantly decreased compared to the dimensionality of a centralized state estimator, as indicated in Table 3.1. This allows for very fast execution times (at least 60 executions per second) and utilization of very detailed power system models (three-phase static or dynamic models, instrumentation inclusive). In addition, the estimation results are very accurate, not only due to the improved modeling, but also due to the measurement redundancy inside a substation. Note that in typical state estimator only few measurements are used per substation. On the contrary, in our approach, it is proposed that all the measurements within the substation should be used. Upon execution of the distributed state estimation on all substations, the results can be collected at a central location (control center) to synthesize the system-wide operating state of the system.

Table 3.1. State estimation dimensionality for a typical substation and a typical ISO/utility.

	Typical Substation	**ISO/Utility**
States	60	40,000
Measurements	1,200	250,000
State Estimation Execution Time	At least 1 execution per cycle	1-3 mins

Distributed state estimation also enables the implementation of wide area monitoring and protection schemes (WAMPS). The first wide area monitoring system is described in [13]. Several WAMPS have been suggested in the literature [39]-[40], [44]-[46], [52], [108] and their architecture suggests the deployment of PMUs in substations from where the synchronized measurements will be sent to a central location and used for several applications (state estimation, voltage stability analysis etc). A typical architecture is illustrated in Figure 3.11. The major disadvantages of this approach are the following. First of all, raw PMU measurements are directly sent and used to the central location

without any validation procedure. In addition this approach does not take advantage of substation automation technology.

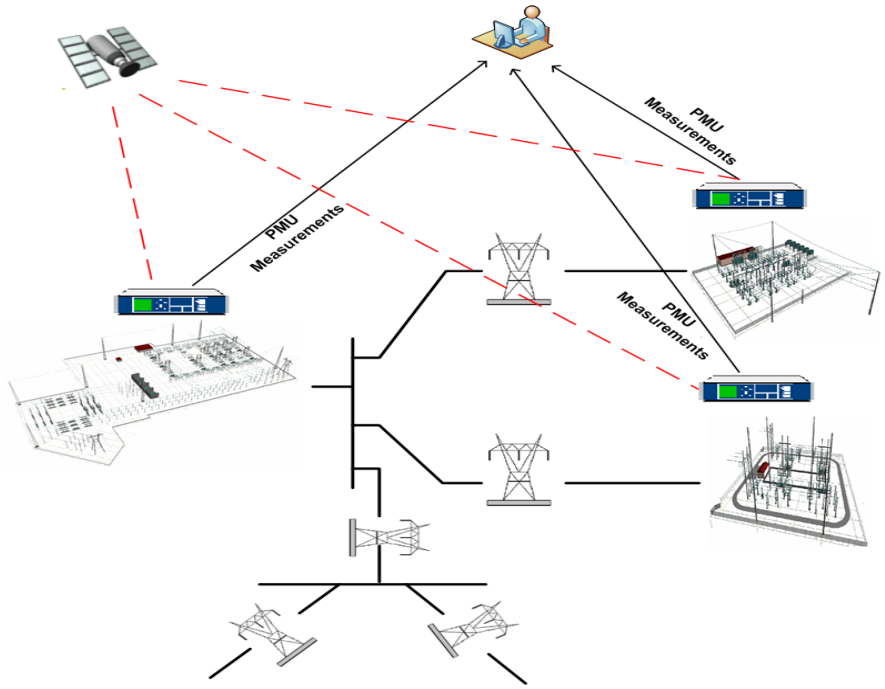

Figure 3.11. Typical wide area monitoring and protection scheme.

In the proposed approach, state estimation is performed at the substation level using all available measurements and a highly accurate dynamic model of the system. Upon execution of the state estimation, only the states are sent to the central location. The major advantages are that the results are validated (since they have been filtered through the estimation algorithm) and the information that has to be sent to the central location is minimal (number of states is significantly less compared to the number of measurements in a substation). As a result there is less communications burden and reduced time latencies for the implementation of the WAMPS. The proposed architecture for WAMPS is illustrated in Figure 3.12.

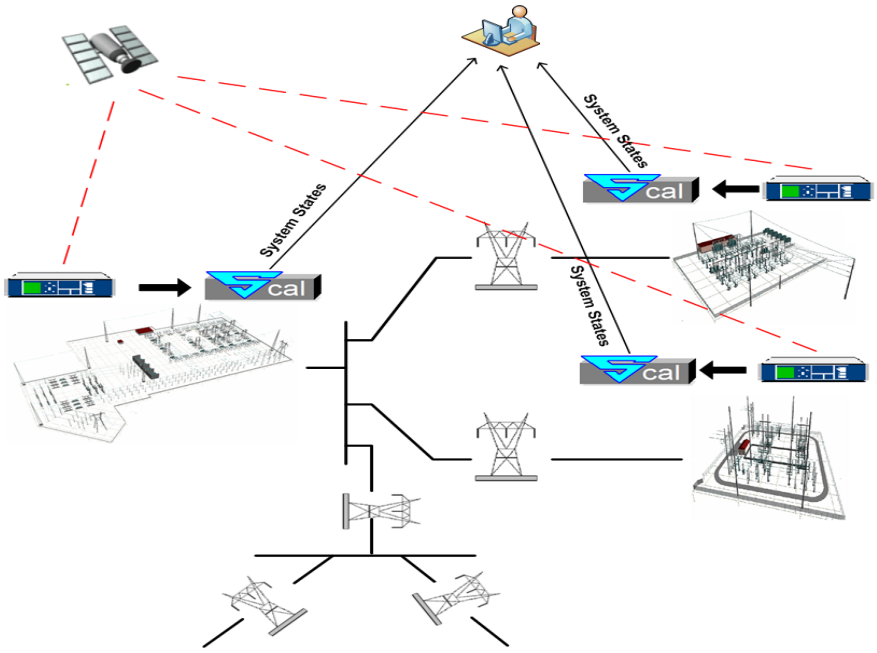

Figure 3.12. Proposed wide area monitoring and protection scheme.

The PMU-based distributed state estimation can be also used as a fundamental component of a system level, consistent, state estimator. For a given control area that the system level state estimator is used for, if all the substations in this area are equipped with PMUs and a distributed state estimator is performed in each substation, then at the central location (control center) there is no need for the execution of another state estimator. In particular, under this assumption, the computed state from each local estimator is sent to the control center where the total system state is synthesized. In addition, given the model of the system and the system state (voltage phasors) synthesized at the central location, additional quantities can be computed such as current flows, real and reactive power flows etc. Note that there is no need for another state estimation, because the computed states from each substation are referenced to the GPS clock, so all the phasors are computed based the same reference angle. In addition, the confidence level of the computed states in each substation is calculated and can be sent to the central location. The bad data detection, identification and rejection that is performed by each local estimator guarantees that the confidence level is acceptable otherwise an alarm can be issued. Finally, another cross check that can be performed is the comparison of states that are computed by several local estimators. To illustrate this better, assume

the system configuration of Figure 3.13. The voltage phasor at the terminal bus of substation 1 ($\tilde{V}_1$) is computed three times, from the local state estimator, and from the estimators in substations 2 and 3, since the substation state is extended to include the state at the terminal of the neighboring substation. As a result, at the central location a cross performance check can be performed, whether a computed value from multiple local estimators is in the expected range, otherwise an alarm can be issued.

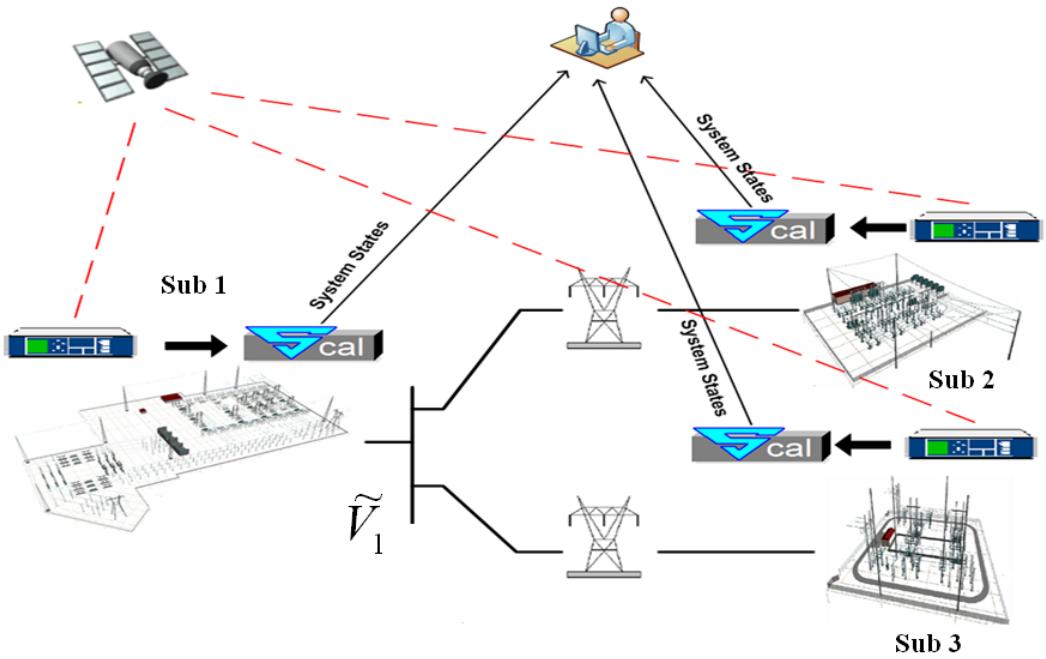

Figure 3.13. Cross performance check.

In the case that not all the substations in the specified control area are equipped with PMUs, then the results from the local state estimators can be used as a part of a PMU assisted centralized state estimator. In particular, a traditional state estimator can be performed in the central location, where the states computed by the PMU-based local estimators can be used as measurements with very small or even with zero error, meaning that these quantities are known. Note that in this case, since in the traditional state estimator the phase angle of a specific bus in the system is used as the reference angle, then all the phase angles computed by the PMU-based local estimators have to be referenced to the system reference angle. Another issue in this case is the different execution speed of the local and the centralized state estimator. While the local estimator

is performed at rates of 60 executions per second, a centralized state estimator is expected to be slower, with rates comparable to the execution speeds of traditional state of the art estimators that are used nowadays. In this case, it is suggested that the time tags of the states computed by the local estimators are utilized, and the most recent states are used.

3.11 Summary

The mathematical formulation and the solution algorithm of the developed PMU-based distributed dynamic state estimator are presented in this chapter. Emphasis is given on the object-oriented modeling approach of the DSE which combined with its distributed architecture (substation based state estimation), enabled by synchrophasor technology, results in DSE execution rates of 60 times per second and eliminates the biases of traditional state estimators.

4 A PREDICTIVE DSE-ENABLED TRANSIENT STABILITY MONITORING SCHEME WITH APPLICATION TO GENERATOR OUT-OF-STEP PROTECTION

4.1 Overview

The real-time dynamic model of the system as computed through the dynamic state estimator can be utilized for the implementation of novel, advanced power system control and protection applications that will improve the operation of the power system. Such an application is introduced in this section. In particular, a predictive transient stability monitoring scheme is presented. It is based on the combination of the dynamic state estimation, as presented in chapter 3, with the application of Lyapunov's direct method to the power system transient stability problem. The proposed scheme enables real-time monitoring of the transients swings of the generator and evaluates its energy based on the information given by the DSE, and as a result characterizes the stability of the system. An application of the transient stability monitoring scheme is also presented which is a novel, predictive, generator out-of-step protection scheme, which is capable of detecting potential generator loss of synchronism after a system disturbance.

4.2 Lyapunov Direct Method Applied to Transient Stability Analysis

Traditional transient stability analysis methods are based on step-by-step integration of the differential equations of the system during and after a disturbance occurrence. Despite the fact that these methods are highly accurate, they cannot be used in on-line and real-time applications since huge computational effort is required. Direct methods belong to a different class of transient stability analysis methods and provide an alternative to conventional approaches that are based on extensive numerical simulations. A direct method for transient stability analysis is defined as a method that is able to determine stability without explicitly integrating the differential equations that describe

the post-fault system. As a result they are advantageous in the sense that they require significantly reduced computational effort.

Lyapunov's direct method is one of the methods that can be used for power systems transient stability analysis. In this section, it is illustrated how Lyapunov's direct method can be utilized in power systems transient stability analysis.

Let $\dot{x} = f_{pre-fault}(x)$, $\dot{x} = f_{fault}(x)$, and $\dot{x} = f_{post-fault}(x)$ be the state space equations describing the response of a generator after a disturbance for the following conditions a) pre-fault b) during fault and c) after fault correspondingly, where the state vector is composed of the generator rotor angle δ and rotor velocity ω, that is $x = [\delta \quad \omega]$. Let also $V(x)$ be a Lyapunov function which guarantees stability of the system around the post fault stable equilibrium point and $V_{\max}$ be the value of this Lyapunov function on the boundary of the stability region. The closed V-contour for which $V(\delta(t), \omega(t)) = V_{\max}$ is called the separatrix and defines the stability region of the system.

Evaluation of $V(x)$ along the system trajectory can be used to determine the critical clearing time and the stability margin of the system. This is illustrated in Figure 4.1. For a stable scenario the trajectory of the system stays within the separatrix and the value of $V(x)$ is always less than $V_{\max}$. On the contrary, for an unstable scenario, the trajectory crosses the separatrix and the value of $V(x)$ exceeds $V_{\max}$. The time instant at which the trajectory crosses the separatrix is the critical clearing time.

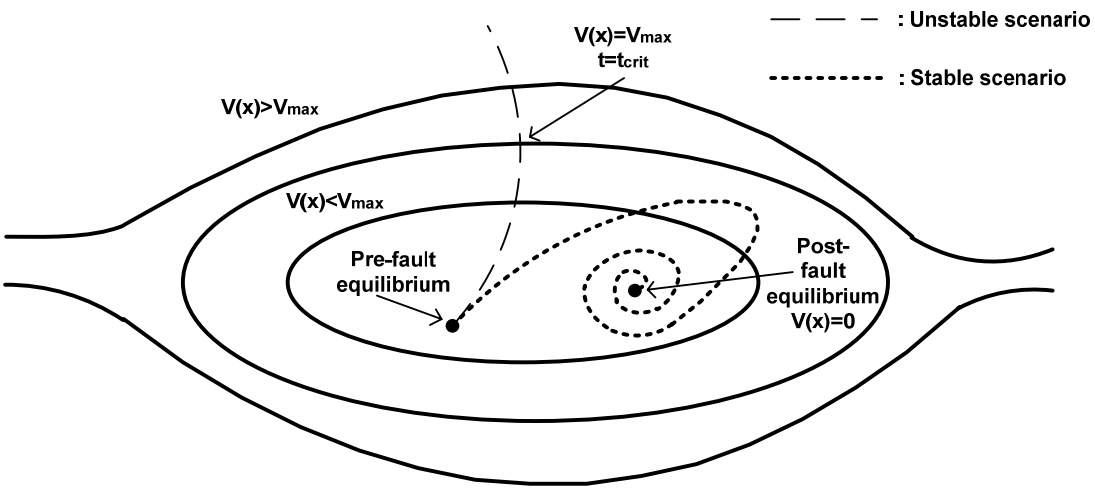

Figure 4.1. System trajectory potential energy function contours.

The selection of the Lyapunov function is not trivial. Several Lyapunov functions have been proposed in the literature for transient stability analysis methods [56]-[74]. In this work, the Lyapunov function that is used is the total energy of the generator, defined as the sum of the potential and the kinetic energy of the generator [109]. A proof that the total energy of the generator is a suitable Lyapunov function, that is, $V(\delta_s,0)=0$, V is positive definite, and $\dot{V}=0$, can be found in [60].

The potential energy is defined as follows: Assume that the equilibrium position of a generator is at $\delta=\delta_s$. It is assumed that the generator position deviates from the equilibrium to an arbitrary position δ and the transition takes place very slow so that the speed of the generator is practically constant equal to the synchronous frequency. At the new position there will be an accelerating power, P_{acc}, acting on the generator. In general this accelerating power is a function of the position of the rotor. The potential energy equals the work done to move the generator from position δ_s to position δ.

$$E_{potential}=\int_{\delta_s}^{\delta}(P_{acc})\cdot d\delta \tag{4.1}$$

The kinetic energy is defined as the energy stored at the rotor and can be calculated in terms of the rotor speed $\omega(t)$ as:

$$E_{kinetic} = \frac{1}{2} \cdot M \cdot \omega^2(t) \tag{4.2}$$

where M is the mass of the generator.

Determination of the critical clearing time using Lyapunov's direct method can be achieved as follows. Consider a single generating unit system that experienced a disturbance. At the end of the disturbance, the generator is at a state described with a certain position $\delta_0 = \delta_{tc}$ and certain speed $\omega_0 = \omega_{tc}$. Further assume that the post fault equilibrium point is at position δ_s. This is expressed with the following model:

$$\frac{d\delta(t)}{dt} = \omega(t) \tag{4.3}$$

$$M \frac{d\omega(t)}{dt} = P_m - P_{e\_pos}(\delta(t)) \tag{4.4}$$

The initial conditions at time $t = t_c$ are: $\delta_{tc} = \delta_0$ and $\omega_{tc} = \omega_0$. The post fault equilibrium point is δ_s given by the solution of the equation $0 = P_m - P_{e\_post}(\delta(t))$.

The Lyapunov test function is defined as the sum of the kinetic and the potential energy of the generator as follows:

$$V(\delta(t), \omega(t)) = E_{kinetic} + E_{potential} \tag{4.5}$$

Where:

$$E_{kinetic} = \frac{1}{2} \cdot M \cdot \omega^2(t) \tag{4.6}$$

$$E_{potential} = \int_{\delta_s}^{\delta} (P_{e\_post}(\delta(t)) - P_m) \cdot d\delta \tag{4.7}$$

In Figure 4.2 a typical V-contour graph is illustrated. Note that the largest closed V-contour defines the stability region.

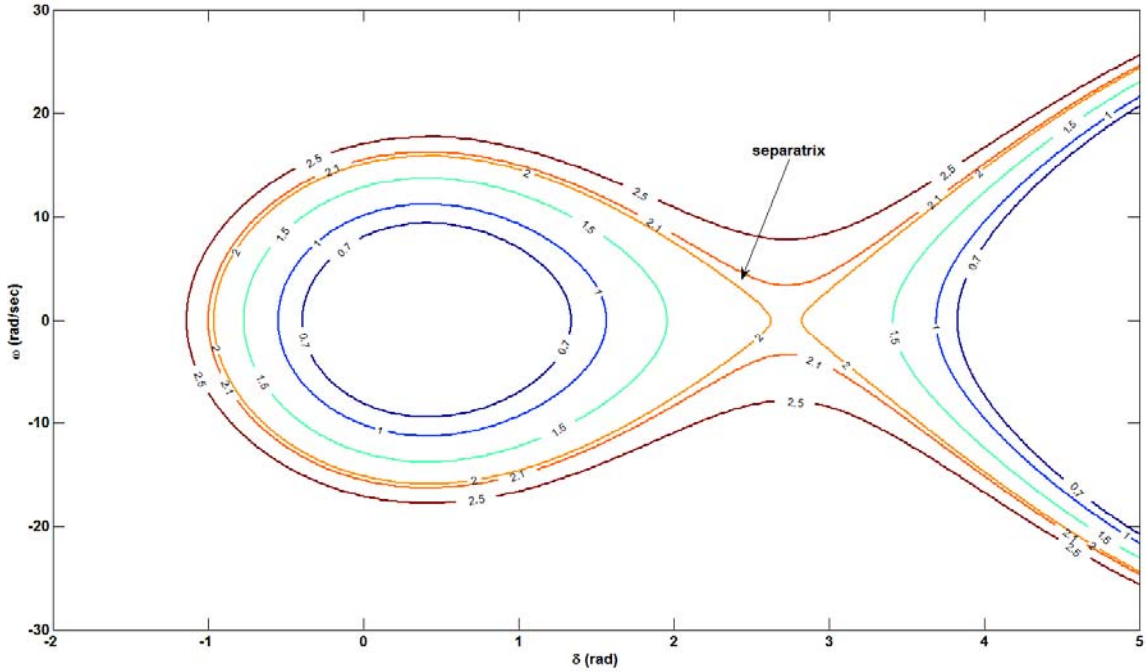

Figure 4.2. Typical V-contour graph.

A typical potential energy function is illustrated in Figure 4.3.

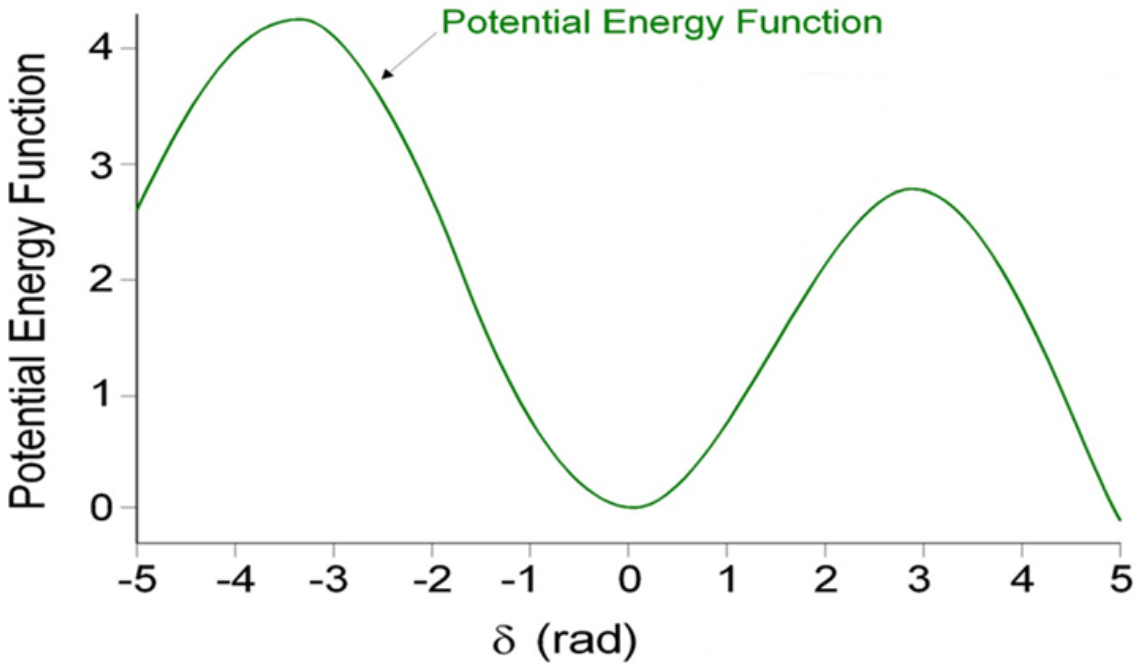

Figure 4.3. Typical potential energy function.

In order to compute the critical clearing time t_{cr}, the state equations during the fault $\dot{x} = f_{during}(x)$ have to be solved until $V(\omega(t_{tc}), \delta(t_{tc})) = V_{\max}$. At that time the system is at the boundary of the stability region and t_c is the critical clearing time, that is $t_c = t_{cr}$.

An alternative of the above approach is the following. $V_{\max}$, which is the maximum energy that a system can have before synchronism is lost (or the value of the energy at the separatrix) equals the smallest maximum value of V(0, δ) around a stable equilibrium point which is by definition:

$$V_{\max} = V(0, \delta_u) = \min(V(0, \delta_{u1}), V(0, \delta_{u2})) \tag{4.8}$$

where δ_{u1}, δ_{u2} are the two unstable equilibrium point surrounding the stable equilibrium point.

The equilibrium point δ_u is called the "closest" unstable equilibrium point. For a clearing time t_c if $V(\omega(t_c), \delta(t_c)) < V_{\max}$ the system is stable.

The critical clearing time can be found as follows: first $\delta(t_{cr})$ is evaluated by solving $V(\omega(t_{cr}), \delta(t_{cr})) = V_{\max}$ and then the faulted state equation is integrated until $\delta(t) = \delta(t_{cr})$.

Consider for example a one machine infinite bus system which experiences a disturbance that disconnects one of the parallel lines, as illustrated in Figure 4.4.

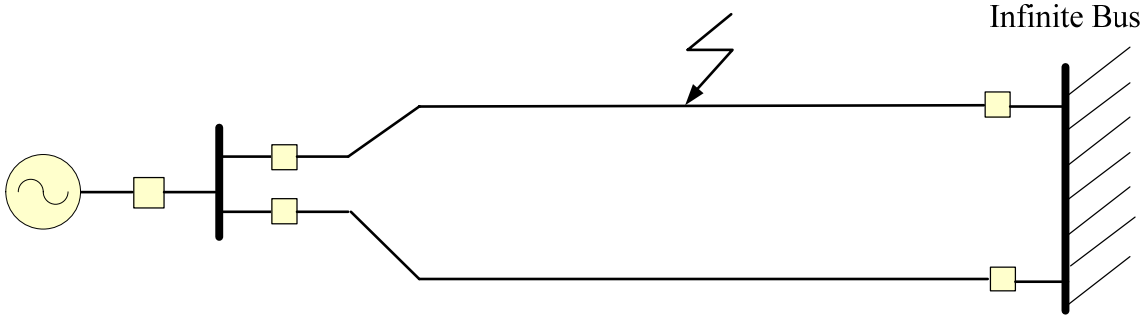

Figure 4.4. A single machine - infinite bus system.

For this system assume that the swing equation for the post fault system is given by the following simplified differential equation.

$$M\frac{d\delta^2(t)}{dt} = P_m - P_{\max}\sin\delta(t) \tag{4.9}$$

The post fault stable equilibrium point is $\delta_s = \sin^{-1}(\frac{P_m}{P_{\max}})$ while the post fault closest unstable equilibrium point is $\delta_u = \pi - \delta_s = \pi - \sin^{-1}(\frac{P_m}{P_{\max}})$.

The potential energy function is calculated to be:

$$E_{potential}(\delta) = \int_{\delta_s}^{\delta}(P_{\max}\sin\delta - P_m)\cdot d\delta = P_{\max}\cos\delta_s - P_{\max}\cos\delta - P_m\cdot\delta + P_m\cdot\delta_s \tag{4.10}$$

The total energy function of the generator is:

$$V(\delta(t),\omega(t)) = \frac{1}{2}M\omega^2(t) + P_{\max}\cos\delta_s - P_{\max}\cos\delta - P_m\cdot\delta + P_m\cdot\delta_s \tag{4.11}$$

The maximum energy that the system can have before losing synchronism is:

$$\begin{aligned} V_{\max} &= E_{potential}(\delta_u) = P_{\max}\cos\delta_s - P_{\max}\cos(\pi-\delta_s) - P_m\cdot(\pi-\delta_s) + P_m\cdot\delta_s \\ &= 2\cdot P_{\max}\cos\delta_s + 2\cdot P_m\cdot\delta_s - P_m\cdot\pi \end{aligned} \tag{4.12}$$

For a clearing time t_c with $x(t_c) = \begin{bmatrix}\delta(t_c) & \omega(t_c)\end{bmatrix}$ if $V(\omega(t_c),\delta(t_c)) < V_{\max}$ the system is stable otherwise it is unstable.

4.3 DSE-Enabled Predictive Transient Stability Monitoring Scheme

This section presents how the dynamic state estimation can be combined with the Lyapunov's direct method as summarized in section 4.2, resulting in the proposed transient stability monitoring scheme.

The real-time dynamic state of the substation, as obtained from the dynamic state estimation results, includes the real-time operating condition of the substation generator, i.e. generator torque angle, generator speed, generator acceleration etc. This information is adequate to monitor the dynamics of the generator and characterize and predict the stability of the system. Stability monitoring is performed on the basis of Lyapunov

energy functions and Lyapunov direct method. Specifically the total energy of a generator that experiences a fault is evaluated as the sum of its kinetic and potential energy.

$$V(\delta(t),\omega(t)) = \frac{1}{2}\cdot M\cdot \omega^2(t) + \int_{\delta_s}^{\delta} (P_{e\_post}(\delta(t)) - P_m)\cdot d\delta \tag{4.13}$$

The computation of the kinetic energy is trivial since the generator speed is evaluated continuously and in real time by the DSE. The major computational challenge is the evaluation of the potential energy of the generator, and it is performed in terms of the center of oscillations (CoO) of the system with the assumption that the fault is cleared at the present time. Detailed description of the methodology is given next.

4.3.1 CoO Definition and Computation

The CoO is identified as the place of the system where the rate of frequency is constant as illustrated in Figure 4.5. Note that multiple CoOs might exist in the system, since the center of oscillations is actually a plane in the system. The evaluation of the CoO is based on an optimization problem and is explained next.

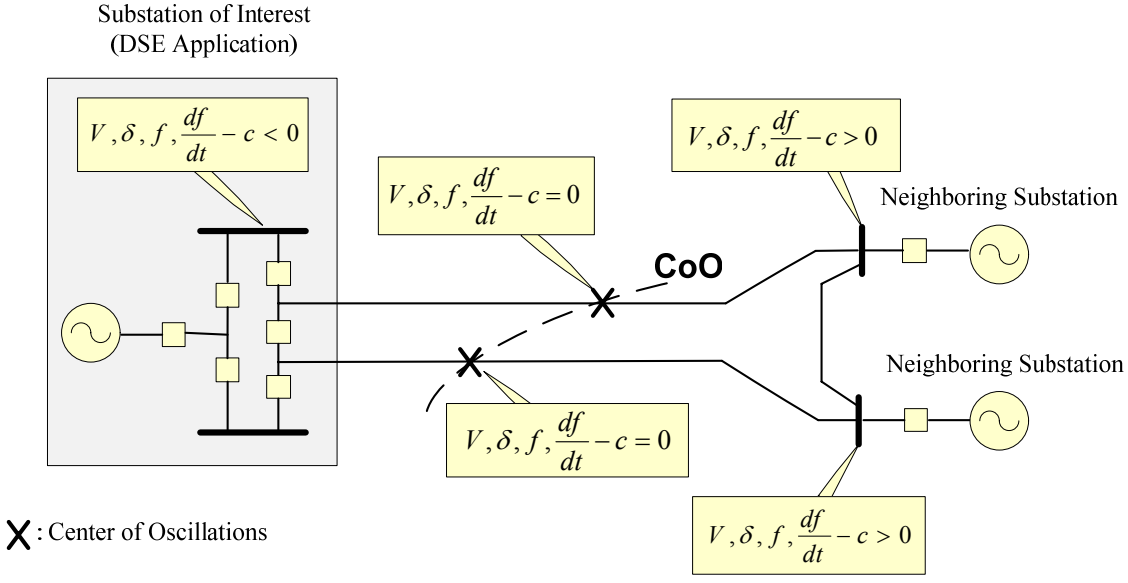

Figure 4.5. Center of oscillations definition.

Assume the system in Figure 4.6, with the substation of interest and the transmission line that connects the substation with the rest of the system.

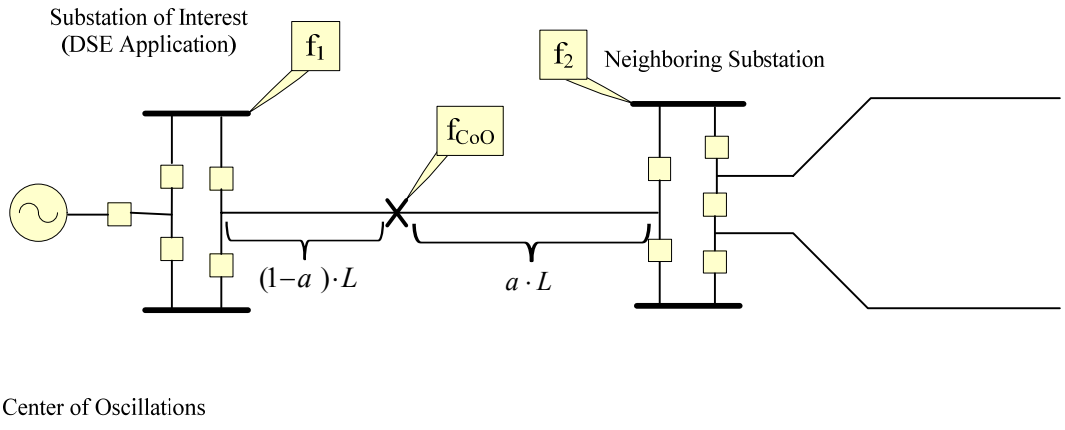

Figure 4.6. Center of oscillations within a transmission line.

Assume that the frequency at the CoO is a straight line with equation:

$$f_{coo}(t) = b + c \cdot t \tag{4.14}$$

and that the frequency at the two ends of the line is given as f_1 and f_2 correspondingly. Further assume that the frequency along the line varies linearly with the distance from one end of the line. Let the CoO be within the line. Then for every time instant t_i, the frequency of the CoO is a convex combination with coefficient a of the frequencies f_1 and f_2 at the two ends of the line, that is:

$$f_{coo}(t_i) = b + c \cdot t_i = a \cdot f_{1,t_i} + (1-a) \cdot f_{2,t_i}. \tag{4.15}$$

The coefficient a along with the equation of the line (parameters b and c) can be found by solving the following optimization problem:

$$\min \; J = \sum_{i=1}^{N} (a \cdot f_{1,t_i} + (1-a) \cdot f_{2,t_i} - b - c \cdot t)^2 \tag{4.16}$$

where N is the number of samples of f_1 and f_2 that are used. The samples of f_1 and f_2 are obtained upon simulation of the system for a few cycles (around 5 simulation cycles) given that the present time is the fault clearing time. In particular, the simulation is

performed for a given fault duration time $t_{fd} = t_{present} - t_{fault}$, where the simulated frequency at the two ends of the line is used as an input to the optimization algorithm for the evaluation of the CoO.

Once the coefficient a is computed, if $0 < a < 1$, then the center of oscillations is found to be along the transmission line at the point $(1-a)\cdot L$ from the first terminal, where L is the length of the line. Thus, the CoO lies within the observable area (the substation of interest or the transmission lines connecting to the neighboring substations). Otherwise it is outside the line. This case will be discussed further in section 6.6 . In case of multiple lines that depart from the substation, the same optimization procedure is performed for each line. An illustration of the CoO computation based on the optimization problem is shown in Figure 4.7.

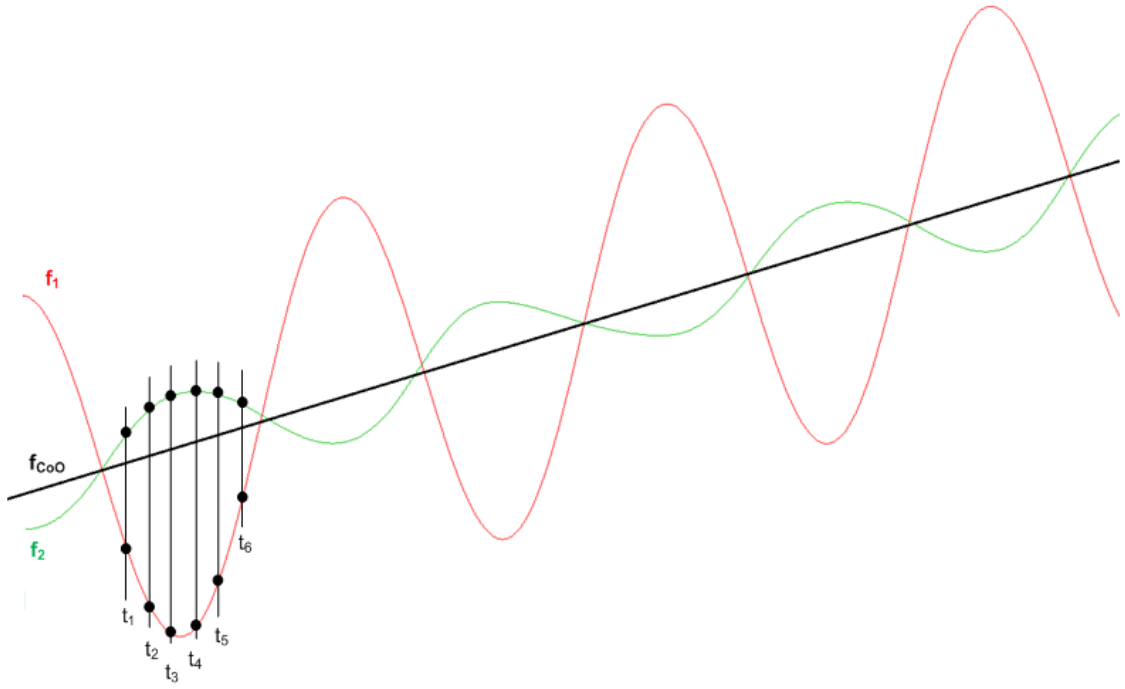

Figure 4.7. Center of oscillations evaluation.

4.3.2 Equivalent System Derivation

Once the CoO is evaluated then an equivalent system can be derived, that is used for the evaluation of the potential energy of the generator. The equivalent system consists of the original system up to the CoO along with the mirror image of this part of the system

with respect to the CoO. The concept of the equivalent system is illustrated in Figure 4.8 and Figure 4.9. In particular, assume that the original system consists of the substation of interest and two transmission lines with lengths L_1 and L_2 respectively, that connect the substation of interest to the neighboring substations and to the rest of the system as in Figure 4.6. Further assume that upon execution of the optimization algorithm for the evaluation of the CoO, it was found to be at the distance $a_1 \cdot L_1$ and $a_2 \cdot L_2$ away from the terminal of the substation of interest, on the two transmission lines respectively. Then the equivalent system consists of the substation of interest and the part of the transmission lines up to the CoO, along with the mirror image as is illustrated in Figure 4.9. Note that the equivalent substation has the same components (generator, transformer, etc) with the substation of interest.

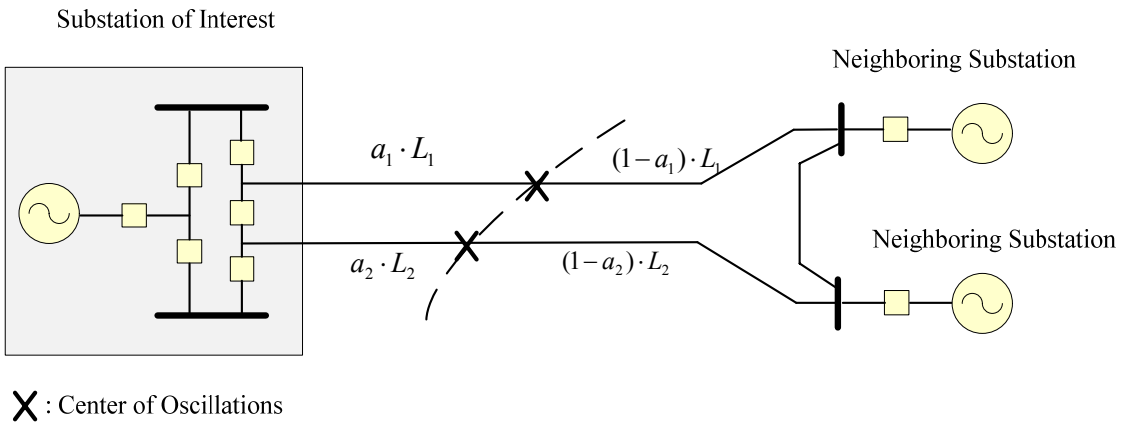

Figure 4.8. Original System.

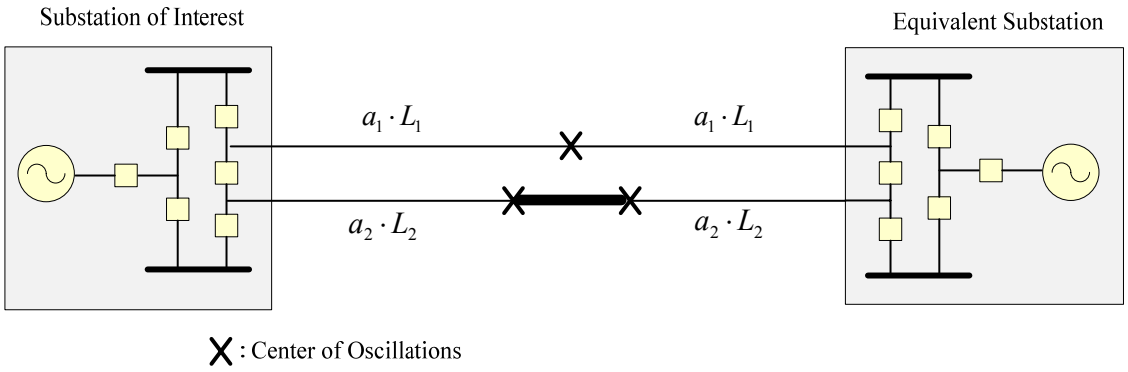

Figure 4.9. Equivalent System.

At this point, the importance but also the reasoning behind the evaluation of the CoO is to be emphasized. By evaluating the CoO of the system, then a very simple equivalent system is created, where the dynamics of the generator of interest are the same in the original and the equivalent system. As a result the potential energy of the generator is evaluated using the equivalent system and it is the same as the potential energy of the generator in the original system. Note that with this method, the complexity of the computation of the potential energy of the generator is significantly reduced since the equivalent system is a small two generator equivalent system. As a result, the potential and kinetic energy of the system can be computed using the well known formulas for a two machine system given next. The swing equations of the two generators are:

$$\frac{2H_1}{\omega_s}\frac{d\delta_1^2}{dt^2} = P_{m1} - P_{e1}(\delta_1 - \delta_2) \tag{4.17}$$

$$\frac{2H_2}{\omega_s}\frac{d\delta_2^2}{dt^2} = P_{m2} - P_{e2}(\delta_1 - \delta_2) \tag{4.18}$$

The single unit equivalent model is:

$$M\frac{d\delta^2}{dt^2} = M\frac{\omega_s}{2H_1}(P_{m1} - P_{e1}(\delta)) - M\frac{\omega_s}{2H_2}(P_{m2} - P_{e2}(\delta)) \tag{4.19}$$

where M is the two generators equivalent mass:

$$M = \frac{2H_1 \cdot H_2}{(H_1 + H_2)\cdot \omega_s} \tag{4.20}$$

The above model permits the evaluation of the potential energy of the generator which is given as follows:

$$E_{potential} = -\int_{\delta_{s1}-\delta_{s2}}^{\delta}\left[M\frac{\omega_s}{2H_1}(P_{m1} - P_{e1}(\delta)) - M\frac{\omega_s}{2H_2}(P_{m2} - P_{e2}(\delta))\right] \tag{4.21}$$

The kinetic energy of the system is:

$$E_k = \frac{1}{2}M(\omega_1 - \omega_2)^2 \tag{4.22}$$

where $\delta = \delta_1 - \delta_2$ is the difference of the generators' torque angles and ω_1 and ω_2 are the generators' speeds. $P_{e1}(\delta)$ and $P_{e2}(\delta)$ are computed based on the equations for the stability evaluation of a multi-machine system, given in Appendix B.

Note that the torque angle (δ_1) and the speed (ω_1) of the generator in the substation of interest are given continuously and in real time by the DSE. The torque angle (δ_2) and the speed (ω_2) of the equivalent generator are computed to be:

$$\delta_2 = 2 \cdot \delta_{CoO} - \delta_1 \tag{4.23}$$

$$\omega_2 = 2 \cdot \omega_{CoO} - \omega_1 \tag{4.24}$$

since the system is symmetric in terms of the CoO as is illustrated in Figure 4.10.

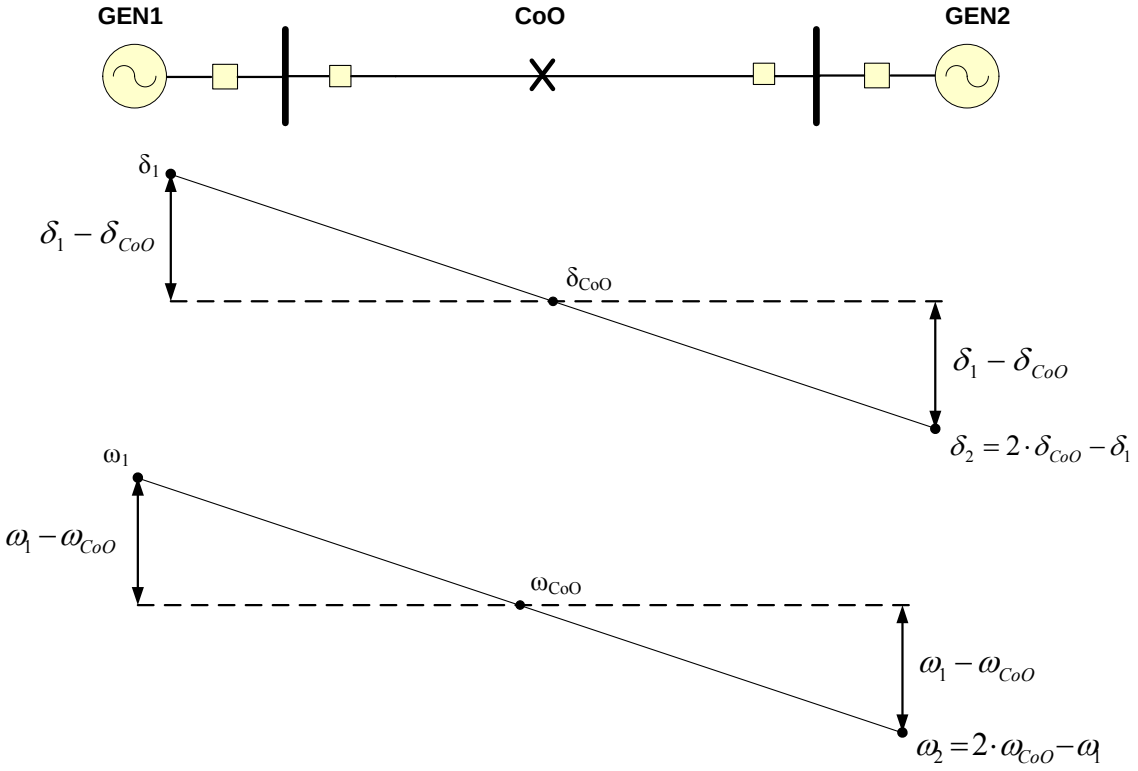

Figure 4.10. Phase angle and frequency computation of the equivalent generator.

The equilibrium point $\delta_s = \delta_{s1} - \delta_{s2}$ is given by the steady state power flow solution of the equivalent system.

4.3.3 Transient Stability Monitoring Scheme Algorithm

The algorithm that describes the implementation of the transient stability monitoring scheme is given next and shown in Figure 4.11. The generator torque angle and speed (frequency) at the substation of interest are monitored continuously through the DSE. After the occurrence of a fault, the type of the fault and the location of the fault can be identified. Given this information the topology of the post fault system is predicted, assuming that the predefined settings of the protective relays are known. This is also facilitated by the breaker oriented power system modeling that is used in this work, which allows for the prediction of the breaker(s) that will operate. These computations are expected to last a few cycles, so there will be a delay of few cycles before the monitoring of the total energy trajectory begins. However this time is expected to be in the order of a few msecs (2-3 cycles), thus it will normally be during the fault period and it is not expected to affect the performance of the scheme.

Now given the topology of the post fault system, at each time step of the algorithm and assuming that the fault is cleared at that time instant, the steps of the algorithm for the proposed transient stability monitoring scheme are the following:

1. the center of oscillations is evaluated by performing the optimization algorithm described in section 4.3.1,
2. the equivalent two generator system is derived, as described in section 4.3.2,
3. the potential energy function of the equivalent system is computed, along with the post fault equilibrium and the barrier value of the potential energy function which is equal to the value of the potential energy function at the closest unstable equilibrium point of the post fault system, as described in section 4.2,
4. the total energy of the generator is computed as the sum of the potential energy and the kinetic energy of the generator at that time instant. Note that for these calculations, the torque angle and the speed of the generator, along with the phase angle and the frequency of the CoO are used, and are given by the DSE that is performed at the substation of interest.

Note that these computations are expected to last a few cycles, so there will be a delay of few cycles before the scheme determines the stability of the system. However

due to the fact that all the computations are performed on a very simple and small two generator equivalent system, this computation time is expected to be in the order of a few msecs (2-3 cycles). Also note that the CoO is moving during the transient swings of the system, thus its evaluation is necessary at each time instant.

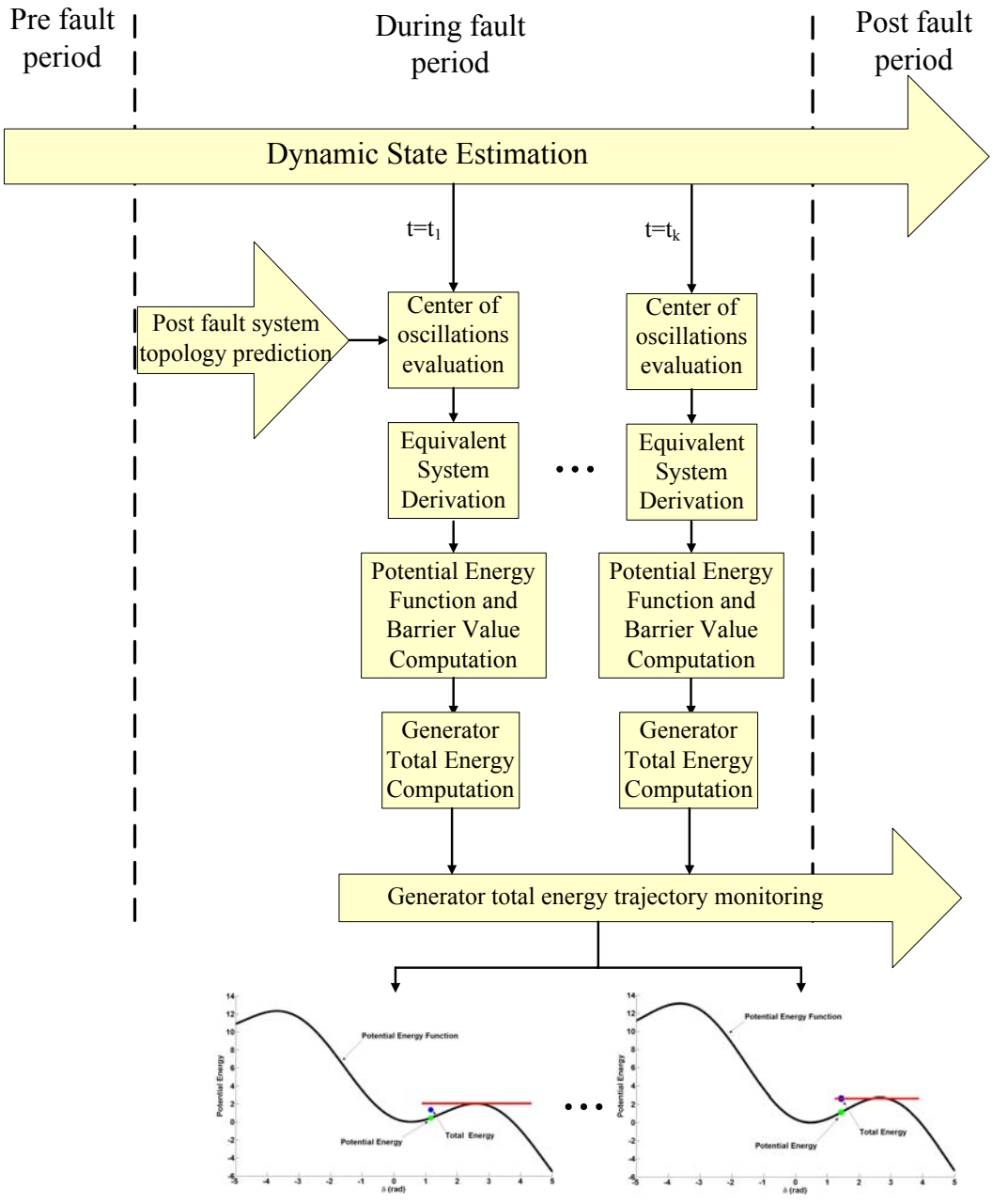

Figure 4.11. Proposed transient stability monitoring scheme conceptual illustration.

As a result, the proposed transient stability monitoring scheme determines in real time the stability of the system. In addition stability indexes such as the stability margin, in

terms of the generator energy or the phase angle can be computed at each time instant. Finally in case of an unstable system the critical clearing time is also determined, since this is the time instant at which the total energy of the generator equals the barrier value.

4.4 Application: Generator Out-of-Step Protection Scheme

An application of the transient stability monitoring scheme is a novel generator out-of-step protection scheme. As mentioned in the literature review section, nowadays, out-of-step protection is based on impedance relays that monitor the impedance trajectory at the terminals of the generator as illustrated in Figure 4.12. For present state-of-the-art out-of-step protection, the most common scheme is a mho relay with a single blinder set. Specifically, the impedance trajectory is monitored and instability is detected when there is a crossing on the two blinders (right and left). The major disadvantages of this scheme are that a) instability is detected when the unit has already slipped a pole and b) additional delay of tripping may be needed to avoid breaker overstresses in case of high generator torque angles.

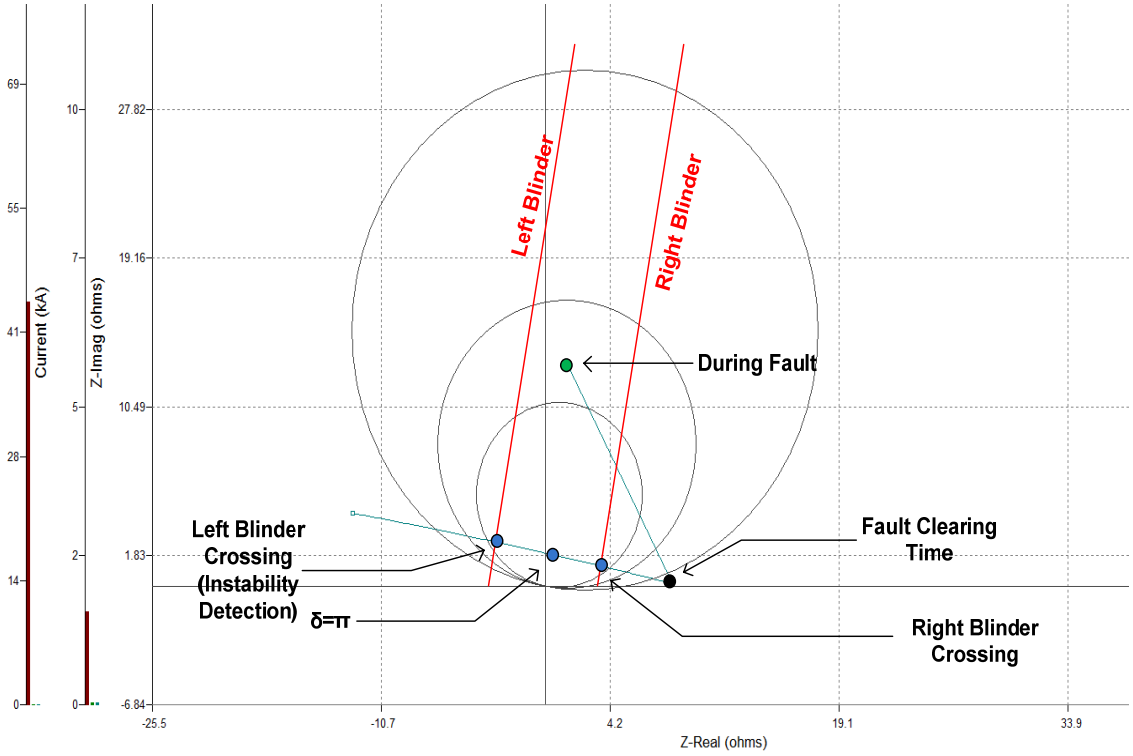

Figure 4.12. Single blinder out-of-step impedance relay operation [107].

Figure 4.13 illustrates in more detail a visualization of the generator total energy trajectory monitoring. The total energy of the generator is computed at each time step, and it is superimposed on the potential energy function. When and if the total energy value exceeds the barrier value $V_{\max}$ then instability is detected and a trip signal can be sent to the generator. Note that $V_{\max}$ is the value of the potential energy function at the "closest equilibrium point" as explained in section 4.2. Also, note that the instability is detected at the critical clearing time of the fault (t_{crit}), resulting in a predictive out-of-step protection scheme. At that time also the value of the torque angle of the generator (δ_{crit}) is typically such that allows the breaker to open without a risk to overstress it. If the total energy value does not exceed the barrier value $V_{\max}$, this means that the system is stable and there is no need for generator tripping. Thus monitoring of the trajectory of the total energy as the disturbance is evolving can lead to the calculation of the exact time that the system loses its synchronism and becomes unstable, and as a result provides us with the exact time that the out-of-step relay should trip the generator.

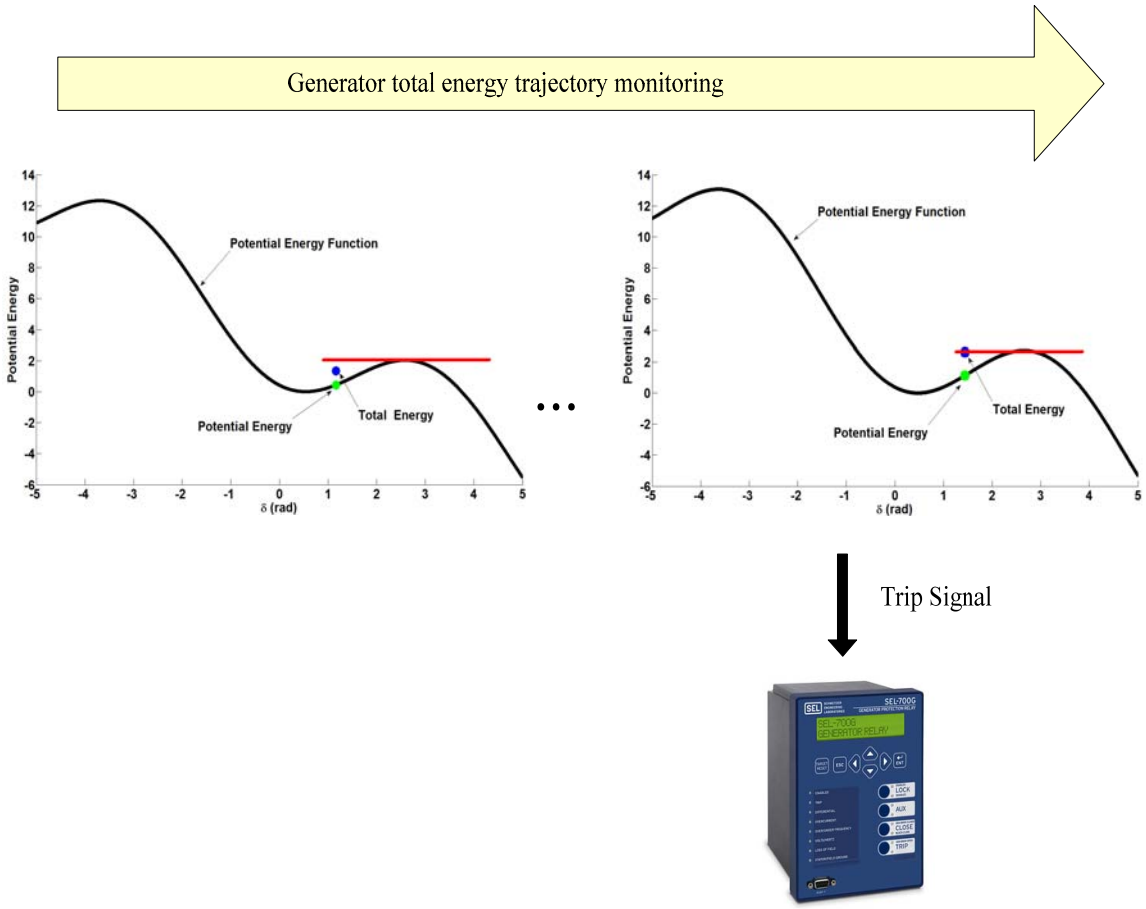

Figure 4.13. Generator out-of-step protection scheme illustration.

Additional visualizations can be also implemented that provide animations of the generator dynamics of the system in real time. The animation indirectly provides a feel of the acceleration of the generating units as their position and/or the arrow size of the speed changes. For example, Figure 4.14 shows the position of each generator according to its torque angle. In addition the speed of the generator (above or below synchronous speed) is shown with arrows that are proportional to the numerical value of the speed.

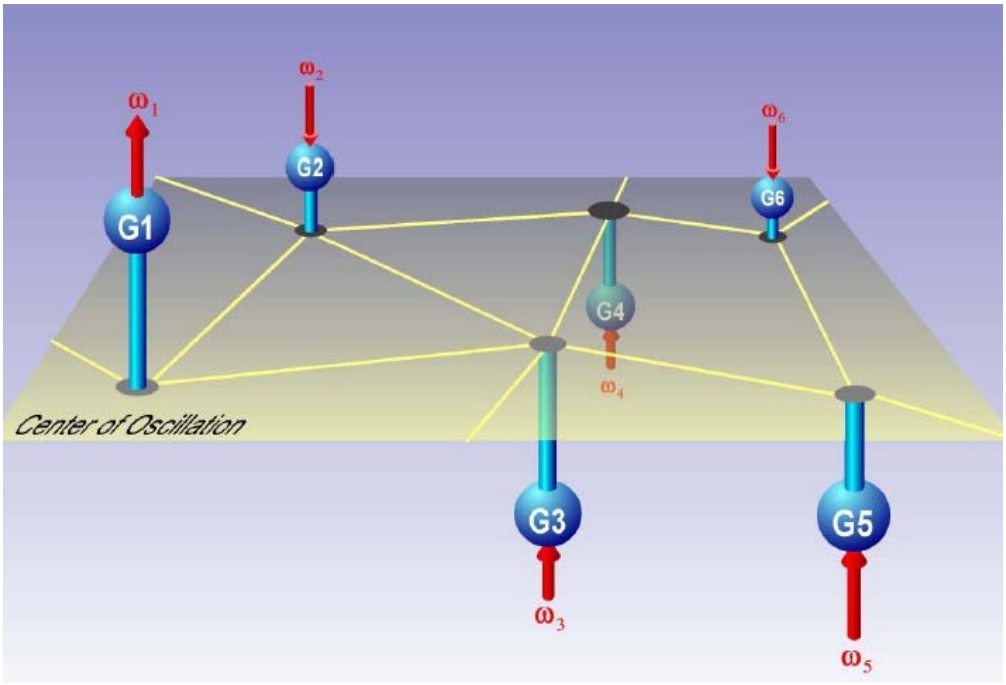

Figure 4.14. Visualization of generator operating state [100].

4.5 Summary

In this chapter, a novel, energy based transient stability monitoring scheme is described that is based on real-time dynamic monitoring of the system's transient swings, and is enabled by the developed dynamic state estimation. A key concept in the scheme is the evaluation of the CoO of the system. Once this is evaluated as part of the algorithm, then a two generator equivalent system is derived that mimics the dynamics of the original system. The equivalent system, along with the necessary information provided by the DSE are used in order to compute in real time the total energy of the generator and extract stability properties from the energy function. In addition an application of the transient stability monitoring scheme is proposed which is a novel, predictive, generator, out-of-step protection scheme. The proposed scheme is advantageous compared to state-of-the-art technology since out-of-step condition can be predicted before its occurrence and therefore relays can act much faster than today's technology.

5 DEMONSTRATING EXAMPLES: DISTRIBUTED DYNAMIC STATE ESTIMATION

5.1 Overview

In this chapter demonstrating examples of the distributed dynamic state estimator are presented. In particular, in section 5.2 the results from the implementation of DSE-Q on a quadratized single axis synchronous generator quasi-static model and on a quadratized two axis synchronous generator quasi-static model are presented. DSE-Q is also tested on three actual substation systems, the USVI LongBay substation, the USVI RHPP substation and the NYPS's Blenheim-Gilboa substation. In section 5.3, DSE-T is demonstrated on the NYPA's Gilboa-Blenheim substation.

5.2 DSE-Q Results

5.2.1 Single-Axis Synchronous Generator DSE-Q

In this section a quadratized single axis quasi-static generator model is presented, which was used in the DSE algorithm for the estimation of the generator states. This is the most common generator model that is used in transient stability studies and is represented by a constant voltage behind a transient impedance, as illustrated in Figure 5.1. The DSE algorithm has been applied to the generator in order to estimate its total state vector. This information can be further used as an input to power systems applications. For example, for transient stability analysis and the developed out-of-step protection scheme, an estimate of the generators' state (that includes the torque angle and the speed) is needed and computed through the DSE in real time.

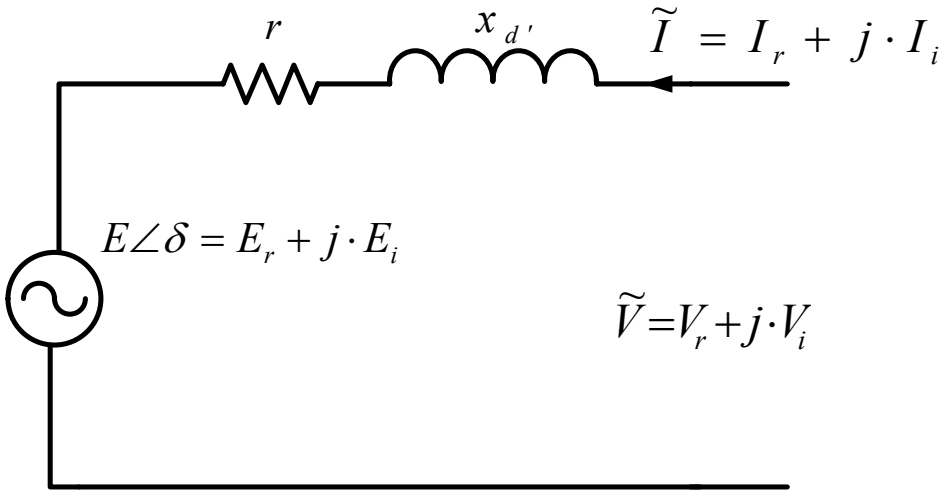

Figure 5.1. Single axis synchronous generator model.

The equations of the quadratized model are:

$$I_r(t) = \frac{E_r(t)}{r} - \frac{V_r(t)}{r} - \frac{E_i(t)}{x_{d'}} + \frac{V_i(t)}{x_{d'}}$$

$$I_i(t) = \frac{E_i(t)}{r} - \frac{V_i(t)}{r} + \frac{E_r(t)}{x_{d'}} - \frac{V_r(t)}{x_{d'}}$$

$$0 = T_e(t) \cdot \omega(t) - P_e(t)$$

$$0 = P_e(t) - \frac{(E_r(t))^2}{r} - \frac{(E_i(t))^2}{r} + \frac{V_r(t) \cdot E_r(t)}{r} + \frac{E_i(t) \cdot V_i(t)}{r} - \frac{E_r(t) \cdot V_i(t)}{x_{d'}} + \frac{E_i(t) \cdot V_r(t)}{x_{d'}}$$

$$0 = y_1(t) - c(t) \cdot (\omega(t) - \omega_0)$$

$$0 = y_2(t) + s(t) \cdot (\omega(t) - \omega_0)$$

(5.1)

$$0 = E_r^2(t) + E_i^2(t) - E_{spec.}$$

$$0 = E_r(t) \cdot s(t) - E_i(t) \cdot c(t)$$

$$\frac{d\delta(t)}{dt} = \omega(t) - \omega_0$$

$$J\frac{d\omega(t)}{dt} = T_m - T_e(t)$$

$$\frac{ds(t)}{dt} = y_1(t)$$

$$\frac{dc(t)}{dt} = y_2(t)$$

where

$\widetilde{I} = I_r + j \cdot I_i$ is the generator current,

$\widetilde{V} = V_r + j \cdot V_i$ is the generator terminal voltage,

$\widetilde{E} = E_r + j \cdot E_i$ is the generator internal voltage,

$\delta(t)$ is the generator torque angle,

$\omega(t)$ is the generator speed,

$T_e(t)$ is the generator electrical torque,

$P_e(t)$ is the generator internal electrical power,

ω_0 is the synchronous speed,

J is the moment of inertia of the generator,

$c(t)$, $s(t)$, $y_1(t)$, $y_2(t)$ are additional states introduced to quadratize the model. In fact, $c(t)$ and $s(t)$ represent the sinus and cosine of the angle $\delta(t)$. T_m is the mechanical power supplied by a prime mover, while E_{spec} is the internal voltage magnitude specified by an excitation system. These two quantities are assumed constant in this simplified model.

The state vector is

$$\left[x^T(t) \quad y^T\right] = \left[\delta(t) \quad \omega(t) \quad s(t) \quad c(t) \quad V_r \quad V_i \quad E_r \quad E_i \quad T_e \quad P_e \quad y_1 \quad y_2\right]^T.$$

It is noted that the states of this component have been separated into "dynamic" states, i.e. states that obey differential equations, and "static" states that obey algebraic equations. Finally it is to be noted that the trigonometric functions have been eliminated by the introduction of the variables $s(t)$ and $c(t)$, without any approximations, thus the model is quadratic.

Given the generator model and the available measurements, the following filter equations are obtained after applying quadratic integration to the differential equations:

$$V_r^m(t) = V_r(t)$$

$$V_i^m(t) = V_i(t)$$

$$I_r^m(t) = \frac{E_r(t)}{r} - \frac{V_r(t)}{r} - \frac{E_i(t)}{x_{d'}} + \frac{V_i(t)}{x_{d'}}$$

$$I_i^m(t) = \frac{E_i(t)}{r} - \frac{V_i(t)}{r} + \frac{E_r(t)}{x_{d'}} - \frac{V_r(t)}{x_{d'}}$$

$$P^m(t) = -\frac{(V_r(t))^2}{r} - \frac{(V_i(t))^2}{r} + \frac{V_r(t)\cdot E_r(t)}{r} + \frac{V_i(t)\cdot E_i(t)}{r} + \frac{V_i(t)\cdot E_r(t)}{x_{d'}} - \frac{V_r(t)\cdot E_i(t)}{x_{d'}}$$

$$Q^m(t) = \frac{(V_r(t))^2}{x_{d'}} + \frac{(V_i(t))^2}{x_{d'}} - \frac{V_r(t)\cdot E_r(t)}{x_{d'}} - \frac{V_i(t)\cdot E_i(t)}{x_{d'}} + \frac{V_i(t)\cdot E_r(t)}{r} - \frac{V_r(t)\cdot E_i(t)}{r}$$

$$\omega^m(t) = \omega(t) \qquad (5.2)$$

$$0 = T_e(t)\cdot\omega(t) - P_e(t)$$

$$0 = P_e(t) - \frac{(E_r(t))^2}{r} - \frac{(E_i(t))^2}{r} + \frac{V_r(t)\cdot E_r(t)}{r} + \frac{E_i(t)\cdot V_i(t)}{r} - \frac{E_r(t)\cdot V_i(t)}{x_{d'}} + \frac{E_i(t)\cdot V_r(t)}{x_{d'}}$$

$$0 = y_1(t) - c(t)\cdot\left(\omega(t) - \omega_0\right)$$

$$0 = y_2(t) + s(t)\cdot\left(\omega(t) - \omega_0\right)$$

$$0 = E_r^2(t) + E_i^2(t) - E_{spec.}$$

$$0 = E_r(t) \cdot s(t) - E_i(t) \cdot c(t)$$

$$0 = Q(t_m)$$

$$0 = \delta(t) - \delta(t-h) - \frac{h}{6}\omega(t) - \frac{2h}{3}\omega(t_m) - \frac{h}{6}\omega(t-h) + h \cdot \omega_0$$

$$0 = \delta(t_m) - \delta(t-h) + \frac{h}{24}\omega(t) - \frac{h}{3}\omega(t_m) - \frac{5h}{24}\omega(t-h) + \frac{h}{2} \cdot \omega_0$$

$$0 = J \cdot \omega(t) - J \cdot \omega(t-h) + \frac{h}{6}T_e(t) + \frac{2h}{3}T_e(t_m) + \frac{h}{6}T_e(t-h) - h \cdot T_m$$

$$0 = J \cdot \omega(t_m) - J \cdot \omega(t-h) - \frac{h}{24}T_e(t) + \frac{h}{3}T_e(t_m) + \frac{5h}{246}T_e(t-h) - \frac{h}{2} \cdot T_m$$

$$0 = s(t) - s(t-h) - \frac{h}{6}y_1(t) - \frac{2h}{3}y_1(t_m) - \frac{h}{6}y_1(t-h)$$

$$0 = s(t_m) - s(t-h) + \frac{h}{24}y_1(t) - \frac{h}{3}y_1(t_m) - \frac{5h}{24}y_1(t-h)$$

$$0 = c(t) - c(t-h) - \frac{h}{6}y_2(t) - \frac{2h}{3}y_2(t_m) - \frac{h}{6}y_2(t-h)$$

$$0 = c(t_m) - c(t-h) + \frac{h}{24}y_2(t) - \frac{h}{3}y_2(t_m) - \frac{5h}{24}y_2(t-h)$$

The first 7 equations refer to actual measurements, while the remaining equations of the form "0=" are the additional virtual measurements (originating from the model equations), considered as measurements with zero value and a very high accuracy. The symbol h refers to the discretization step.

Implementation and application of the dynamic state estimator on the single axis generator model will be demonstrated on the generating units of New York Power Authority's (NYPA) Gilboa-Blenheim substation. A short description of the Gilboa-Blenheim substation model is given in Appendix C. DSE was performed on the first generator of the substation. The system is simulated in WinIGS (a power system analysis software, using a three-phase system representation with detailed component modeling). The measurements involve steady state and transient conditions, after a three-phase fault at the terminal of Freizer Substation. The fault is initiated at t=0.5 sec and lasts for 0.1 sec. The measurement set consists of the terminal voltage phasor of the generating unit

(both magnitude and phase), the unit current phasor (both magnitude and phase), the generator speed and scalar measurements of the active and reactive power injections of the generator. The measurement set is illustrated in Figure 5.2.

The estimated generator states are computed after applying the described DSE algorithm to the measurement set of Figure 5.2 and presented in Figure 5.3. DSE time step was 16.67 msec (one estimation per cycle). Standard deviation of 1% is assumed for each actual measurement, while a higher precision, of an order of magnitude greater, is assumed for the virtual measurements. Estimates of the terminal voltage, the torque angle and the frequency are shown in Figure 5.3, as an illustrative subset of the generator state vector. The DSE results (dotted lines) are superimposed on the simulation results (solid lines). The results show that the estimation is highly accurate both for pre-fault but also for post-fault conditions.

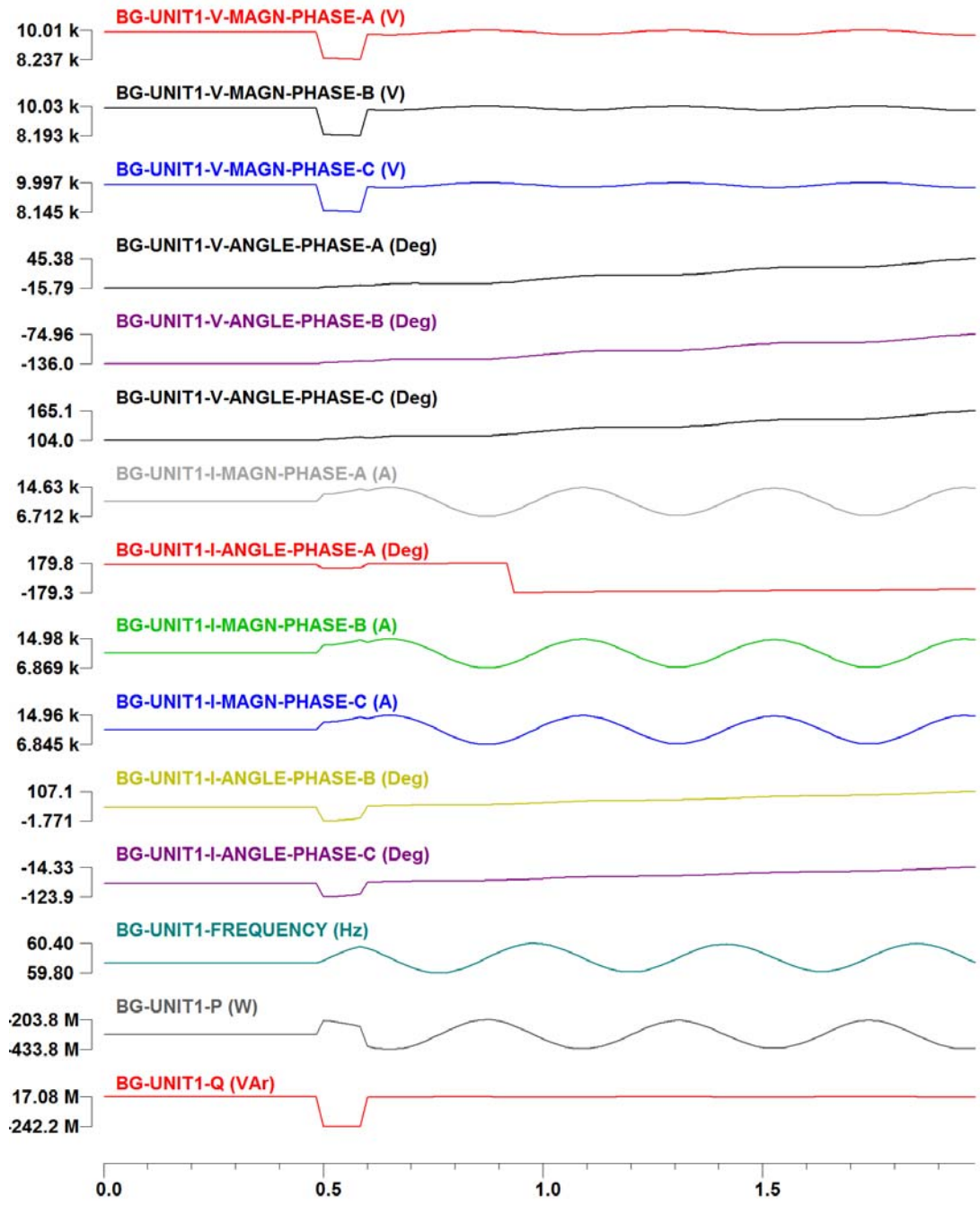

Figure 5.2. Single-axis generator DSE - measurement set.

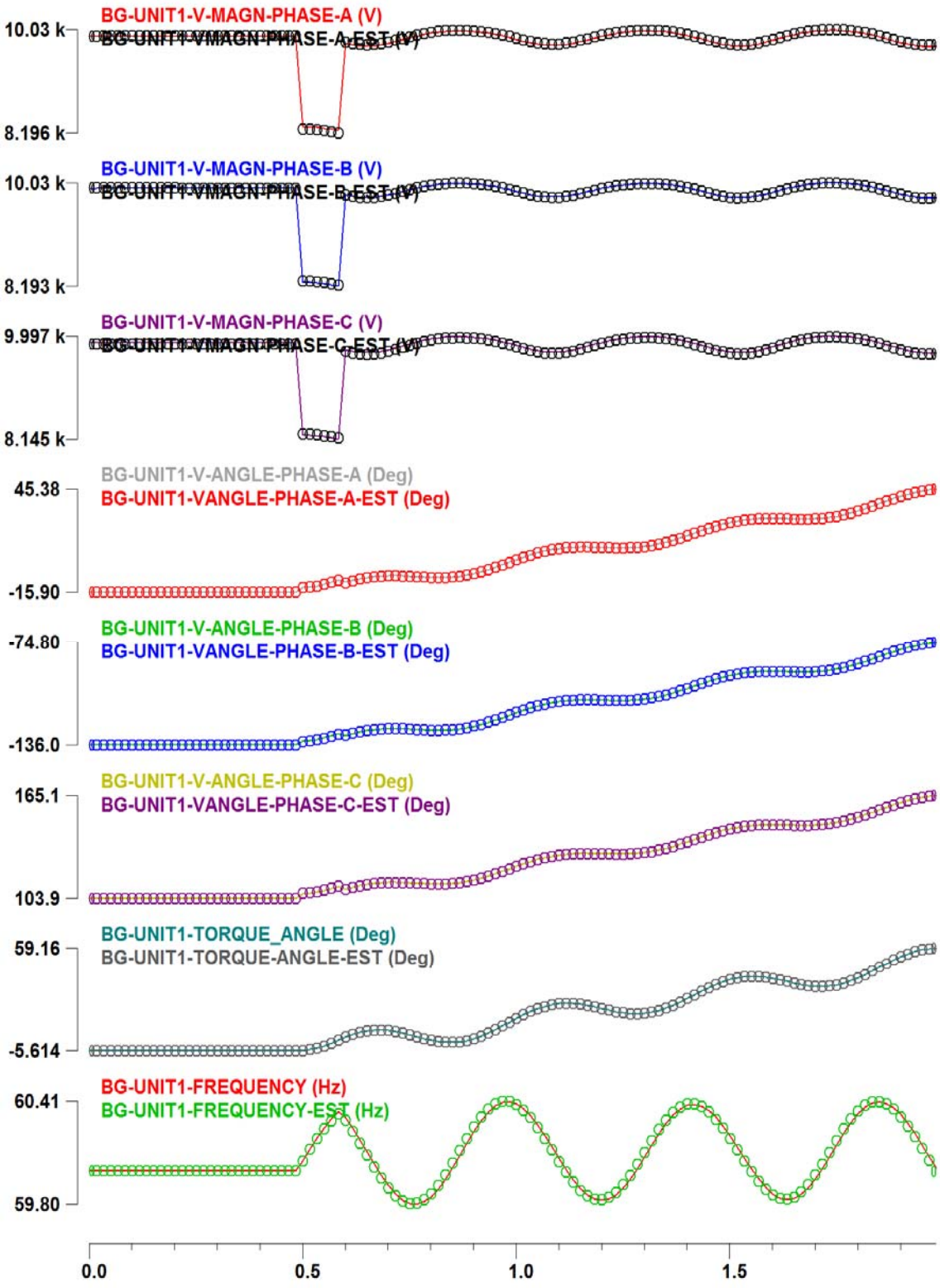

Figure 5.3. Single axis generator DSE - estimated states.

5.2.2 Two-Axis Synchronous Generator DSE-Q

In this section a quadratized, two-axis, quasi-static generator model is presented, which was used in the DSE algorithm for the estimation of the generator states. The objective of the DSE algorithm is to obtain an estimate of the total state of the generator in real time that will be further used as an input for the out-of-step protection scheme.

The phasor diagram of the generator model is illustrated in Figure 5.4.

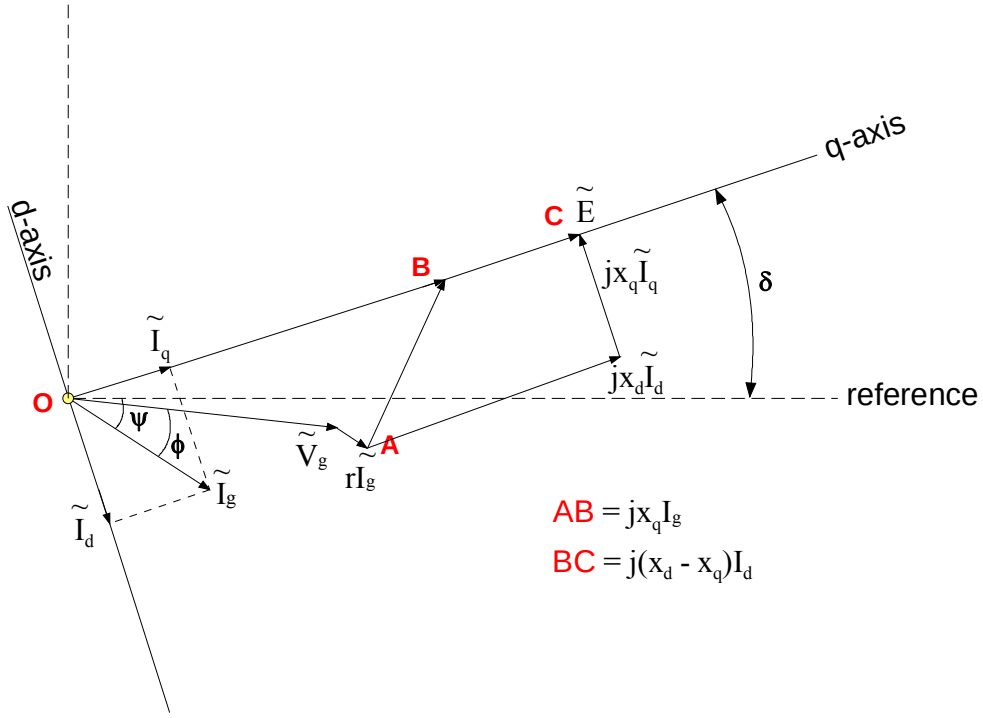

Figure 5.4. Two-axis synchronous machine phasor diagram.

In Figure 5.4:

$\tilde{I}_g$: armature current (positive direction is into the generator)

r : armature resistance

x_d : direct-axis synchronous reactance

x_q : quadrature-axis synchronous reactance

$\tilde{V}_g$: terminal voltage

The rotor angle is defined as

$$\delta(t) = \theta(t) - \omega_0 t - \frac{\pi}{2}, \tag{5.3}$$

where $\delta(t) + \frac{\pi}{2}$ is the angle difference between the rotor (d-axis), rotating at speed $\omega(t)$, and a synchronously rotating reference frame at speed ω_0. $\theta(t)$ is the position of the rotor. Upon differentiation the following hold:

$$\frac{d\delta(t)}{dt} = \frac{d\theta(t)}{dt} - \omega_0 = \omega(t) - \omega_0, \tag{5.4}$$

and

$$\frac{d^2\delta(t)}{dt^2} = \frac{d^2\theta(t)}{dt^2} = \frac{d\omega(t)}{dt}. \tag{5.5}$$

The state vector is defined as

$$X^T = \begin{bmatrix} x^T & y^T \end{bmatrix}$$

$$x^T = \begin{bmatrix} \delta(t) & \omega(t) & s(t) & c(t) \end{bmatrix}$$

$$y^T = \begin{bmatrix} V_{gr} & V_{gi} & E_r & E_i & I_{dr} & I_{di} & I_{qr} & I_{qi} & z_1 & z_2 & T_e & y_1 & y_2 \end{bmatrix}$$

Subscripts r and i denote the real and imaginary part of the corresponding phasor. Igr and Idr are through variables of the model. The equations of the model are as follows:

$$I_{gr}(t) = I_{dr}(t) + I_{qr}(t)$$

$$I_{gi}(t) = I_{di}(t) + I_{qi}(t)$$

$$0 = E_r(t) - V_{gr}(t) + rI_{dr}(t) + rI_{qr}(t) - x_d I_{di}(t) - x_q I_{qi}(t)$$

$$0 = E_i(t) - V_{gi}(t) + rI_{di}(t) + rI_{qi}(t) + x_d I_{dr}(t) + x_q I_{qr}(t)$$

$$0 = E_r(t) \cdot s(t) - E_i(t) \cdot c(t)$$

$$0 = E_r(t) \cdot I_{dr}(t) + E_i(t) \cdot I_{di}(t)$$

$$0 = E_i(t) \cdot I_{qr}(t) - E_r(t) \cdot I_{qi}(t)$$

$$0 = z_1(t) \cdot \omega(t) - E_r(t) \tag{5.6}$$

$$0 = z_2(t) \cdot \omega(t) - E_i(t)$$

$$0 = E_r(t)^2 + E_i(t)^2 - E_{spec.}$$

$$0 = T_e(t) - 3 \cdot \left[z_1(t) \cdot \left(I_{dr}(t) + I_{qr}(t) \right) + z_2(t) \cdot \left(I_{di}(t) + I_{qi}(t) \right) \right]$$

$$0 = y_1(t) - c(t) \cdot \left(\omega(t) - \omega_0 \right)$$

$$0 = y_2(t) + s(t) \cdot \left(\omega(t) - \omega_0 \right)$$

$$\frac{d\delta(t)}{dt} = \omega(t) - \omega_0$$

$$J \frac{d\omega(t)}{dt} = T_m - T_e(t)$$

$$\frac{ds(t)}{dt} = y_1(t)$$

$$\frac{dc(t)}{dt} = y_2(t)$$

Based on the generator model, the available measurements and virtual measurements the following filter equations are obtained after applying quadratic integration to the differential equations:

$$
\begin{aligned}
&V_{gr}{}^{m}(t) = V_{gr}(t),\\
&V_{gi}{}^{m}(t) = V_{gi}(t),\\
&I_{gr}{}^{m}(t) = I_{dr}(t) + I_{qr}(t),\\
&I_{gi}{}^{m}(t) = I_{di}(t) + I_{qi}(t),\\
&\omega^{m}(t) = \omega(t),\\
&P^{m}(t) = V_{gr}(t)\cdot I_{dr}(t) + V_{gr}(t)\cdot I_{qr}(t)\\
&\qquad - V_{gi}(t)\cdot I_{di}(t) - V_{gi}(t)\cdot I_{qi}(t),\\
&Q^{m}(t) = V_{gr}(t)\cdot I_{di}(t) + V_{gr}(t)\cdot I_{qi}(t)\\
&\qquad + V_{gi}(t)\cdot I_{dr}(t) + V_{gi}(t)\cdot I_{qr}(t),
\end{aligned}
$$

$$
\begin{aligned}
&0 = E_r(t) - V_{gr}(t) + rI_{dr}(t) + rI_{qr}(t) - x_d I_{di}(t) - x_q I_{qi}(t)\\
&0 = E_i(t) - V_{gi}(t) + rI_{di}(t) + rI_{qi}(t) + x_d I_{dr}(t) + x_q I_{qr}(t)\\
&0 = E_r(t)\cdot s(t) - E_i(t)\cdot c(t)\\
&0 = E_r(t)\cdot I_{dr}(t) + E_i(t)\cdot I_{di}(t)\\
&0 = E_i(t)\cdot I_{qr}(t) - E_r(t)\cdot I_{qi}(t)\\
&0 = z_1(t)\cdot\omega(t) - E_r(t)\\
&0 = z_2(t)\cdot\omega(t) - E_i(t)\\
&0 = E_r(t)^2 + E_i(t)^2 - E_{spec.}\\
&0 = T_e(t) - 3\cdot\left[z_1(t)\cdot\left(I_{dr}(t) + I_{qr}(t)\right) + z_2(t)\cdot\left(I_{di}(t) + I_{qi}(t)\right)\right]\\
&0 = y_1(t) - c(t)\cdot\left(\omega(t) - \omega_0\right)\\
&0 = y_2(t) + s(t)\cdot\left(\omega(t) - \omega_0\right)
\end{aligned}
\qquad (5.7)
$$

$$
0 = Q(t_m)
$$

$$0 = \delta(t) - \delta(t-h) - \frac{h}{6}\omega(t) - \frac{2h}{3}\omega(t_m) - \frac{h}{6}\omega(t-h) + h \cdot \omega_0$$

$$0 = \delta(t_m) - \delta(t-h) + \frac{h}{24}\omega(t) - \frac{h}{3}\omega(t_m) - \frac{5h}{24}\omega(t-h) + \frac{h}{2} \cdot \omega_0$$

$$0 = J \cdot \omega(t) - J \cdot \omega(t-h) + \frac{h}{6}T_e(t) + \frac{2h}{3}T_e(t_m) + \frac{h}{6}T_e(t-h) - h \cdot T_m$$

$$0 = J \cdot \omega(t_m) - J \cdot \omega(t-h) - \frac{h}{24}T_e(t) + \frac{h}{3}T_e(t_m) + \frac{5h}{246}T_e(t-h) - \frac{h}{2} \cdot T_m$$

$$0 = s(t) - s(t-h) - \frac{h}{6}y_1(t) - \frac{2h}{3}y_1(t_m) - \frac{h}{6}y_1(t-h)$$

$$0 = s(t_m) - s(t-h) + \frac{h}{24}y_1(t) - \frac{h}{3}y_1(t_m) - \frac{5h}{24}y_1(t-h)$$

$$0 = c(t) - c(t-h) - \frac{h}{6}y_2(t) - \frac{2h}{3}y_2(t_m) - \frac{h}{6}y_2(t-h)$$

$$0 = c(t_m) - c(t-h) + \frac{h}{24}y_2(t) - \frac{h}{3}y_2(t_m) - \frac{5h}{24}y_2(t-h)$$

The first group of the filter equations refers to the actual measurements. The second group refers to the algebraic (linear or quadratic) internal equations of the model that are introduced as virtual measurements. This set of equations (renamed as $Q(t)$) is also evaluated at the intermediate time t_m resulting in the set of equation $0 = Q(t_m)$ that are also introduced as virtual measurements. Finally, the last group refers to the integrated (using quadratic integration) dynamic equations of the model which are also introduced as virtual measurements.

Implementation and application of the dynamic state estimator on the two axis generator model will be also demonstrated on the generating units of NYPA's Gilboa-Blenheim substation. DSE was performed on the second generator of the substation. The system is simulated in WinIGS. The measurements involve steady state and transient conditions, after a three-phase fault at the terminal of Freizer Substation. The fault is initiated at t=0.5 sec and lasts for 0.1 sec. The measurement set consists of the terminal voltage phasor of the generating unit (both magnitude and phase), the unit current phasor

(both magnitude and phase), the generator speed and scalar measurements of the active and reactive power injections of the generator. The measurement set is illustrated in Figure 5.5.

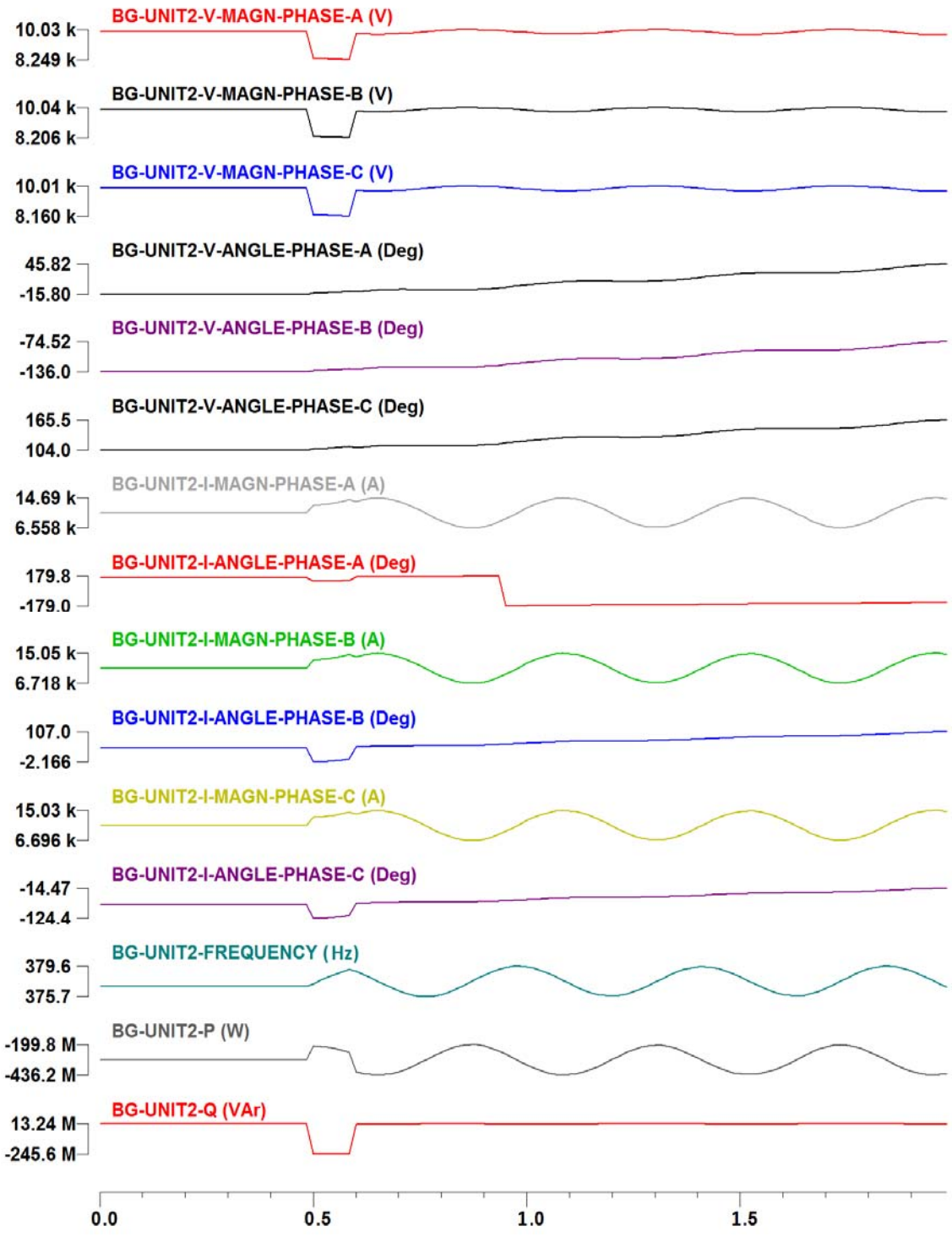

Figure 5.5. Two axis generator DSE - measurement set.

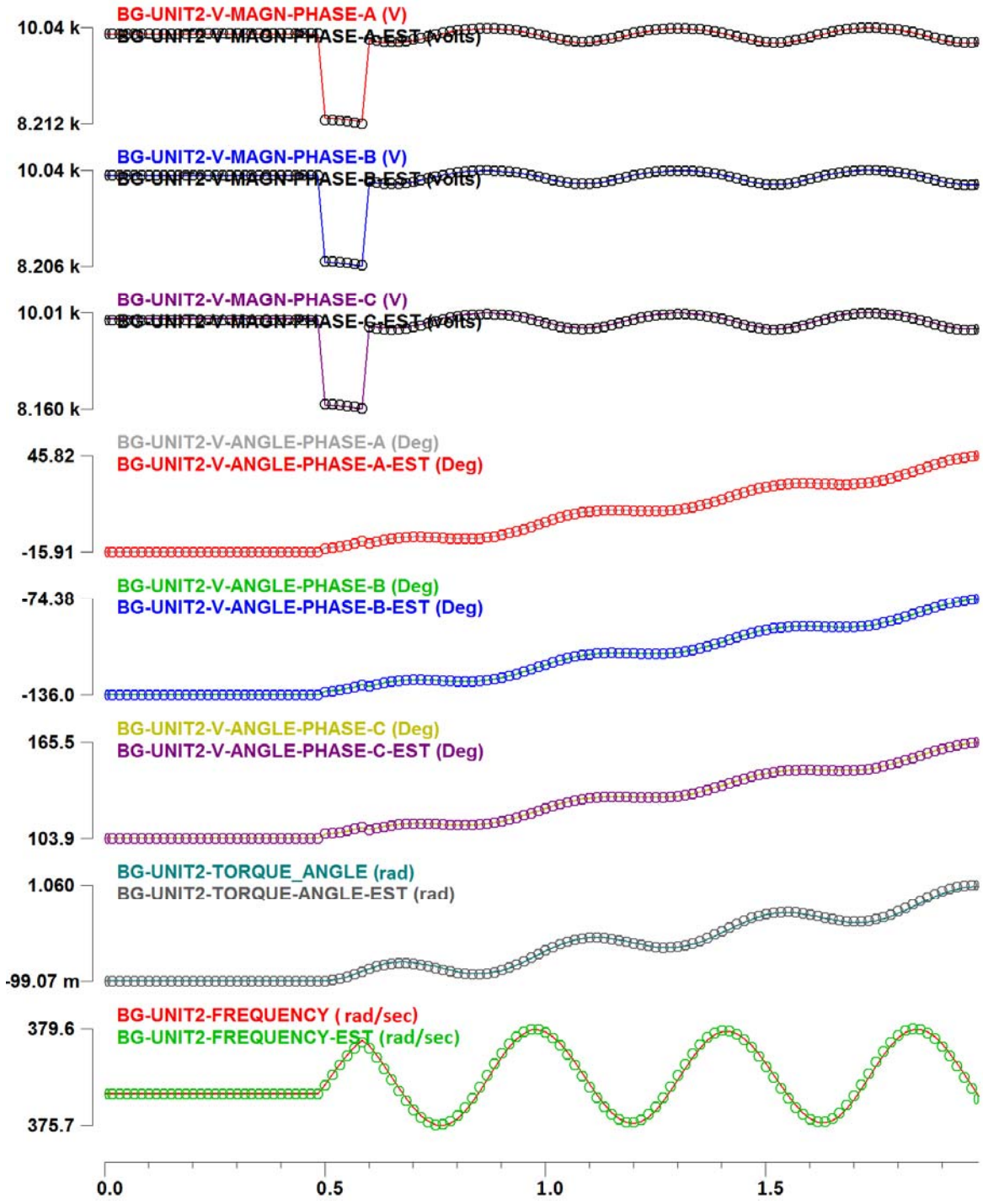

Figure 5.6. Two axis generator DSE - estimated states.

The estimated generator states are computed after applying the described DSE algorithm to the measurement set of Figure 5.5. DSE time step was 16.67 msec (one estimation per cycle). Standard deviation of 1% is assumed for each actual measurement,

while a higher precision, of an order of magnitude greater, is assumed for the virtual measurements. Estimates of the terminal voltage, the torque angle and the frequency are shown in Figure 5.6, as an illustrative subset of the generator state vector. The DSE results (dotted lines) are superimposed on the simulation results (solid lines). The results show that the estimation is highly accurate both for pre fault but also for post fault conditions.

5.2.3 USVI Long Bay DSE-Q

The DSE-Q was also implemented and tested for the Long Bay Substation of the US Virgin Islands system. A description of the Long Bay substation model is given in Appendix D. The results include steady state and transient conditions after a three-phase fault that was simulated close to RHPP substation. The estimation time step was 16.67 msec (1 estimation per cycle). Figure 5.7 to Figure 5.12 illustrate demonstrative results of the estimated states. The estimation results (dotted lines) are superimposed on the simulation results (solid lines). In particular, Figure 5.7 and Figure 5.8 illustrate the voltage magnitudes and phase angles of the three phases for bus 3-0A0B1 (Substation Terminal Bus) respectively. Figure 5.9 and Figure 5.10 illustrate the voltage magnitudes and phase angles of the three phases for bus LB-T1-T (Substation Transformer1 34.5 kV Bus) respectively. Finally Figure 5.11 and Figure 5.12 illustrate the voltage magnitudes and phase angles of the three phases for bus UG350 (Neighboring Bus). The results show that the estimation is highly accurate both for pre fault but also for post fault conditions.

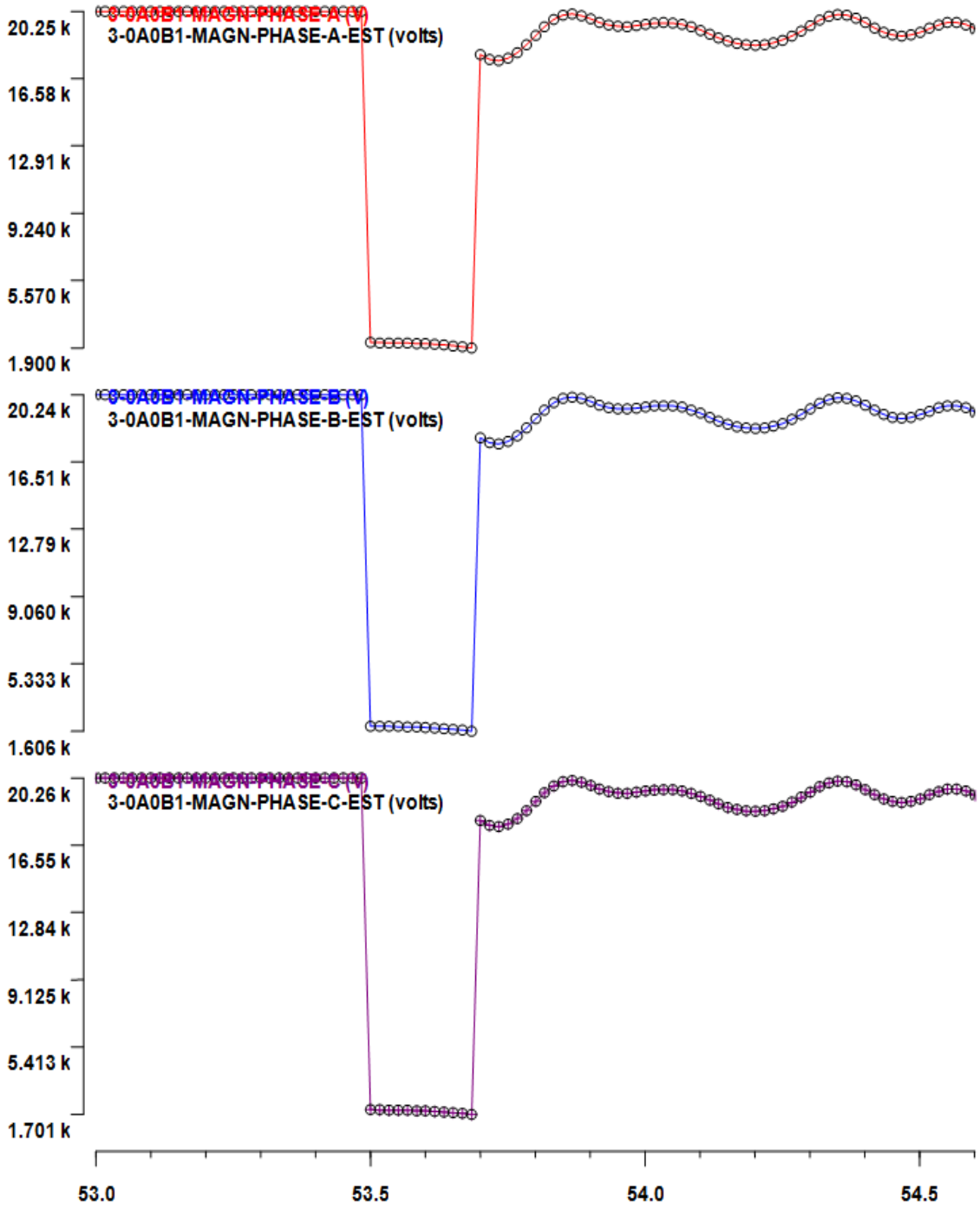

Figure 5.7. Simulated and estimated voltage magnitude of bus 3-0A0B1.

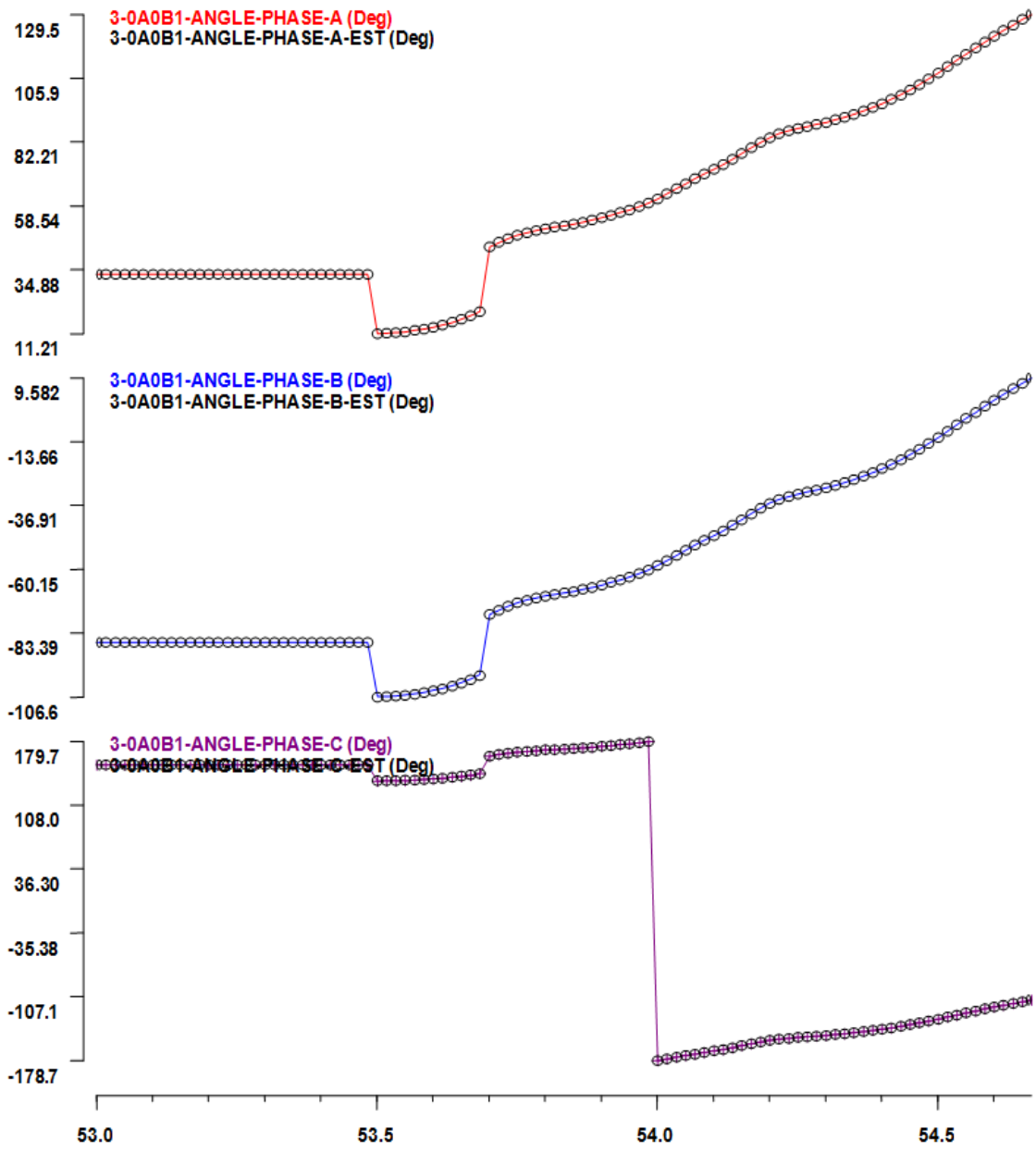

Figure 5.8. Simulated and estimated voltage phase angle of bus 3-0A0B1.

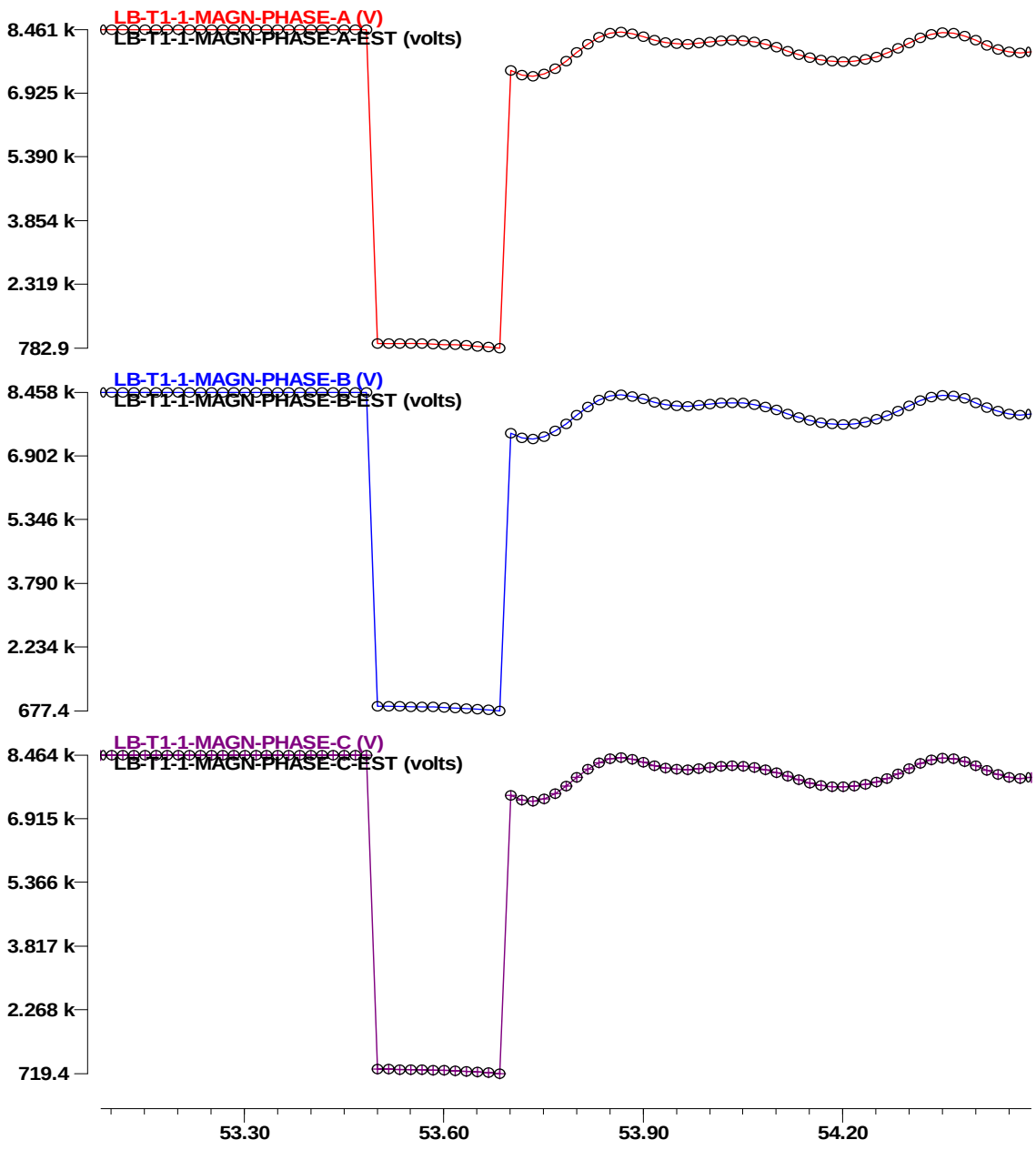

Figure 5.9. Simulated and estimated voltage magnitude of bus LB-T1-1.

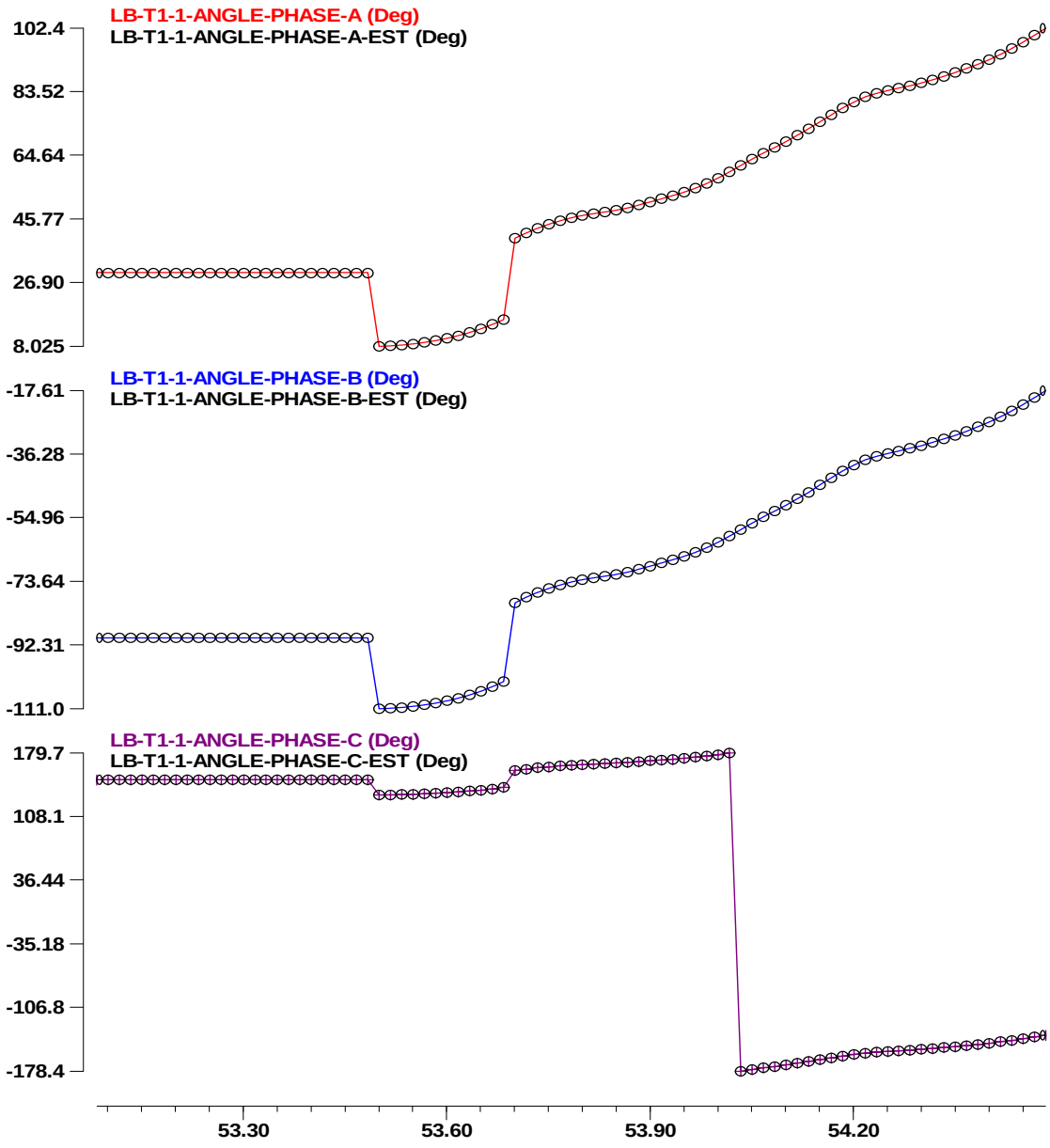

Figure 5.10. Simulated and estimated voltage phase angle of bus LB-T1-1.

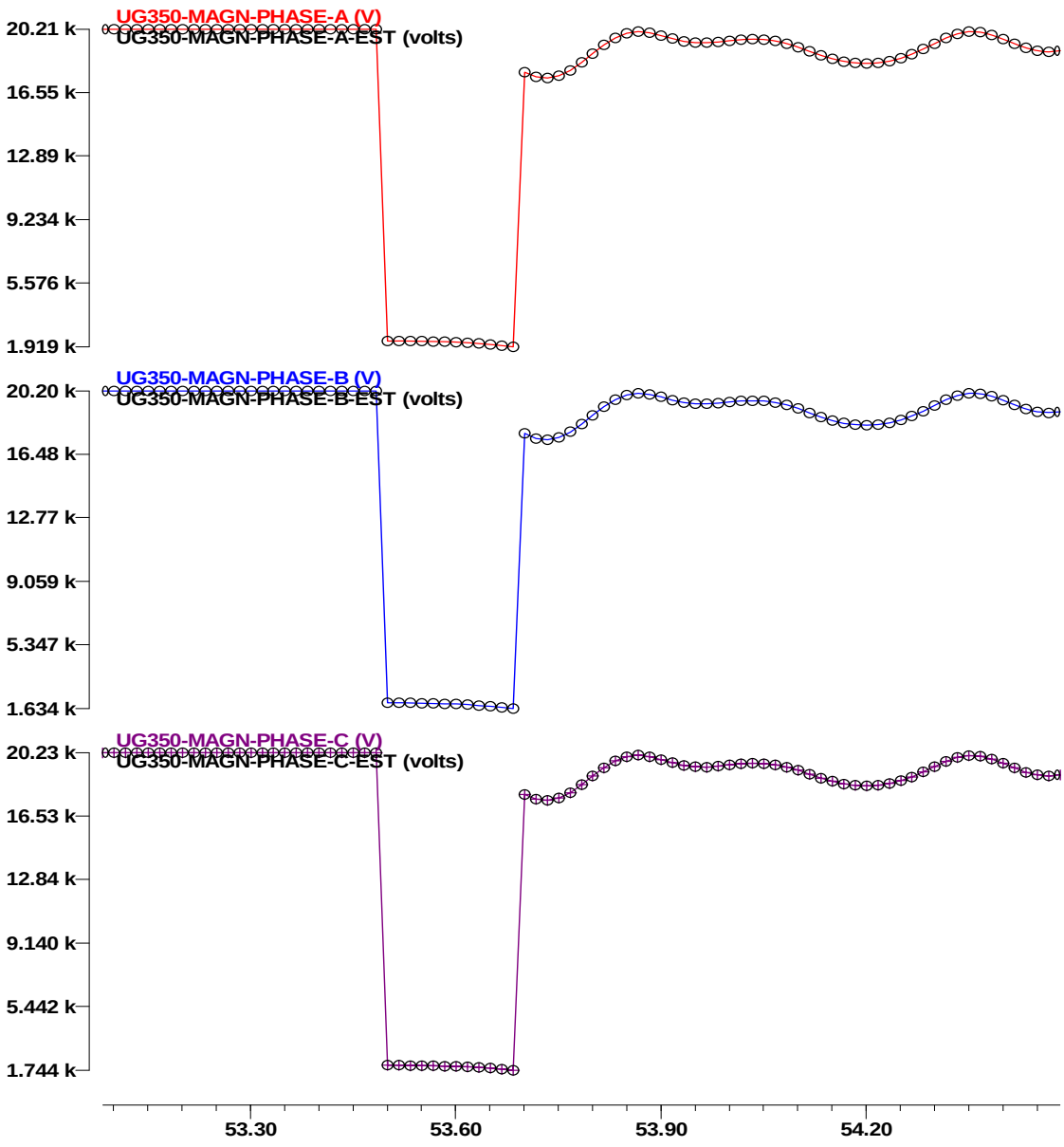

Figure 5.11. Simulated and estimated voltage magnitude of bus UG350.

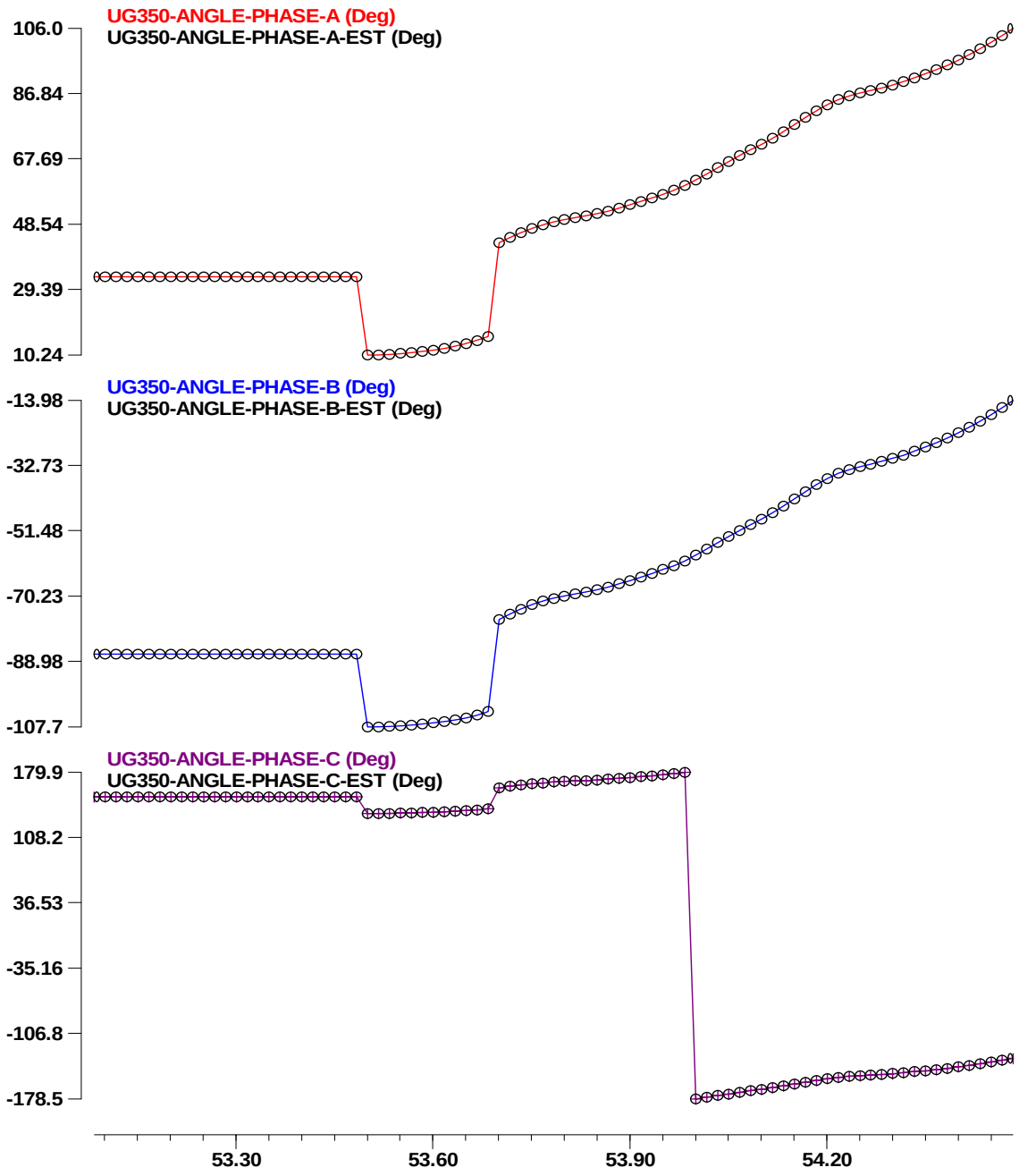

Figure 5.12. Simulated and estimated voltage phase angle of bus UG350.

Timing results were performed for the execution of DSE-Q on the Longbay Substation. Table 5.1 summarizes the number of the system states, the actual measurements and the total measurements (both actual and virtual measurements). The average execution time for each time step is 0.42 msec with a variability of 0.05 msec. The timing experiments were performed on a personal computer with a i7-860, 2.8 GHz processor and 8 GB

RAM. As a result, the timing results prove that a real-time execution of DSE-Q in the substation level with one estimation per cycle is feasible.

Table 5.1. Timing experiment summary of the DSE-Q for LongBay substation.

System States	**82**
Actual Measurements	**171**
Total Measurements (Actual + Virtual)	**784**
Average QSE Execution Time per Time Step	**0.42 msec**
Variability	**0.05 msec**

5.2.4 USVI RHPP DSE-Q

The DSE-Q was also implemented and tested for the RHPP Substation of the US Virgin Islands system. A description of the RHPP substation model is given in Appendix D. The results include steady state and transient conditions after a three-phase fault that was simulated close to LongBay substation. The estimation time step was 16.6 msec (1 estimation per cycle). Figure 5.13 to Figure 5.18 illustrate demonstrative results of the estimated states. The estimation results (circles) are superimposed on the simulation results. In particular, Figure 5.13 and Figure 5.14 illustrate the voltage magnitudes and phase angles of three phases for bus FDR11-GC (substation terminal bus) respectively. Figure 5.15 and Figure 5.16 illustrate the voltage magnitudes and phase angles of three phases for bus XF15-2 (substation transformer) respectively. Finally Figure 5.17 and Figure 5.18 illustrate the voltage magnitudes and phase angles of three phases for bus UG388 (neighboring substation terminal bus).

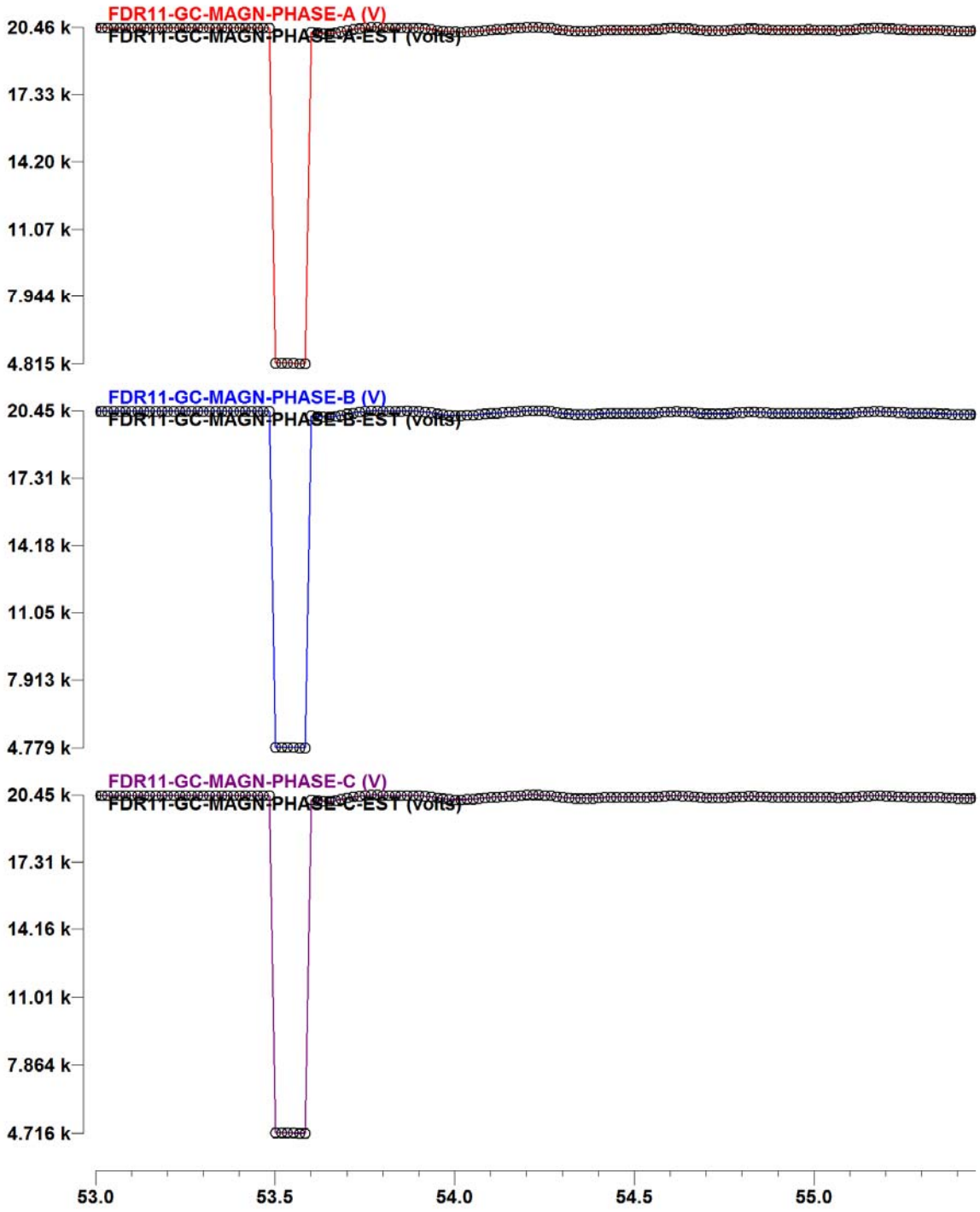

Figure 5.13. Estimated and simulated voltage magnitude of bus FDR11-GC.

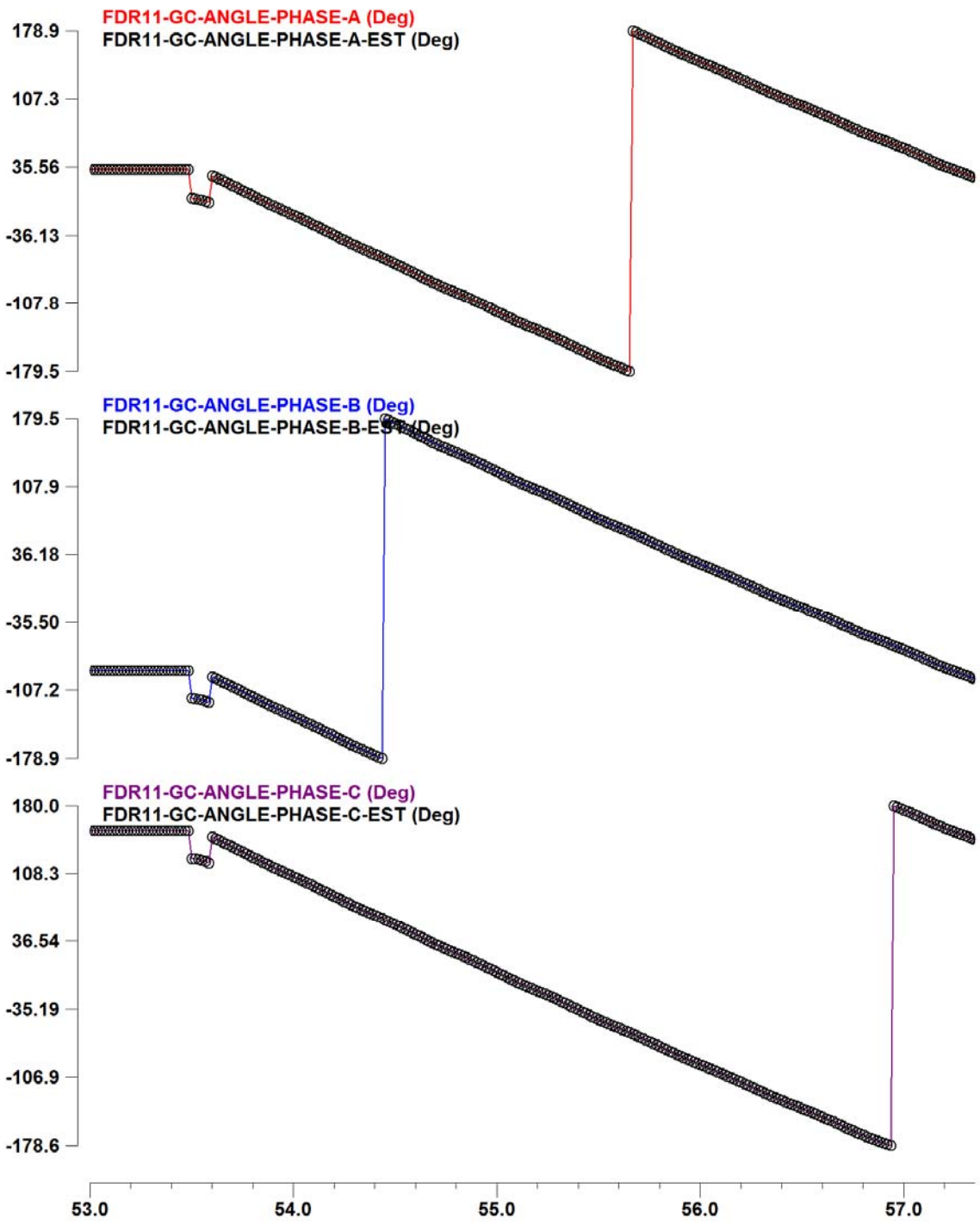

Figure 5.14. Estimated and simulated voltage phase angle of bus FDR11-GC.

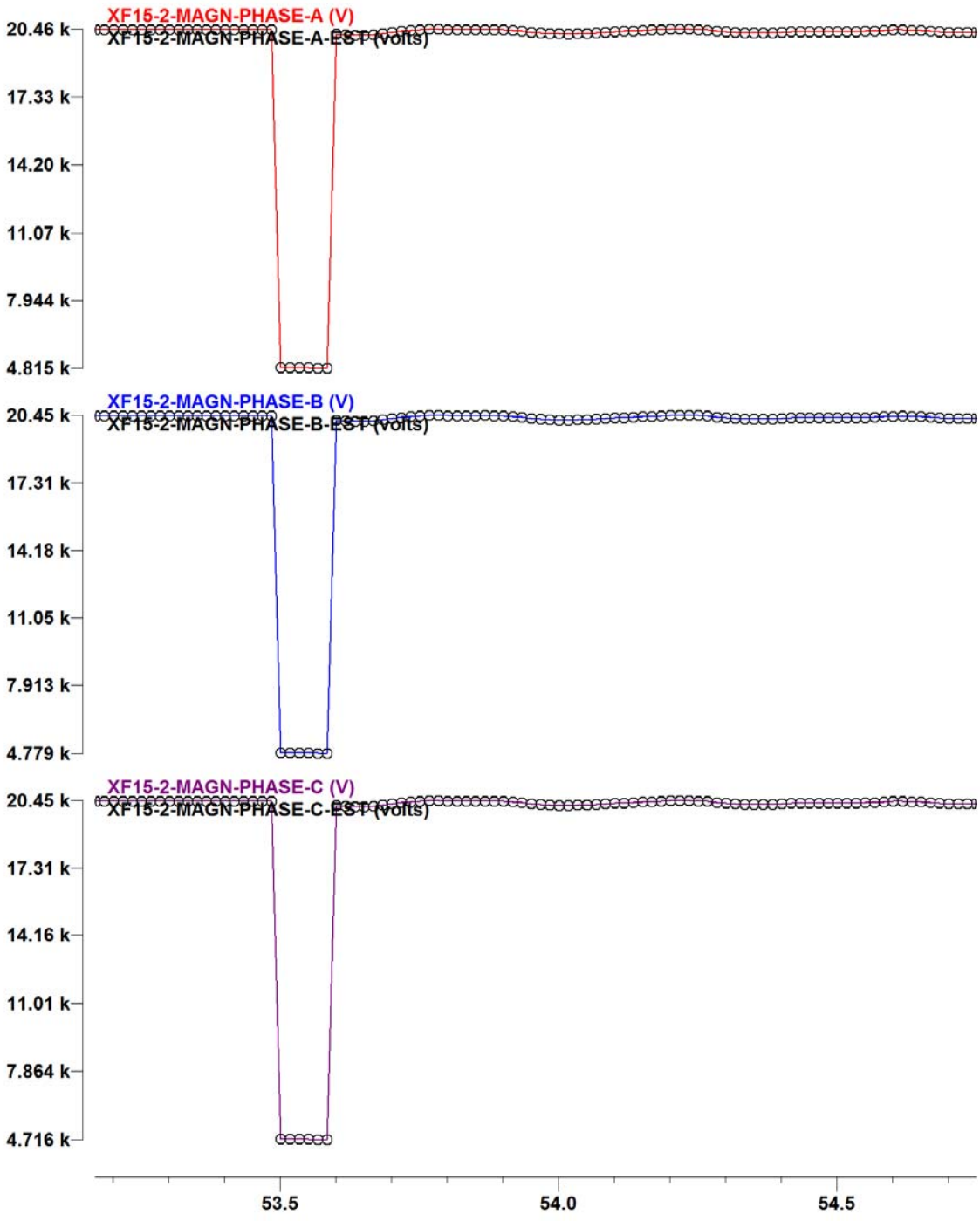

Figure 5.15. Estimated and simulated voltage magnitude of bus XF15-2.

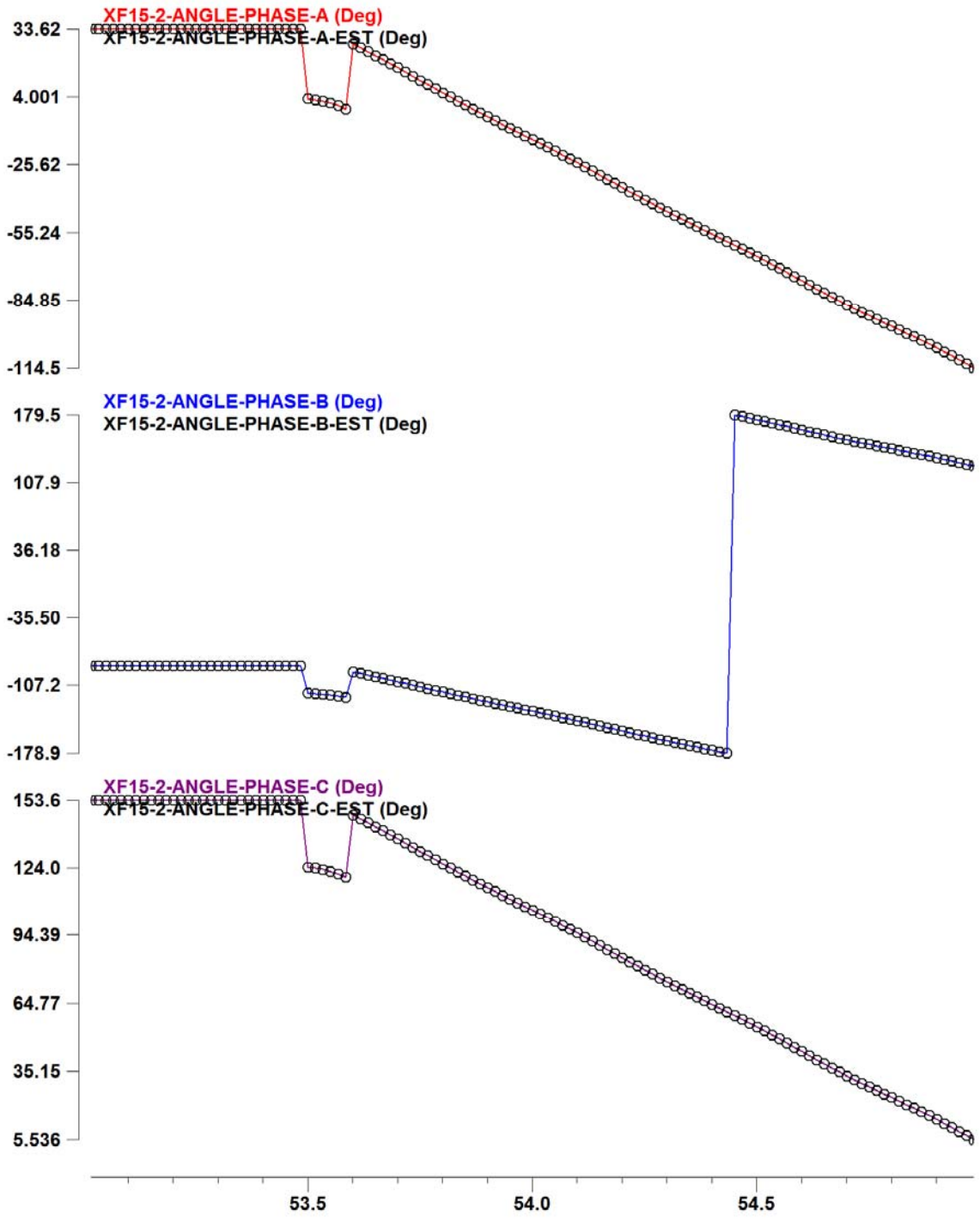

Figure 5.16. Estimated and simulated voltage phase angle of bus XF15-2.

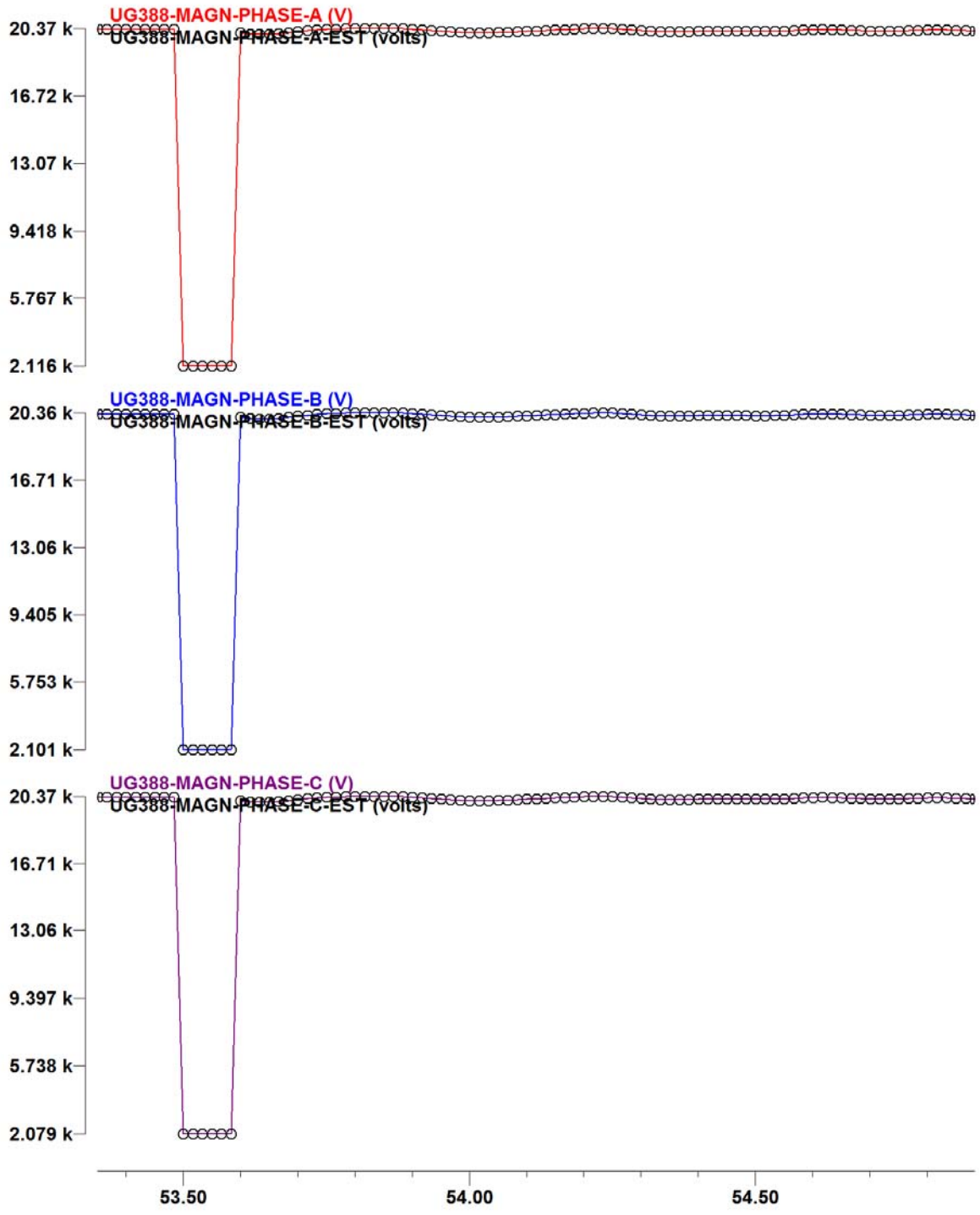

Figure 5.17. Estimated and simulated voltage magnitude of bus UG388.

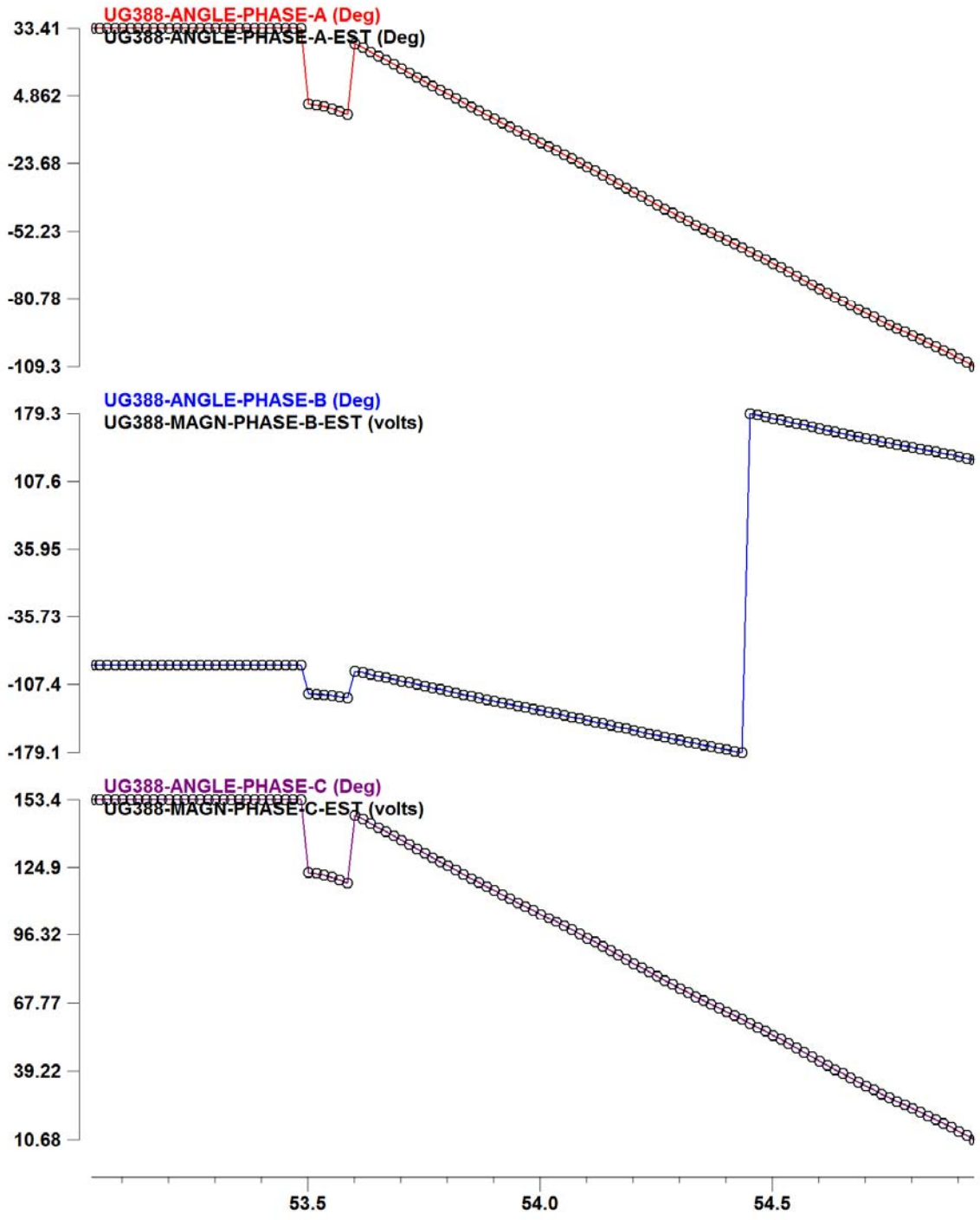

Figure 5.18. Estimated and simulated voltage phase angle of bus UG388.

Table 5.2 summarizes the number of the system states, the actual measurements and the total measurement (both actual and virtual measurements). The average execution time for each time step is 0.4 msec with a variability of 0.04 msec.

Table 5.2. Timing experiment summary of the DSE-Q for RHPP Substation

System States	**66**
Actual Measurements	**176**
Total Measurements (Actual + Virtual)	**824**
Average QSE Execution Time per Time Step	**0.4 msec**
Variability	**0.04 msec**

5.2.5 NYPA Blenheim-Gilboa Plant DSE-Q

The DSE-Q was implemented on the NYPA's system (Blenheim-Gilboa Plant), which has a full description on Appendix C. Synchronized voltage and current measurements from both sides of the 4 step-up transformers of the 278 MVA generators, and synchronized voltage and current measurements at the substation terminals of the 345 kV transmission lines of Fraser-Gilboa, Gilboa-New Scotland, and Gilboa-Leeds, were assumed. To verify the validity of the DSE-Q, a three-phase line to ground fault is simulated near the bus BG-FRAZER and the estimation results show that the DSE-Q can capture the dynamic behavior of the system due to the fault with high accuracy, both for the states inside the NYPA substation and the states at the remote sides of the 345 kV transmission lines. Figure 5.19 to Figure 5.24 show the voltage magnitudes and phases of the buses BG_UNIT1 (generator terminals), BG_LEEDS (high side of the step-up transformer) and LEEDS345 (remote side of the 345 kV transmission line) respectively.

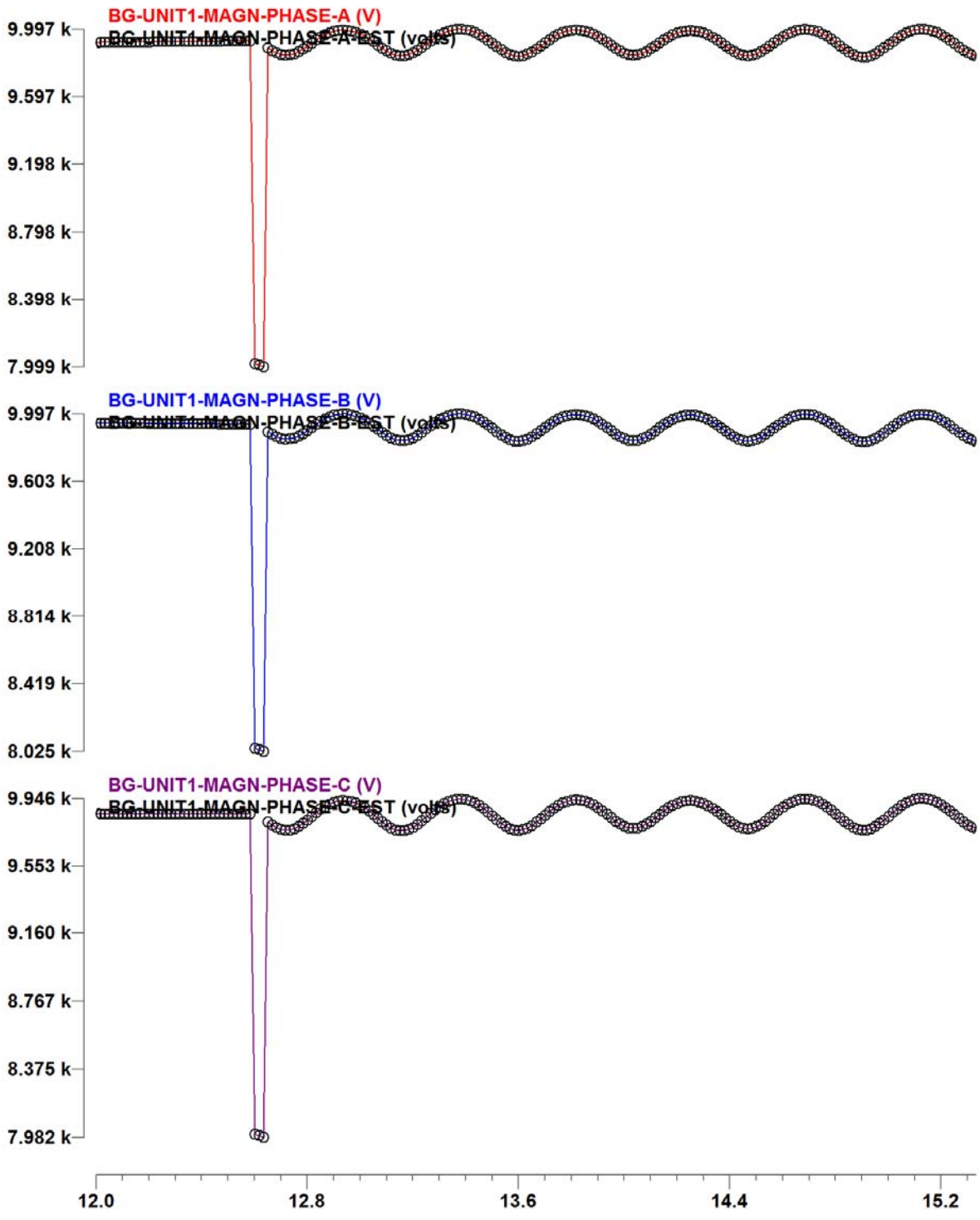

Figure 5.19. Simulated and estimated voltage magnitude of bus BG-UNIT1.

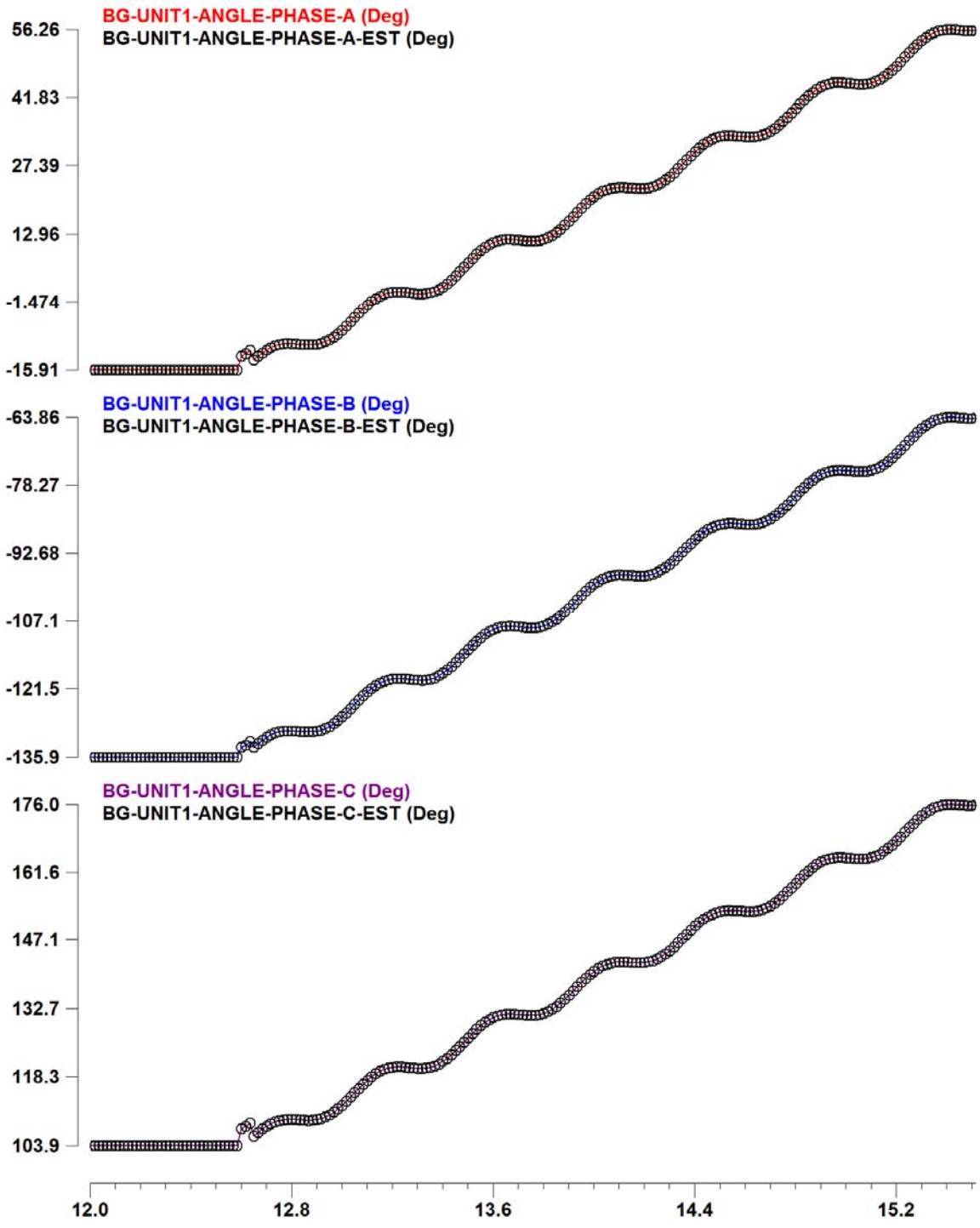

Figure 5.20. Simulated and estimated voltage phase angle of bus BG-UNIT1.

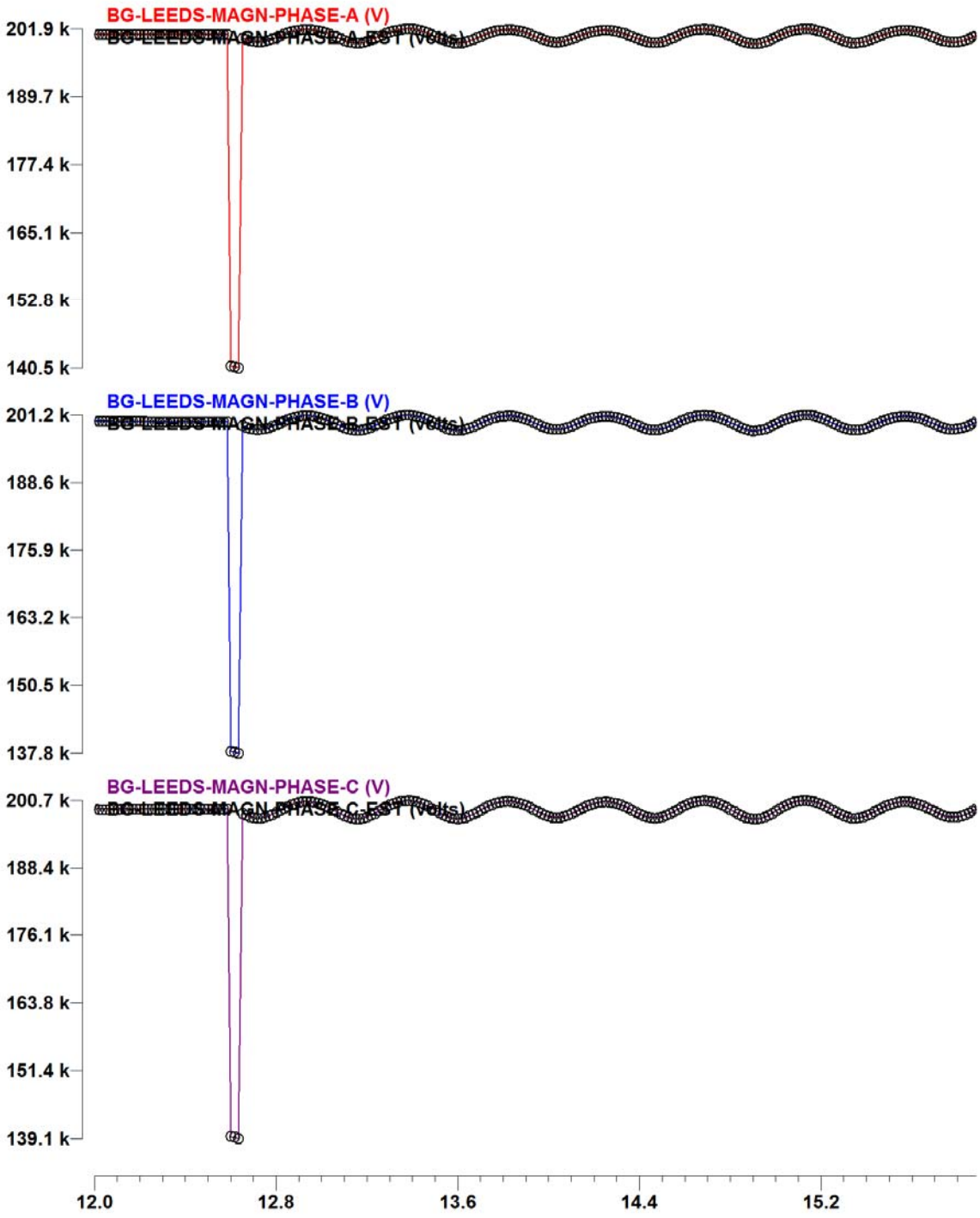

Figure 5.21. Simulated and estimated voltage magnitude of bus BG_LEEDS.

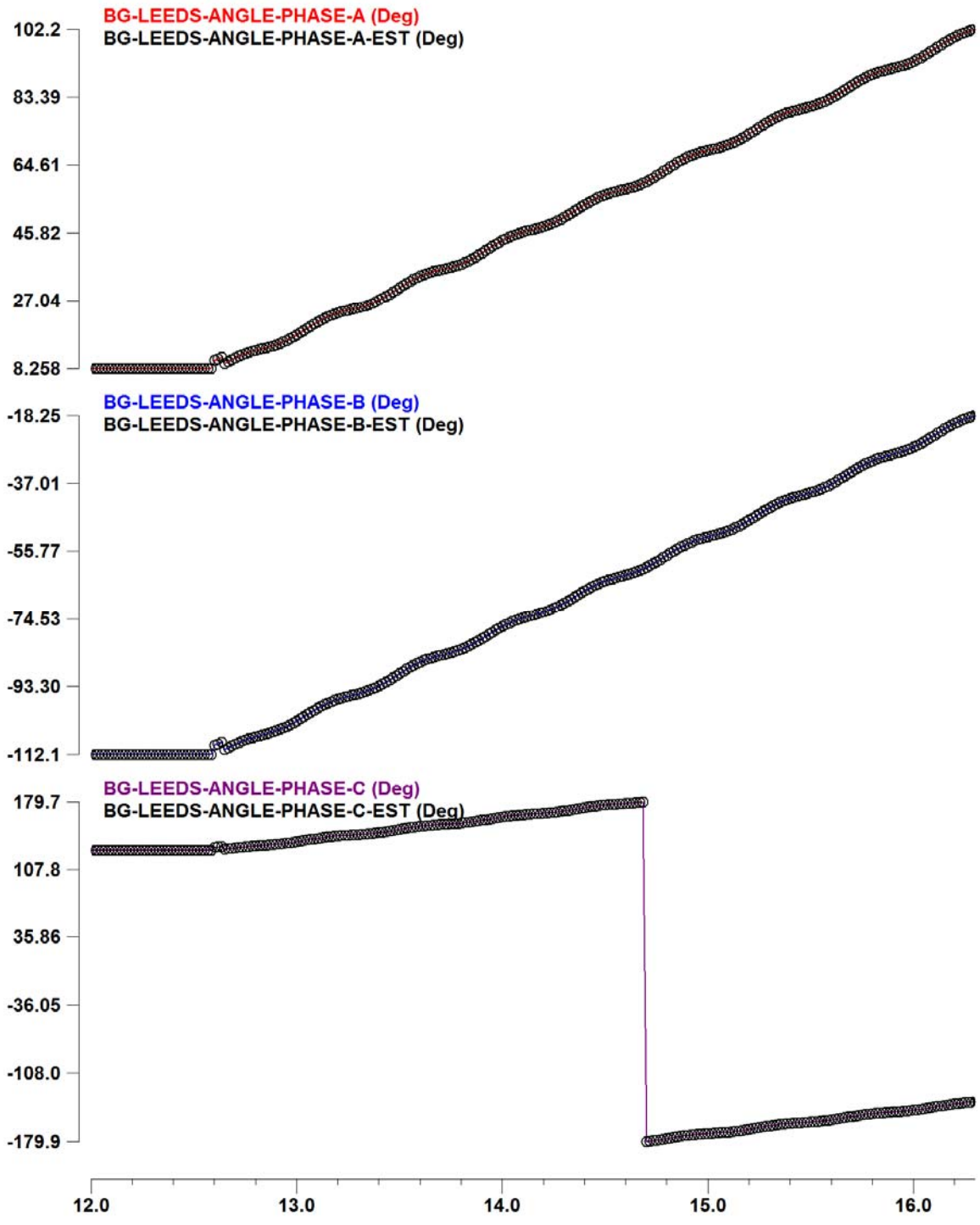

Figure 5.22. Simulated and estimated voltage phase angle of bus BG-LEEDS.

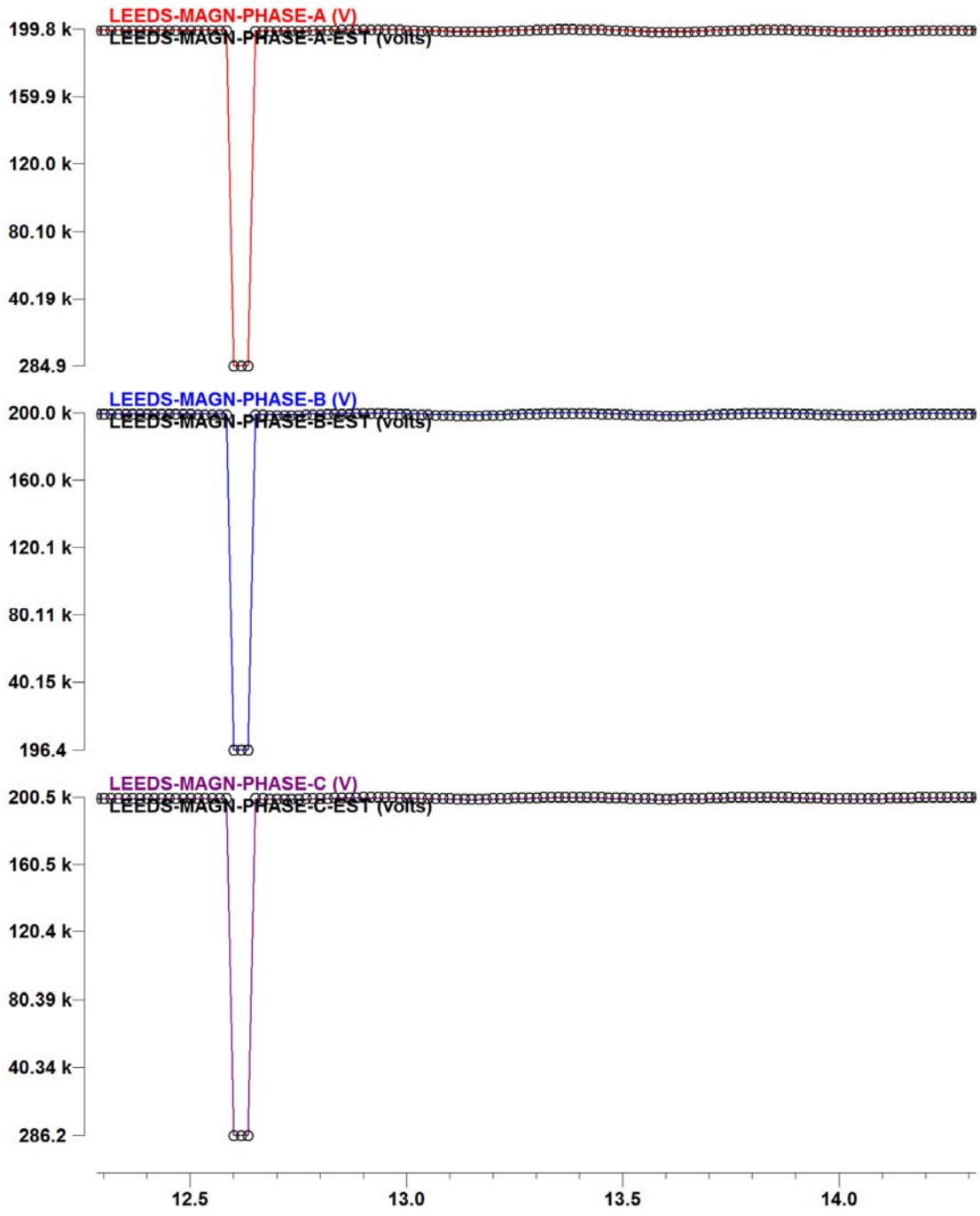

Figure 5.23. Simulated and estimated voltage magnitude of bus LEEDS.

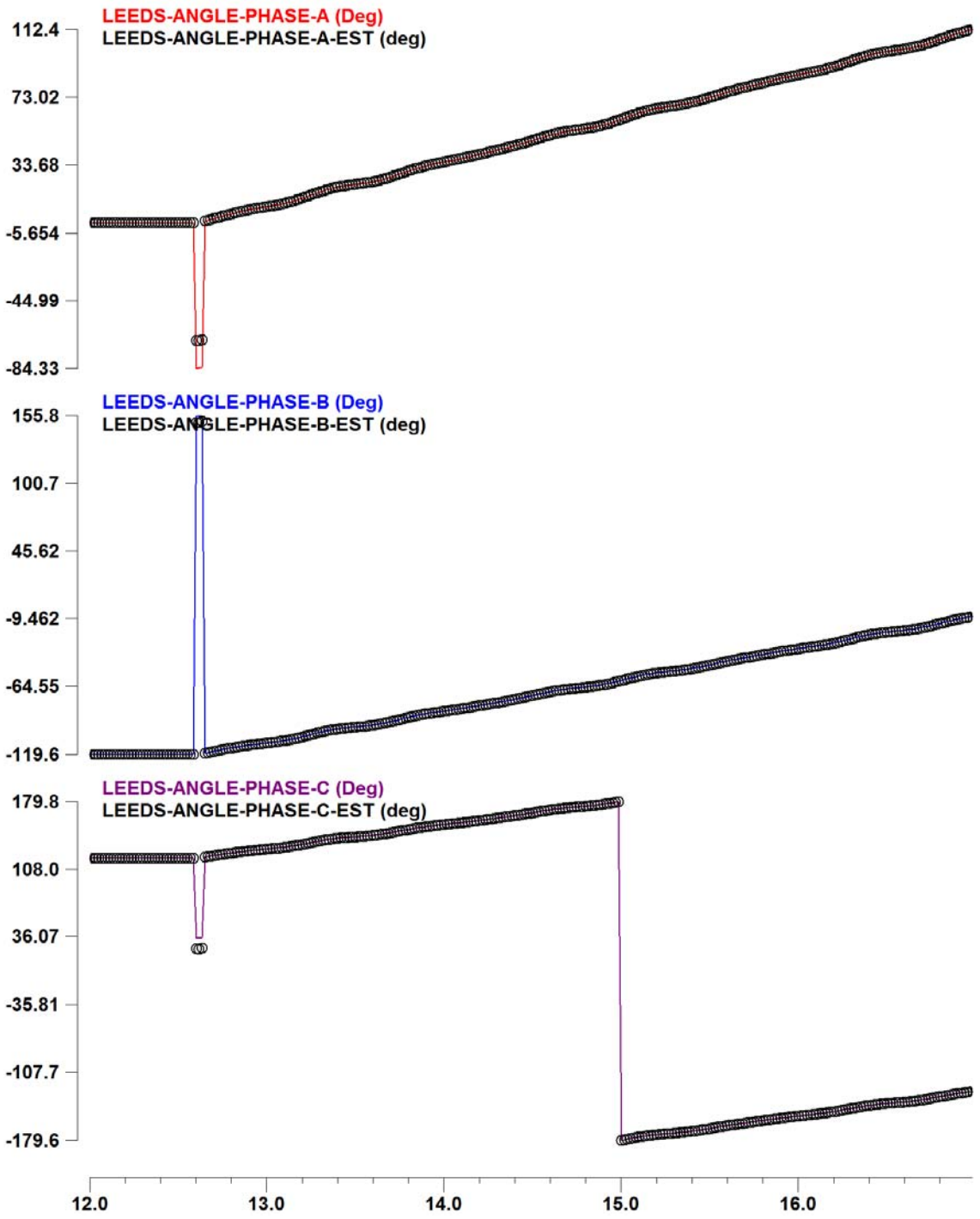

Figure 5.24. Simulated and estimated voltage phase angle of bus LEEDS.

Table 5.3 summarizes the number of the system states, the actual measurements and the total measurement (both actual and virtual measurements) in the QSE. The average execution time for each time step is 0.51 msec with a variability of 0.05 msec. This timing is for a system with all measurements being GPS synchronized.

Table 5.3. Timing experiment summary of the DSE-Q for NYPA system

System States	**58**
Actual Measurements	**192**
Total Measurements (Actual + Virtual)	**880**
Average QSE Execution Time per Time Step	**0.51 msec**
Variability	**0.05 msec**

5.3 DSE-T Results

5.3.1 NYPA Blenheim-Gilboa Plant DSE-T

This section illustrates results from the execution of DSE-T on NYPA's Blenheim-Gilboa substation. The results include steady state and transient conditions after a three-phase fault that was simulated close to RHPP substation. The estimation time step was 0.5 msec. Figure 5.25 and Figure 5.26 illustrate demonstrative results of the estimated states. The estimation results (dotted lines) are superimposed on the simulation results (solid lines). In particular, Figure 5.25 illustrates the three-phase voltage of bus BG-GA345, while Figure 5.26 illustrates the three-phase voltage of bus BG-Unit1. Note that in DSE-T the time domain waveforms of the corresponding quantities are estimated. The results show that the estimation is highly accurate both for pre fault but also for post fault conditions.

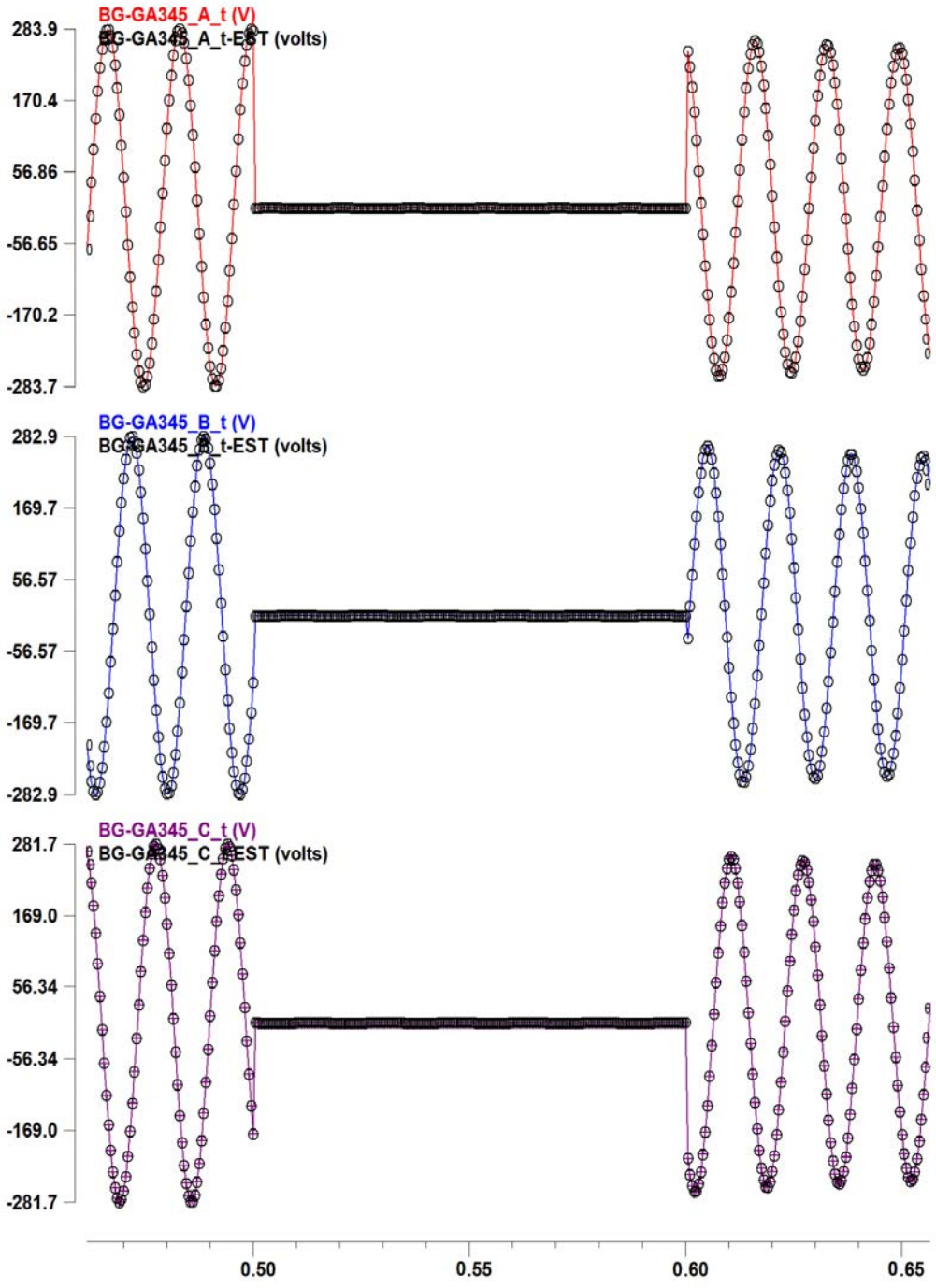

Figure 5.25. Simulated and estimated voltage of bus BG-GA345.

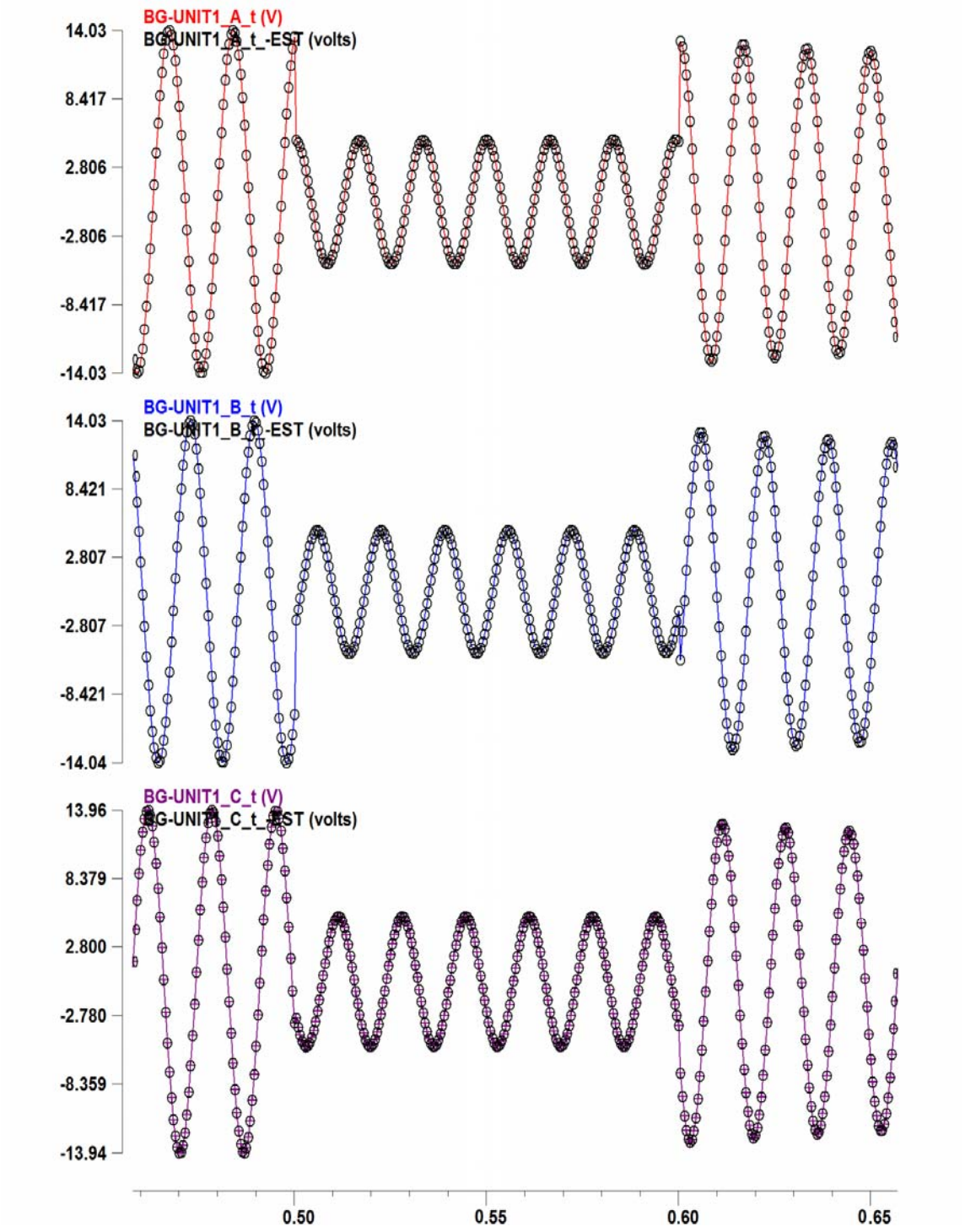

Figure 5.26. Simulated and estimated voltage of bus BG-Unit1.

5.4 Summary

In this chapter numerical experiments on the DSE were initially performed on dynamic generator models. The developed DSE has been also tested on actual substations of NYPA and USVI systems. For these cases timing experiments have been also performed. It is concluded that DSE can capture with high accuracy the dynamics of the system. In addition, the timing results validated that DSE can be performed at rates of 60 times per second for a typical substation.

6 DEMONSTRATING EXAMPLES: TRANSIENT STABILITY MONITORING AND GENERATOR OUT-OF-STEP PROTECTION SCHEME

6.1 Overview

In this chapter, demonstrating results on the transient stability monitoring and generator out-of-step protection scheme are presented. Initially, the method is demonstrated on a simple, two-machine system which is used as a proof-of-concept test case. In this system, results are presented assuming that information is available from both substations, but also for the case where only information from the substation of interest is used, in which case the concept of the calculation of the CoO is used.

Next, in section 6.3, the schemes are presented on a five substation system for a specific fault scenario. In this case a single CoO point exists in the system and is computed. In section 6.4, a three substation system is tested for a specific fault scenario, with the difference that in this case multiple CoOs exist in the system. In section 6.5, the scheme is implemented on the NYPA's Blenheim Gilboa plant, where also multiple CoOs exist. For all the examined test cases, the developed predictive generator out-of-step protection scheme is compared with the state-of-the-art, impedance trajectory monitoring based out-of-step protection method, and the superiority of the developed method in terms of the time when instability is detected, is evaluated.

Finally, in section 6.6 a test case is demonstrated and discussed, in which the CoO is found to be outside the observable area of the substation of interest.

6.2 Two-Machine System - Proof of Concept Test Case

In this section, the proposed transient stability and generator out-of-step protection scheme is demonstrated on a two substation system with two generating units, two step-up transformers and two overhead transmission lines connected in parallel as is illustrated in Figure 6.1. The parameters of the system are presented in Table 6.1.

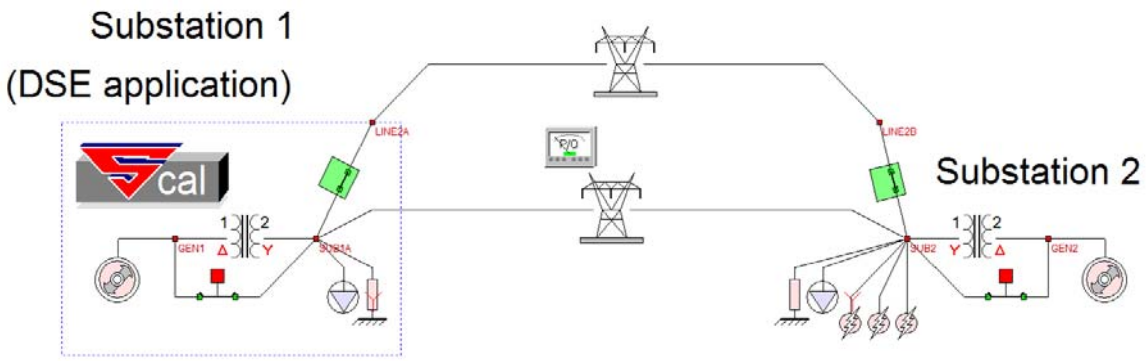

Figure 6.1. Single line diagram of the two generator system.

Table 6.1. Test system parameters.

Gen1	100MVA	z= 0.001+j0.18 pu	H=2.5 sec	15 kV
Gen2	200MVA	z= 0.001+j0.18 pu	H= 3.0 sec	18 kV
XFMR1	100MVA	z=0.001+j0.07 pu	15 kV/115kV	
XFMR2	200MVA	z=0.001+j0.08 pu	115 kV/18kV	
Transmission Line 1		z=0.028+0.2698 pu	115 kV	50 miles
Transmission Line 2		z=0.028+0.2698 pu	115 kV	50 miles
Load 1		S=0.4+j0.1 pu	115 kV	
Load 2		S=1.5+j0.2 pu	115 kV	
Common S_{base}=100 MVA				

Here the focus is on the stability monitoring and out-of-step protection of the generator in the first substation, which is the substation of interest. The fault scenario that is examined is a three-phase fault at the terminal of the second substation. The system is simulated in WinIGS.

6.2.1 Using data from both substations

In this section, the energy based transient stability monitoring of the system is demonstrated assuming that the required information (generator's torque angle and speed) is available from both substations.

In particular, a single machine equivalent is derived using the equations presented in section 4.3.2. For this test system, the equilibrium point of the post fault system is computed to be at:

$$\delta_s = \delta_{s1} - \delta_{s2} = 18.17^0 - 5.03^0 = 13.14^0$$

Two test cases have been simulated. The first one corresponds to a three-phase fault that resulted in a stable system, and the second case corresponds to a three-phase fault that resulted in an unstable case. The fault is initiated at t=1 sec. The duration of the fault was 0.3 sec in the stable case and 0.4 sec in the unstable one. The fault is cleared by disconnecting the second (upper) transmission line. In Tables Table 6.2Table 6.3 the generators' torque angles and speeds at the fault clearing time are given.

Table 6.2. Generators' torque angle & frequency at fault clearing time – stable scenario.

Generator 1	Generator 2
δ_1=154.3 deg	δ_2=80.7 deg
f_1=62.57 Hz	f_2=61.4 Hz

Table 6.3. Generators' torque angle & frequency at fault clearing time – unstable scenario.

Generator 1	Generator 2
δ_1=262.2 deg	δ_2=139.1 deg
f_1=63.41 Hz	f_2=61.85 Hz

The total energy (sum of potential and kinetic energy) of the system is computed next using equations 4.17-4.22. Figure 6.2 illustrates the total energy of the system superposed on the corresponding potential energy function for the stable case at the time when the fault was cleared (t=1.3 sec). It is clear in this case that the total energy is below the highest value of the potential energy, thus indicating a stable system.

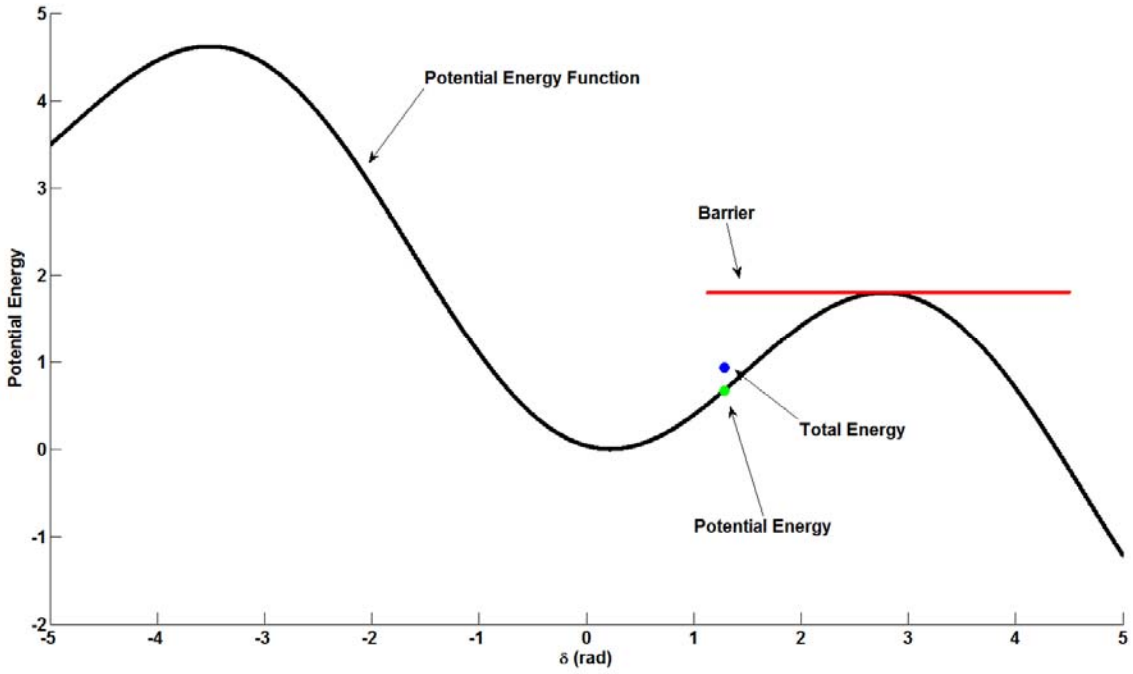

Figure 6.2. Total and potential system energy - stable case.

In Figure 6.3 the unstable case is depicted. Note that in this case, the total energy at the fault clearing time (t=1.4 sec) exceeds the highest value of the potential energy function, thus indicating an unstable system.

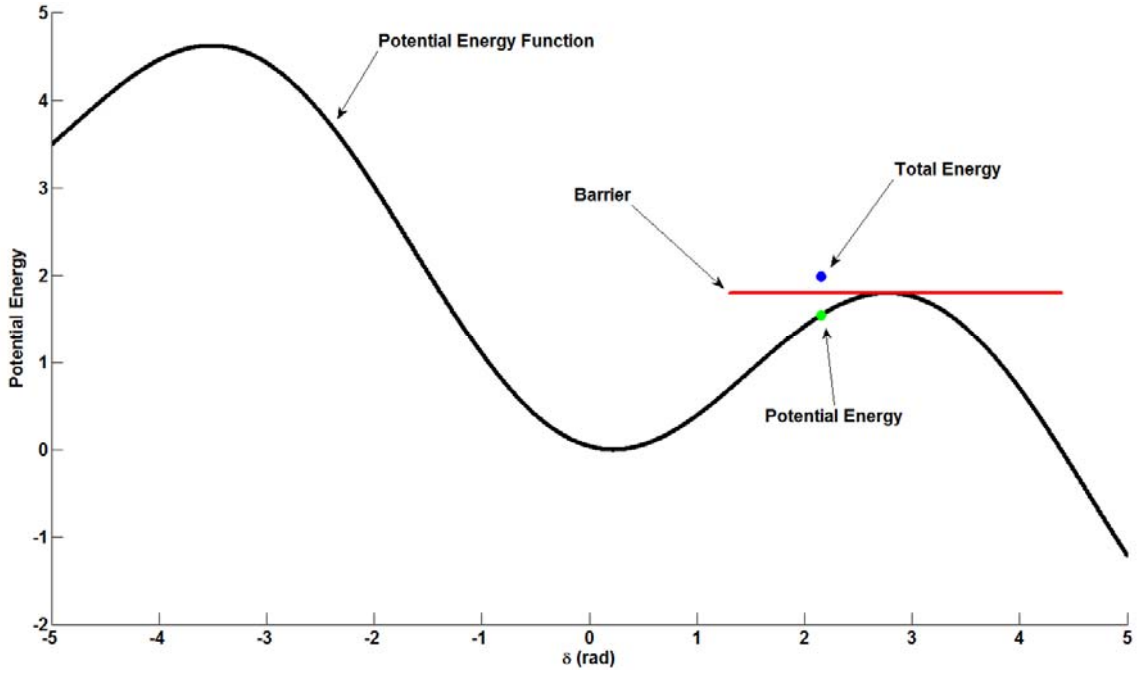

Figure 6.3. Total and potential system energy - unstable case.

Next, it is illustrated how the proposed out-of-step protection scheme can predict instability before its occurrence for the unstable scenario described before. In particular, Figure 6.4 illustrates the trajectory of the potential and total energy of the generator for the unstable scenario. The total energy is continuously monitored and compared to the peak (barrier) value of the potential energy. When the total energy becomes higher than the barrier value, this indicates instability and a trip signal is issued to the generator. Note that this is a totally predictive out-of-step scheme that is taking place in real time. Specifically, in the described unstable scenario the fault is cleared at t=1.4 sec (0.4 sec after its initiation). Visualization of the total energy trajectory as illustrated in Figure 6.4 verifies that instability is asserted when δ=109.5 degrees at t=1.37 seconds.

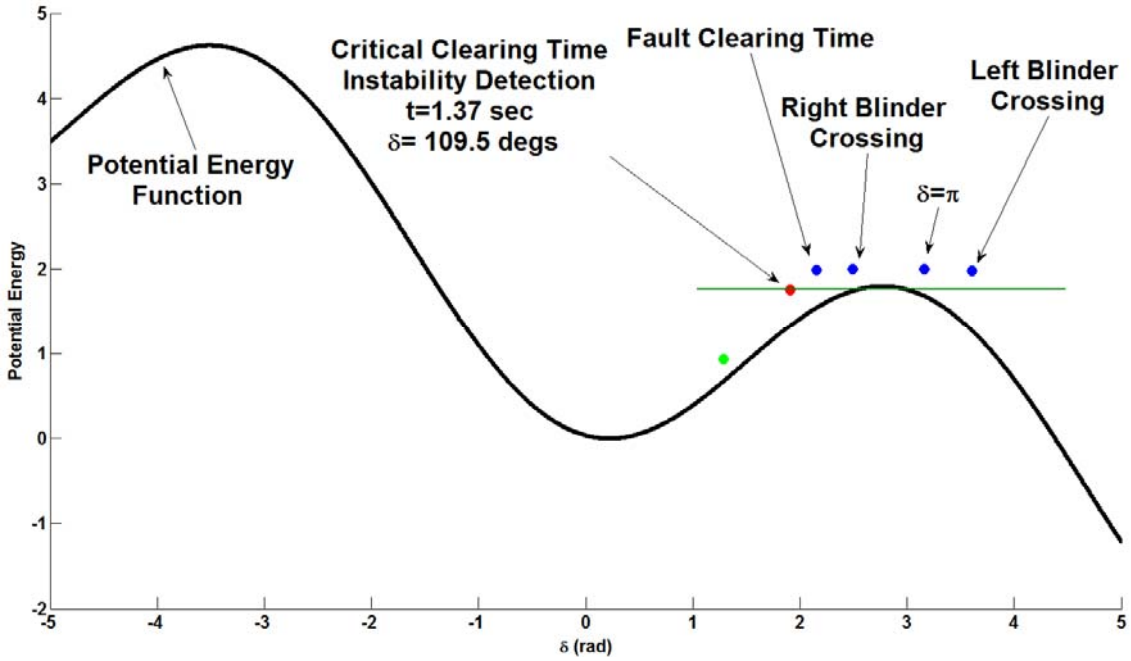

Figure 6.4. Total and potential system energy trajectory.

Next, the energy based scheme for stability monitoring and out-of-step protection is compared with the single blinder out-of-step protection method. In order to perform the comparison, the out-of-step function of the impedance relay is simulated for the same unstable scenario. Observing Figure 6.5, it is evaluated that the impedance trajectory crosses the right blinder at t=1.44 seconds. The left blinder is crossed at t=1.58 seconds. Additional delay is needed before generator tripping is issued. As a result the proposed approach and the generator total energy visualization predicted instability 0.21 seconds before the impedance relay, without considering additional delay of the impedance relay tripping due to the high value of the angle when the instability is detected. Note that comparison of Figure 6.4 and Figure 6.5 illustrates that in the developed scheme, instability detection was achieved before the fault clearing time, when the impedance was still between the two blinders (Figure 6.5- During Fault point).

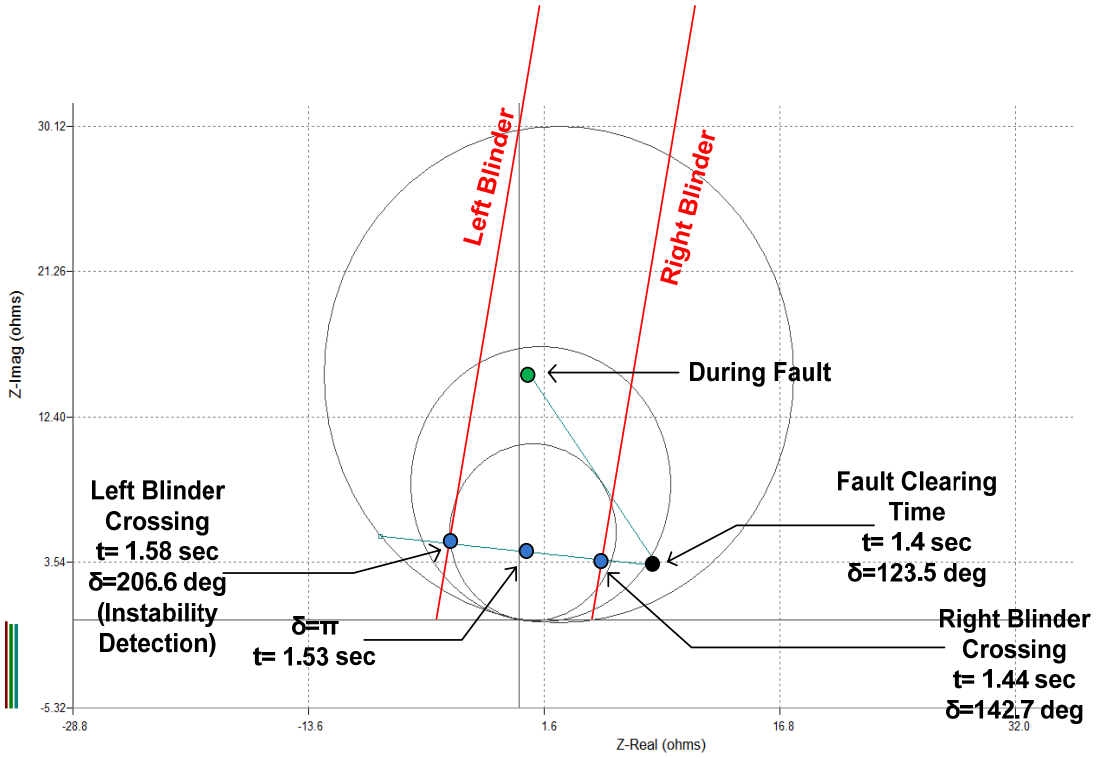

Figure 6.5. Impedance trajectory monitoring.

6.2.2 Using data only from the substation of interest

The same test case is presented here, with the difference that now it is assumed that only information from the DSE that is performed at the substation of interest is available. In this case, which is the general case since for the developed scheme only information from the substation of interest is utilized, the potential energy function and the total energy of the generator of interest are computed in real time, in terms of the CoO as described in section 4.3.

The energy of the system is computed next for two time instants, t=1.25 sec and t=1.37 sec. In particular, the energy of the system is computed at time t=1.25 sec. Assuming that this is the fault clearing time, after a few cycles simulation of the system, the frequency at the two ends of the line that connects the two substations is given in Figure 6.6. Given the frequency at the two terminals of the line it is concluded that the CoO is within this line and it is evaluated by the optimization method described in section 4.3.1. The results are summarized in Table 6.4.

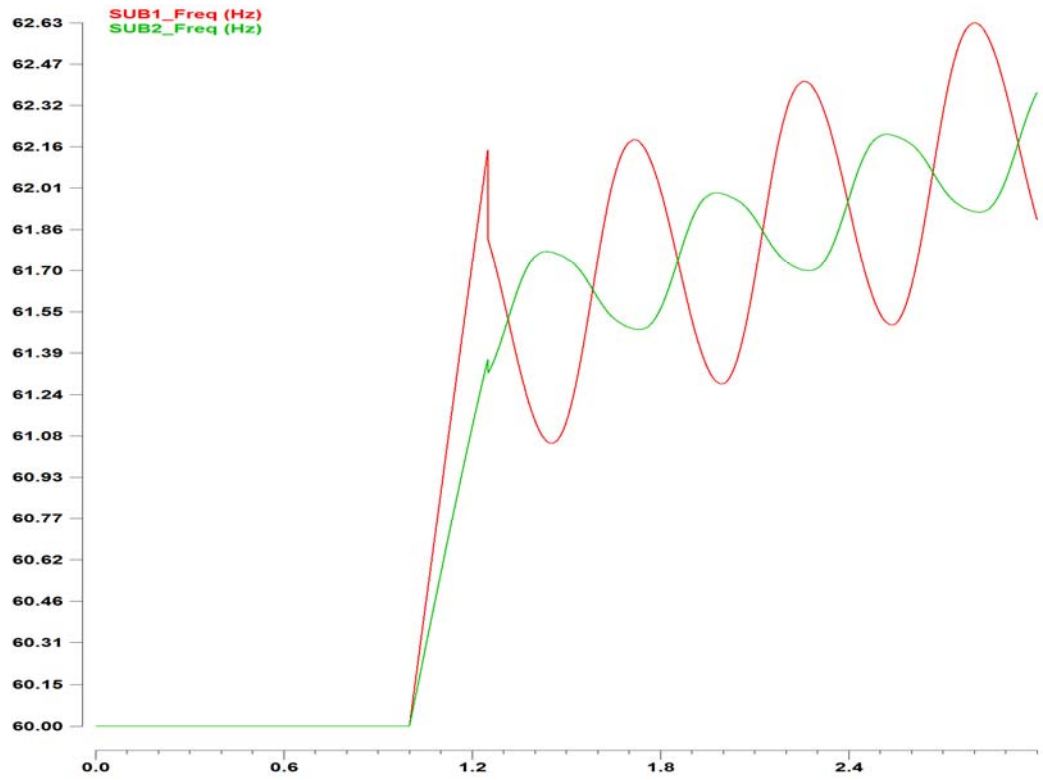

Figure 6.6. Frequency at the terminals of the line - fault clearing time t=1.25 sec.

Table 6.4. CoO calculation results - fault clearing time t=1.25 sec.

Line	α	b	c	CoO Length (miles)(away from Sub1)	Line Length (miles)	Coo Frequency Equation
SUB1-SUB2	0.36	61.49	0.42	32.0	50.0	$f_{CoO}(t) = 61.49 + 0.42 \cdot t$

The frequency at the two terminals of the line, along with the simulated frequency at the CoO and the equation of the frequency of the CoO are shown in Figure 6.7. Note that the simulated frequency at the CoO is well approximated by the computed CoO frequency.

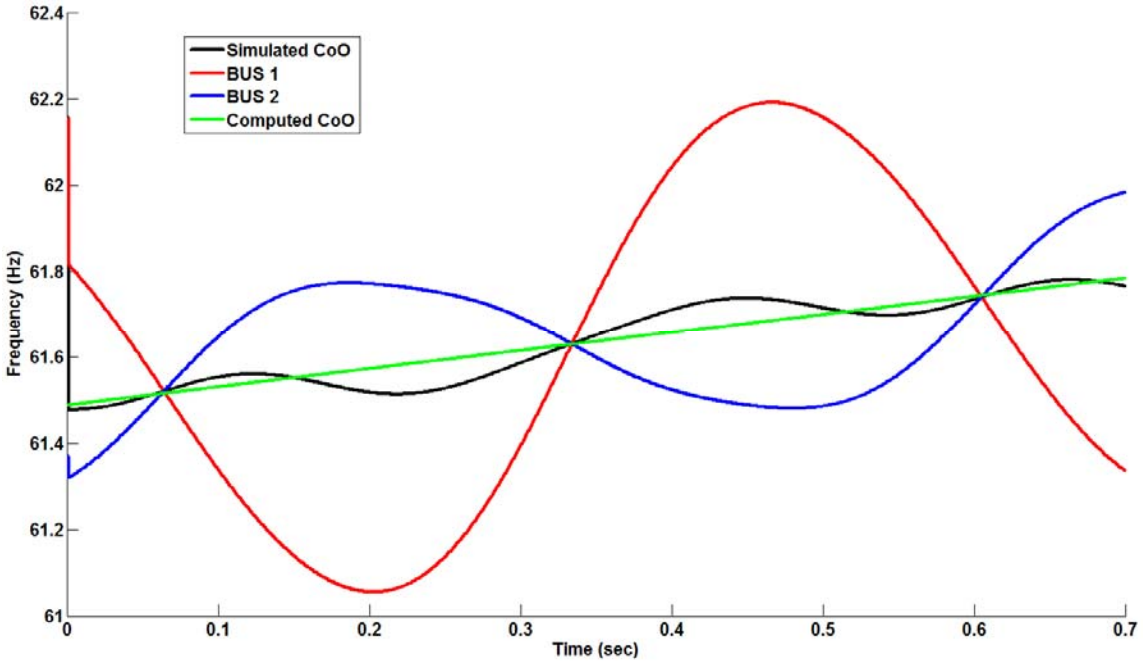

Figure 6.7. Comparison of simulated and computed CoO frequency - fault clearing time t=1.25 sec.

Once the CoO is computed, a two generator equivalent was built as explained in section 4.3.2. The equivalent is shown in Figure 6.8.

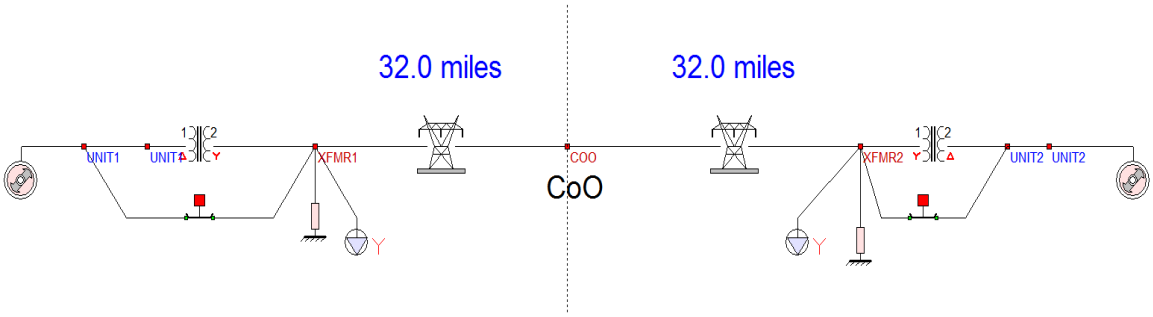

Figure 6.8. Equivalent system - fault clearing time t=1.25 sec.

In order to evaluate the accuracy of the equivalent model, the dynamics of the original system and the equivalent system are compared. In particular, the initial conditions (torque angle and speed) of the generator in the substation of interest were set to the values that the system had at the assumed fault clearing time. The initial conditions (torque angle and speed) of the generator in the second substation (mirror image part of the system) were set to be symmetric to the initial conditions of the first generator in

terms of the CoO, as explained in section 4.3.2. The initial conditions at the equivalent system are given in Table 6.5.

Table 6.5. Generators' torque angle & frequency - fault clearing time t=1.25 sec.

Generator 1	CoO	Generator 2
δ_1=113.3 deg	δ_{CoO}=68.0 deg	δ_2=22.6 deg
f_1=62.2 Hz	f_{CoO}=61.52 Hz	f_2=60.82 Hz

The torque angle and frequency of the generator of interest, the CoO phase angle and the relative angle between the generator's torque angle and the CoO phase angle are compared between the original and the equivalent system in Figure 6.9. As expected, the dynamics of the equivalent system are very close to the dynamics of the original system.

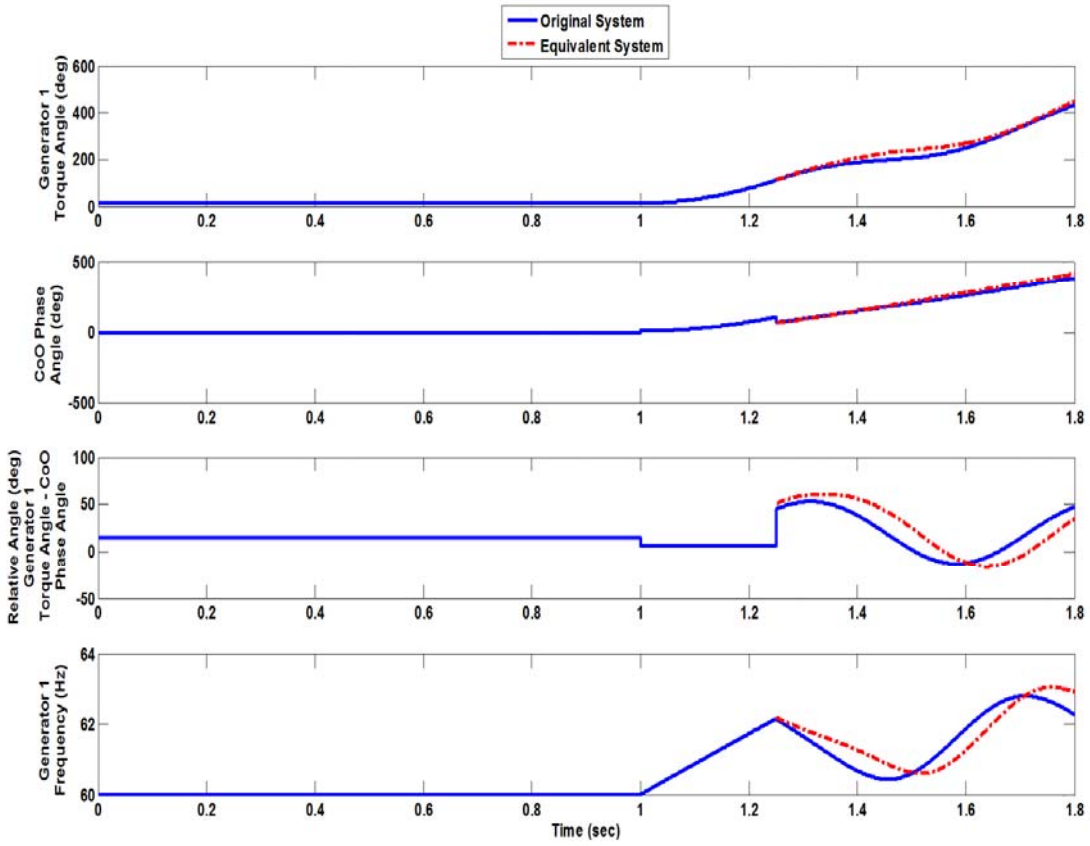

Figure 6.9. Comparison of original and equivalent system dynamics - fault clearing time t=1.25 sec.

In order to evaluate the stability of the system for this assumed fault clearing time, the potential energy function of the equivalent system was evaluated. The total energy of the system is also computed and it is superposed on the corresponding potential energy function, as illustrated in Figure 6.10. For this computation the torque angle and the frequency of the two generators of the equivalent system at the assumed clearing time (Table 6.5) are used. Note that the total energy is below the barrier, thus indicating that the system is stable.

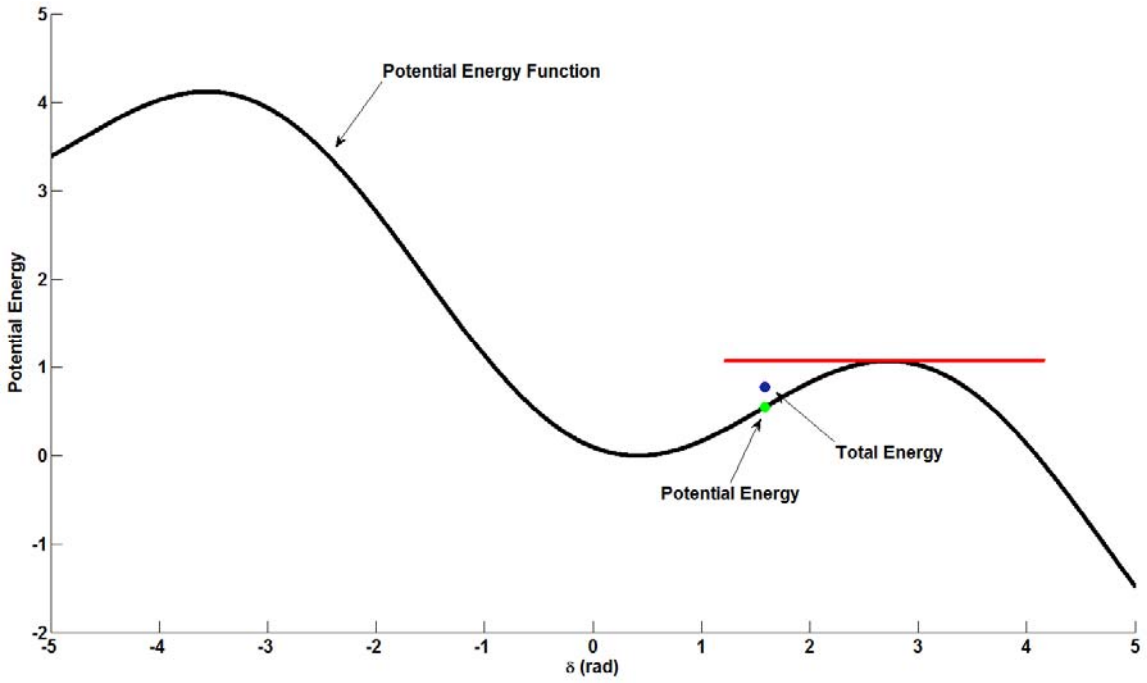

Figure 6.10. System total energy evaluation and stability characterization - fault clearing time t=1.25 sec.

The same steps as before are followed again for the time instant t=1.37 sec. In particular, assuming that this is the fault clearing time, the frequency at the two ends of the line is simulated for a few cycles as shown in Figure 6.11. Given the frequency at the two terminals of the line, the CoO is computed to be within this line, as shown in the results in Table 6.6.

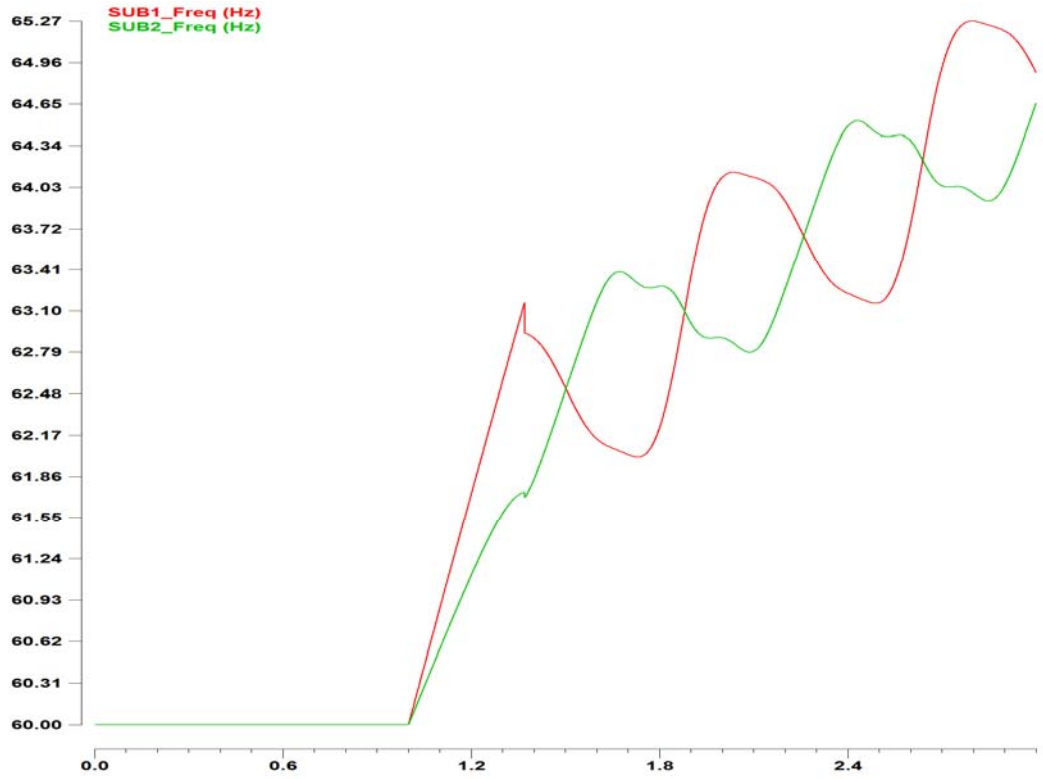

Figure 6.11. Frequency at the terminals of the line - fault clearing time t=1.37 sec.

Table 6.6. CoO calculation results - fault clearing time t=1.37 sec.

Line	α	b	c	CoO Length (miles)(away from Sub1)	Line Length (miles)	Coo Frequency Equation
SUB1-SUB2	0.72	62.28	1.63	14.0	50.0	$f_{CoO}(t) = 62.28 + 1.63 \cdot t$

The frequency at the two terminals of the line, along with the simulated frequency at the CoO is computed and the equation of the frequency of the CoO are shown in Figure 6.12. Note that the simulated frequency at the CoO is well approximated by the computed CoO frequency. However the accuracy is decreased compared with the previous case since the system approaches the instability region.

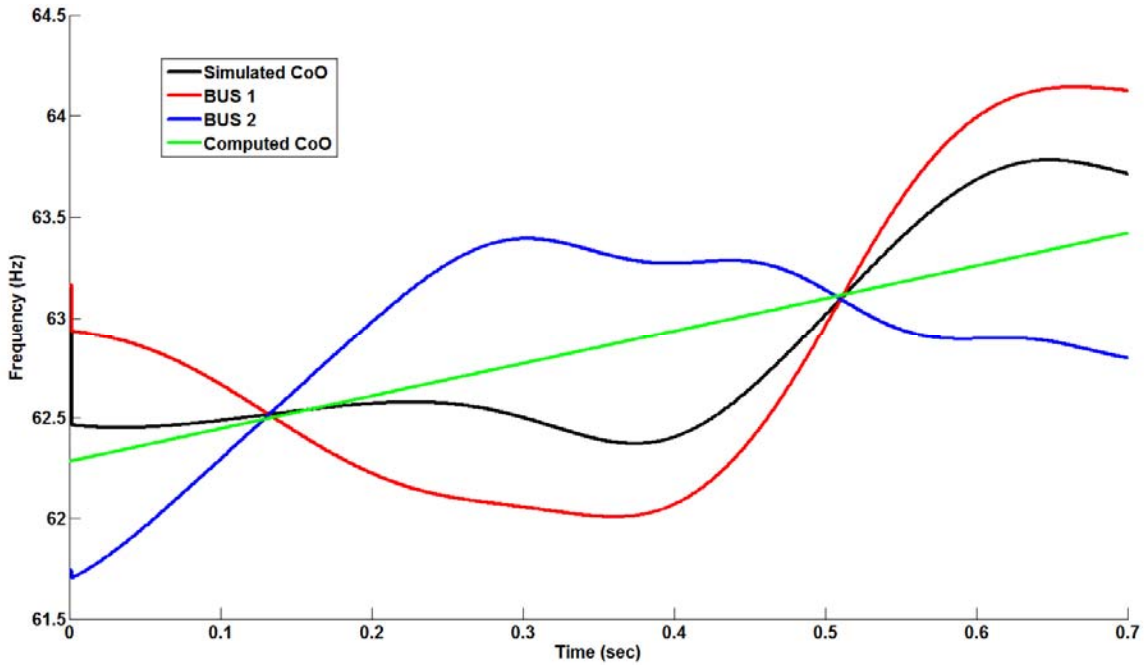

Figure 6.12. Comparison of simulated and computed CoO frequency - fault clearing time t=1.37 sec.

Once the CoO is computed, a two generator equivalent was built as shown in Figure 6.13.

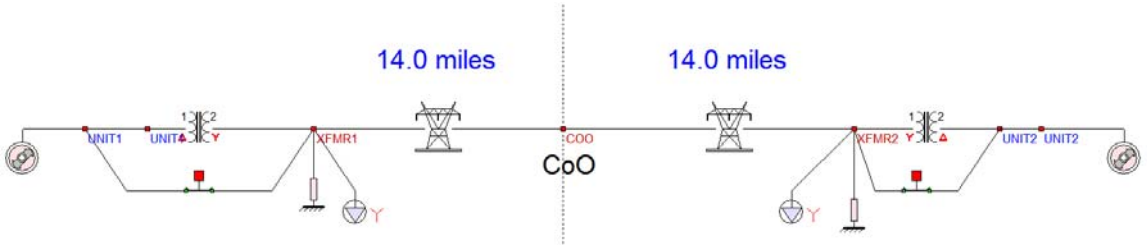

Figure 6.13. Equivalent system - fault clearing time t=1.37 sec.

The accuracy of the equivalent model is evaluated by comparing the dynamics of the original system and the equivalent system, as shown in Figure 6.14. The initial conditions of the equivalent system, calculated based on the generator of interest torque angle and speed along with the CoO phase angle and frequency, given in real time by the DSE that is performed at the substation of interest are given in Table 6.7.

Table 6.7. Generators' torque angle & frequency - fault clearing time t=1.37 sec.

Generator 1	CoO	Generator 2
δ_1=227.0 deg	δ_{CoO}=164.5 deg	δ_2=102.0 deg
f_1=63.1 Hz	f_{CoO}=62.43 Hz	f_2=61.75 Hz

As expected, the dynamics of the equivalent system are very close to the dynamics of the original system.

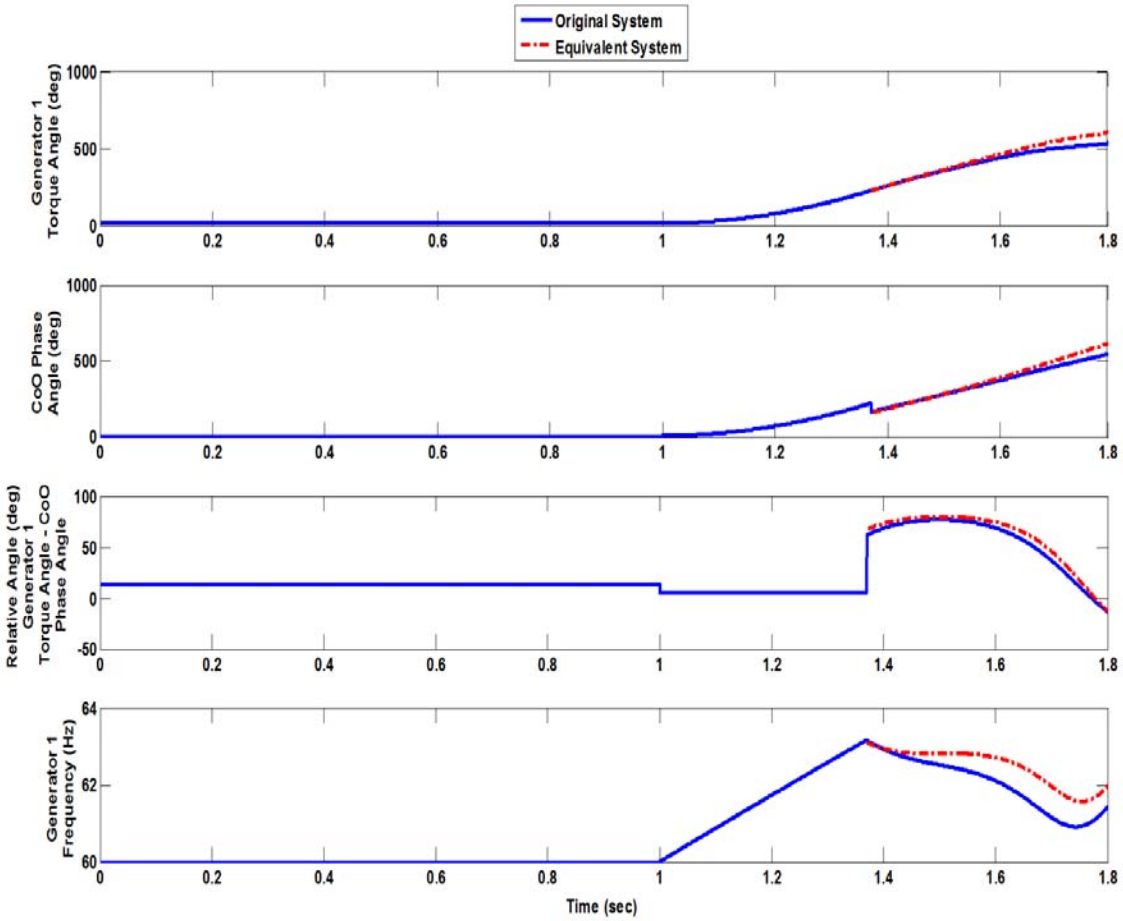

Figure 6.14. Comparison of original and equivalent system dynamics - fault clearing time t=1.37 sec.

For this assumed fault clearing time, the stability of the system is evaluated by computing the potential energy function and the total energy of the system. The total

energy of the system superposed on the corresponding potential energy function is shown in Figure 6.15. The total energy is equal to the barrier value of the energy, thus indicating that t=1.37 sec is the critical clearing time for the system and for the specific fault. Note that the total energy is computed given the torque angle and the frequency of the two generators of the equivalent system at the assumed clearing time (Table 6.7). Note also that, as expected, this is the same clearing time that was evaluated in section 6.2.1.

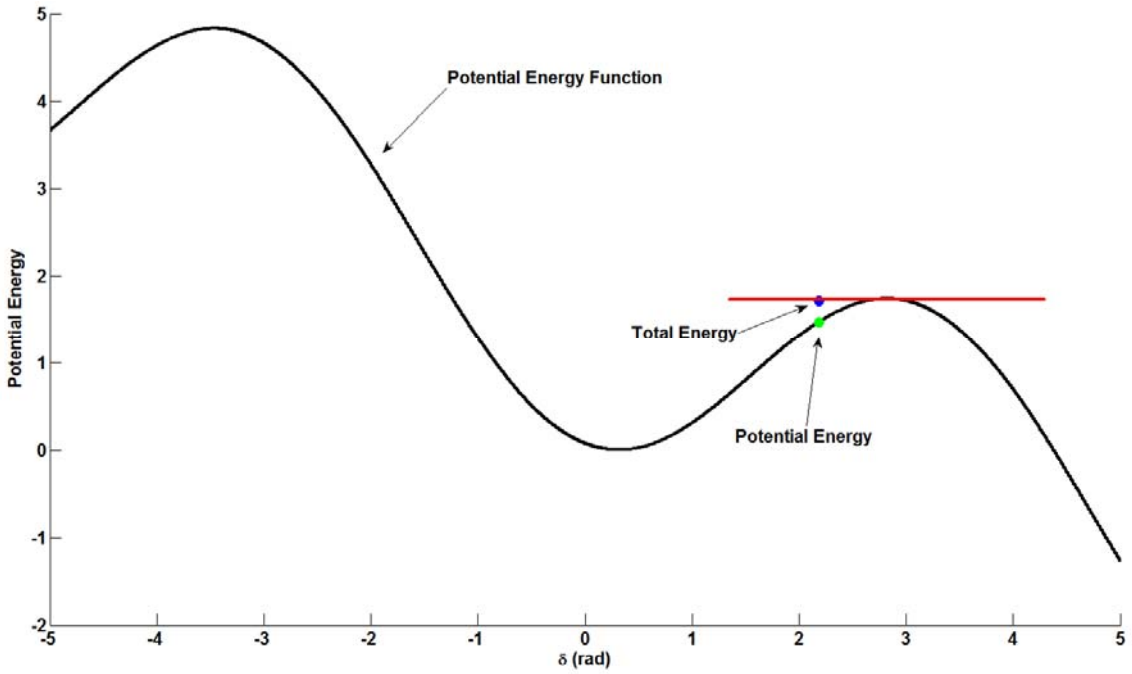

Figure 6.15. System total energy evaluation and stability characterization - fault clearing time t=1.37 sec.

6.3 Five Substation Test System - Single CoO Case

In this section the developed transient stability monitoring and generator out-of-step protection scheme are presented on a more complex five substation system. The test system consists of five substations, three of which are generating substations as is illustrated in Figure 6.16. The substation of interest, where the DSE and the transient stability monitoring scheme is applied is the first substation. The parameters of the system are presented in Table 6.8.

Table 6.8. Five substation test system parameters.

Gen1	450MVA	z= 0.001+j0.18 pu	H=2.5 sec	18 kV
Gen2	400MVA	z= 0.001+j0.18 pu	H= 2.5 sec	18 kV
Gen3	650MVA	z= 0.001+j0.18 pu	H= 2.5 sec	25 kV
XFMR1	450MVA	z=0.004+j0.1047 pu	18 kV/138kV	
XFMR2	450MVA	z=0.004+j0.1047 pu	18kV/138 kV	
XFMR3	700MVA	z=0.004+j0.1047 pu	25kV/230 kV	
AXFMR1	300MVA	z=0.03+j0.06 pu	138/230kV	
AXFMR2	300MVA	z=0.03+j0.06 pu	138/230kV	
Trans. Line Sub1-Sub4		z=0.02+0.16 pu	138 kV	41 miles
Trans. Line Sub1-Sub5		z=0.02+0.143 pu	138 kV	37 miles
Trans. Line Sub4-Sub5		z=0.025+0.185 pu	138 kV	48 miles
Trans. Line Sub4-Sub2		z=0.006+0.068 pu	230 kV	62 miles
Trans. Line Sub5-Sub2		z=0.003+0.038 pu	230 kV	35 miles
Trans. Line Sub5-Sub3		z=0.003+0.035 pu	230 kV	32 miles
Trans. Line Load2		z=0.005+0.05 pu	230 kV	40 miles
Load Sub1		S=1.8+j0.4 pu	138 kV	
Load Sub2		S=3.0+j0.8 pu	230 kV	
Load AXFMR1-PR		S=2.1+j0.5 pu	230 kV	
Load AXFMR2-PR		S=0.7+j0.1 pu	230 kV	
Load AXFMR2-SEC		S=0.8+j0.1 pu	138 kV	
Common S_{base}=100 MVA				

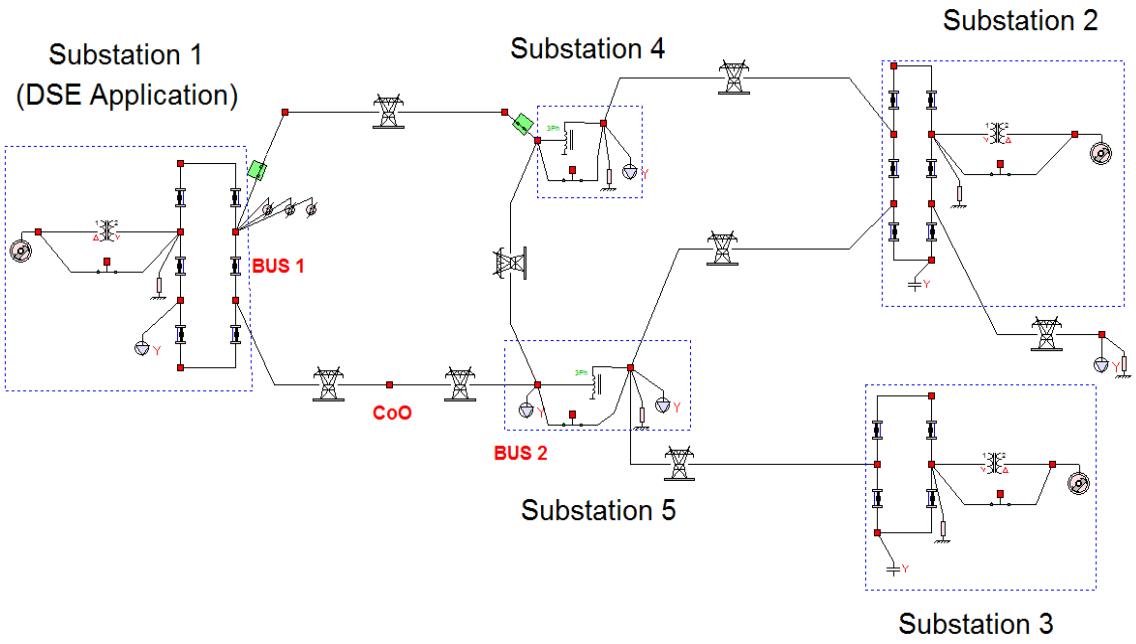

Figure 6.16. Single line diagram of the five substation test system.

The fault that will be examined is a three-phase fault at the terminal of the substation of interest and is cleared by disconnection of the line "Trans. Line Sub1-Sub4". The fault initiates at t=1 sec and different hypothetical clearing times are examined next.

6.3.1 Hypothetical fault clearing time = 1.1 sec

Assuming that t=1.1 sec is the fault clearing time, the frequency at the two terminals of line "Trans. Line Sub1-Sub5" is calculated upon simulation of the system and is illustrated in Figure 6.17.

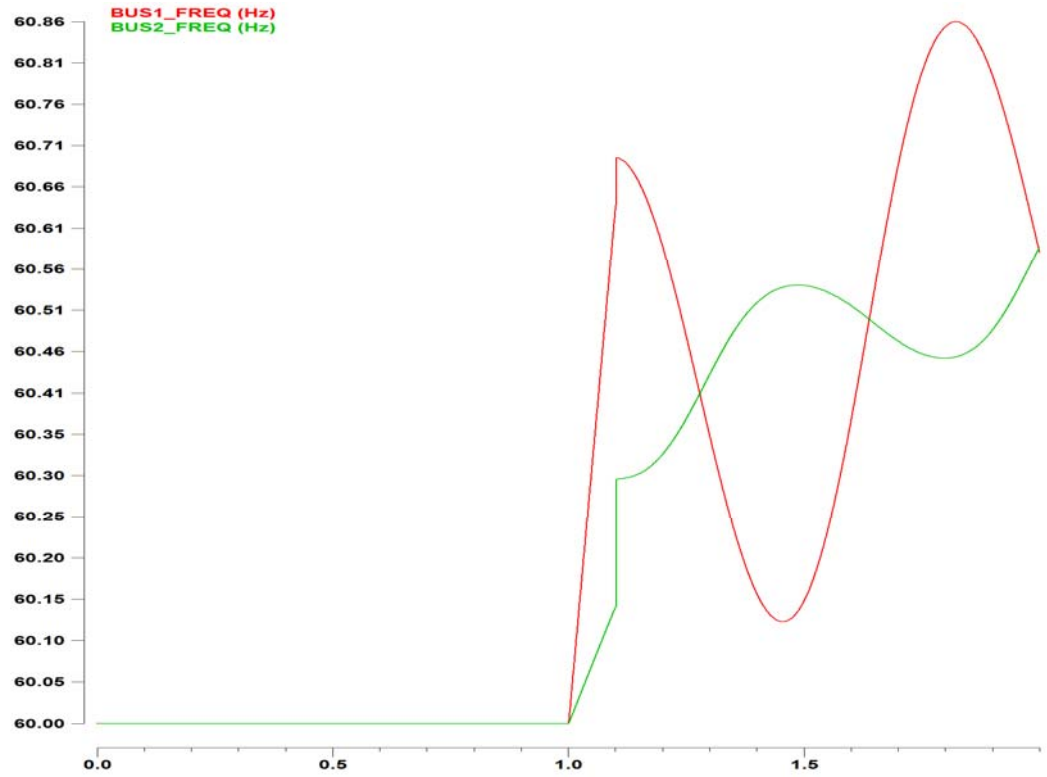

Figure 6.17. Frequency at the terminals of the line - fault clearing time t=1.1 sec.

Given the frequency at the two terminals of the line it is concluded that the CoO is within this line and it is evaluated by the CoO calculation optimization method. The results are summarized in Table 6.9.

Table 6.9. CoO calculation results - fault clearing time t=1.1 sec.

Line	α	b	c	CoO Length (miles)(away from Sub1)	Line Length (miles)	Coo Frequency Equation
SUB1-SUB5	0.208	60.366	0.235	29.3	37.0	$f_{CoO}(t) = 60.366 + 0.235 \cdot t$

The frequency at the two terminals of the line, along with the simulated frequency at the CoO and the equation of the frequency of the CoO are shown in Figure 6.18. Note that

the simulated frequency at the CoO is almost a straight line and is very well approximated by the computed CoO frequency.

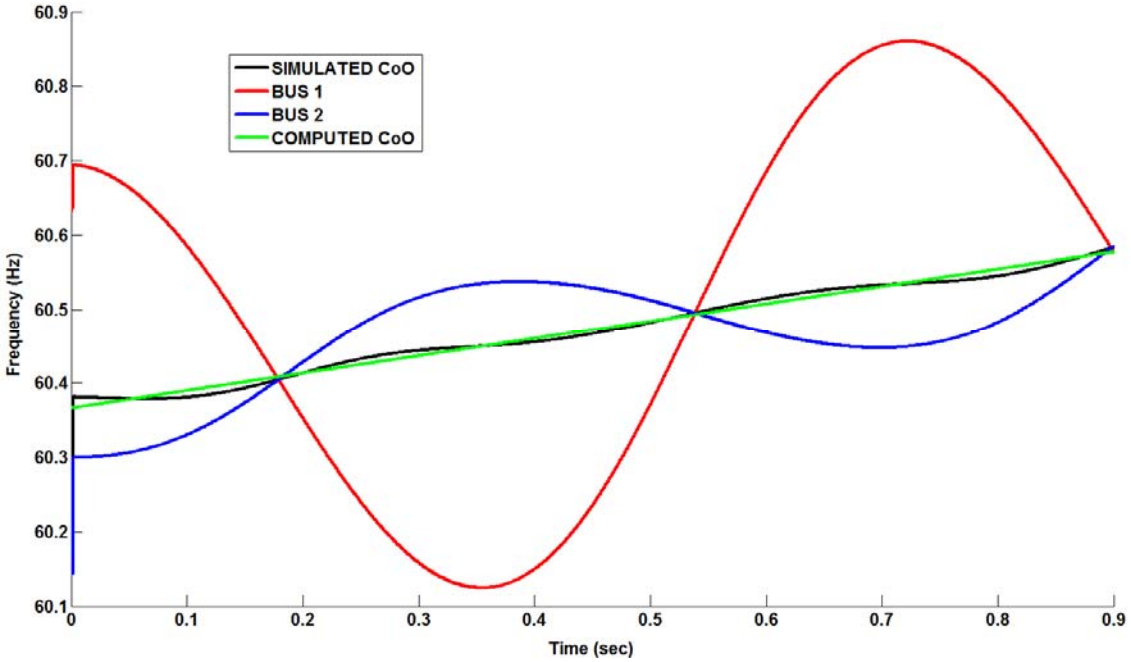

Figure 6.18. Comparison of simulated and computed CoO frequency - fault clearing time t=1.1 sec.

Once the CoO is computed, a two generator equivalent is derived, shown in Figure 6.19.

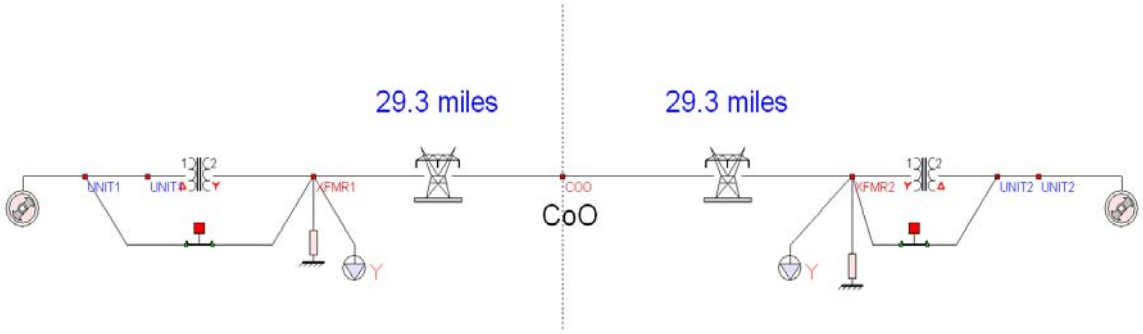

Figure 6.19. Equivalent system - fault clearing time t=1.1 sec.

Next, the dynamics of the original system and the equivalent system are compared as shown in Figure 6.20, in order to evaluate the accuracy of the equivalent model. The initial conditions that were used for the equivalent system, are calculated based on the DSE results that is running in the substation of interest, and provides the operating condition of the system at the assumed fault clearing time, given in Table 6.10. At this

point, it is reminded that the DSE provides an estimation of the states inside the substation of interest (including the generator states) along with an estimate of the state at the terminal(s) of the neighboring substation(s). So the observable area includes the departing line(s) from the substation of interest, and as a result the phase angle and the frequency of the CoO are given by the DSE as long as it lies in the observable area.

Table 6.10. Generators' torque angle & frequency - fault clearing time t=1.1 sec.

Generator 1	CoO	Generator 2
δ_1=28.83 deg	δ_{CoO}=3.1 deg	δ_2=-22.63 deg
f_1=60.84 Hz	f_{CoO}=60.38 Hz	f_2=59.92 Hz

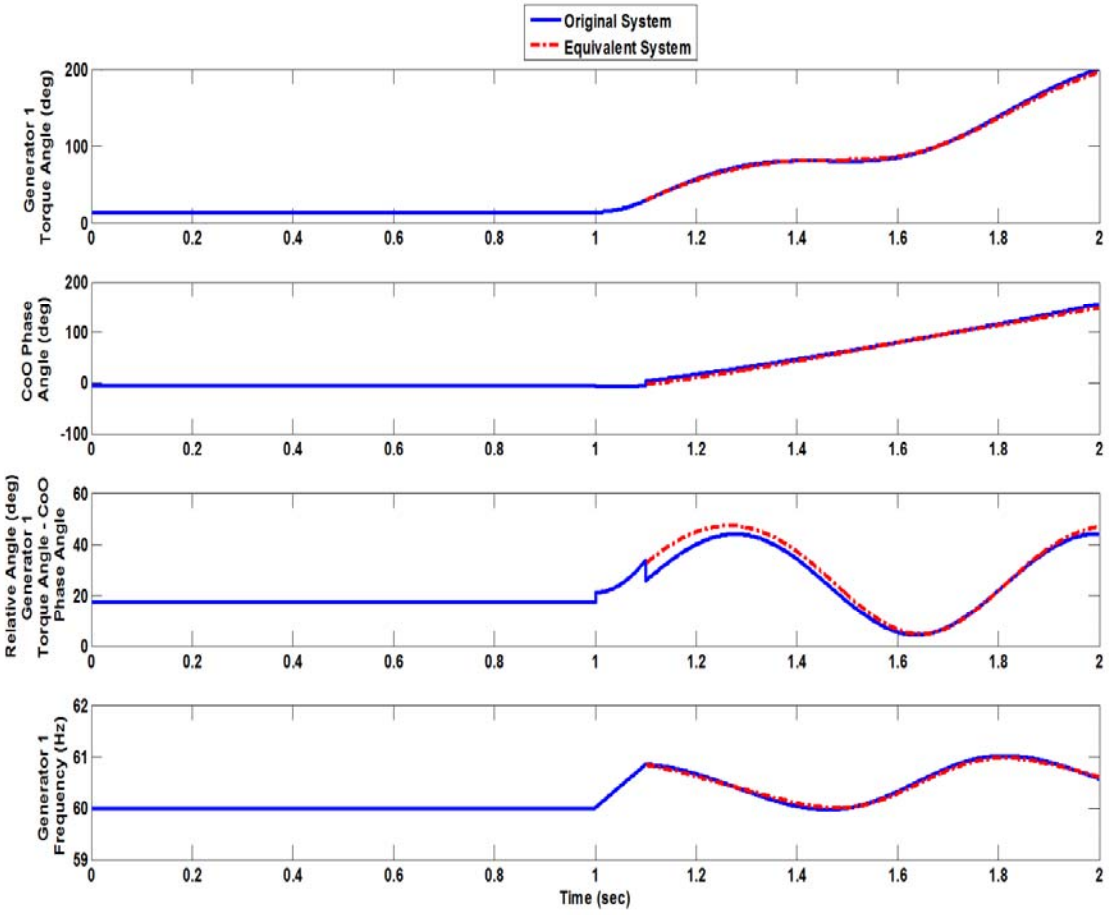

Figure 6.20. Comparison of original and equivalent system dynamics - fault clearing time t=1.1 sec.

As expected, the dynamics of the equivalent system are very close to the dynamics of the original system.

In order to evaluate the stability of the system for this assumed fault clearing time, the potential energy function of the equivalent system was evaluated as illustrated in Figure 6.21. The total energy of the system is also computed given the torque angle and the frequency of the two generators of the equivalent system at the assumed clearing time (Table 6.10), and it is superposed on the corresponding potential energy function. It is clear in this case that the total energy is below the barrier, thus indicating a stable system.

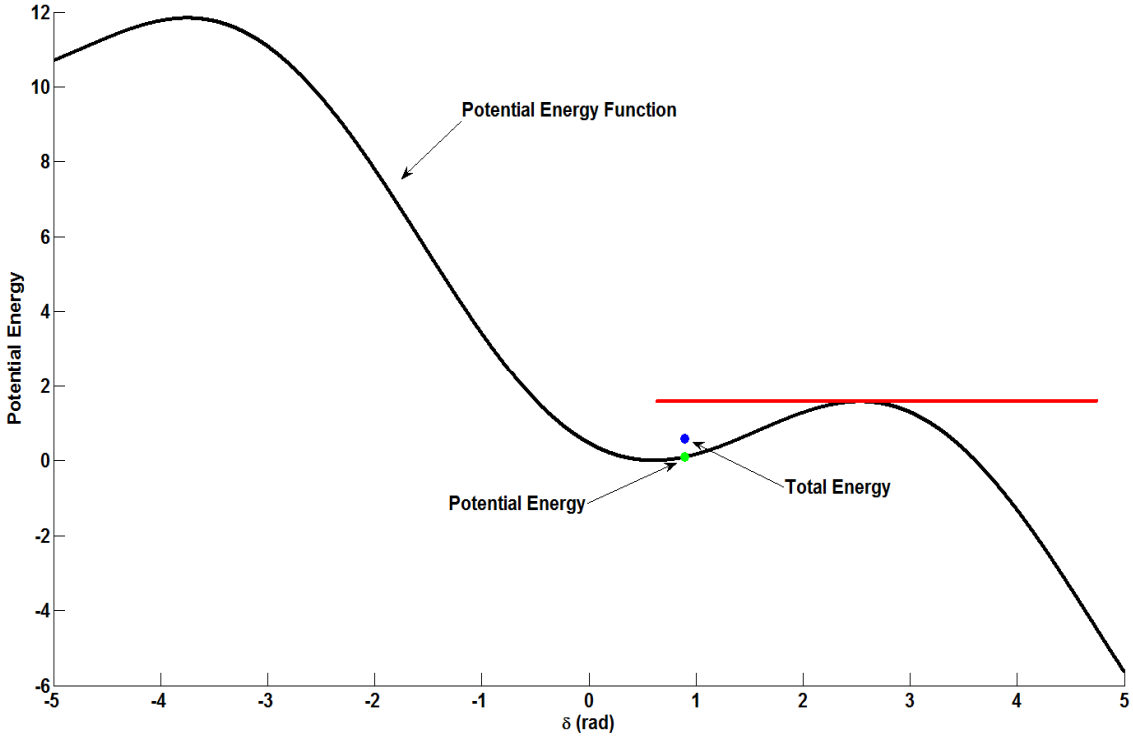

Figure 6.21. System total energy evaluation and stability characterization - fault clearing time t=1.1 sec.

6.3.2 Hypothetical fault clearing time = 1.15 sec

For this hypothetical clearing time, the frequency at the two terminals of line "Trans. Line Sub1-Sub5" is illustrated in Figure 6.22. Given the frequency at the two terminals of the line it is concluded that the CoO is within this line, and it is computed as shown in Table 6.11.

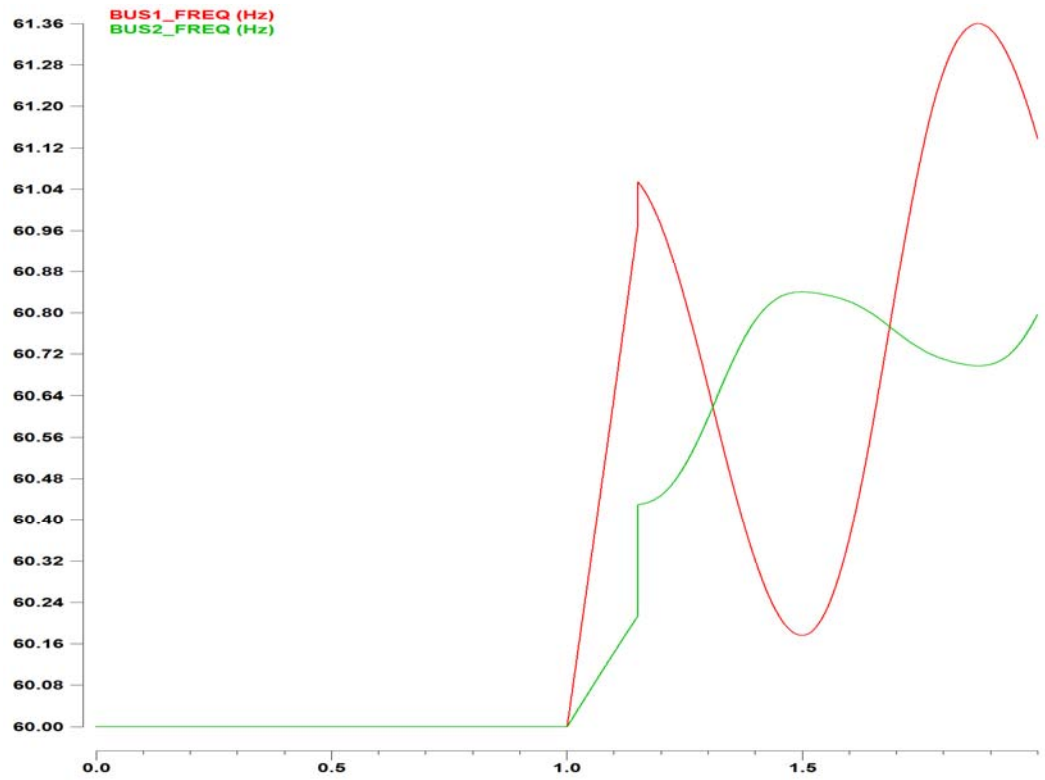

Figure 6.22. Frequency at the terminals of the line - fault clearing time t=1.15 sec.

Table 6.11. CoO calculation results - fault clearing time t=1.15 sec.

Line	α	b	c	CoO Length (miles)(away from Sub1)	Line Length (miles)	Coo Frequency Equation
SUB1-SUB5	0.32	60.56	0.36	25.2	37.0	$f_{CoO}(t) = 60.56 + 0.36 \cdot t$

The simulated frequency at the two terminals of the line, along with comparison of the simulated frequency and the approximated with a straight line frequency at the CoO, are shown in Figure 6.23. Note that the simulated frequency at the CoO is well approximated by the computed CoO frequency.

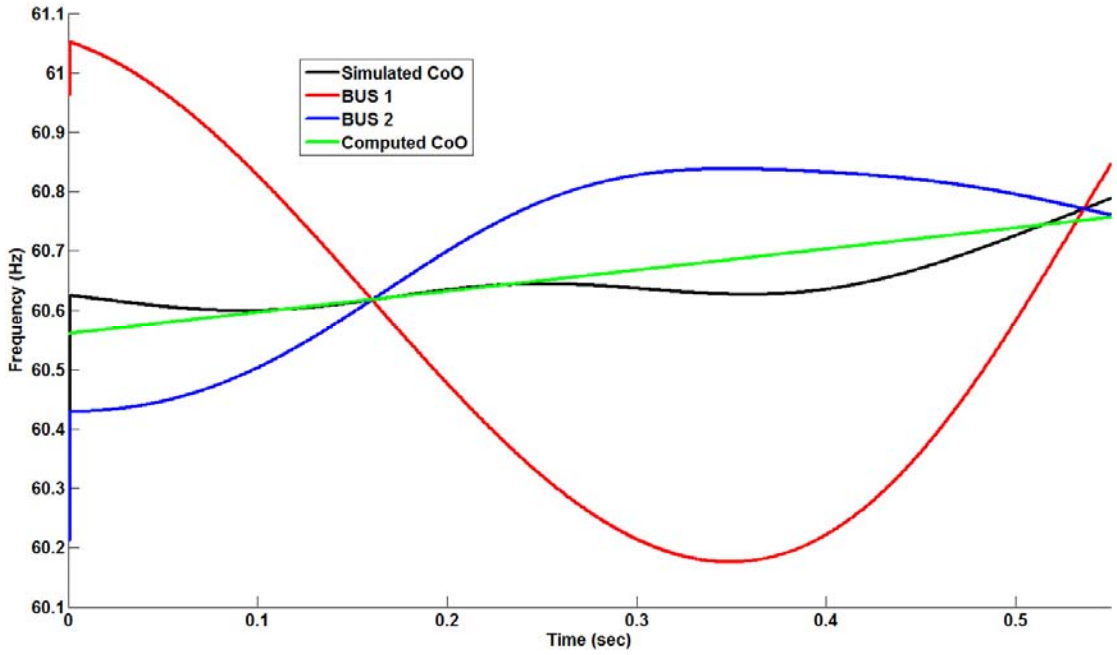

Figure 6.23. Comparison of simulated and computed CoO frequency - fault clearing time t=1.15 sec.

Once the CoO is computed, a two generator equivalent was built as shown in Figure 6.24.

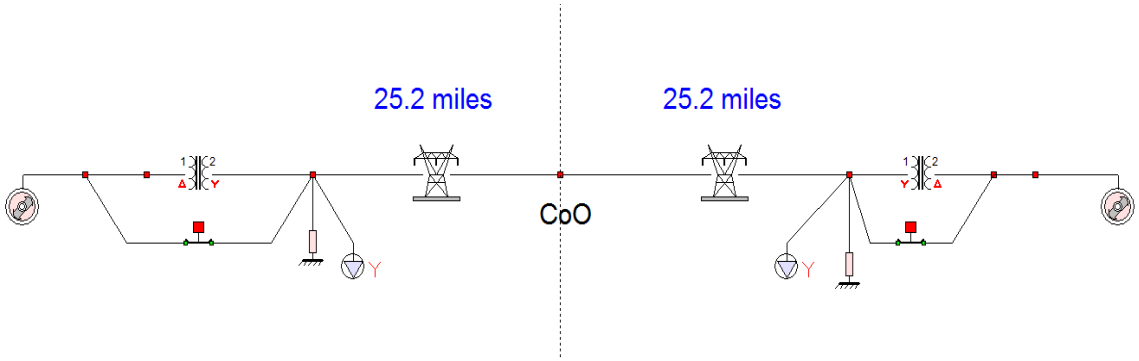

Figure 6.24. Equivalent system - fault clearing time t=1.15 sec.

The accuracy of the equivalent model is evaluated by comparing the dynamics of the original system and the equivalent system as shown in Figure 6.25. The initial conditions of the equivalent system are given in Table 6.12. As expected, the dynamics of the equivalent system are very close to the dynamics of the original system.

Table 6.12. Generators' torque angle & frequency - fault clearing time t=1.15 sec.

Generator 1	CoO	Generator 2
δ_1=47.58 deg	δ_{CoO}=14.36 deg	δ_2=-18.87 deg
f_1=61.25 Hz	f_{CoO}=60.63 Hz	f_2=60.00 Hz

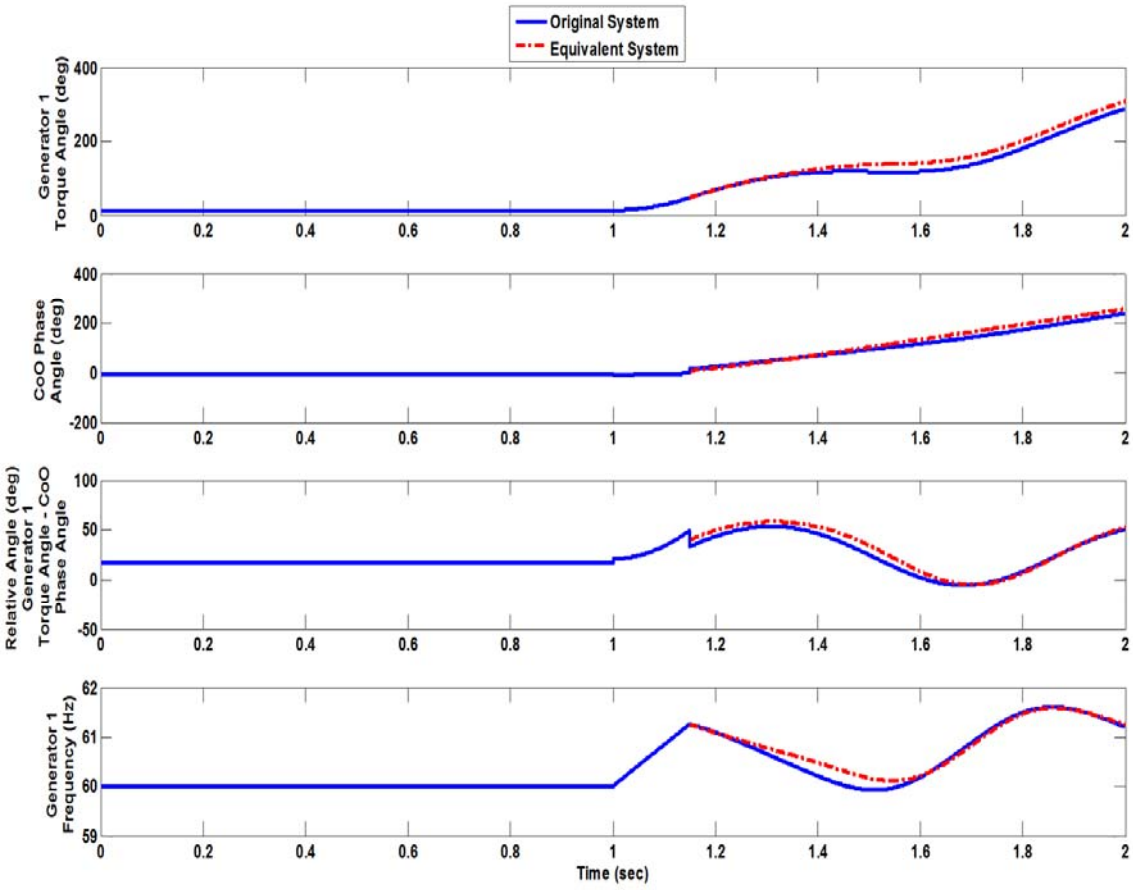

Figure 6.25. Comparison of original and equivalent system dynamics - fault clearing time t=1.15 sec.

In order to evaluate the stability of the system for this assumed fault clearing time, the potential energy function of the equivalent system is evaluated. The total energy of the system is also computed and it is superposed on the corresponding potential energy function, shown in Figure 6.26. The total energy is still below the barrier, thus indicating a stable system.

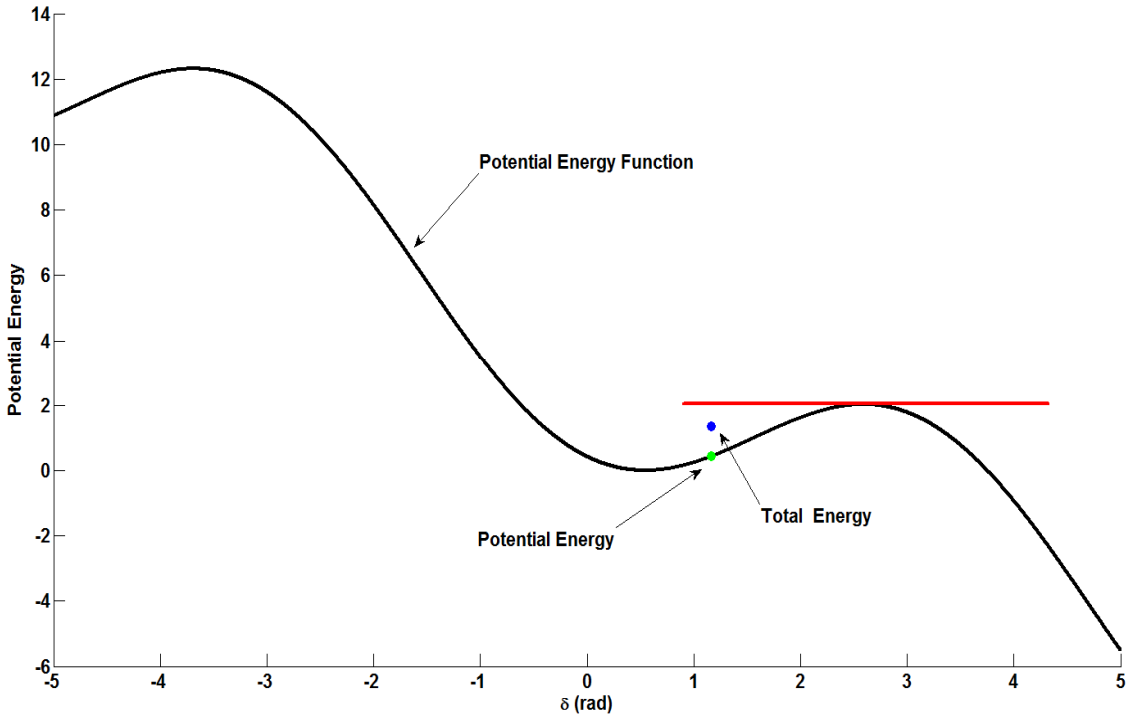

Figure 6.26. System total energy evaluation and stability characterization - fault clearing time t=1.15 sec.

6.3.3 Hypothetical fault clearing time = 1.2 sec

For this clearing time, the frequency at the two terminals of line "Trans. Line Sub1-Sub4" is illustrated in Figure 6.27.

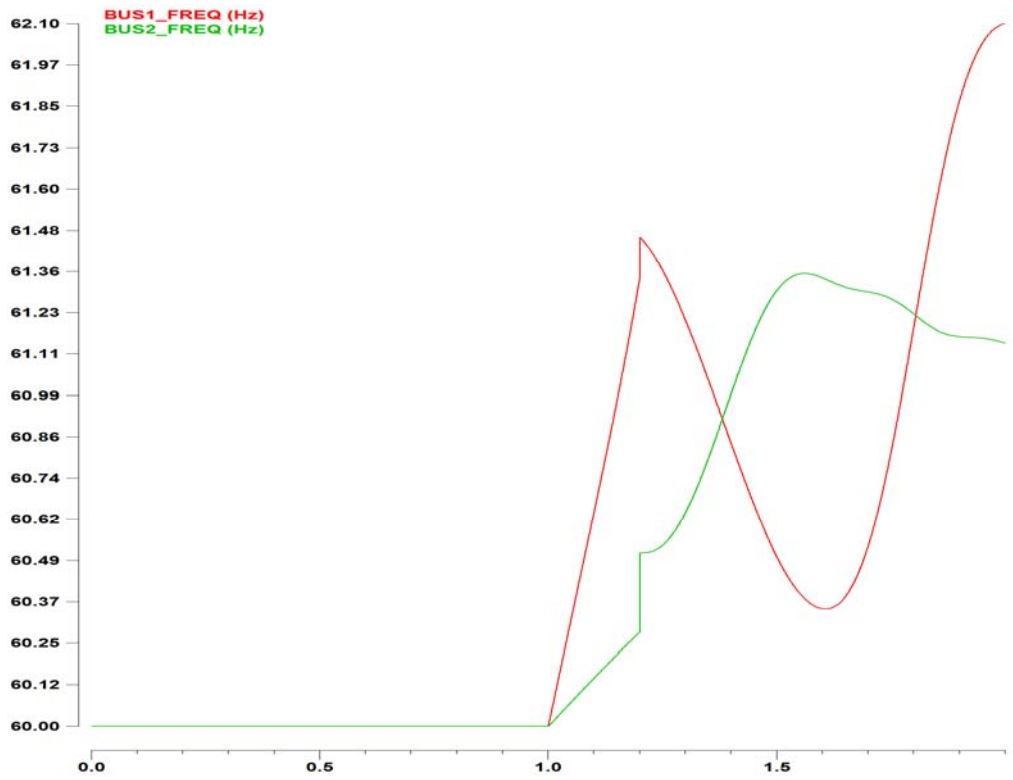

Figure 6.27. Frequency at the terminals of the line - fault clearing time t=1.2 sec.

Based on the frequency at the two terminals of the line it is concluded that the CoO is within this line and its computation is summarized in Table 6.13.

Table 6.13. CoO calculation results - fault clearing time t=1.2 sec.

Line	α	b	c	CoO Length (miles)(away from Sub1)	Line Length (miles)	Coo Frequency Equation
SUB1-SUB5	0.45	60.82	0.51	20.3	37.0	$f_{CoO}(t) = 60.82 + 0.51 \cdot t$

The frequency at the two terminals of the line, along with the comparison between the simulated and the computed frequency at the CoO, are shown in Figure 6.28. The simulated frequency at the CoO is well approximated by the computed CoO frequency.

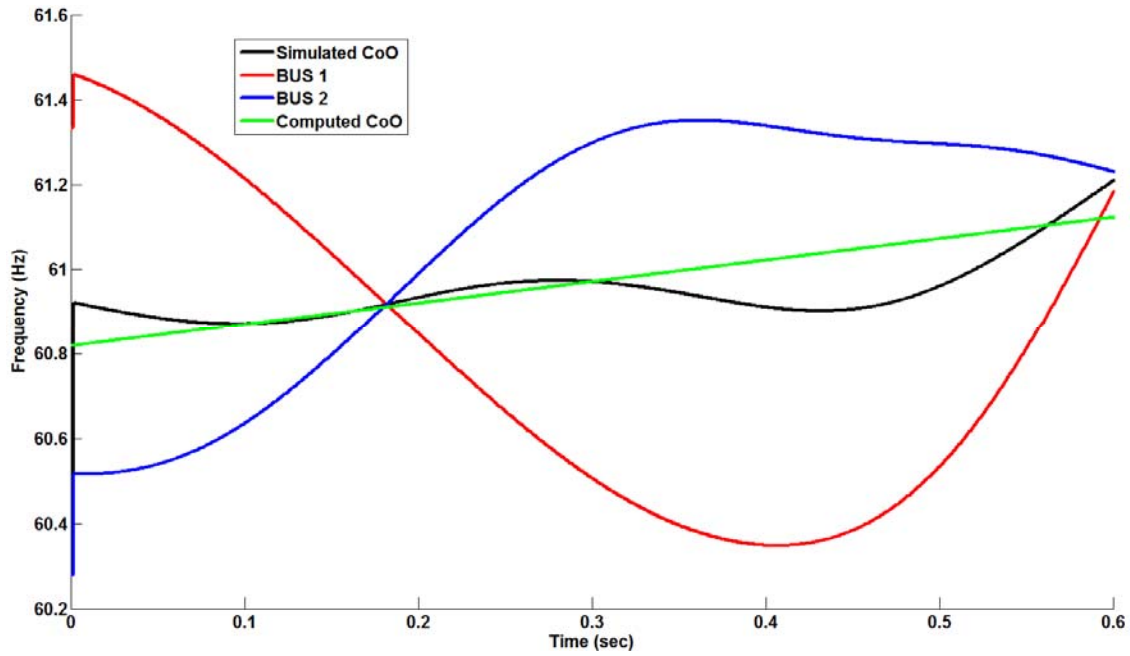

Figure 6.28. Comparison of simulated and computed CoO frequency - fault clearing time t=1.2 sec.

Next, a two generator equivalent was built as explained, shown in Figure 6.29.

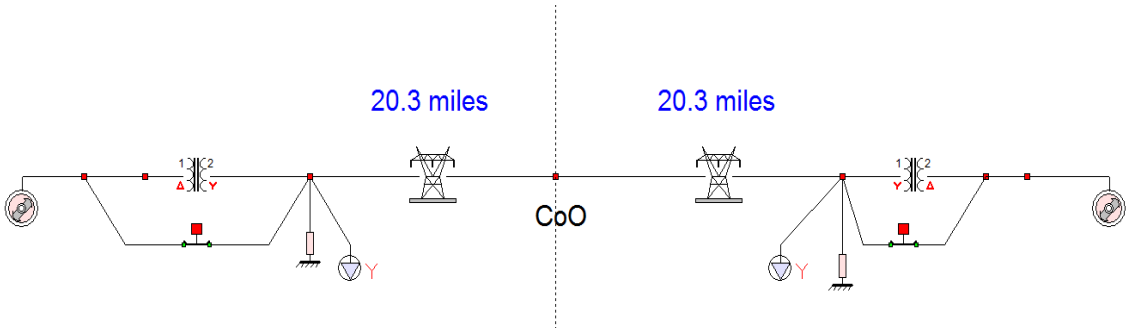

Figure 6.29. Equivalent system - fault clearing time t=1.2 sec.

The accuracy of the equivalent model is again evaluated by comparing the dynamics of the original system and the equivalent system, as illustrated in Figure 6.30. The state of the generators (torque angle and frequency) of the equivalent system, at the examined hypothetical fault clearing time are given in Table 6.14. As expected, the dynamics of the equivalent system are close to the dynamics of the original system, although the accuracy is decreased compared to the previous cases, given that the system is approaching the instability region and the nonlinearities become more dominant.

Table 6.14. Generators' torque angle & frequency - fault clearing time t=1.2 sec.

Generator 1	CoO	Generator 2
δ_1=74.27 deg	δ_{CoO}=32.94 deg	δ_2=-8.4 deg
f_1=61.68 Hz	f_{CoO}=60.89 Hz	f_2=60.09 Hz

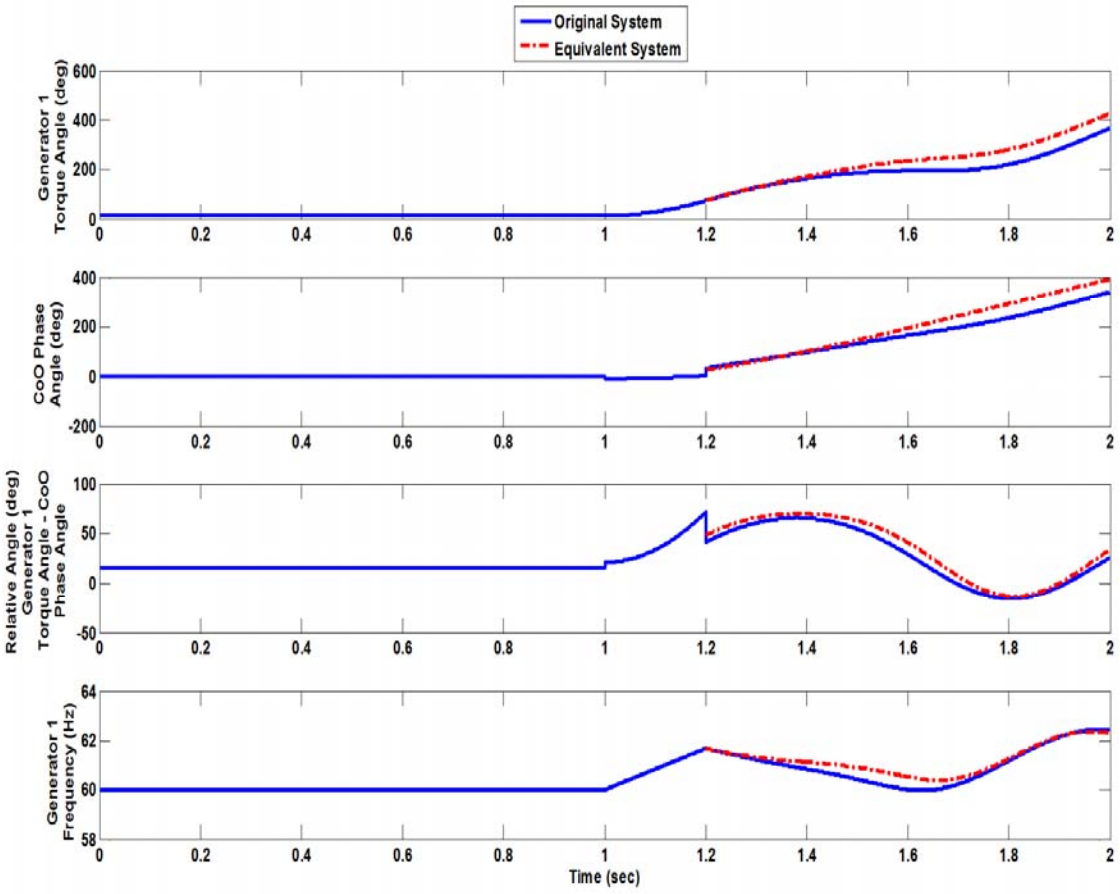

Figure 6.30. Comparison of original and equivalent system dynamics - fault clearing time t=1.2 sec.

Finally, the stability of the system is evaluated for this hypothetical fault clearing time. The potential energy function of the equivalent system is first evaluated. Then, the total energy of the system is computed given the state (torque angle and frequency) of the two generators of the equivalent system (Table 6.14) and it is superposed on the corresponding potential energy function, as illustrated in Figure 6.31. Note that in this

case the total energy is equal to the barrier value of the energy, thus indicating that this is the critical clearing time of the system.

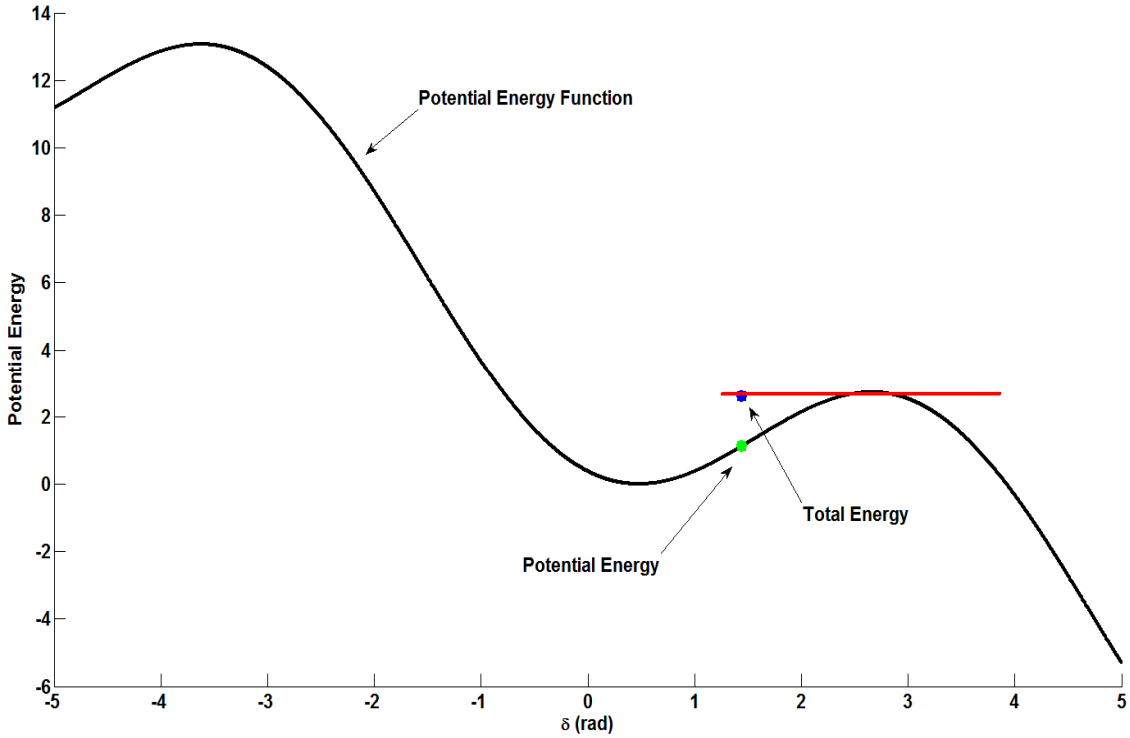

Figure 6.31. System total energy evaluation and stability characterization - fault clearing time t=1.2 sec.

As a result, the critical clearing time (CCT) as computed in real time by the proposed method is evaluated to be 0.2 sec. Simulations of the system indicate that the actual critical clearing time for the examined fault is 0.22 sec. Thus, there is an error of 0.02 sec (approximately 1 cycle) in the evaluation of the CCT, which is reasonable considering that the derivation of the equivalent system was made under the assumption that the frequency and the phase angle along the line varies linearly with the distance from the terminals of the line. The accuracy of this assumption is decreased as the system gets closer to the instability region and the nonlinearities become more severe.

6.3.4 Comparison with conventional out-of-step protection method

Based on the results from the previous sections, it is concluded that the developed stability monitoring scheme evaluated in real time the CCT of the system to be at t=1.2 sec (0.2 sec after the fault initiation). As a result, at this time instant, instability of the

generator is detected and a trip signal can be sent to generator. In this section, the functionality of a state-of-the-art, impedance monitoring based, out-of-step relay is simulated and the instability detection time is evaluated for an unstable scenario with clearing time t=1.25 sec (0.25 sec after fault initiation). The results are summarized in Figure 6.32. In particular, monitoring of the trajectory of the impedance at the terminals of the generator indicates that the right blinder and the left blinder are crossed at t=1.34 sec and t=1.51 sec respectively. As a result, the impedance based relay detected instability at t=1.51 sec, thus the developed method in this work predicted instability 0.31 sec before the conventional relay. Note that this time difference is actually higher, considering the fact that when the left blinder is crossed the value of the phase angle is high and the generator trip has to be delayed in order to avoid breaker overstress.

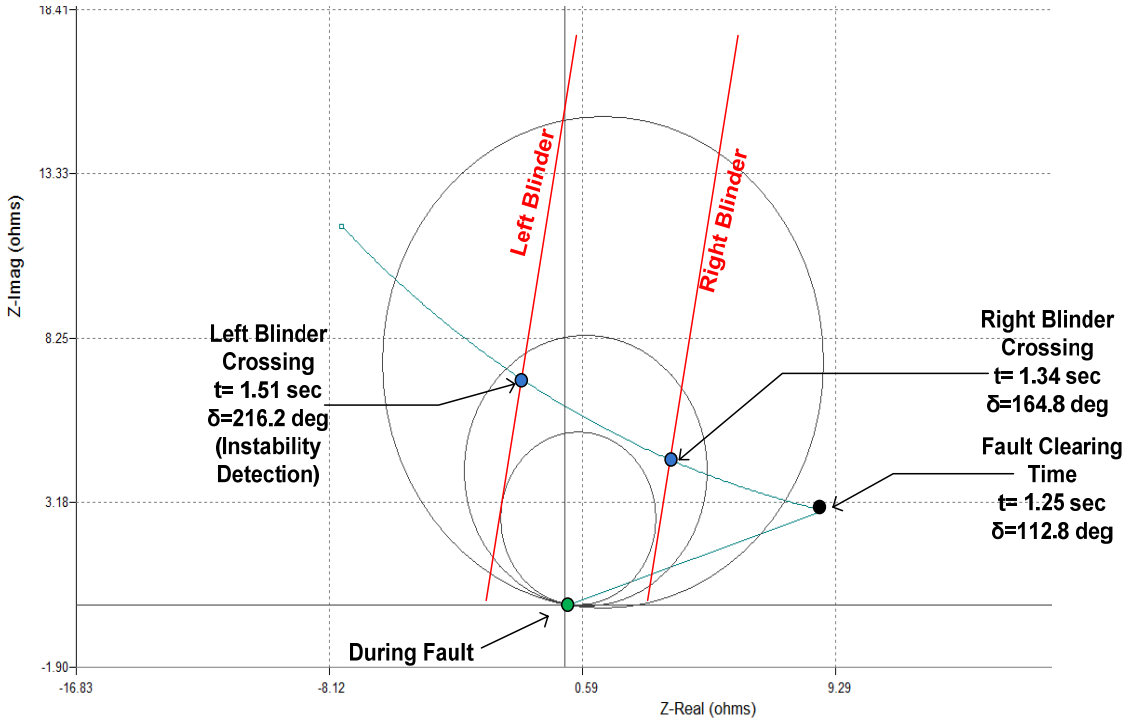

Figure 6.32. Impedance trajectory monitoring - five substation system.

6.4 Three Substation Test System - Multiple CoO Case

In this section the transient stability monitoring and generator out-of-step protection schemes are demonstrated on a three substation system. In particular, the test system consists of three generating substations, five overhead transmission lines that connect the

three substations and three constant power loads that have to be served. It is assumed that a three-phase fault occurs at the terminal of the second substation (substation of interest) which causes the trip of one of the two parallel transmission lines that connect the first with the second substation. The fault initiates at t=1 sec and different hypothetical fault clearing times are examined next. Note that at the post-fault system, there are two lines departing from the substation of interest, thus it is expected that there will be two CoO points, one on each line. The described test system is illustrated in Figure 6.33. Its parameters are presented in Table 6.15.

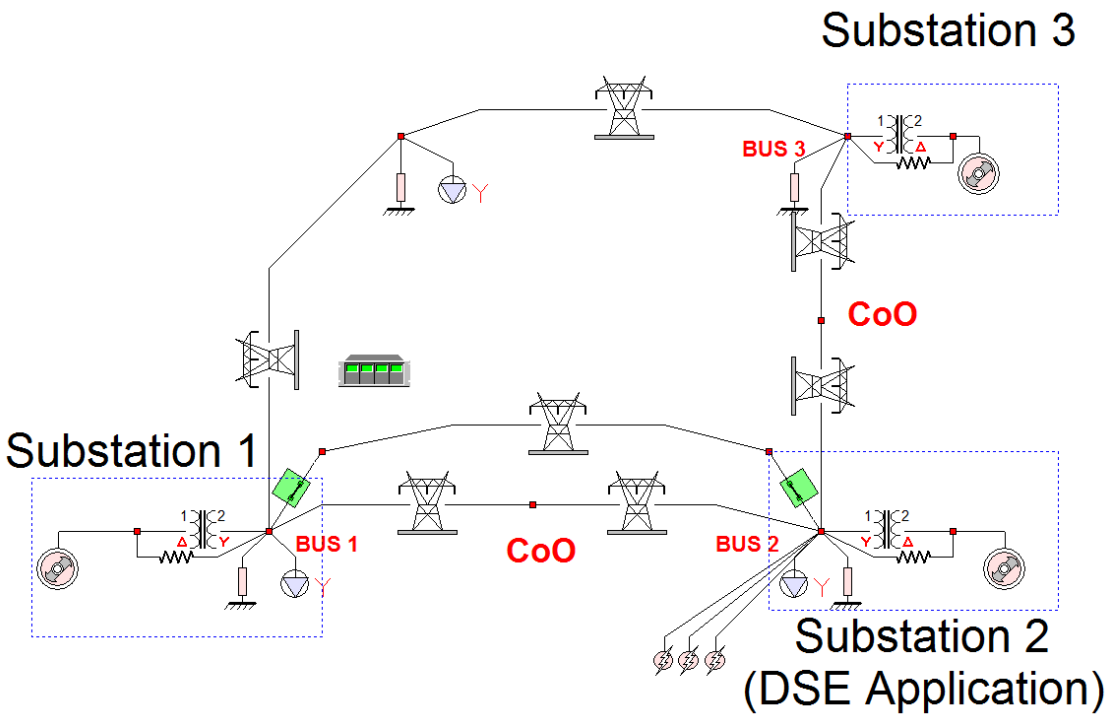

Figure 6.33. Single line diagram of the three substation test system.

Table 6.15. Three substation test system parameters.

Gen1	100MVA	z= 0.001+j0.2 pu	H=2.5 sec	15 kV
Gen2	300MVA	z= 0.001+j0.18 pu	H= 3.0 sec	18 kV
Gen3	200MVA	z= 0.001+j0.18 pu	H= 2.5 sec	20 kV
XFMR1	100MVA	z=0.001+j0.07 pu	15 kV/115kV	
XFMR2	300MVA	z=0.001+j0.08 pu	115 kV/18kV	
XFMR3	200MVA	z=0.001+j0.07 pu	115 kV/20kV	
Trans. Line1 Sub1-Sub2		z=0.024+j0.235 pu	115 kV	43.5 miles
Trans. Line2 Sub1-Sub2		z=0.024+j0.235 pu	115 kV	43.5 miles
Trans. Line1 Sub1-Sub3		z=0.019+j0.19 pu	115 kV	35 miles
Trans. Line2 Sub1-Sub2		z=0.008+j0.082 pu	115 kV	15 miles
Trans. Line Sub2-Sub3		z=0.028+j0.272 pu	115 kV	20 miles
Load 1		S=1.33+j0.1 pu	115 kV	
Load 2		S=0.56+j0.1 pu	115 kV	
Load 3		S=1.5+j0.1 pu	115 kV	
Common Sbase=100 MVA				

6.4.1 Hypothetical fault clearing time = 1.2 sec

For this hypothetical fault clearing time, the frequency at the terminals of the lines that connect the substation of interest with the neighboring substations (BUS1, BUS2 and BUS3) is illustrated in Figure 6.34. Given the frequency at the terminals of the lines it can be concluded that the CoO is within the lines that connect the second substation with the first and the third substation. The optimization algorithm was executed for the determination of the CoO in the two lines and the results are summarized in Table 6.16.

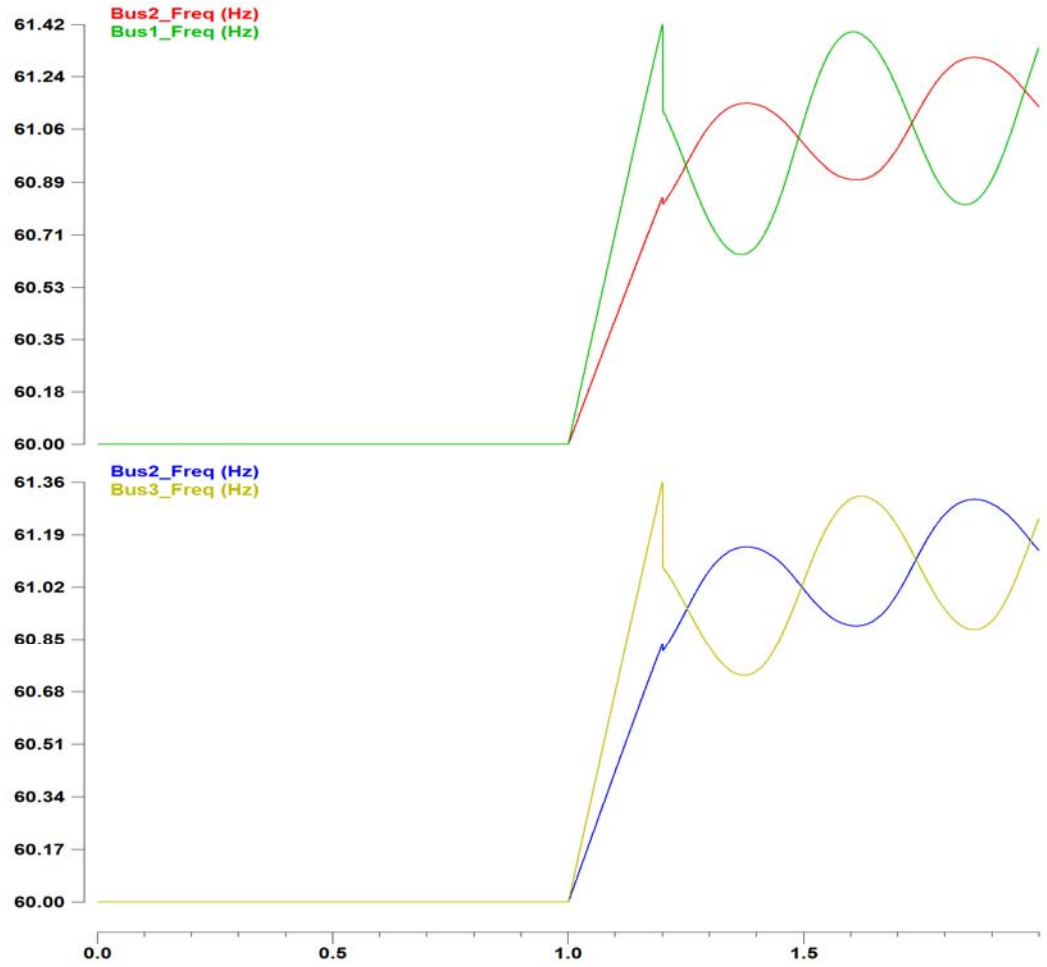

Figure 6.34. Frequency at the terminals of the lines - fault clearing time t=1.2 sec.

Table 6.16. CoO calculation results - fault clearing time t=1.2 sec.

Line	α	b	c	CoO Length (miles)(away from Sub2)	Line Length (miles)	Coo Frequency Equation
SUB2-SUB1	0.668	60.94	0.3	14.5	43.5	$f_{CoO}(t) = 60.94 + 0.3 \cdot t$
SUB2-SUB3	0.597	60.93	0.32	8.1	20.0	$f_{CoO}(t) = 60.93 + 0.32 \cdot t$

The frequency at the two terminals of the lines, along with the simulated and computed frequency at the CoO points, are shown in Figure 6.35 and Figure 6.36, respectively. Note that in both cases, the simulated frequency at the CoO is almost a straight line and is very well approximated by the computed CoO frequency.

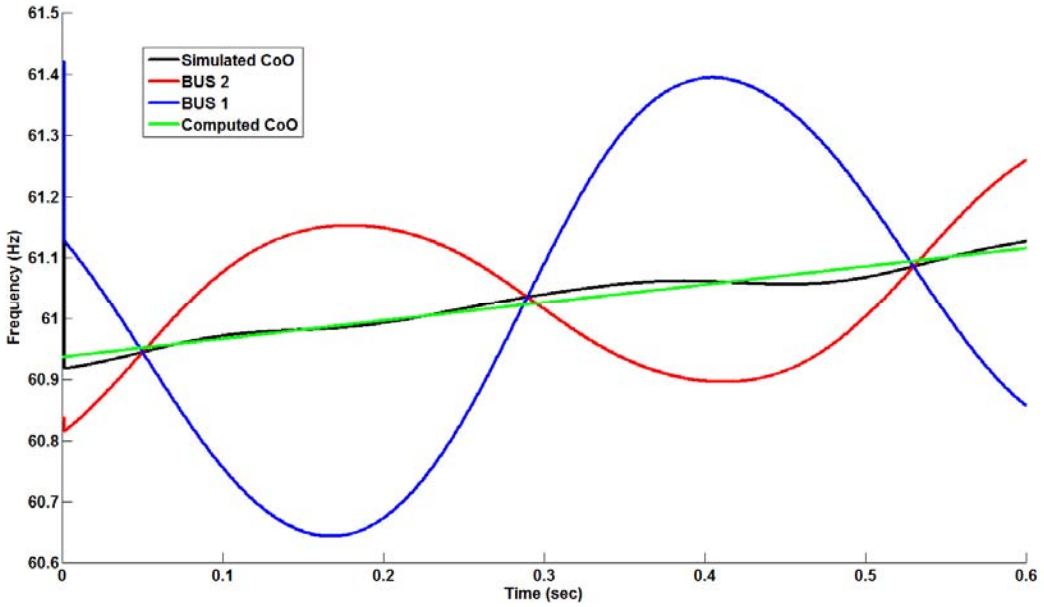

Figure 6.35. Comparison of simulated and computed CoO1 frequency - fault clearing time t=1.2 sec.

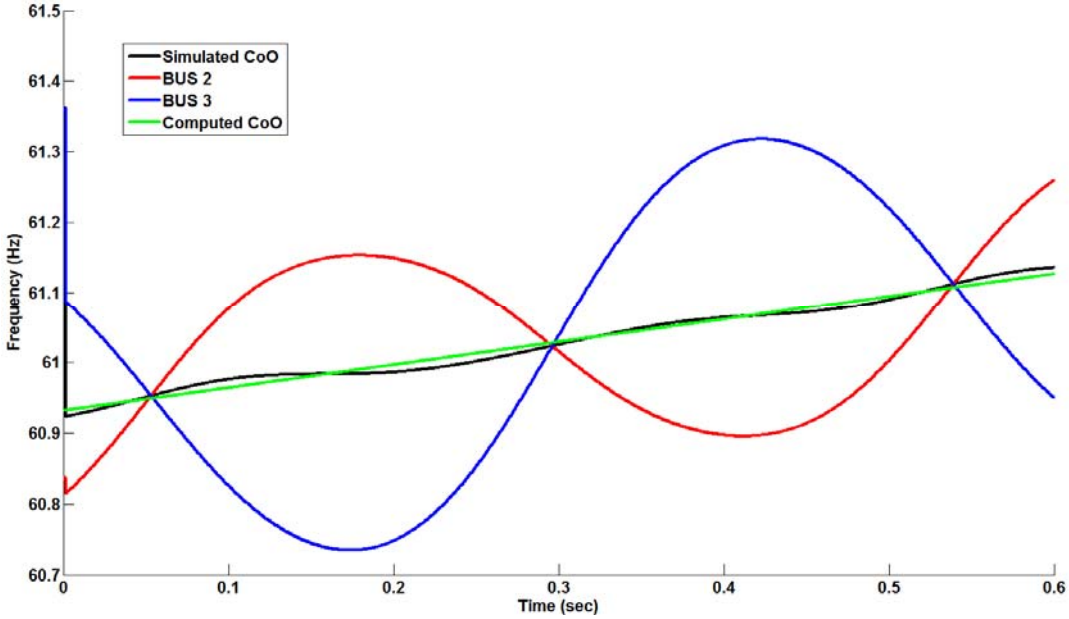

Figure 6.36. Comparison of simulated and computed CoO2 frequency - fault clearing time t=1.2 sec.

Once the CoO is computed, a two generator equivalent was built. The equivalent is shown in Figure 6.37. Note that since there are two CoO points in the original system, there are two CoO points in the equivalent system too, one on each of the parallel lines.

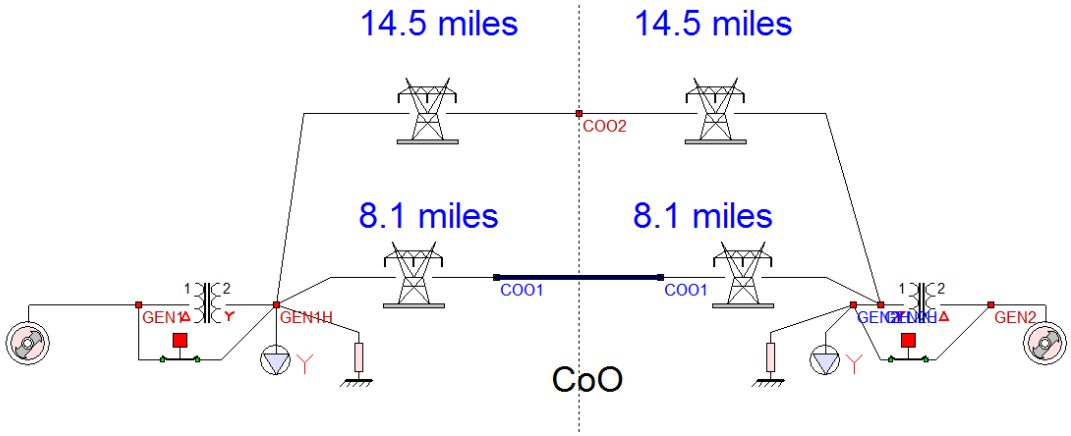

Figure 6.37. Equivalent system - fault clearing time t=1.2 sec.

In order to evaluate the accuracy of the equivalent model, the dynamics of the original system and the equivalent system are compared. In particular, the initial conditions (torque angle and speed) of the generator in the substation of interest were set to the values that the system had at the hypothetical fault clearing time. The initial conditions (torque angle and speed) of the generator in the second substation (mirror image part of the system) were set to be symmetric in terms of the CoO, as explained in section 4.3.2. Since now there are two CoO points in the system, the average of the phase angle and the frequency at the two CoO points was calculated and was used as a reference for the evaluation of the torque angle and the frequency of the second generator in the equivalent system. At this point, it is emphasized again that these values are computed in real time based on the DSE that is performed at the substation of interest, as explained in previous sections. The results are shown in Table 6.17.

Table 6.17. Generators' torque angle & frequency - fault clearing time t=1.2 sec.

Generator 1	CoO1	CoO2	Generator 2
δ_1=38.35 deg	δ_{CoO}=27.5 deg	δ_{CoO}=29.7 deg	δ_2=18.84 deg
f_1=61.31 Hz	f_{CoO}=60.92 Hz	f_{CoO}=60.92 Hz	f_2=60.53 Hz

The second generator's torque angle and frequency, the phase angle of the two CoO points and the relative angle between the second generator's torque angle and the phase angle of the two CoO points, are compared between the original and the equivalent system in Figure 6.38. As expected, the dynamics of the equivalent system are very close to the dynamics of the original system.

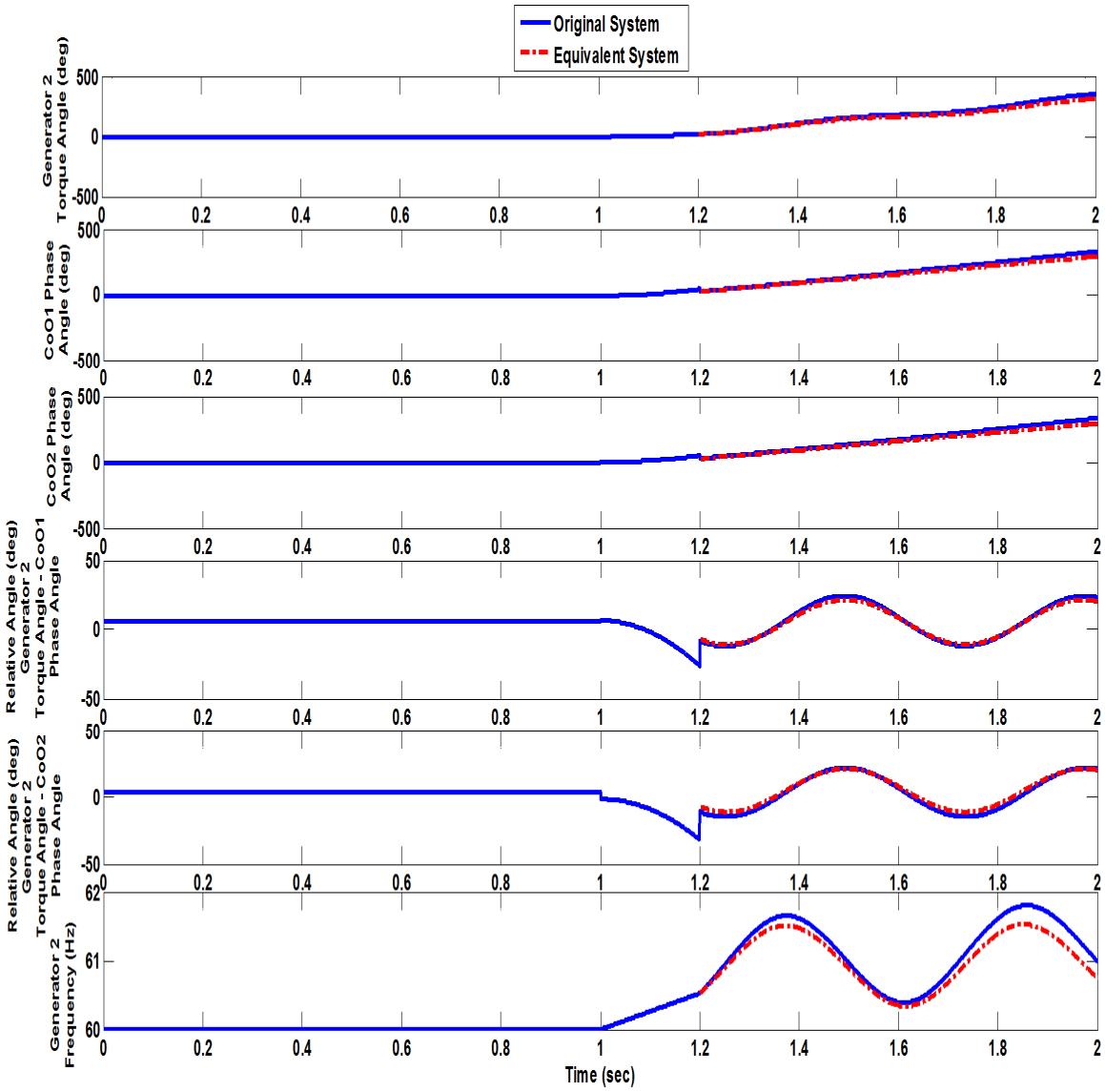

Figure 6.38. Comparison of original and equivalent system dynamics - fault clearing time t=1.2 sec.

In order to evaluate the stability of the system for this hypothetical fault clearing time, the potential energy function of the equivalent system was evaluated. The total energy of

the system is also computed based on the state of the equivalent system generators given in Table 6.17, and it is superposed on the corresponding potential energy function, as illustrated in Figure 6.39. It is clear in this case that the total energy is below the barrier, thus indicating a stable system. Note that the barrier value is the smallest value among the potential energy value of the unstable equilibrium points that surround a stable equilibrium point as explained in section 4.2.

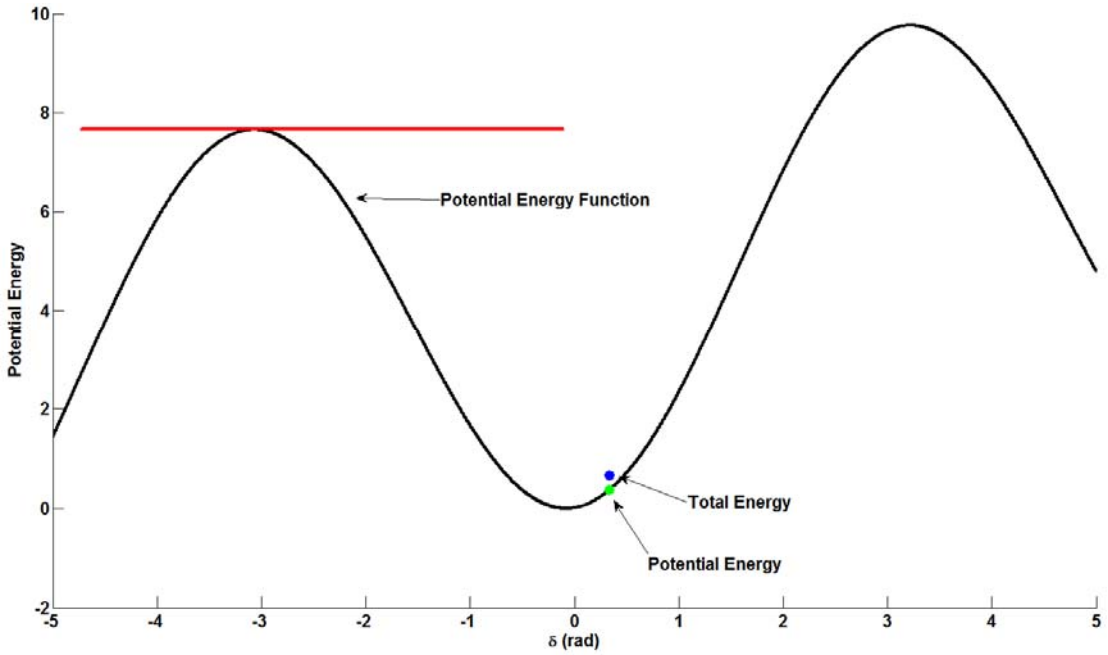

Figure 6.39. System total energy evaluation and stability characterization - fault clearing time t=1.2 sec.

6.4.2 Hypothetical fault clearing time = 1.3 sec

In this section assuming that the fault clearing time is t=1.3 sec, the same analysis as before is performed. In particular, the frequency at the terminals of the lines that connect the substation of interest with the neighboring substations (BUS1, BUS2 and BUS3) is calculated based on a few cycles simulation and is illustrated in Figure 6.40. Based on the frequency at the terminals of the lines, it is clear that two CoO points exist in the system, one on each line that connects the second substation with the first and the third substation. The CoO calculation optimization routine was executed for the determination of the CoO points and the results are summarized in Table 6.18.

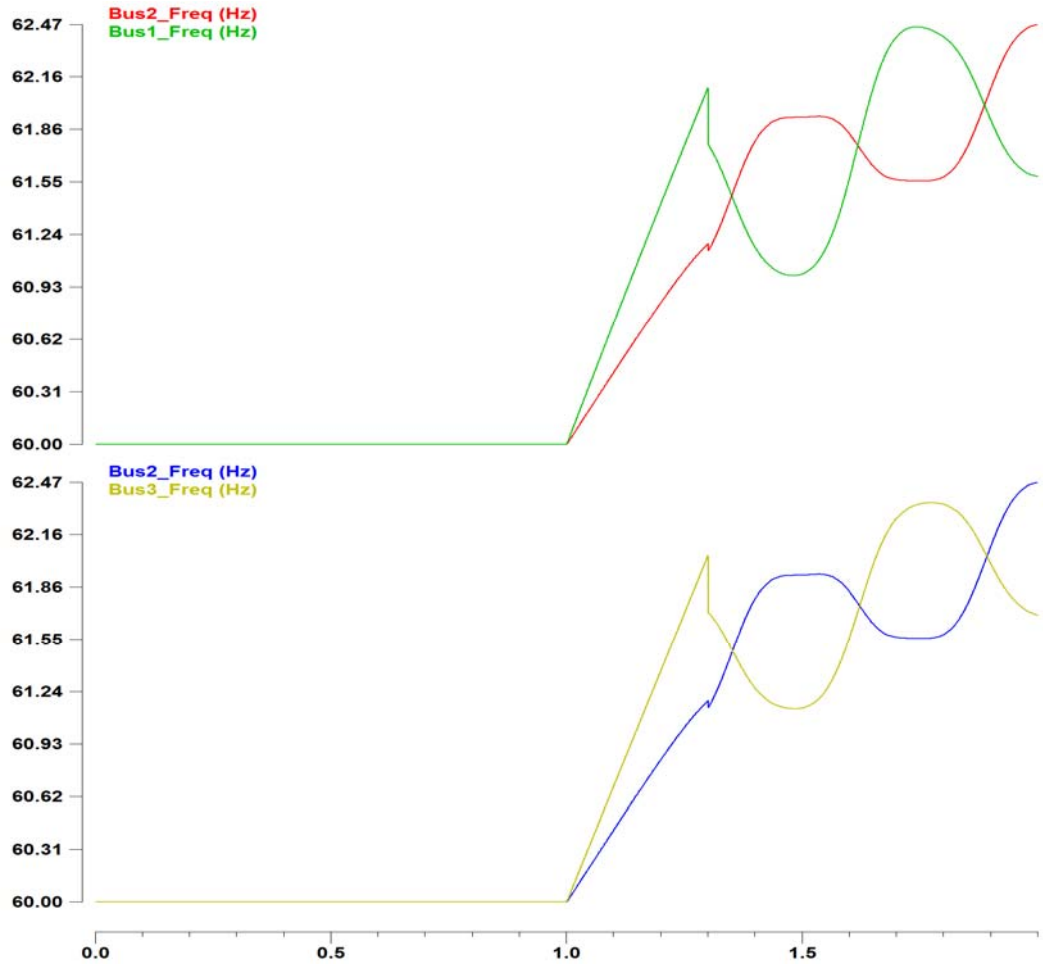

Figure 6.40. Frequency at the terminals of the lines - fault clearing time t=1.3 sec.

Table 6.18. CoO calculation results - fault clearing time t=1.3 sec.

Line	α	b	c	CoO Length (miles)(away from Sub2)	Line Length (miles)	Coo Frequency Equation
SUB2-SUB1	0.64	61.42	1.03	15.6	43.5	$f_{CoO}(t) = 61.42 + 1.03 \cdot t$
SUB2-SUB3	0.59	61.43	0.99	8.2	20.0	$f_{CoO}(t) = 61.43 + 0.99 \cdot t$

Comparison of the simulated and the computed frequency at the CoO is shown in Figure 6.41 and Figure 6.42, for each CoO point respectively. Note that in both cases the simulated frequency at the CoO is almost a straight line and is well approximated by the computed CoO frequency.

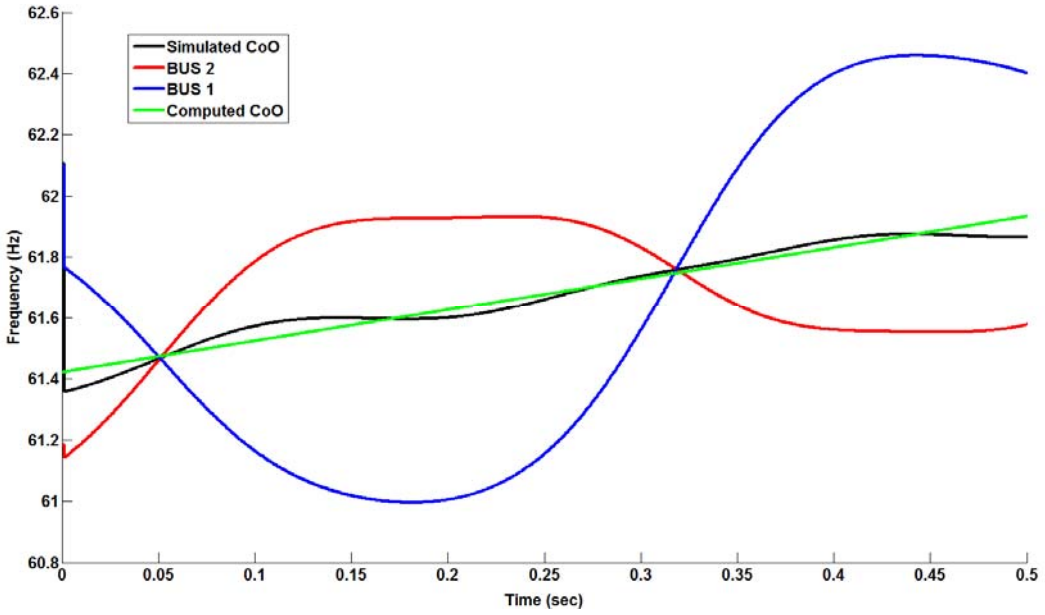

Figure 6.41. Comparison of simulated and computed CoO1 frequency - fault clearing time t=1.3 sec.

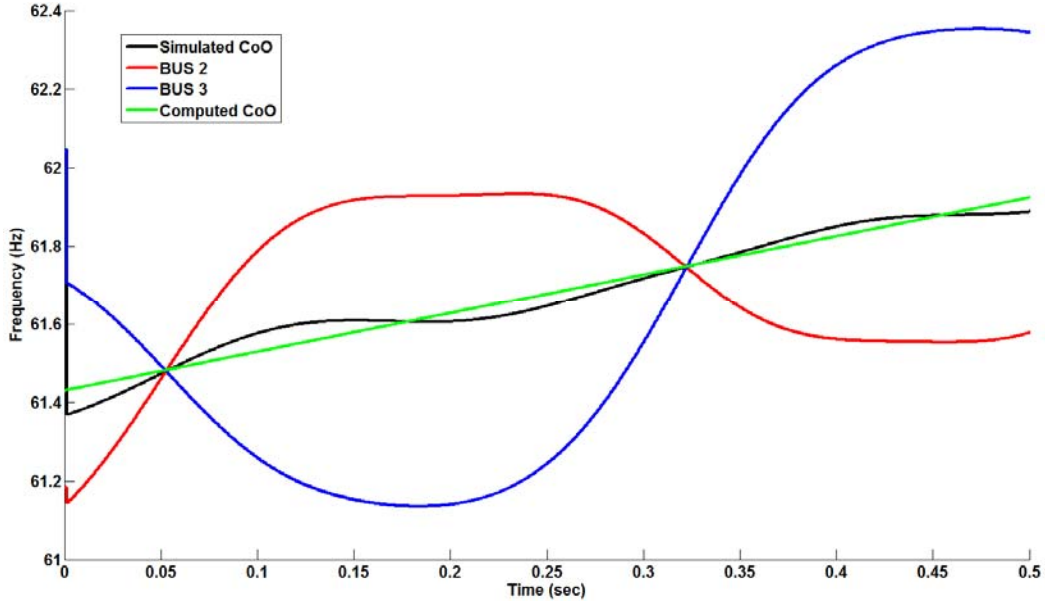

Figure 6.42. Comparison of simulated and computed CoO2 frequency - fault clearing time t=1.3 sec.

Next, a two generator equivalent was built. The equivalent is shown in Figure 6.43.

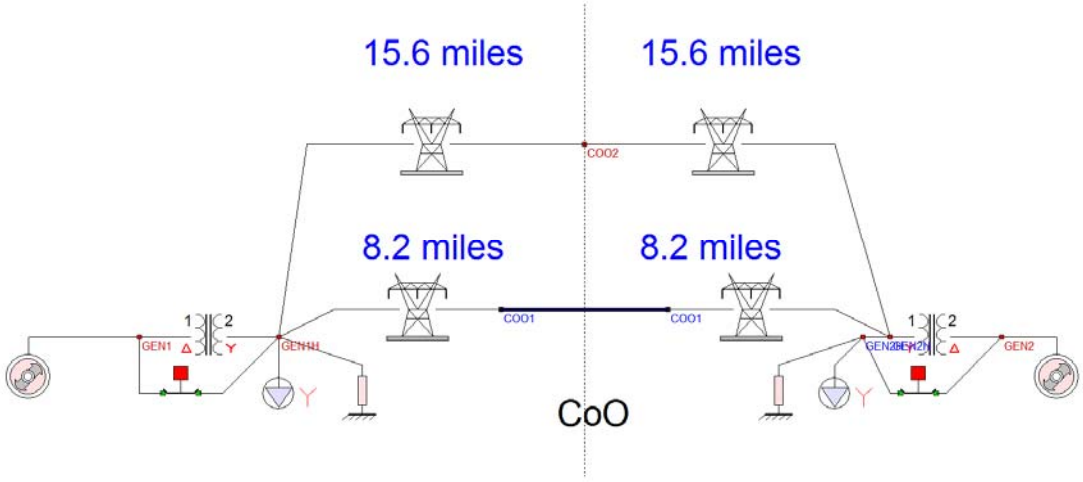

Figure 6.43. Equivalent system - fault clearing time t=1.3 sec.

The accuracy of the equivalent model is evaluated next, by comparing the dynamics of the original system and the equivalent system, as shown in Figure 6.44. The initial conditions of the equivalent system are summarized in Table 6.19. As expected, the dynamics of the equivalent system are very close to the dynamics of the original system.

Table 6.19. Generators' torque angle & frequency - fault clearing time t=1.3 sec.

Generator 1	CoO1	CoO2	Generator 2
δ_1=97.74 deg	δ_{CoO}=69.1 deg	δ_{CoO}=71.2 deg	δ_2=42.46 deg
f_1=61.92 Hz	f_{CoO}=61.36 Hz	f_{CoO}=61.36 Hz	f_2=60.8 Hz

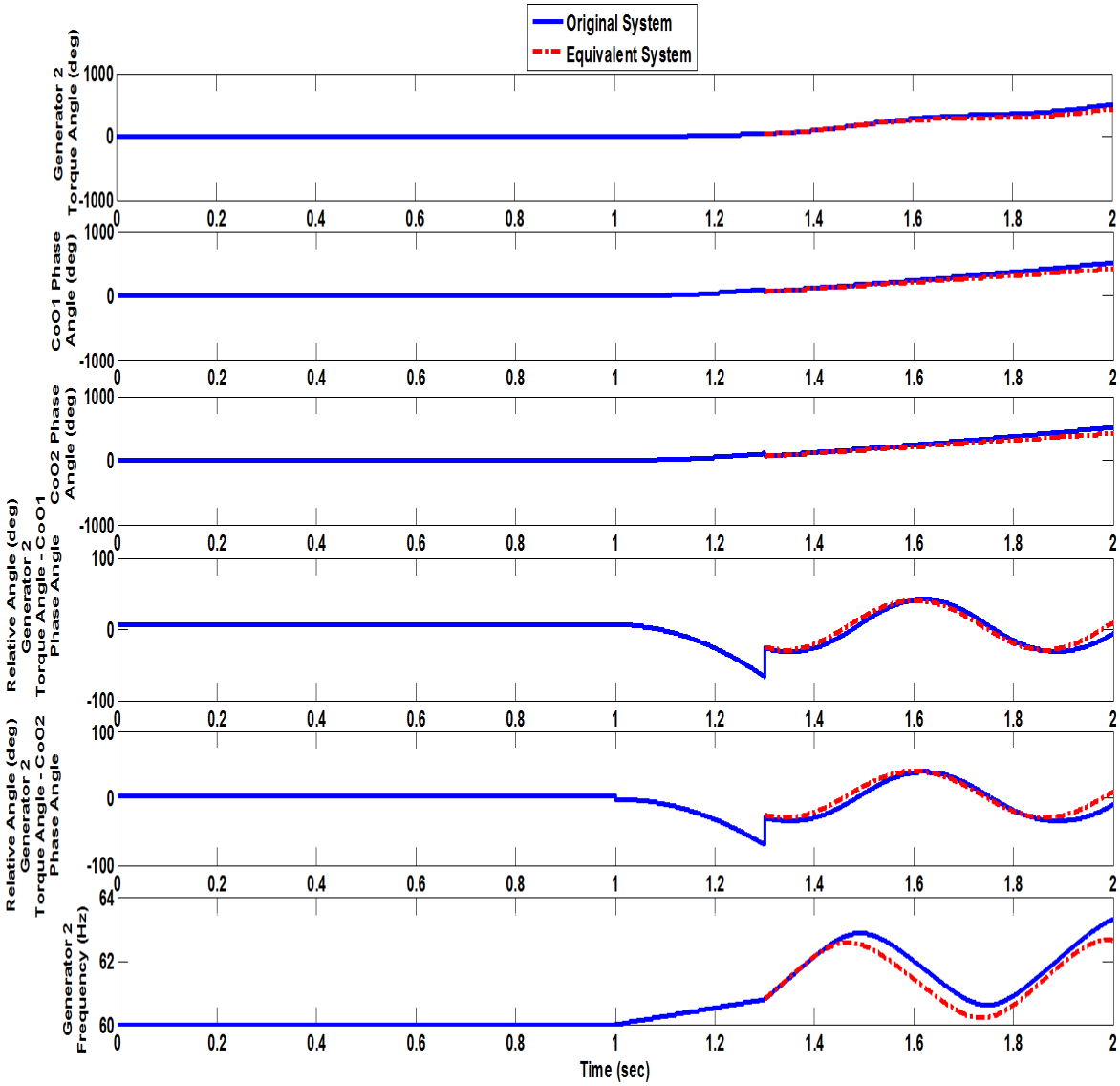

Figure 6.44. Comparison of original and equivalent system dynamics - fault clearing time t=1.3 sec.

The stability of the system for this hypothetical fault clearing time is evaluated. The potential energy function of the equivalent system is calculated along with the total energy of the system given the state of the equivalent system at the hypothetical clearing time (Table 6.19), and it is superposed on the corresponding potential energy function. It is clear that in this case the system is still stable since the total energy is below the barrier, as shown in Figure 6.45.

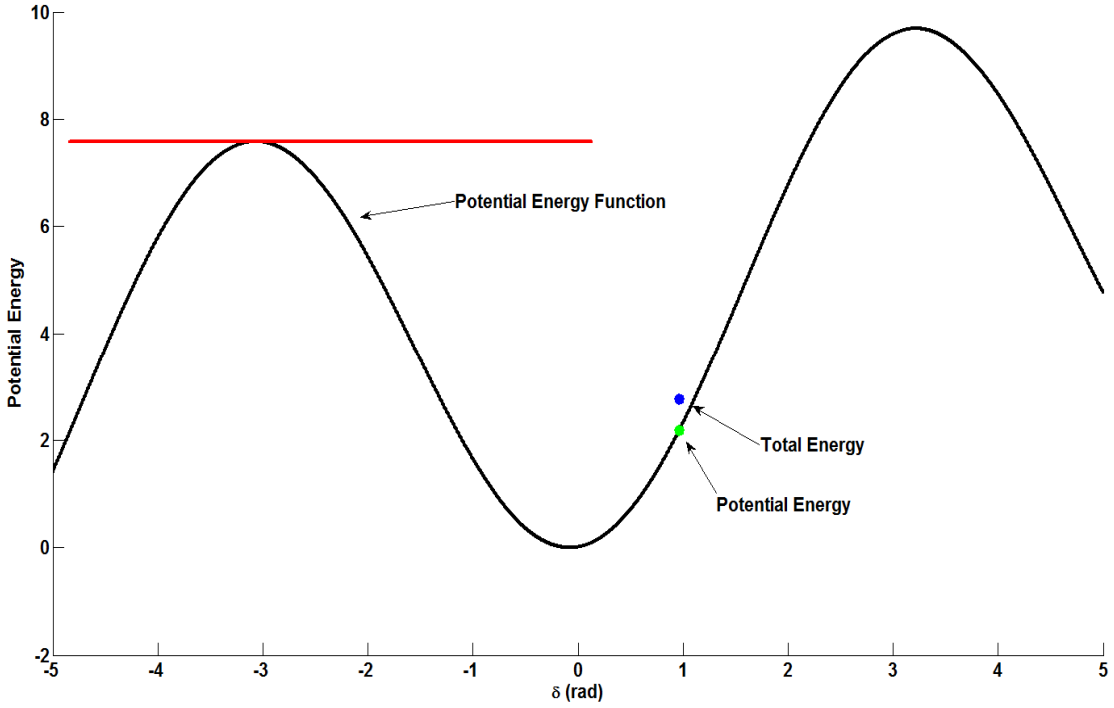

Figure 6.45. System total energy evaluation and stability characterization - fault clearing time t=1.3 sec.

6.4.3 Hypothetical fault clearing time = 1.38 sec

Under the assumption that the fault clearing time is t=1.38 sec, the same steps as before are followed. The frequency at the terminals of the lines that connect the second substation with the neighboring substations (BUS1, BUS2 and BUS3) is calculated based on a few cycles simulation as illustrated in Figure 6.46. It is concluded that two CoO points exist in the system, one on each line that connects the second substation with the first and the third substation. The CoO points that were calculated upon execution of the optimization routine are summarized in Table 6.20.

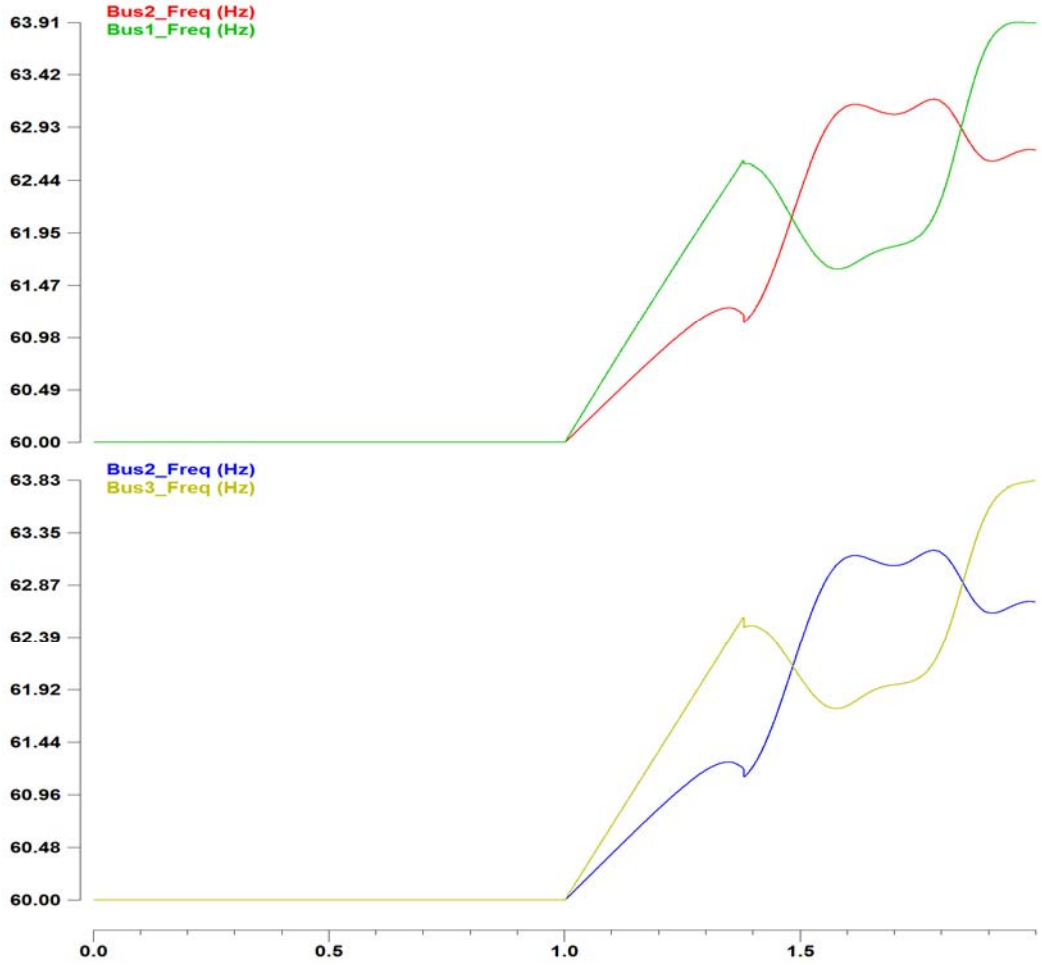

Figure 6.46. Frequency at the terminals of the lines - fault clearing time t=1.38 sec.

Table 6.20. CoO calculation results - fault clearing time t=1.38 sec.

Line	α	b	c	CoO Length (miles)(away from Sub2)	Line Length (miles)	Coo Frequency Equation
SUB2-SUB1	0.483	61.87	2.15	22.5	43.5	$f_{CoO}(t) = 61.87 + 2.15 \cdot t$
SUB2-SUB3	0.5	61.9	2.0	10.0	20.0	$f_{CoO}(t) = 61.9 + 2.0 \cdot t$

The simulated frequency is compared with the computed frequency at the CoO in Figure 6.47 and Figure 6.48, for each CoO point respectively, and the simulated frequency at the CoO is well approximated by the computed CoO frequency.

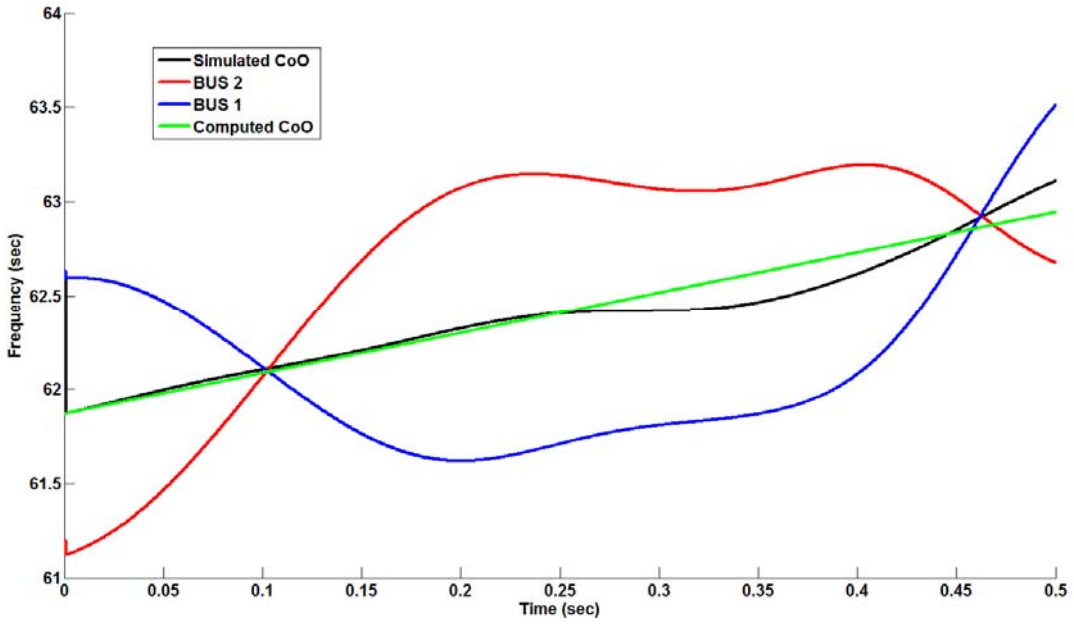

Figure 6.47. Comparison of simulated and computed CoO1 frequency - fault clearing time t=1.38 sec.

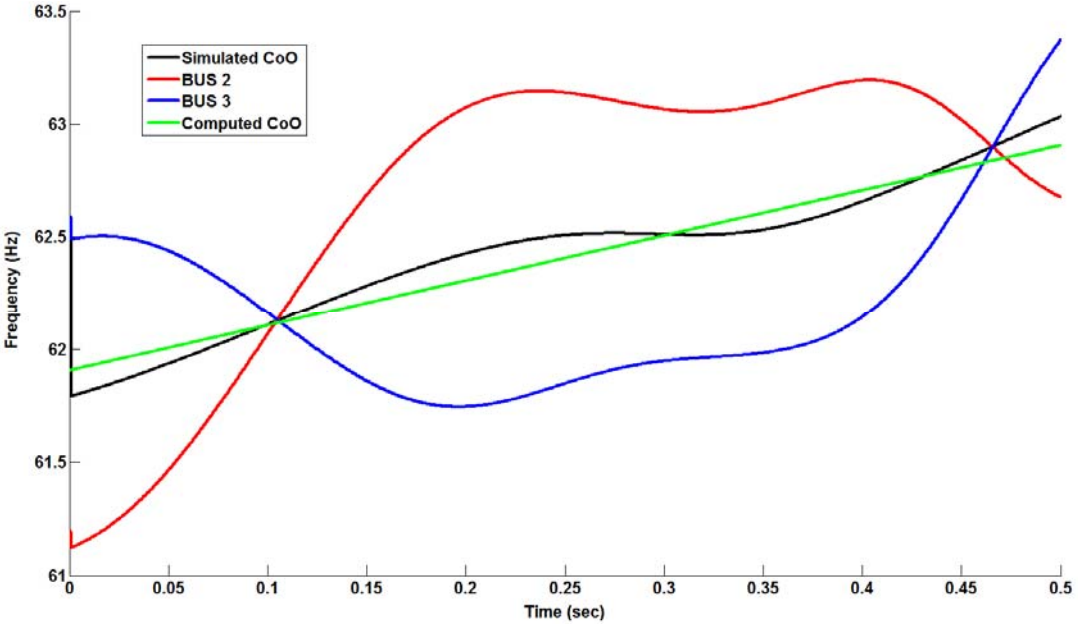

Figure 6.48. Comparison of simulated and computed CoO2 frequency - fault clearing time t=1.38 sec.

Once the CoO is computed, a two generator equivalent was derived. The equivalent is shown in Figure 6.49.

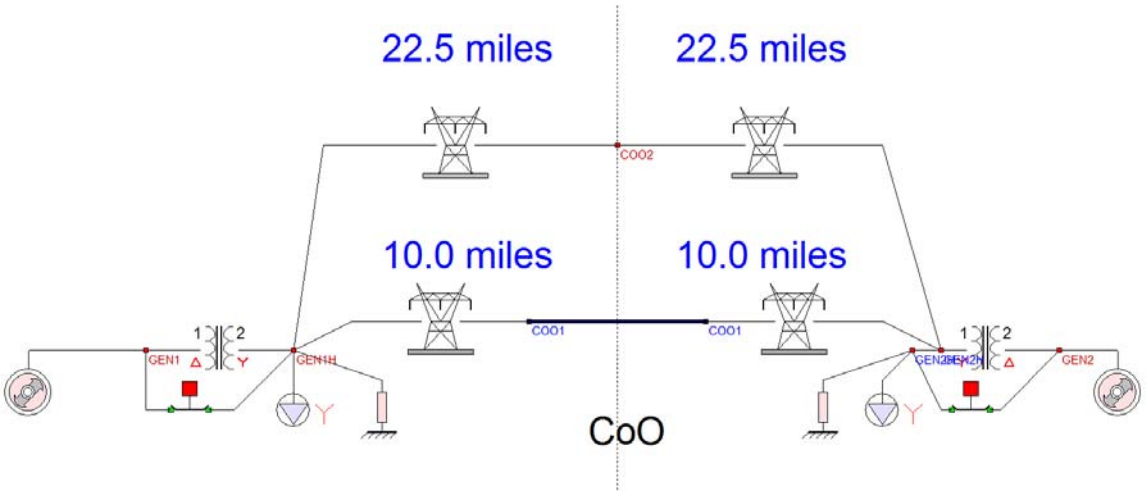

Figure 6.49. Equivalent system - fault clearing time t=1.38 sec.

In order to evaluate the accuracy of the equivalent model, the dynamics of the original system and the equivalent system are compared as illustrated in Figure 6.50. The initials conditions that were used for the equivalent system are shown in Table 6.21.

Table 6.21. Generators' torque angle & frequency - fault clearing time t=1.38 sec.

Generator 1	CoO1	CoO2	Generator 2
δ_1=172.2 deg	δ_{CoO}=120.4 deg	δ_{CoO}=120.2 deg	δ_2=68.4 deg
f_1=62.7 Hz	f_{CoO}=61.82 Hz	f_{CoO}=61.88 Hz	f_2=61.00 Hz

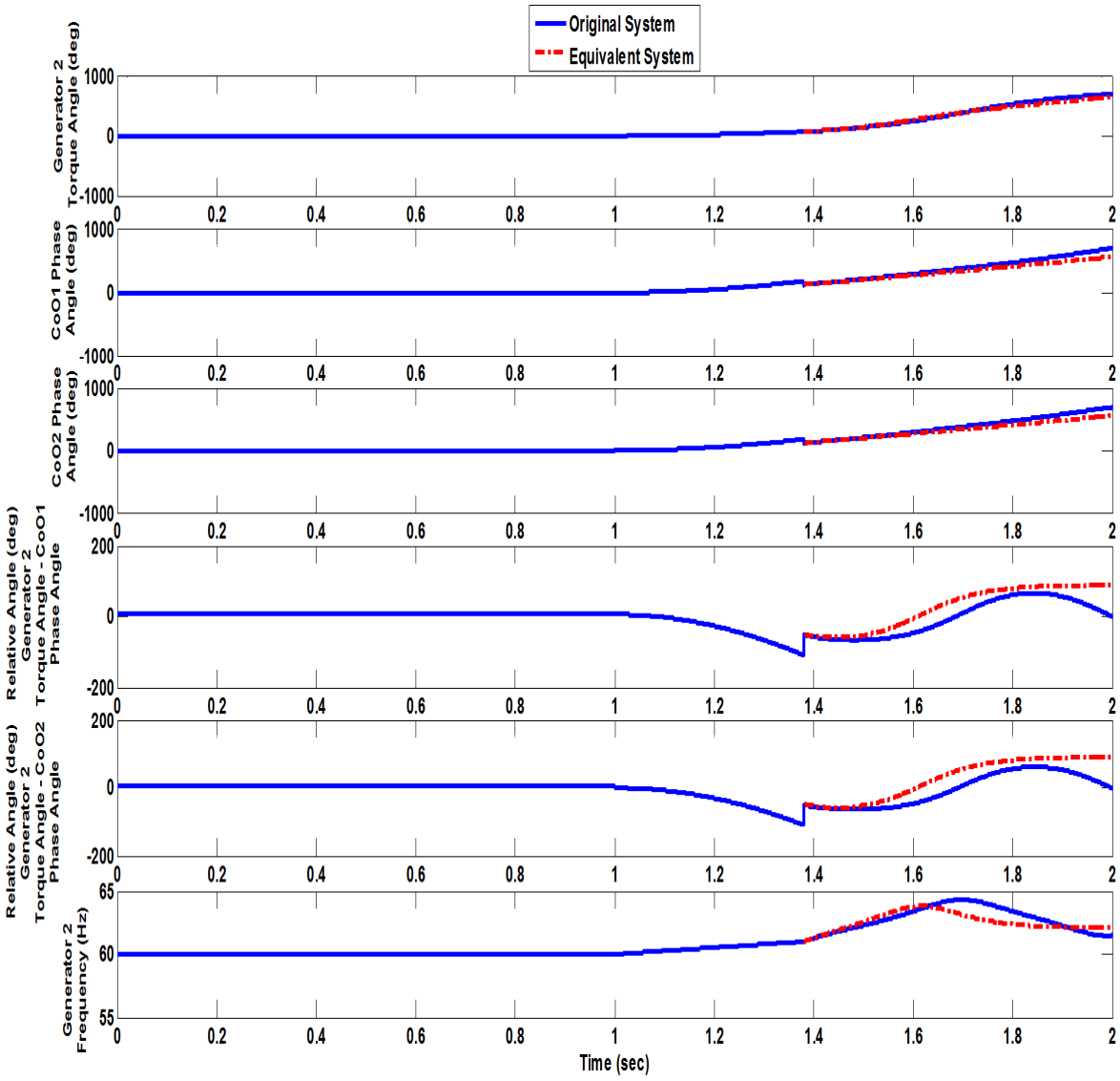

Figure 6.50. Comparison of original and equivalent system dynamics - fault clearing time t=1.38 sec.

Finally, in order to evaluate the stability of the system for this fault clearing time, the potential energy function of the equivalent system is evaluated. The total energy of the system is also computed and it is superposed on the corresponding potential energy function. In this case that the total energy is equal to the barrier value of the energy, as illustrated in Figure 6.51, thus indicating that this is the critical clearing time of the system.

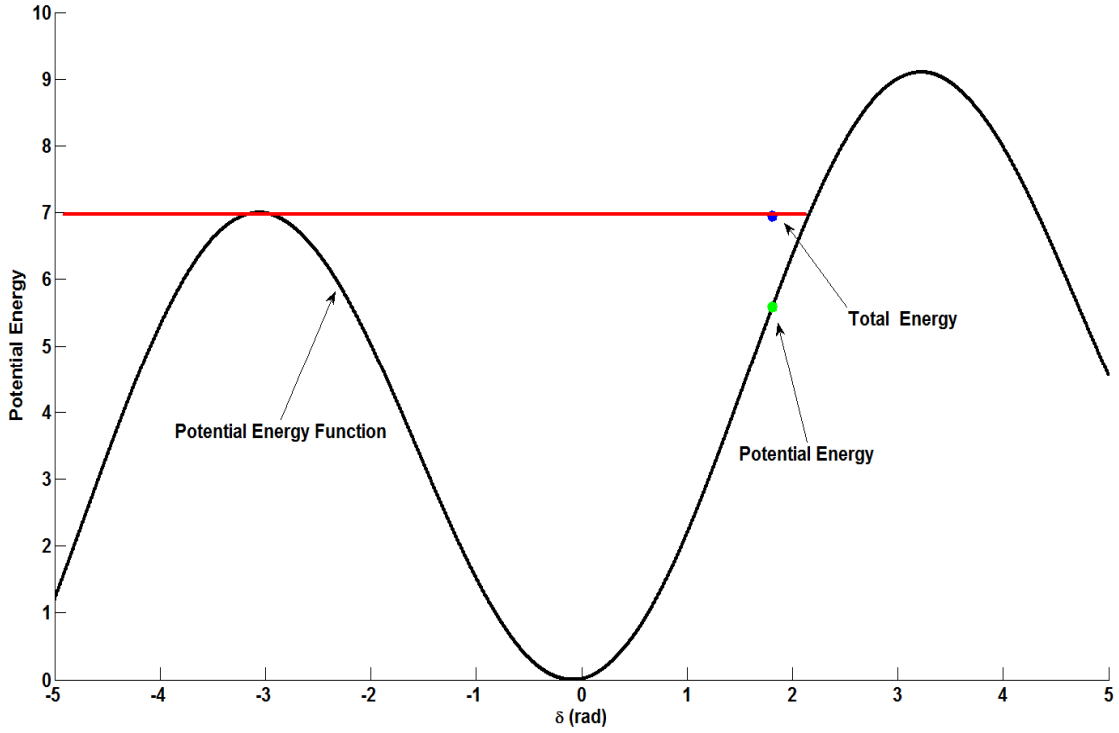

Figure 6.51. System total energy evaluation and stability characterization - fault clearing time t=1.38 sec.

As a result, the critical clearing time (CCT) as computed by the developed method is evaluated to be 0.38 sec after the initiation of the fault, for the specific disturbance. Upon simulations of the system, it was found that the critical clearing time for this fault is 0.39 sec. Thus, there is an error of 0.01 sec in the evaluation of the CCT.

6.4.4 Comparison with conventional out-of-step protection method

The developed transient stability monitoring scheme evaluated the CCT of the system to be at t=1.38 sec (0.38 sec after the fault initiation). At this time instant, instability of the generator is detected and a trip signal can be sent to generator. In this section, comparison between the developed out-of-step protection scheme and the response of a conventional, impedance based, out-of-step relay is performed. In particular, the functionality of an impedance monitoring out-of-step relay is simulated for an unstable scenario with clearing time t=1.4 sec (0.4 sec after fault initiation). The results are summarized in Figure 6.52. In particular, monitoring of the trajectory of the impedance at the terminals of the generator indicates that the left blinder and the right blinder are

crossed at t=1.43 sec and t=1.64 sec respectively. As a result, the impedance based relay detected instability at t=1.64 sec. Thus, it is concluded that the developed method predicted instability 0.26 sec before the conventional relay. Note that this time difference does not consider the fact that when the second blinder is crossed the value of the phase angle is high and the generator trip has to be delayed to avoid breaker overstress.

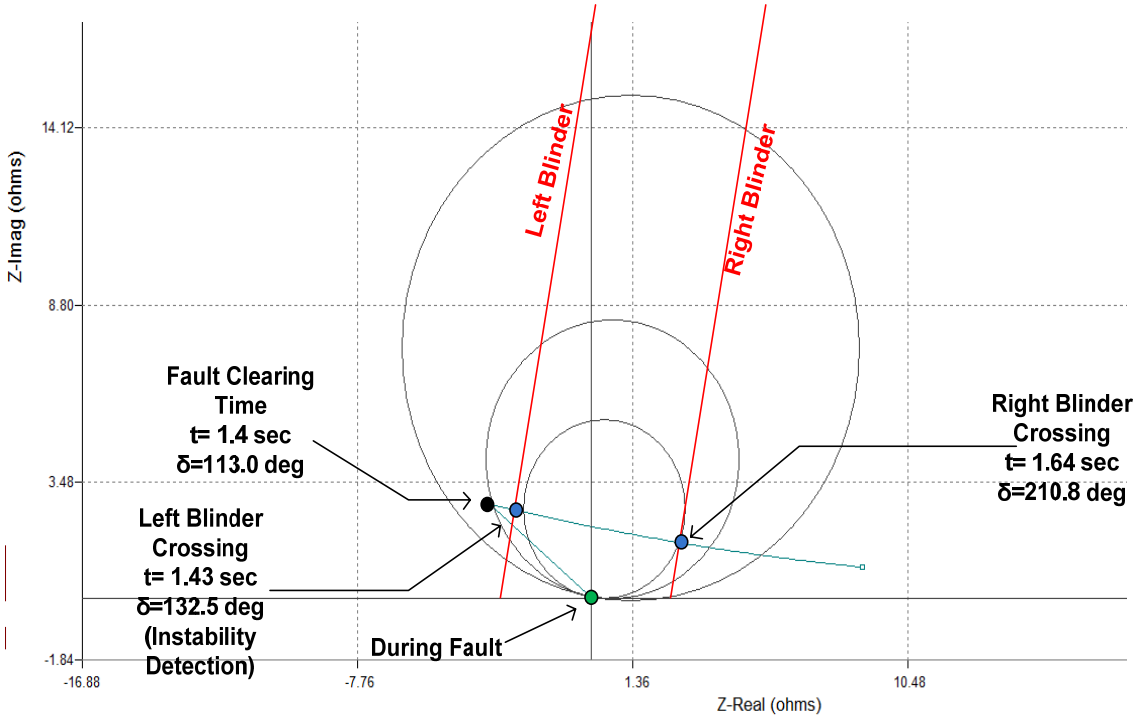

Figure 6.52. Impedance trajectory monitoring - three substation system.

6.5 NYPA Blenheim-Gilboa Substation

The transient stability monitoring scheme was also tested on the NYPA Blenheim-Gilboa substation. The details of the substation model are given in Appendix C. It was assumed that all four generators were operational, providing the same amount of power, so a single equivalent generator was used. The fault that will be examined is a three phase fault at the terminal of the substation and the fault is cleared by disconnecting the line that connects the Blenheim-Gilboa substation with Frazer substation. The fault initiates at t=1 sec and different clearing times are examined next.

6.5.1 Hypothetical fault clearing time = 1.1 sec

Assuming that the fault is cleared at t=1.1 sec, the frequency at the terminal of the Blenheim Gilboa substation (B-G bus) and the neighboring substations (NSCOTLAND bus and LEEDS bus) is simulated and is shown in Figure 6.53.

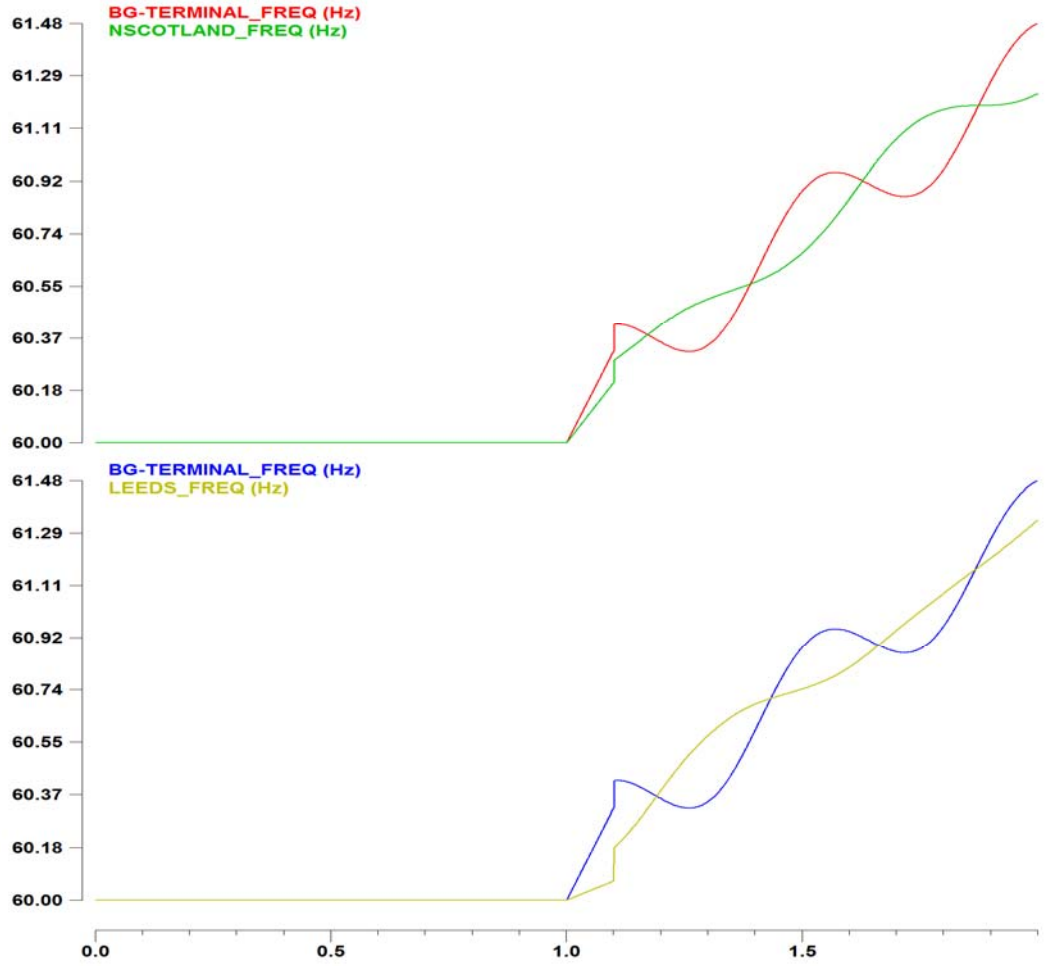

Figure 6.53. Frequency at the terminals of the lines - fault clearing time t=1.1 sec.

Given the frequency at the terminals of the lines it is concluded that there is a CoO point within each of the lines that connect the Blenheim-Gilboa substation with the neighboring substations (Nscotland and Leeds). The optimization algorithm was executed for the determination of the CoO points in the two lines and the results are summarized in Table 6.22.

Table 6.22. CoO calculation results - fault clearing time t=1.1 sec.

Line	α	b	c	CoO Length (miles)(away from B-G Sub)	Line Length (miles)	Coo Frequency Equation
BG-NSCOTLAND	0.181	60.32	0.82	29.0	35.4	$f_{CoO}(t) = 60.32 + 0.82 \cdot t$
BG-LEEDS	0.276	60.24	1.4	21.9	30.3	$f_{CoO}(t) = 60.24 + 1.4 \cdot t$

The frequency at the terminals of the two lines, along with comparison between the simulated and the computed frequency at the CoO points are shown in Figure 6.54 and Figure 6.55. Note that the simulated frequency at the CoO is almost a straight line and is well approximated by the computed CoO frequency.

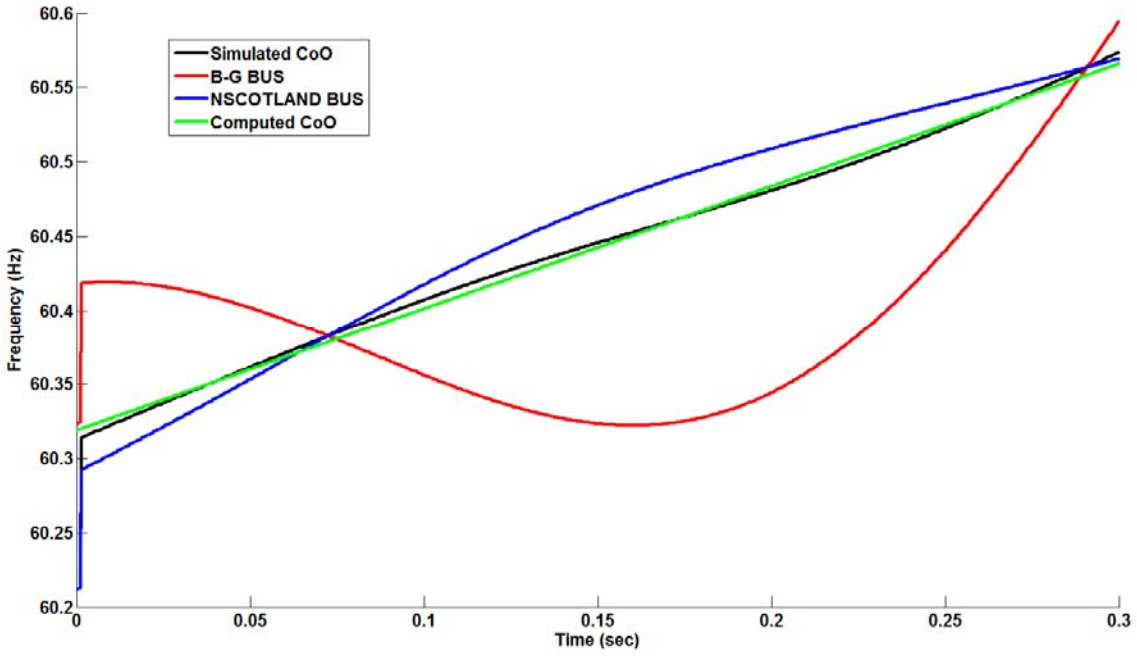

Figure 6.54. Comparison of simulated and computed CoO1 frequency - fault clearing time t=1.1 sec.

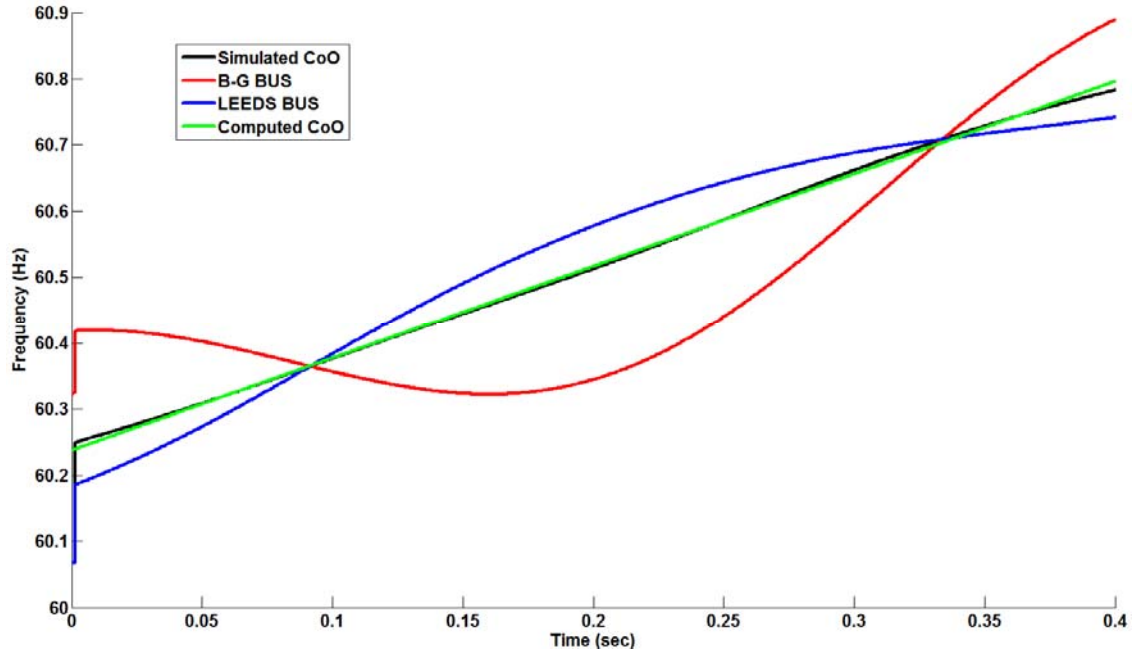

Figure 6.55. Comparison of simulated and computed CoO2 frequency - fault clearing time t=1.1 sec.

The two generator equivalent that was built upon calculation of the CoO points is shown in Figure 6.56.

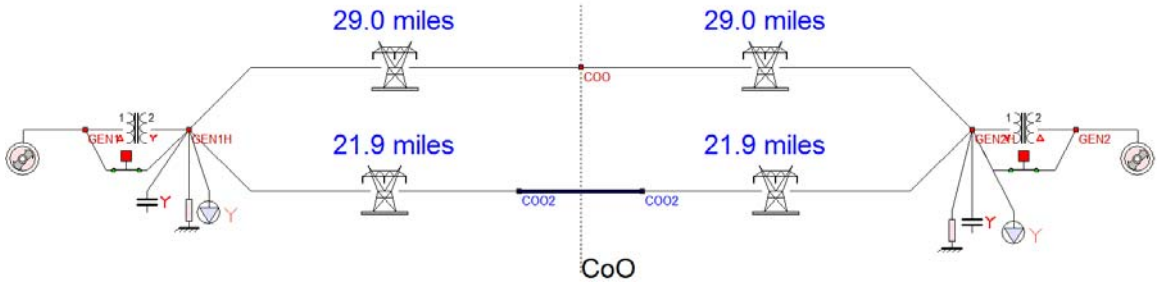

Figure 6.56. Equivalent system - fault clearing time t=1.1 sec.

The accuracy of the equivalent model is evaluated next, by comparing the dynamics of the original system and the equivalent system. In particular, the initial conditions (torque angle and speed) of the generator in the substation of interest were set to the values that the system had at the fault clearing time, as computed by the DSE in the substation. The initial conditions (torque angle and speed) of the generator in the second substation (mirror image part of the system) were set to be symmetric to the values of the first generator in terms of the CoO, as explained in section 4.3.2, and are shown in Table 6.23.

Table 6.23. Generators' torque angle & frequency - fault clearing time t=1.1 sec.

Generator 1	CoO1	CoO2	Generator 2
δ_1=4.4 deg	δ_{CoO}=-10.56 deg	δ_{CoO}=-13.32 deg	δ_2=-28.28 deg
f_1=60.74 Hz	f_{CoO}=60.26 Hz	f_{CoO}=60.30 Hz	f_2=59.82 Hz

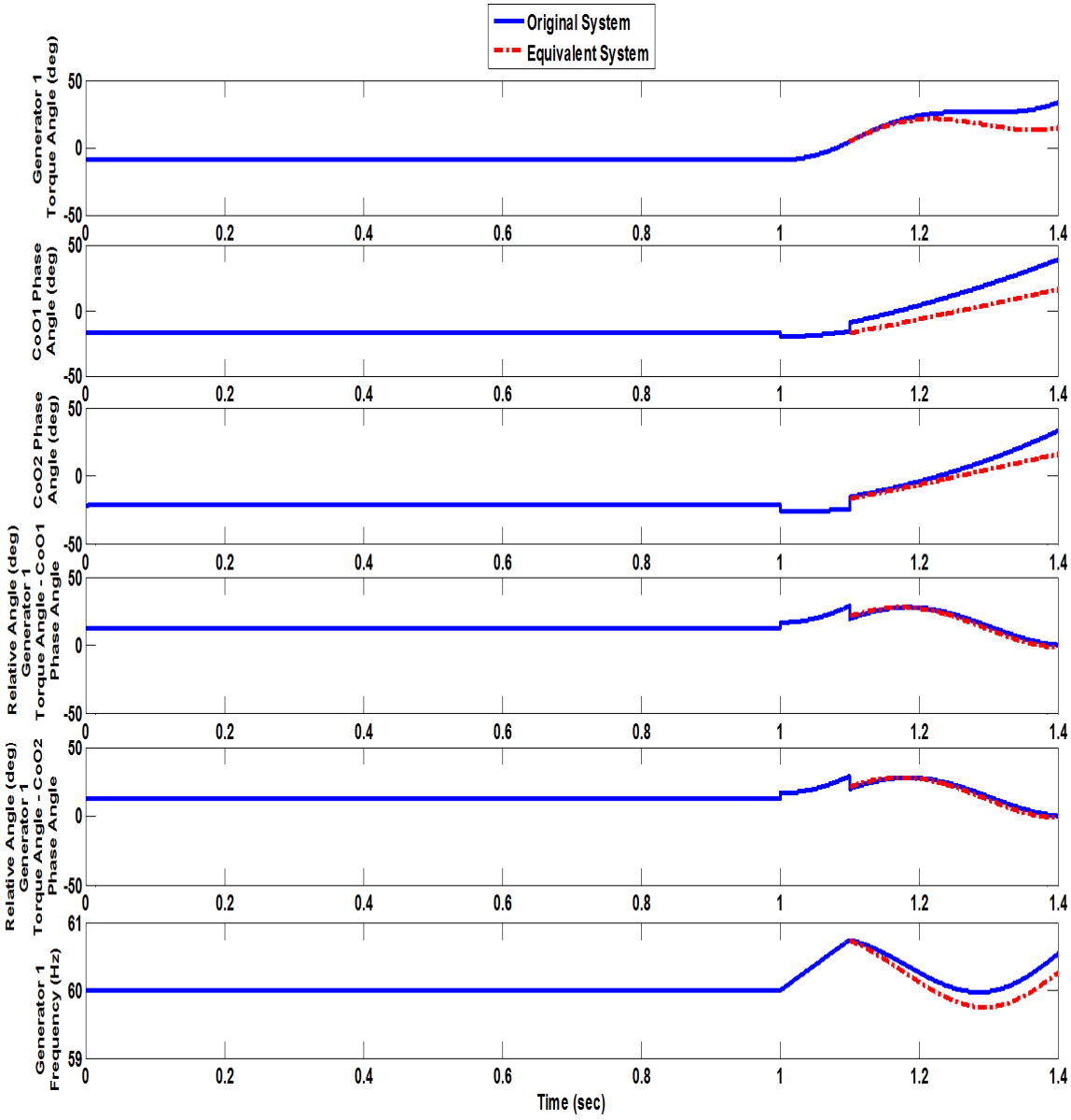

Figure 6.57. Comparison of original and equivalent system dynamics - fault clearing time t=1.1 sec.

As expected, the dynamics of the equivalent system are very close to the dynamics of the original system, as shown in Figure 6.57.

In order to evaluate the stability of the system for this hypothetical fault clearing time, the potential energy function of the equivalent system was evaluated along with the total energy of the system which is superposed on the corresponding potential energy function, as illustrated in Figure 6.58. It is clear in this case that the total energy is below the barrier energy value, thus indicating a stable system.

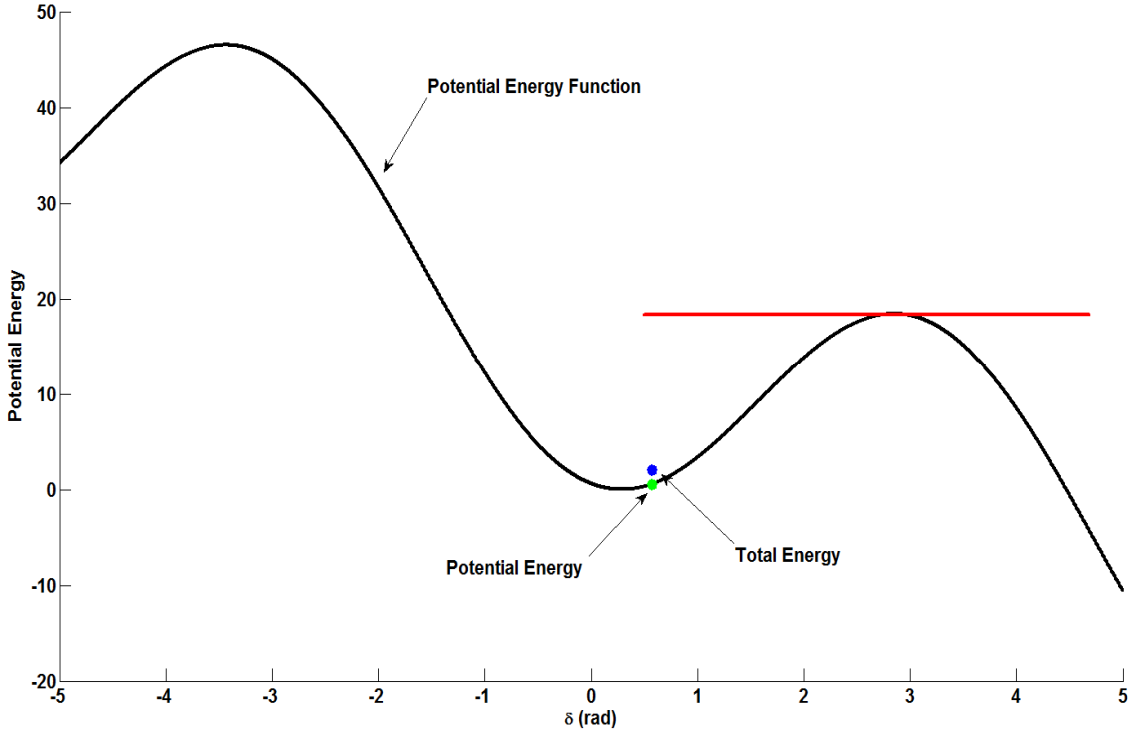

Figure 6.58. System total energy evaluation and stability characterization - fault clearing time t=1.1 sec.

6.5.2 Hypothetical fault clearing time = 1.2 sec

For this hypothetical fault clearing time, the same analysis is performed. In particular, the frequency at the terminals of the Blenheim-Gilboa and its neighboring substations are shown in Figure 6.59.

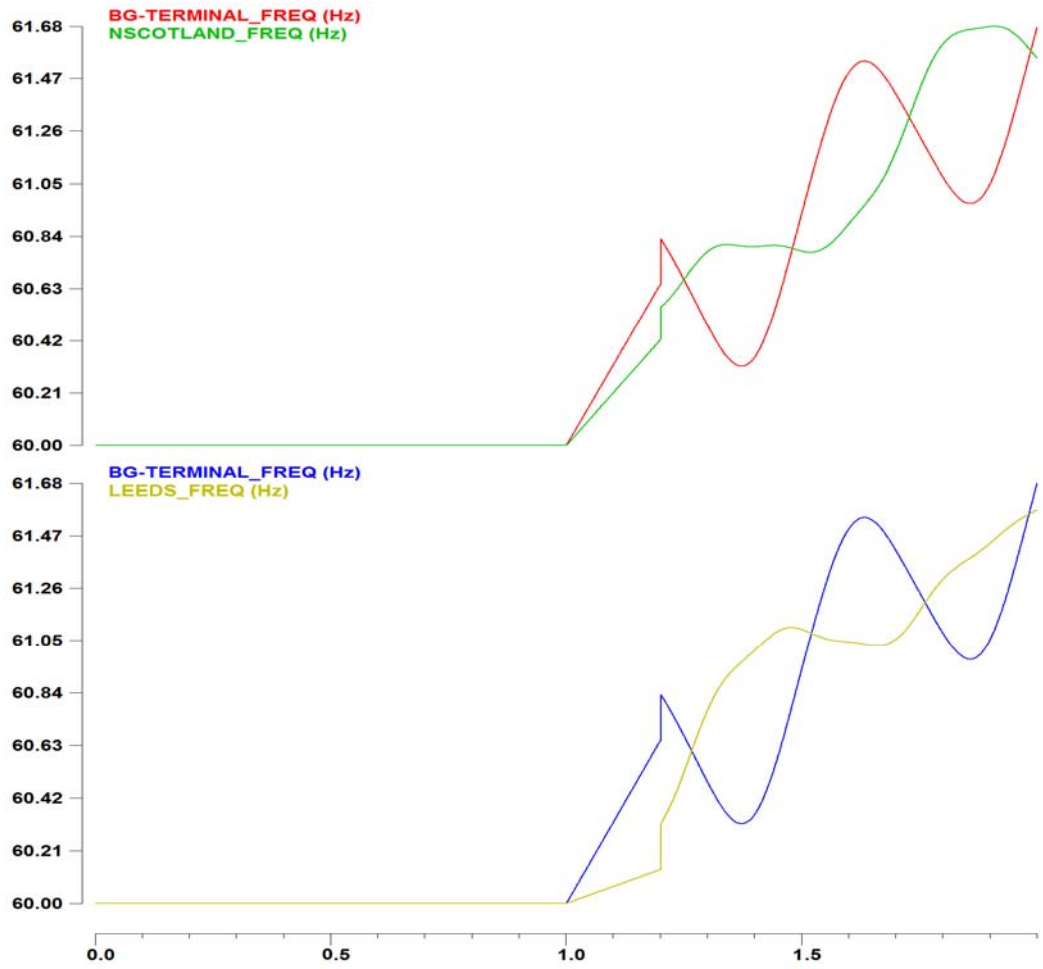

Figure 6.59. Frequency at the terminals of the lines - fault clearing time t=1.2 sec.

Given the computed frequencies, it is concluded that there is a CoO point on each of the two lines and the optimization algorithm was executed for the determination of the CoO points. The results are summarized in Table 6.24.

In Figure 6.60 and Figure 6.61, the simulated frequency is compared with the computed frequency for the two CoO points.

Table 6.24. CoO calculation results - fault clearing time t=1.2 sec.

Line	α	b	c	CoO Length (miles)(away from B-G sub)	Line Length (miles)	Coo Frequency Equation
BG-NSCOTLAND	0.277	60.64	0.5	25.6	35.4	$f_{CoO}(t) = 60.64 + 0.5 \cdot t$
BG-LEEDS	0.366	60.47	1.84	19.2	30.3	$f_{CoO}(t) = 60.47 + 1.84 \cdot t$

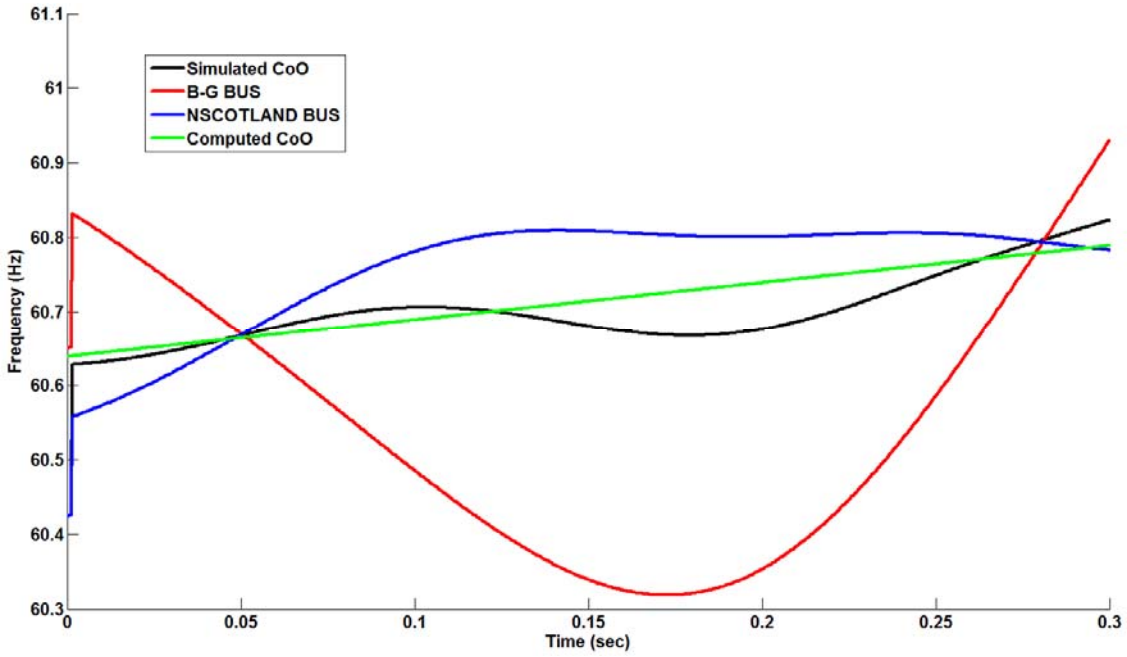

Figure 6.60. Comparison of simulated and computed CoO1 frequency - fault clearing time t=1.2 sec.

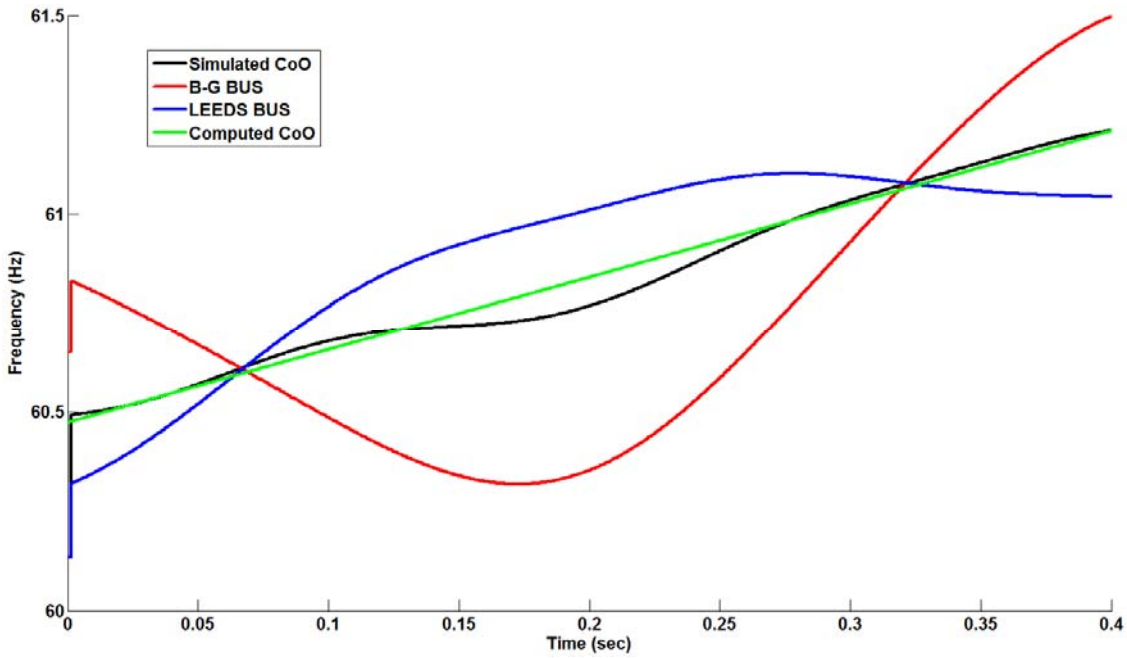

Figure 6.61. Comparison of simulated and computed CoO2 frequency - fault clearing time t=1.2 sec.

Once the CoO is computed, a two generator equivalent was built. The equivalent is shown in Figure 6.62.

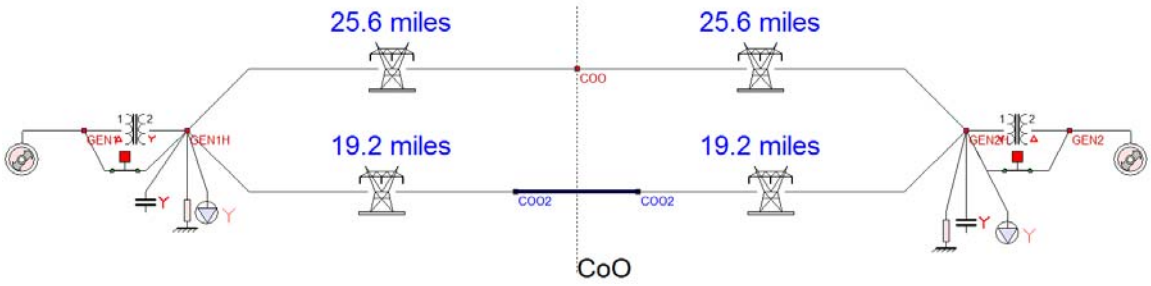

Figure 6.62. Equivalent system - fault clearing time t=1.2 sec.

Next the accuracy of the equivalent model is evaluated by comparing the dynamics of the original system and the equivalent system as shown in Figure 6.63. The initial conditions of the equivalent system as computed by the DSE results and the phase angle and frequency at the CoO points is shown in Table 6.25. As expected, the dynamics of the equivalent system are very close to the dynamics of the original system.

Table 6.25. Generators' torque angle & frequency - fault clearing time t=1.2 sec.

Generator 1	CoO1	CoO2	Generator 2
δ_1=44.7 deg	δ_{CoO}=4.9 deg	δ_{CoO}=3.5 deg	δ_2=-36.3 deg
f_1=61.46 Hz	f_{CoO}=60.57 Hz	f_{CoO}=60.53 Hz	f_2=59.64 Hz

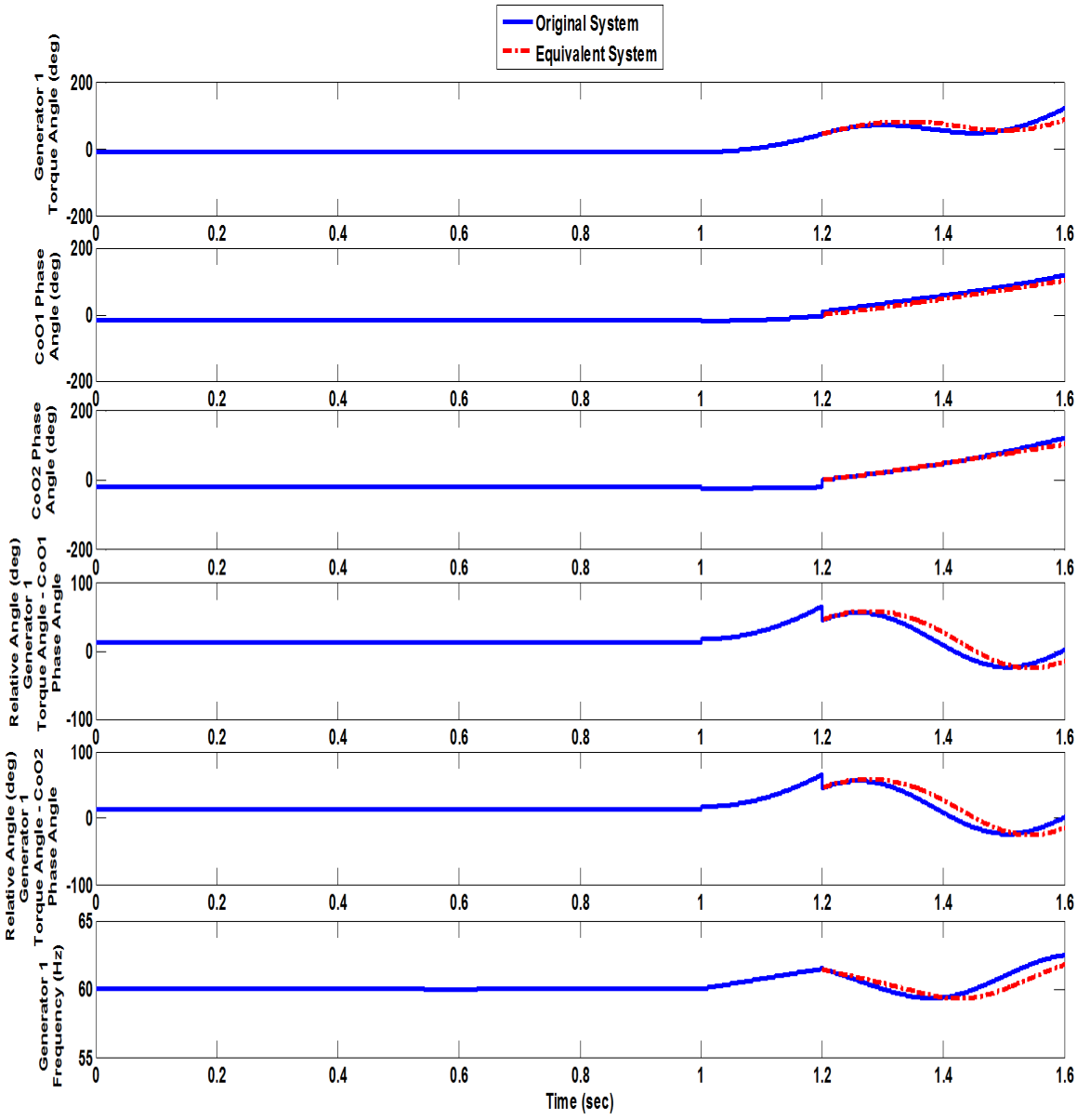

Figure 6.63. Comparison of original and equivalent system dynamics - fault clearing time t=1.2 sec.

The stability of the system is evaluated for this assumed fault clearing time. Given the equivalent system, the potential energy function was evaluated. The total energy of the system is also computed and it is superposed on the corresponding potential energy function as illustrated in Figure 6.64. The total energy is below the barrier in this case too, thus the system is still in the stable region.

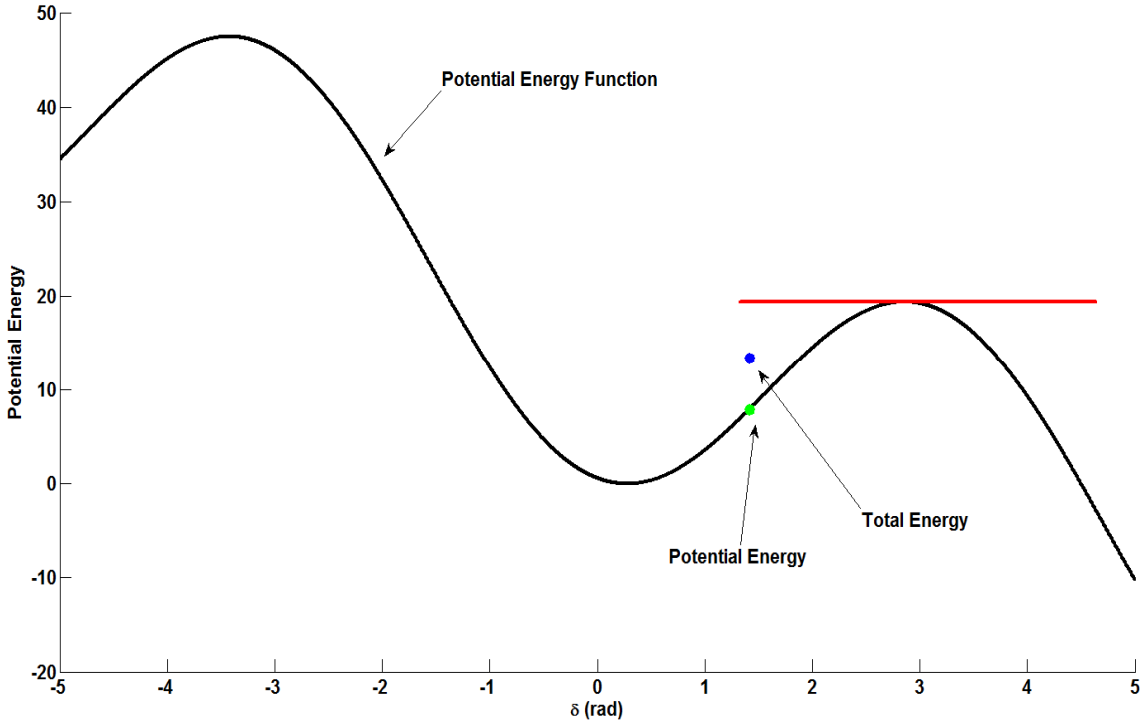

Figure 6.64. System total energy evaluation and stability characterization - fault clearing time t=1.2 sec.

6.5.3 Hypothetical fault clearing time = 1.27 sec

Assuming that the fault clearing time is t=1.27 sec, the frequency at the B-G bus (terminal of Blenheim-Gilboa substation) and the neighboring substations (NSCOTLAND bus and LEEDS bus) is illustrated in Figure 6.65. It is concluded that the CoO lies on the two lines that connect the Blenheim-Gilboa substation with the neighboring substations and upon execution of the optimization algorithm, the CoO points were evaluated as shown in Table 6.26.

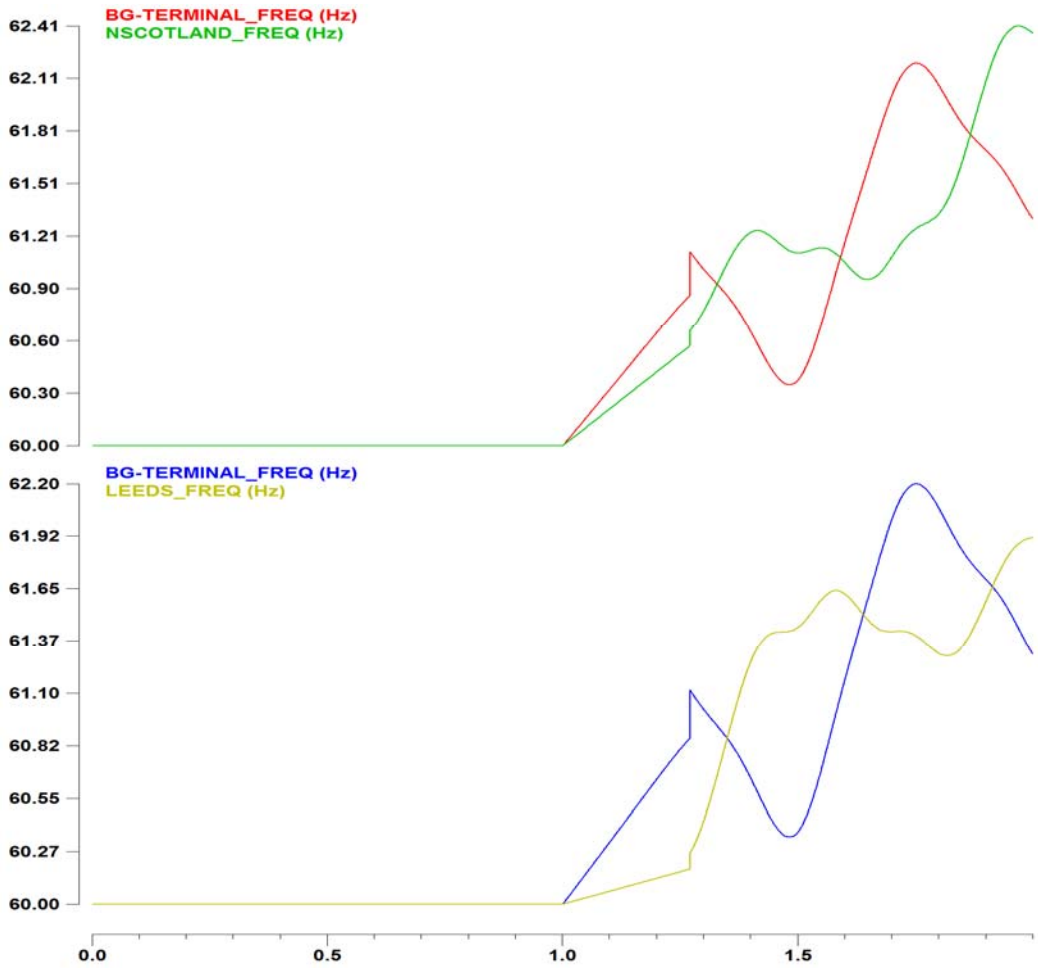

Figure 6.65. Frequency at the terminals of the lines - fault clearing time t=1.27 sec.

Table 6.26. CoO calculation results - fault clearing time t=1.27 sec.

Line	α	b	c	CoO Length (miles)(away from B-G substation)	Line Length (miles)	Coo Frequency Equation
BG-NSCOTLAND	0.62	60.89	0.56	13.4	35.4	$f_{CoO}(t) = 60.89 + 0.56 \cdot t$
BG-LEEDS	0.64	60.63	2.37	10.9	30.3	$f_{CoO}(t) = 60.63 + 2.37 \cdot t$

Comparison of the simulated and the computed frequency for the two CoO points is illustrated in Figure 6.66 and Figure 6.67. However the accuracy is decreased compared with the previous cases since the system approaches its instability region and the nonlinearities become more severe for this complex system. This can be observed also by the simulated frequencies in Figure 6.65.

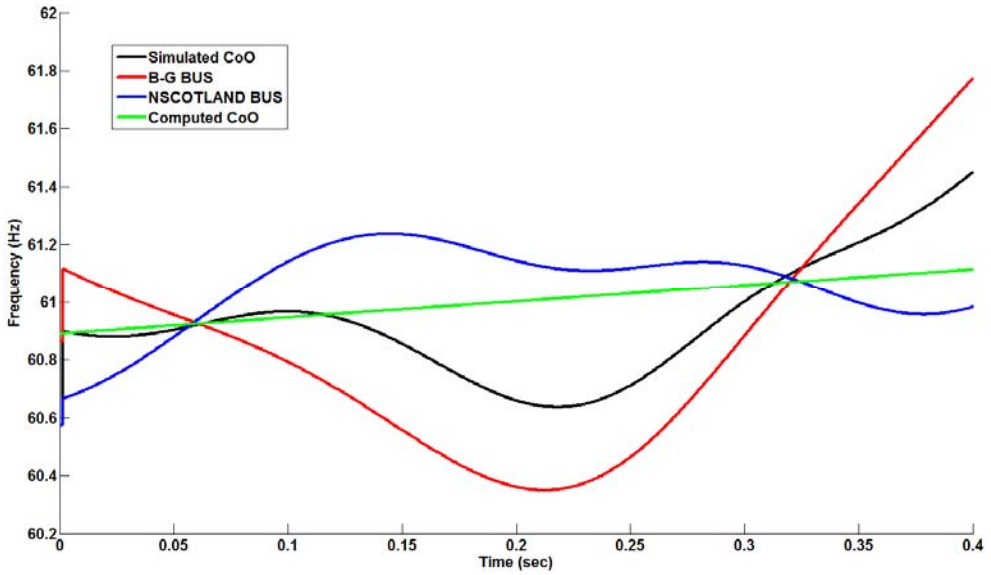

Figure 6.66. Comparison of simulated and computed CoO1 frequency - fault clearing time t=1.27 sec.

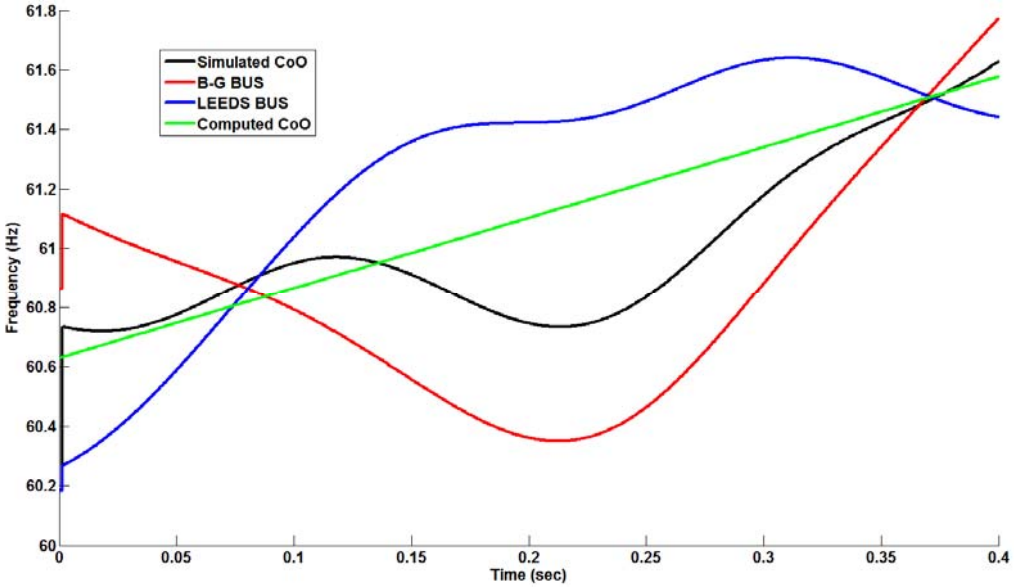

Figure 6.67. Comparison of simulated and computed CoO2 frequency - fault clearing time t=1.27 sec.

The two generator equivalent that was derived is shown in Figure 6.68.

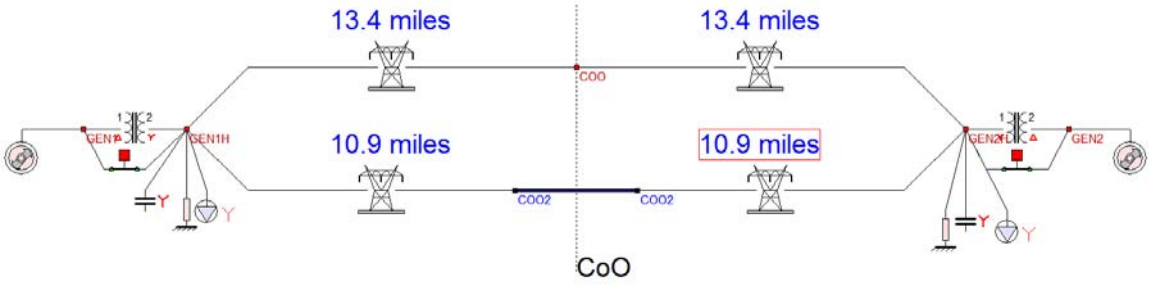

Figure 6.68. Equivalent system - fault clearing time t=1.27 sec.

In order to evaluate the accuracy of the equivalent model, the dynamics of the original system and the equivalent system are compared in Figure 6.69. The initial conditions (torque angle and speed) of the generators in the equivalent system that are computed based on the DSE results are summarized in Table 6.27. In this case, it is noted that the accuracy is decreased compared to the previous case. This was expected due to the fact that the system is very close to the instability region and the nonlinearities are more dominant. As a result the assumption that the CoO frequency is a straight line is less accurate, and given that the derivation of the equivalent system was made under the assumption that the frequency and the phase angle along the lines in the system varies linearly with the distance from the terminals of the line, the accuracy of the equivalent system is reduced.

Table 6.27. Generators' torque angle & frequency - fault clearing time t=1.27 sec.

Generator 1	CoO1	CoO2	Generator 2
δ_1=88.3 deg	δ_{CoO}=31.98 deg	δ_{CoO}=33.72 deg	δ_2=-22.6 deg
f_1=62.01 Hz	f_{CoO}=60.96 Hz	f_{CoO}=61.02 Hz	f_2=59.96 Hz

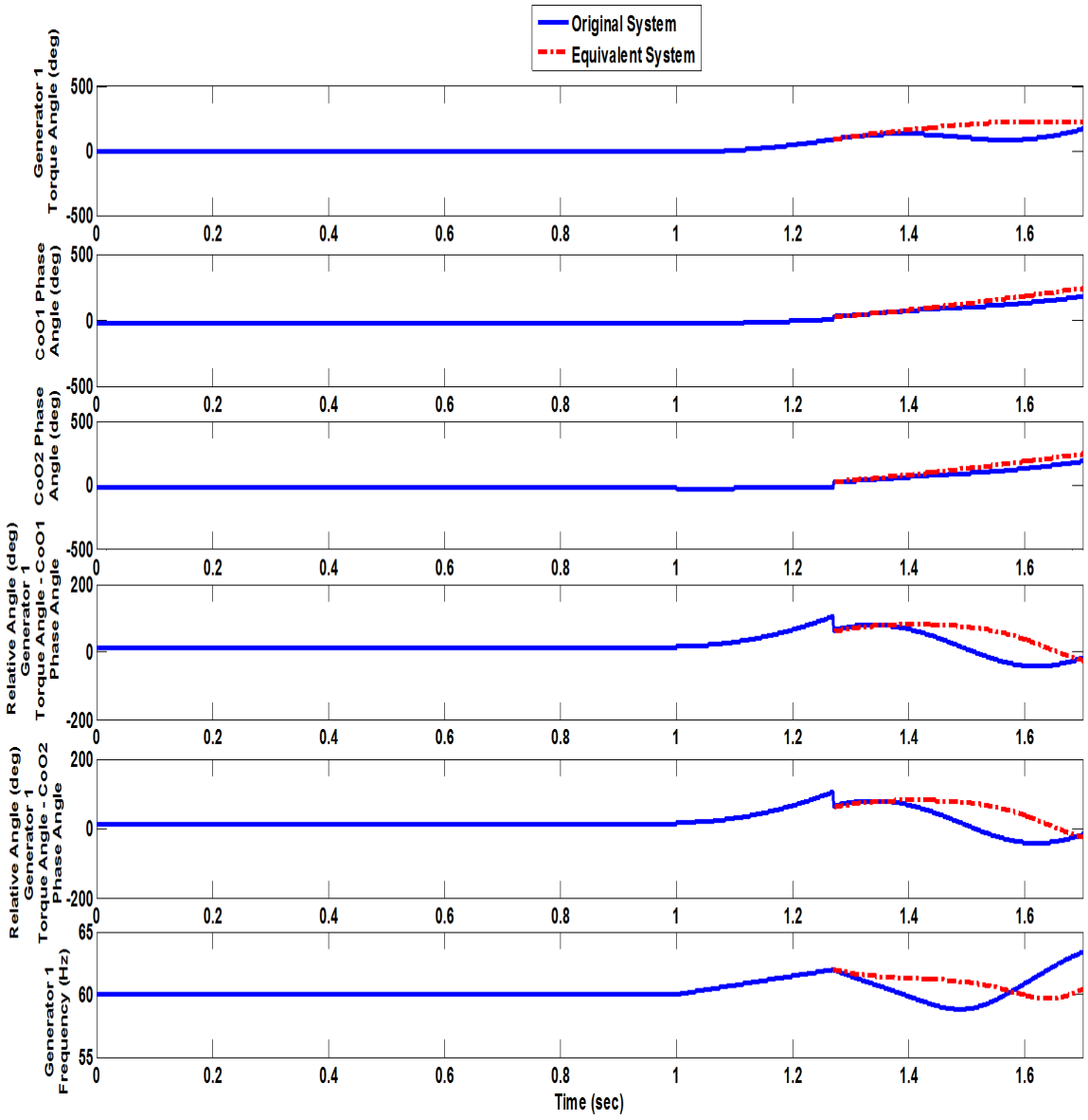

Figure 6.69. Comparison of original and equivalent system dynamics - fault clearing time t=1.27 sec.

Finally, the stability of the system is evaluated for this hypothetical fault clearing time. Again, the potential energy function of the equivalent system was evaluated along with the total energy of the system which is superposed on the corresponding potential energy function, as illustrated in Figure 6.70. In this case that the total energy is equal to the barrier value of the energy, thus indicating that this is the critical clearing time of the system.

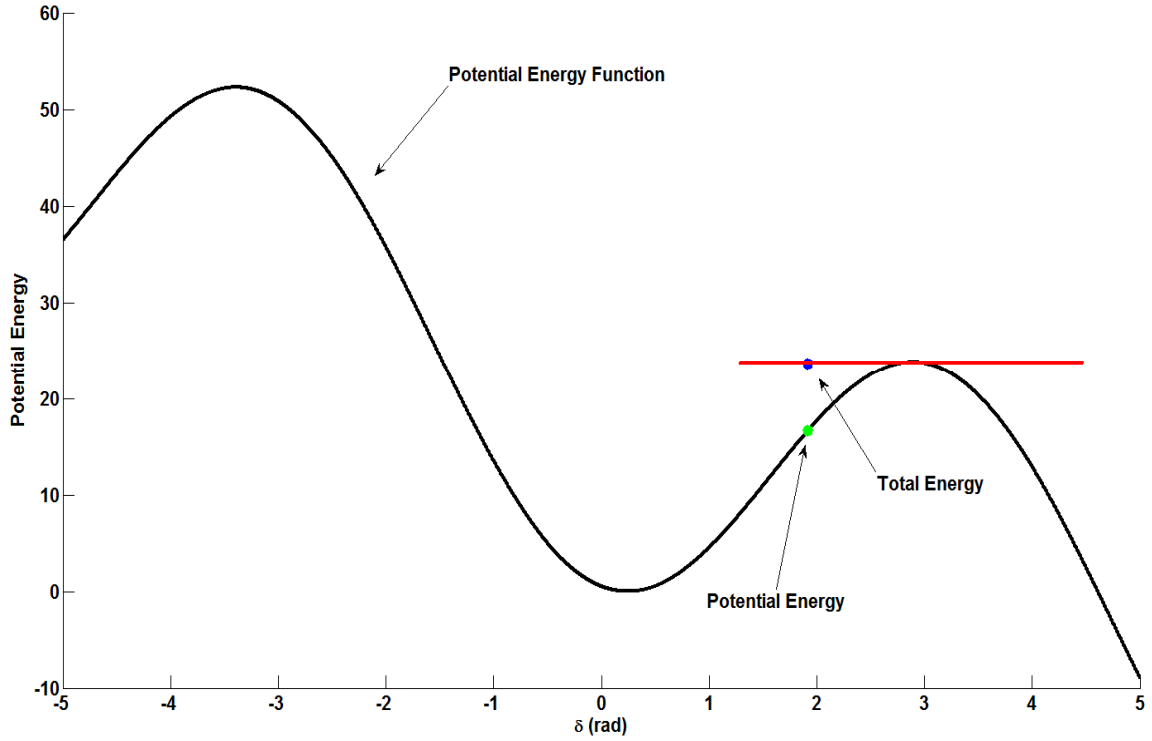

Figure 6.70. System total energy evaluation and stability characterization - fault clearing time t=1.27 sec.

As a result, the critical clearing time (CCT) as computed by the developed method is evaluated to be 0.27 sec after the fault initiation. Simulations of the system indicate that the actual critical clearing time for this system and for this type of fault is 0.31 sec. Thus, there is an error of 0.04 sec (approximately 2.5 cycles) in the evaluation of the CCT, which is reasonable based on the assumptions that were made for the derivation of the equivalent system and the computation of the total energy of the system as was explained before.

6.5.4 Comparison with conventional out-of-step protection method

Based on the results from the previous sections, it was concluded that the developed stability monitoring scheme evaluated in real time the CCT of the system to be at t=1.27 sec (0.27 sec after the fault initiation). As a result, at this time instant, instability of the generator is detected and a trip signal can be sent to generator. In this section, the functionality of a state-of-the-art, impedance monitoring based, out-of-step relay is simulated and the instability detection time is evaluated for an unstable scenario with

clearing time t=1.35 sec (0.35 sec after fault initiation). The results are summarized in Figure 6.71. In particular, monitoring of the trajectory of the impedance at the terminals of the generator indicates that the right blinder and the left blinder are crossed at t=1.37 sec and t=1.47 sec respectively. As a result, the impedance based relay detected instability at t=1.47 sec, thus the developed method in this work predicted instability 0.2 sec before the relay. Note that this time difference is actually higher, considering the fact that when the left blinder is crossed the value of the phase angle is high and the generator trip has to be delayed in order to avoid breaker overstress.

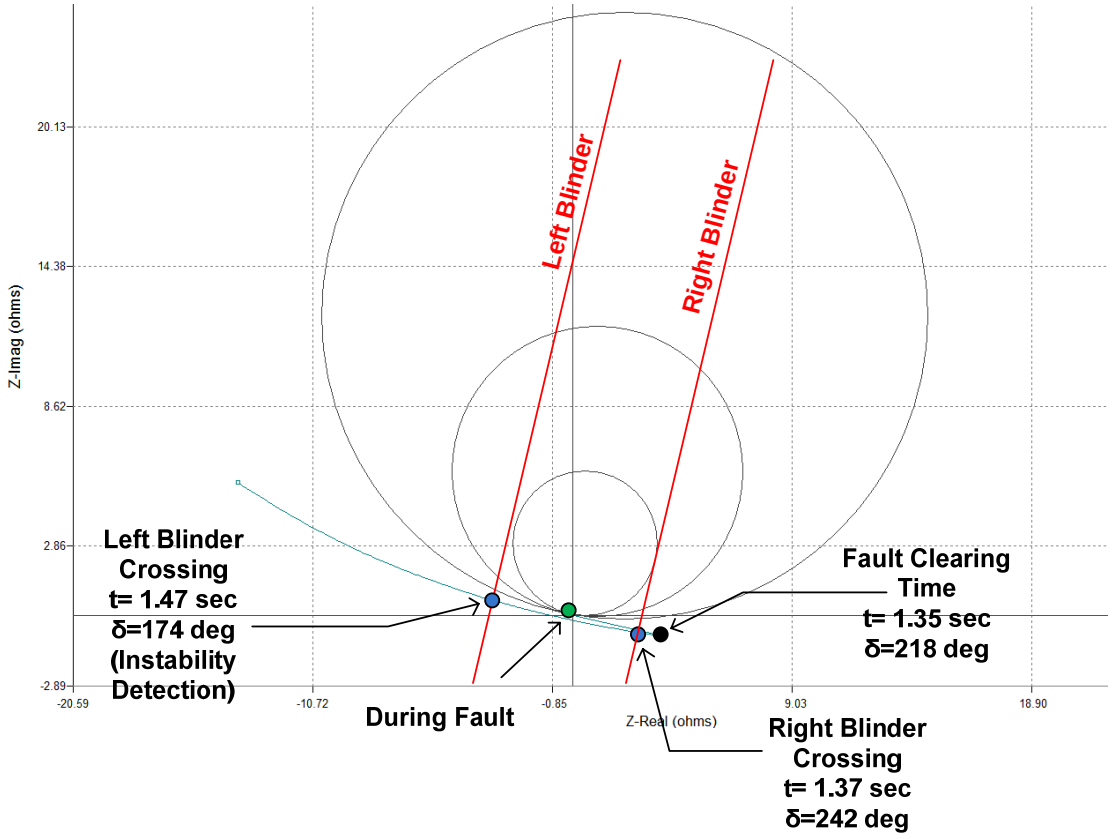

Figure 6.71. Impedance trajectory monitoring - NYPA B-G system.

6.6 Test Case with CoO Outside Observable Area

In this section, a test case is examined in which the CoO lies outside the observable area of the DSE that is performed at the substation of interest. As was discussed in chapter 3, the observable area of the DSE that is performed in a substation is up to the terminal of the neighboring substations. For the application of the transient stability

monitoring scheme using only local information derived by the DSE in the substation of interest, the CoO has to lie in the observable area. However, it is quite common that a generating substation is connected via a short line to a non generating substation, thus it is possible, depending on the disturbance, that the CoO lies outside the observable area. The test system that was used to demonstrate this scenario is shown in Figure 6.72. Note that it is the same test system as in section 6.3, with the difference that the length of the line "Trans. Line Sub1-Sub4" was changed to be 5 miles.

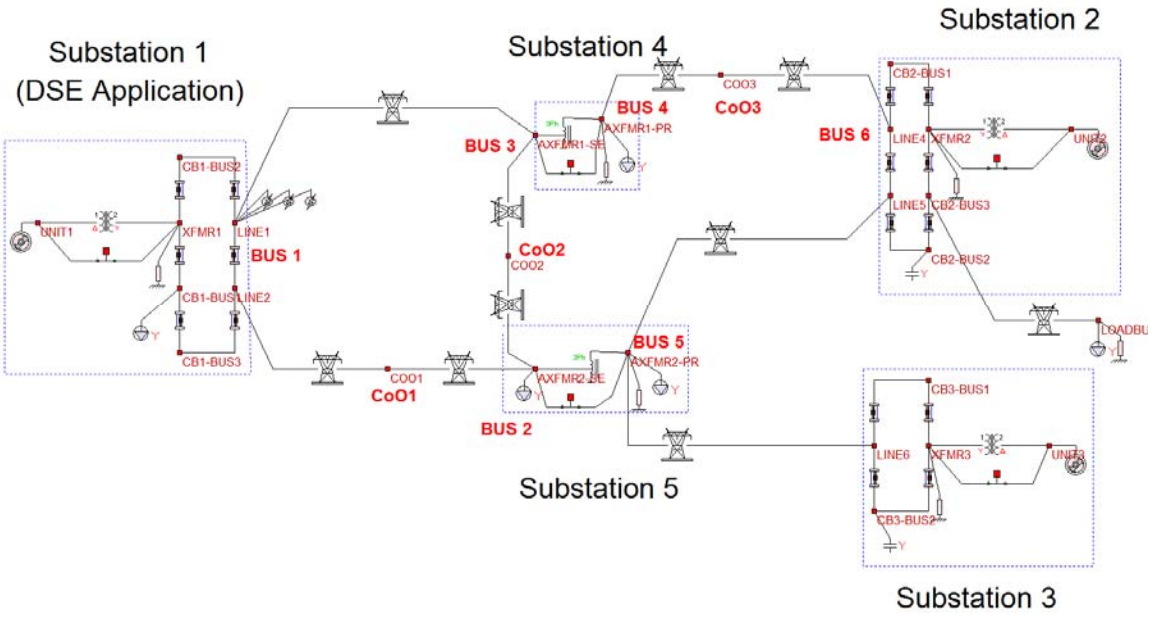

Figure 6.72. Single line diagram of five substation test system.

A three-phase fault was simulated at the terminal of the substation of interest. The fault initiates at t=1 sec and it is cleared 0.25 sec after its initiation, without a change in the system configuration. The frequency at the terminal of the substation of interest (substation 1) and the neighboring substations (Bus 2 and Bus3) are illustrated in Figure 6.73.

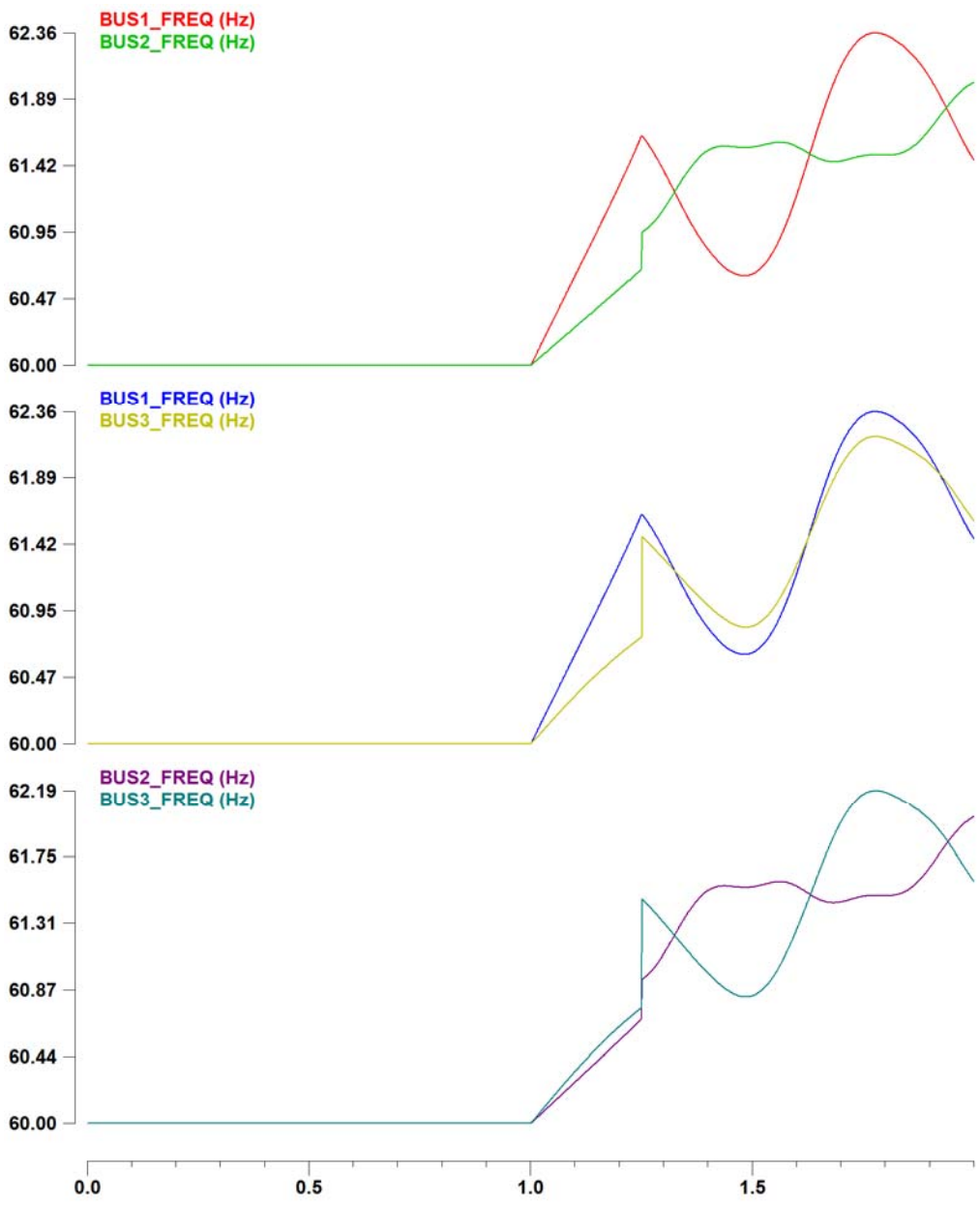

Figure 6.73. Frequency at the terminals of the lines - fault clearing time t=1.25 sec.

It is clear that a CoO point lies on the line that connects substation 1 with substation 5, and another CoO point on the line that connects substation 4 with substation 5. Upon execution of the optimization routine for the determination of the CoO points, the results are summarized in Table 6.28.

Table 6.28. CoO calculation results - fault clearing time t=1.25 sec.

Line	α	b	c	CoO Length (miles)	Line Length (miles)
BUS1-BUS2	0.23	61.15	0.98	28.5	37
BUS1-BUS3	-2.1	-	-	-	5
BUS3-BUS2	0.29	61.15	0.99	34.1	48

Note that given the frequency at Bus 1 and Bus 3, the coefficient a of the optimization routine is negative ($0 < a < 1$), indicating that there is no CoO point on the line that connects substation 1 with substation 4. However, there is an additional CoO point that lies outside the observable area and could not be observed. In particular, Figure 6.74 illustrates the frequency at Bus 4 and Bus 6 of the system.

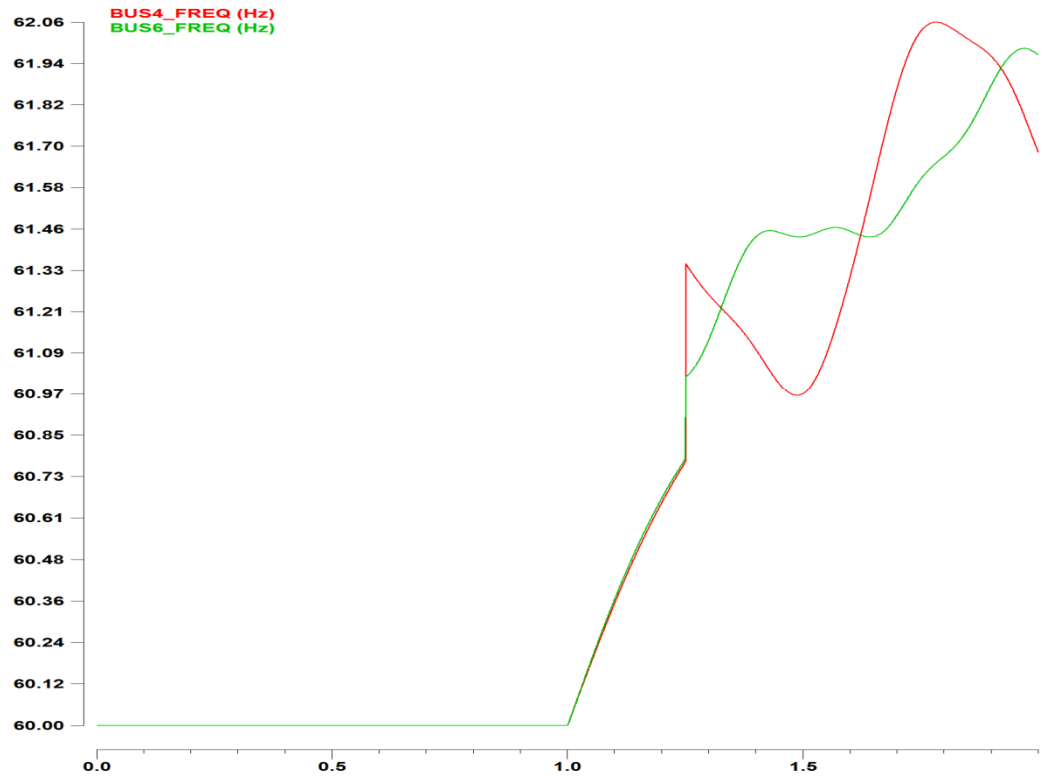

Figure 6.74. Frequency at the terminals of the remote line - fault clearing time t=1.25 sec.

It is clear that there is a CoO point on the line that connects Substation 4 with Substation 2. This CoO point cannot be determined by the DSE that is performed in the substation of interest, so in this case it is required that a DSE is also performed in substation 4 that will increase the observability of the system up to the terminal of substation 2. The CoO point on the line that connects substation 4 with substation 2 is found to be 48.8 miles away from Bus 4.

As a result, for the transient stability monitoring scheme to be applied, the results of the DSE that is performed in substation 4 have to be sent to substation 1, where the real-time model of the extended system will be synthesized and the transient stability monitoring and out-of-step protection scheme can be applied. The disadvantage in this case is that there is expected to be a delay in the characterization of the stability of the system due to the required communication of the DSE state that is computed in substation 4 to substation 1, and the associated delays.

Given the extended real-time model of the system as computed by the DSE performed in substation 1 and substation 4, the equivalent system that is derived for the computation of the total energy of the system and the characterization of its stability is shown in Figure 6.75.

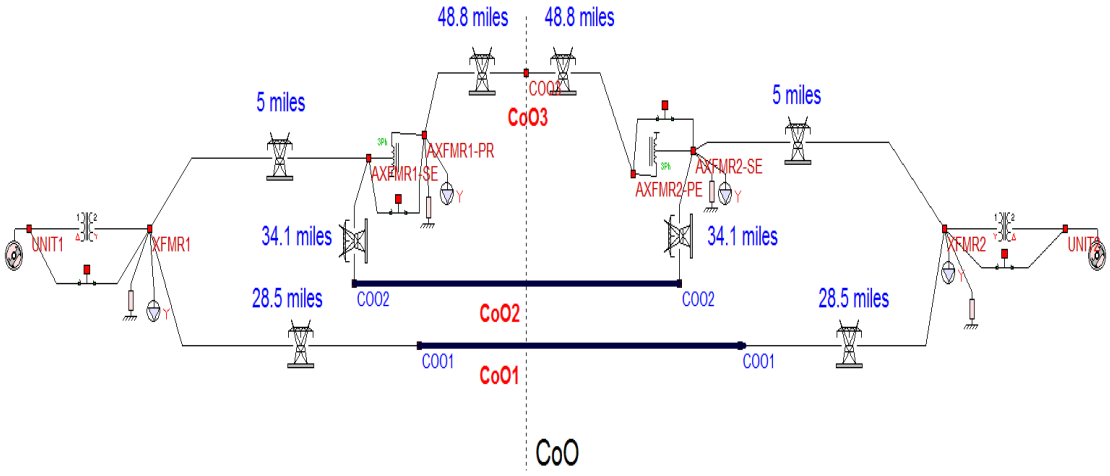

Figure 6.75. Equivalent system.

6.7 Summary

In this chapter, the developed transient stability monitoring and generator out-of-step protection scheme are demonstrated on several test systems with single or multiple CoO points, including the NYPA's Blenheim Gilboa generating substation. It is concluded that the developed scheme can characterize in real-time the stability of the system and evaluate with high accuracy the critical clearing time of a disturbance, before the system becomes unstable. Thus it can predict eminent system instability much earlier than traditional methods

The predictive generator out-of-step protection scheme is also demonstrated. The simulation results indicate that the scheme can predict the generator's instability much earlier than traditional methods such as present day out-of-step relays. The prediction time is of such magnitude that the generating unit can be tripped before it actually slips a pole as it is the case with present out of step relaying systems.

7 CONTRIBUTIONS AND POTENTIAL FUTURE WORK

7.1 Conclusions

The presented research work consists mainly of two parts: (a) a PMU-based distributed dynamic state estimator that is performed at the substation level with rates more than 60 times per second and can capture with high accuracy the dynamics of the system and (b) a predictive, energy-based, transient stability monitoring scheme that is enabled by the dynamic state estimator and characterizes in real time the stability of the system. As an application of the transient stability monitoring scheme, a predictive generator out-of-step protection scheme that can protect a generator from a potential loss of synchronism has also been developed.

In particular, initially a distributed dynamic state estimator has been presented. DSE is performed at the substation level by utilizing only local measurements available from PMUs, meters, FDRs etc in the substation only, thus avoiding all issues associated with transmission of data and associated time latencies. A three-phase, asymmetric and breaker oriented power system model is used in order to account for system imbalances, asymmetries and topology changes. In general the problem is nonlinear. However, the quadratic power system component modeling that is used, converts the problem in quadratic and improves the convergence characteristics of the algorithm. The solution is further simplified if only synchronized measurements are used and the associated devices are linear, in which case the state estimation becomes linear and has a direct solution. Emphasis is also given on the object-oriented formulation of the algorithm. The distributed architecture of the DSE (substation based) but also the object-oriented formulation of the algorithm results in very fast DSE update rate which can go up to more than 60 executions per second. The DSE has been tested in numerous test systems including the actual models of the USVI's Longbay and RHPP substations and NYPA's Blenheim-Gilboa substation. Timing results indicate that the method can be performed at rates of 60 times per second for a typical substation. Finally it is concluded that DSE can be used as the major component of a PMU-based wide area monitoring system.

An energy-based transient stability monitoring scheme is also presented in this work. The scheme is enabled by the dynamic state estimator since it utilizes the estimated state of the substation, monitors in real-time the transient swings of the system and characterizes the stability of the system. In particular, the real-time dynamic model of the system, as given by the DSE, is utilized to evaluate the system's energy function based on Lyapunov's direct method and extract stability properties from the energy function. The two major components of the scheme are a) the calculation of the center of oscillations of the system and b) the derivation of an equivalent, reduced sized model which is used for the calculation of the potential and kinetic energy of the system based on which the stability of the system is determined. The mathematical formulation for the calculation of the center of oscillations and the methodology for the equivalent derivation are presented in detail. The overall algorithm of the stability monitoring scheme and in particular how the information given by the dynamic state estimation is used for the real-time characterization of the stability of the system, are also given. Finally an application of this scheme, which is a novel, predictive, generator out-of-step protection scheme is described. Given the DSE results, the energy of the generator is computed and continuously monitored and if it exceeds a predefined threshold then instability is asserted and a trip signal can be sent to the generator. The schemes have been demonstrated on various test systems, including the NYPA's Blenheim-Gilboa generating substation, in order to demonstrate their efficiency and accuracy along with comparison with the state-of-the art technology for generator out-of-step protection in order to demonstrate the superiority of the developed method. The major advantage of the scheme is that the out-of-step condition is predicted before its occurrence and therefore relays can act much faster than today's technology. It is concluded that the scheme can predict the generator's instability much earlier than traditional methods such as present day out-of-step relays. The prediction time is of such magnitude that the generating unit can be tripped before it actually slips a pole as it is the case with present out of step relaying systems.

7.2 Potential Future Work

The real-time dynamic model of the system as computed by the DSE can be used in various applications. Apart from the developed transient stability monitoring and generator out-of-step protection schemes other monitoring, control and protection applications can be also developed. An example could be a short-term and a long-term voltage stability monitoring scheme that is based on the DSE results. Potential protection schemes that can be developed are component protection schemes, for devices such as transmission lines or transformers, or system protection schemes. The DSE results could be also used for applications of component parameter estimation such as generator and transmission line parameter identification.

Another promising topic is the integration of renewable sources (wind, solar etc) and of storage devices into the grid. This integration will increase the complexity of the system but on the same time allows for the implementation of control and optimization schemes that can coordinate the operation of the non-dispatchable units with the bulk power system with the objective being the maximization of the utilization of the available resources but on the same time improvement of the operation and reliability of the system. Maximum utilization of these resources requires fast and accurate monitoring and control for the purpose of continuous coordination and optimization of the system. If storage is added to the system then there is a need to continuously optimize the store/retrieve functions with the wind/PV availability for the purpose of mitigating the effects of wind/PV source variability and maximizing the amount of energy retrieved from wind and PV. Towards this goal, DSE can be used as the major component of such a monitoring scheme that will provide a more accurate and more frequent real-time model of the system, and will enable new approaches for control, operation and protection of the system.

7.3 Publications and Awards

7.3.1 Publications

1. E. Farantatos, R. Huang, G. Cokkinides, and A. P. Meliopoulos, "A Predictive Out-of-Step Protection Scheme based on PMU enabled Dynamic State Estimation," in *Proc. 2011 PES General Meeting*, Detroit, MI, July 24-29 2011.
2. E. Farantatos, R. Huang, G. Cokkinides, A. P. Meliopoulos, Bruce Fardanesh and George Stefopoulos, "Advanced Disturbance Recording and Playback enabled by a Distributed Dynamic State Estimation Including Bad Data Detection and Topology Change Identification", in *Proc. 2012 PES General Meeting*, San Diego, CA, July 22-26, 2012
3. E. Farantatos, G. K. Stefopoulos, G. J. Cokkinides, A. P. Meliopoulos, "PMU-Based Dynamic State Estimation for Electric Power Systems," in *Proc. 2009 PES General Meeting*, Calgary, Alberta, Canada, July 2009.
4. A. P. Meliopoulos, E. Farantatos, G. Cokkinides, S. Mohagheghi, and G. K. Stefopoulos, "A new out-of-step protection scheme via GPS-Synchronized data," in *Proc. of the 2008 Power Systems Computation Conference (PSCC)*, Glasgow, Scotland, UK, July 2008.
5. R. Huang, E. Farantatos, G. Cokkinides, A. P. Meliopoulos, Bruce Fardanesh and George Stefopoulos, "Object-Oriented 3-Phase Distributed Dynamic State Estimator," in *Proc. 2011 PES General Meeting*, Detroit, MI, July 2011.
6. A.P Meliopoulos, G. Cokkinides, R. Huang, E. Farantatos, S. Choi, Y. Lee , "Wide Area Dynamic Monitoring and Stability Controls," in *Proc. IREP Symposium 2010, Bulk Power System Dynamics and Control VIII*, Buzios, Brazil, Aug. 2010.
7. R. Huang, E. Farantatos, G. Cokkinides, and A. P. Meliopoulos, "Substation Based Dynamic State Estimator - Numerical Experiment," in *Proc. 2010 Transmission and Distribution Conference and Exposition*, New Orleans, Louisiana, Apr. 2010.
8. Evangelos Farantatos, Renke Huang, George Cokkinides and A. P. Meliopoulos, "Implementation of a 3-Phase State Estimation Tool Suitable for Advanced

Distribution Management Systems," in *Proc. of the 2011 Power Systems Conference & Exposition*, Phoenix, AZ, Mar. 2011.

9. A. P. Meliopoulos, G. Cokkinides, S.Choi, E. Farantatos, R. Huang and Y. Lee, "Symbolic integration and autonomous state estimation: Building blocks for an intelligent power grid", *in Proc. 16th International Conference on Intelligent System Applications to Power Systems (ISAP)*, Hersonissos, Crete, Greece, Sept. 25-28, 2011.
10. A. P. Meliopoulos, E. Farantatos, R. Huang, Y. Cho, E. Polymeneas, Z. Tan and G. Cokkinides, "Methodology for Monitoring, Control and Operation of Power Systems with Wind Farms", *in Proc. 2012 PES General Meeting*, San Diego, CA, July 22-26, 2012.

7.3.2 Awards

1. 2nd best student paper-poster award, 2011 IEEE PES General Meeting for the paper "A Predictive Out-of-Step Protection Scheme based on PMU enabled Dynamic State Estimation"
2. Clayton Griffin student paper award, 2012 Georgia Tech Protective Relaying Conference, for the paper "A Predictive Out-of-Step Protection Scheme based on GPS-Synchronized Measurements"

APPENDICES

Appendix A: Quadratic Integration

Quadratic integration method is a numerical integration method that assumes that time domain functions vary quadratically within the integration time step. This assumption is illustrated in Figure A.1. Note that the three points, $x(t-h)$, x_m and $x(t)$ fully define the quadratic function in the interval $[t-h, t]$. The method is an implicit numerical integration method (it can be easily observed that it makes use of information at the unknown point $x(t)$) and therefore demonstrates the desired advanced numerical stability properties compared to explicit methods.

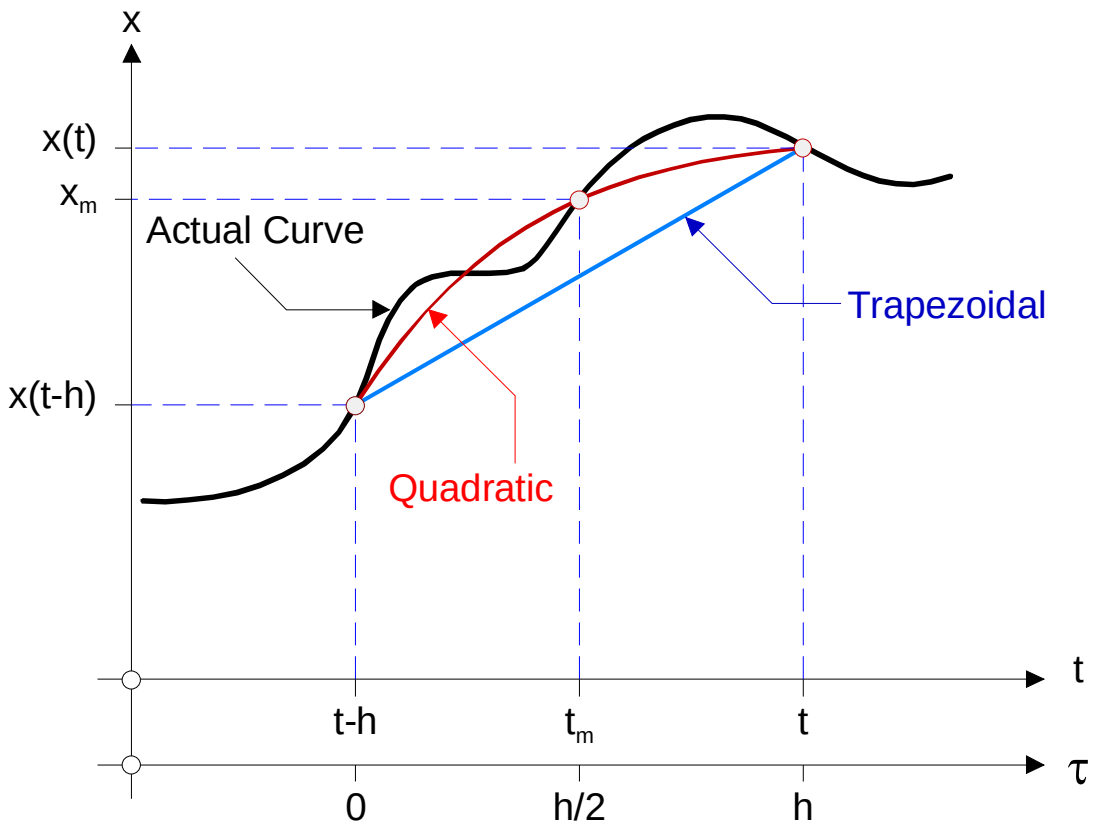

Figure A.1. Illustration of the quadratic integration method [101].

The general integration results are listed as follows,

Integration over time interval $[t-h, t_m]$:

$$\int_{t-h}^{t_m} x(\tau)d\tau = \frac{5h}{24}x(t-h) + \frac{h}{3}x_m - \frac{h}{24}x(t)$$

Integration over time interval $[t-h, t]$:

$$\int_{t-h}^{t} x(\tau)d\tau = \frac{h}{6}x(t-h) + \frac{2h}{3}x_m + \frac{h}{6}x(t)$$

Integration over time interval $t_m, t]$:

$$\int_{t_m}^{t} x(\tau)d\tau = -\frac{h}{24}x(t-h) + \frac{h}{3}x_m + \frac{5h}{24}x(t)$$

Appendix B: Multi-Machine System Potential Energy Computation

In this section, the methodology for deriving the expression of the power output of the generators in a multi-machine power system as a function of the units' rotor position δ is described. For the derivation, the following assumptions are made:

- The positive sequence model of the multi-machine power system will be used.
- The machines are represented by a constant voltage $E_i \angle \delta_i$ behind the generator impedance
- The loads in the system are represented as constant admittance loads

Consider the multi-machine power system in Figure A.2 with m buses, n of which represent generator buses.

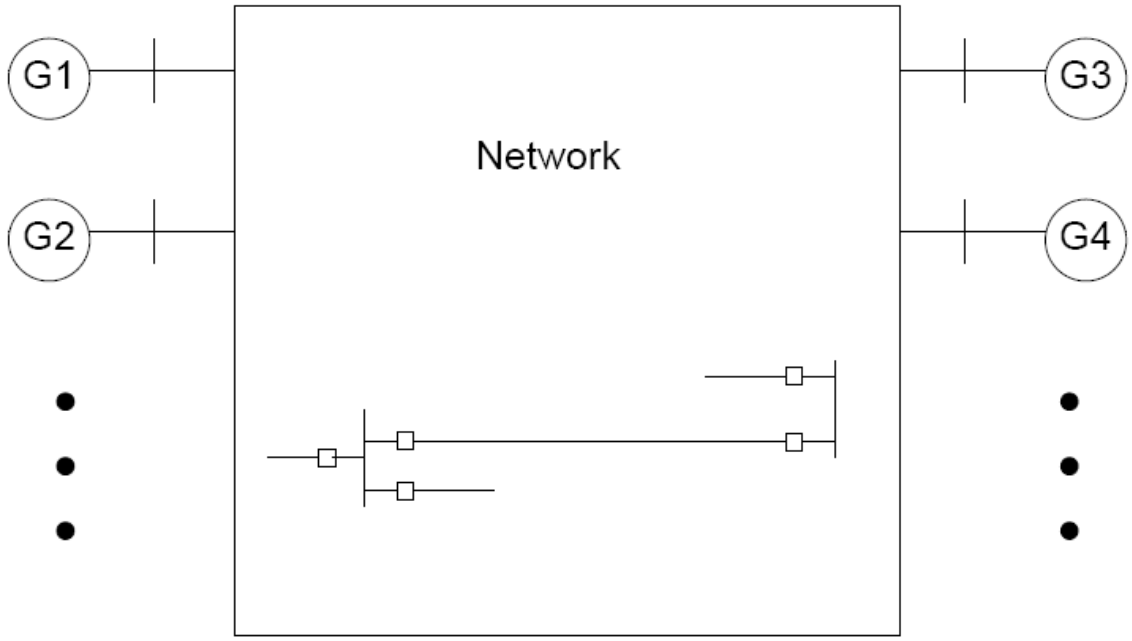

Figure A.2. Multi-machine power system.

Upon converting the voltage sources into current sources and applying nodal analysis it holds that:

$$\begin{bmatrix} \frac{E_1 \cdot e^{\delta_1}}{j \cdot x'_{d1}} \\ \vdots \\ \frac{E_n \cdot e^{\delta_n}}{j \cdot x'_{dn}} \\ 0 \\ \vdots \\ 0 \end{bmatrix} = \begin{bmatrix} Y_{11} & \cdots & Y_{1n} & \cdots & Y_{1m} \\ \vdots & \ddots & \vdots & \ddots & \vdots \\ Y_{n1} & \cdots & Y_{nn} & \cdots & Y_{nm} \\ \vdots & \ddots & \vdots & \ddots & \vdots \\ Y_{m1} & \cdots & Y_{mn} & \cdots & Y_{mm} \end{bmatrix} \cdot \begin{bmatrix} \widetilde{V}_1 \\ \widetilde{V}_2 \\ \vdots \\ \widetilde{V}_m \end{bmatrix}$$

where Y is the admittance matrix of the system, that is the diagonal terms Y_{ii} are the self admittance terms, equal to the sum of the admittances of all devices incident to bus i, while the off-diagonal terms, Y_{ij}, are equal to the negative of the sum of the admittances connecting the two buses i and j.

The nodal equations can be written in compact form as follows:

$$\begin{bmatrix} I_G \\ 0 \end{bmatrix} = \begin{bmatrix} Y_{GG} & Y_{GN} \\ Y_{NG} & Y_{NN} \end{bmatrix} \cdot \begin{bmatrix} V_G \\ V_N \end{bmatrix}$$

where $I_G = \begin{bmatrix} \frac{E_1 \cdot e^{\delta_1}}{j \cdot x'_{d1}} & \cdots & \frac{E_n \cdot e^{\delta_n}}{j \cdot x'_{dn}} \end{bmatrix}^T$, $V_G = \begin{bmatrix} V_{G,1} & \cdots & V_{G,n} \end{bmatrix}^T$, $V_N = \begin{bmatrix} V_{N,(n+1)} & \cdots & V_{N,m} \end{bmatrix}^T$.

Expanding the matrix equations it holds that:

$$I_G = Y_{GG} \cdot V_G + Y_{GN} \cdot V_N$$
$$0 = Y_{NG} \cdot V_G + Y_{NN} \cdot V_N$$

The second equation can be solved for V_N yielding:

$$V_N = -Y_{NN}^{-1} \cdot Y_{NG} \cdot V_G$$

Substitution in the first equation and upon solution for V_G yields:

$$V_G = (Y_{GG} - Y_{GN} \cdot Y_{NN}^{-1} \cdot Y_{NG})^{-1} \cdot I_G$$

or equivalently:

$$\widetilde{V}_1 = \widetilde{a}_{11} \cdot e^{\delta_1} + \cdots + \widetilde{a}_{1n} \cdot e^{\delta_n}$$
$$\vdots$$
$$\widetilde{V}_n = \widetilde{a}_{n1} \cdot e^{\delta_1} + \cdots + \widetilde{a}_{nn} \cdot e^{\delta_n}$$

From the computed voltages the electric power can be computed as:

$$P_{e1} = \mathrm{Re}\left[\widetilde{V}_1 \cdot \left(\frac{E_1 \cdot e^{\delta_1}}{j \cdot x'_{d1}}\right)^*\right] = f_1(e^{\delta_2-\delta_1}, \cdots, e^{\delta_n-\delta_1}) =$$
$$A_1 + B_{1,2} \cdot \cos(\delta_2 - \delta_1) + C_{1,2} \cdot \sin(\delta_2 - \delta_1) + \cdots + B_{1,n} \cdot \cos(\delta_n - \delta_1) + C_{1,n} \cdot \sin(\delta_n - \delta_1)$$
$$\vdots$$
$$P_{en} = \mathrm{Re}\left[\widetilde{V}_n \cdot \left(\frac{E_n \cdot e^{\delta_n}}{j \cdot x'_{dn}}\right)^*\right] = f_n(e^{\delta_1-\delta_n}, \cdots, e^{\delta_{n-1}-\delta_n}) =$$
$$A_n + B_{1,n} \cdot \cos(\delta_1 - \delta_n) + C_{1,n} \cdot \sin(\delta_1 - \delta_n) + \cdots + B_{n-1,n} \cdot \cos(\delta_{n-1} - \delta_n) + C_{n-1,n} \cdot \sin(\delta_{n-1} - \delta_n)$$

A simple example of a two generator system shown in Figure A.3 follows next.

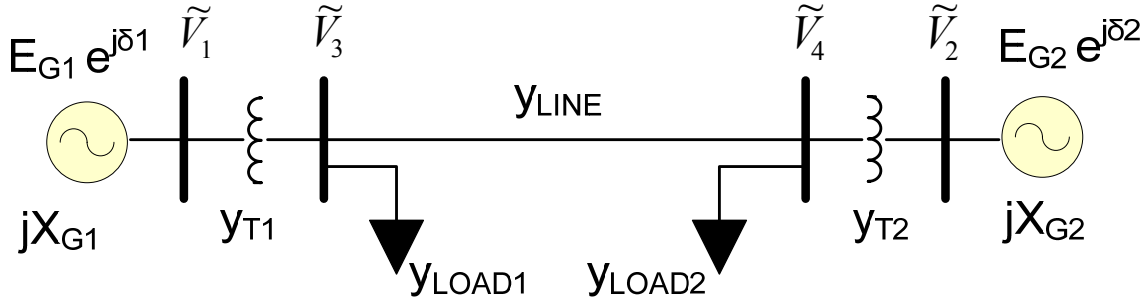

Figure A.3. Two generator system - potential energy computation example.

The nodal equations can be written in compact form as follows:

$$\begin{bmatrix} I_G \\ 0 \end{bmatrix} = \begin{bmatrix} Y_{GG} & Y_{GN} \\ Y_{NG} & Y_{NN} \end{bmatrix} \cdot \begin{bmatrix} V_G \\ V_N \end{bmatrix}$$

where: $I_G = \left[\frac{E_1 \cdot e^{\delta_1}}{j \cdot x'_{d1}} \quad \frac{E_2 \cdot e^{\delta_2}}{j \cdot x'_{d2}} \right]^T$, $V_G = \left[\widetilde{V}_1 \quad \widetilde{V}_2 \right]^T$, $V_N = \left[\widetilde{V}_3 \quad \widetilde{V}_4 \right]^T$,

$$Y_{GG} = \begin{bmatrix} y_{G1} + y_{T1} & 0 \\ 0 & y_{G2} + y_{T2} \end{bmatrix}, \qquad Y_{GN} = Y_{NG} = \begin{bmatrix} -y_{T1} & 0 \\ 0 & -y_{T2} \end{bmatrix},$$

$$Y_{NN} = \begin{bmatrix} y_{T1} + y_{LINE} + y_{LOAD1} & -y_{LINE} \\ -y_{LINE} & y_{T2} + y_{LINE} + y_{LOAD2} \end{bmatrix}.$$

The voltages at the terminals of the generators are computed to be:

$$\widetilde{V}_1 = Y_{inv}(1,1) \cdot \frac{E_1 \cdot e^{\delta_1}}{j \cdot x'_{d1}} + Y_{inv}(1,2) \cdot \frac{E_2 \cdot e^{\delta_2}}{j \cdot x'_{d2}}$$

$$\widetilde{V}_2 = Y_{inv}(2,1) \cdot \frac{E_1 \cdot e^{\delta_1}}{j \cdot x'_{d1}} + Y_{inv}(2,2) \cdot \frac{E_2 \cdot e^{\delta_2}}{j \cdot x'_{d2}}$$

where $Y_{inv} = (Y_{GG} - Y_{GN} \cdot Y_{NN}^{-1} \cdot Y_{NG})^{-1}$

From the computed voltages the electric power can be computed as:

$$P_{e1} = \mathrm{Re}\left[\widetilde{V}_1 \cdot \left(\frac{E_1 \cdot e^{\delta_1}}{j \cdot x'_{d1}} \right)^* \right] = A_1 + B_{1,2} \cdot \cos(\delta_2 - \delta_1) + C_{1,2} \cdot \sin(\delta_2 - \delta_1)$$

$$P_{e2} = \mathrm{Re}\left[\widetilde{V}_2 \cdot \left(\frac{E_2 \cdot e^{\delta_2}}{j \cdot x'_{d2}} \right)^* \right] = A_2 + B_{2,1} \cdot \cos(\delta_1 - \delta_2) + C_{2,1} \cdot \sin(\delta_1 - \delta_2)$$

Appendix C: NYPA Model

This section describes NYPA's Blenheim-Gilboa substation model on which the distributed dynamic state estimator has been implemented. NYPA's Blenheim-Gilboa electric power system is a special type of hydroelectric facility that is located at the base of Brown Mountain, Southwest of Albany. It has four 278 MVA generators (total of 1,112 MVA) which can generate more than one million kilowatts during peak demands and supply electricity to New York customers via three 345 kV transmission lines as represented in Figure A.4. A computer model of the NYPA Blenheim-Gilboa electric power system has been constructed in WinIGS which includes the Fraser-Gilboa, Gilboa-New Scotland, and Gilboa-Leeds 345kV transmission lines. A single line diagram of the system is illustrated in Figure A.4. The specific ratings of transmission lines and transmission tower types are built based on the given actual data.

A breaker oriented, three-phase and physical model of the power plant was developed based on the collected data from a field visit. Multi-vendor numerical relays are installed at NYPA Blenheim-Gilboa plant, some of which support GPS-synchronized measurement. Figure A.5 illustrates the system model of the Blenheim-Gilboa plant along with the numerical relays installed.

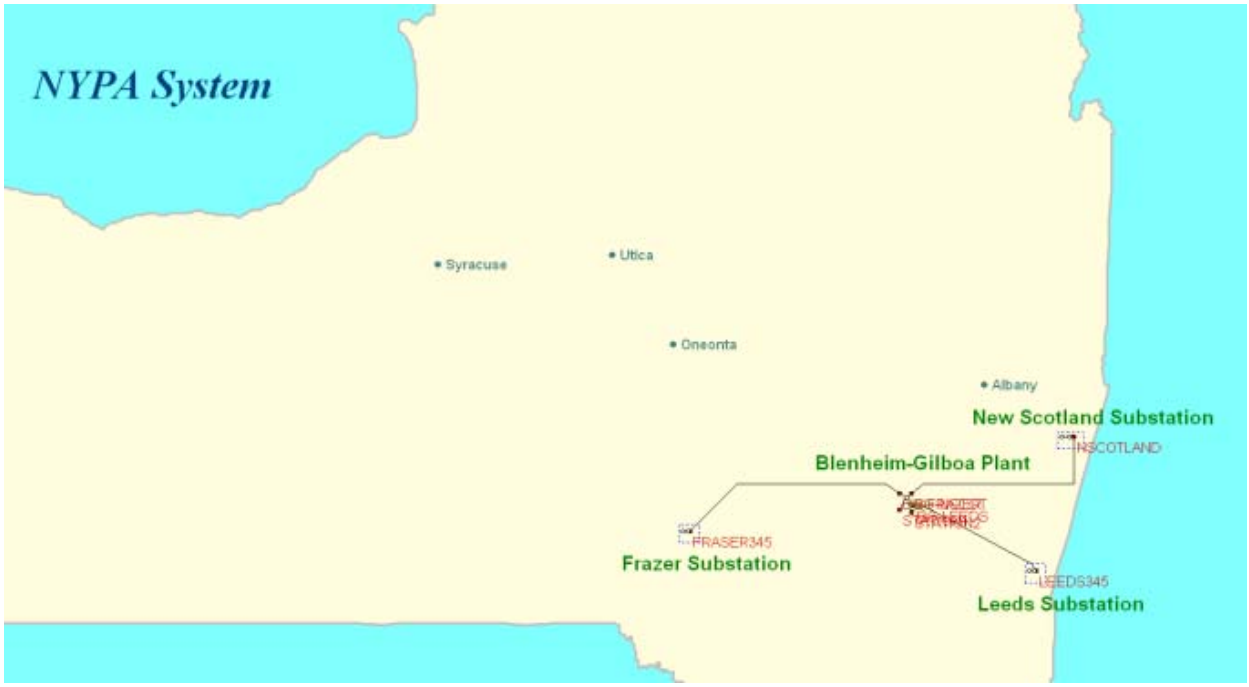

Figure A.4. Single line diagram of NYPA electric power system.

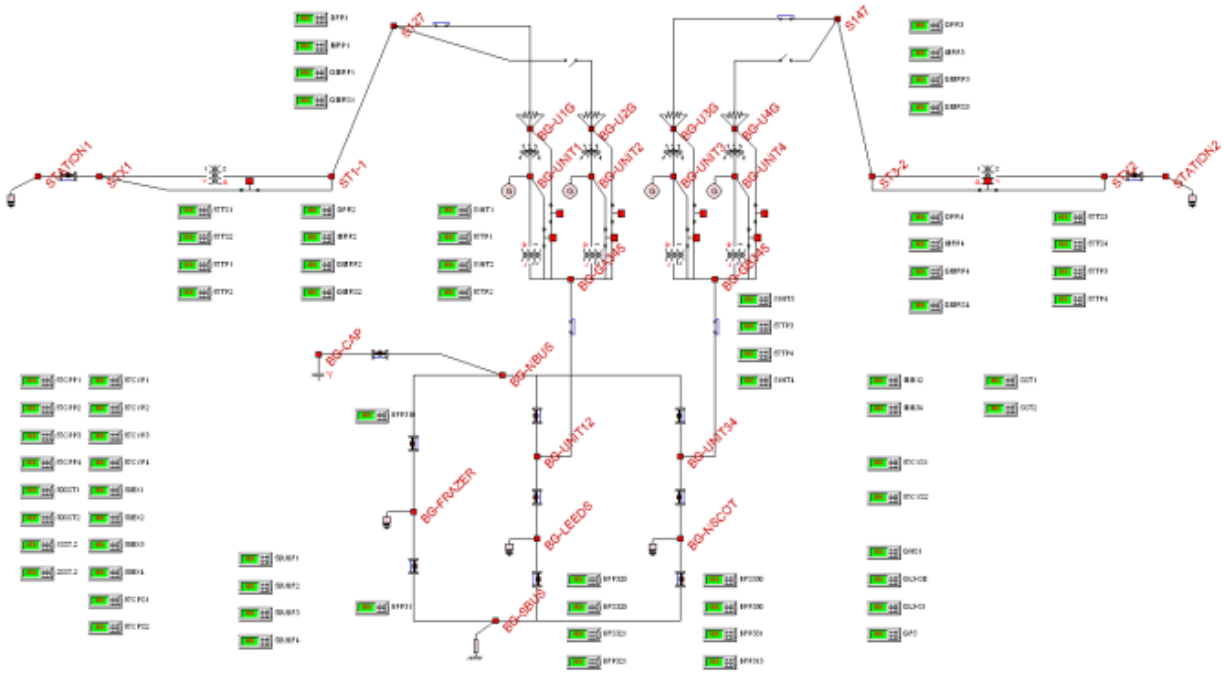

Figure A.5. Single line diagram of Blenheim-Gilboa system including relays.

Appendix D: USVI Model

This section describes the USVI-WAPA electric power system model on which the distributed dynamic state estimator has been implemented. A computer model of the USVI-WAPA electric power system serving the islands of St Thomas and St John has been constructed in WinIGS which includes the USVI-WAPA power plant (R.H.P.P.), the five substations of the system and the interconnecting 35 kV and 13 kV transmission and distribution lines. A single line diagram of the system is illustrated in Figure A.6.

US Virgin Islands consist of the main islands of St. Croix, St. John, and St. Thomas, and many other surrounding minor islands. The electric power network is a stand-alone system i.e. not connected to the US national power grid, and the system is operated by the USVI Water and Power Authority (WAPA). The system consists of five substations: Randolph Harley Power Plant (RHPP), Long Bay, Tutu, East End, and St. John. In the main island, i.e. St. Thomas, there is a single generating plant (RHPP) with eight units that has a total capacity of nearly 200 MW. The generating plant is connected to two networks: the 35 kV transmission network and the 13 kV distribution network. The distribution network that is directly connected to the generators consists of unbalanced loads. The transmission systems consist of overhead lines, underground cables and two submarine cables that interconnect the power systems of two islands, St. Thomas and St. John. A breaker oriented, three-phase and physical model of the power plant was developed based on the collected data from a field visit. Multi-vendor numerical relays are installed at the substations, some of which support GPS-synchronized measurement. Figure A.7 illustrates the system model of the LongBay substation along with the numerical relays installed. Figure A.8 illustrates the system model of the RHPP substation along with the numerical relays installed.

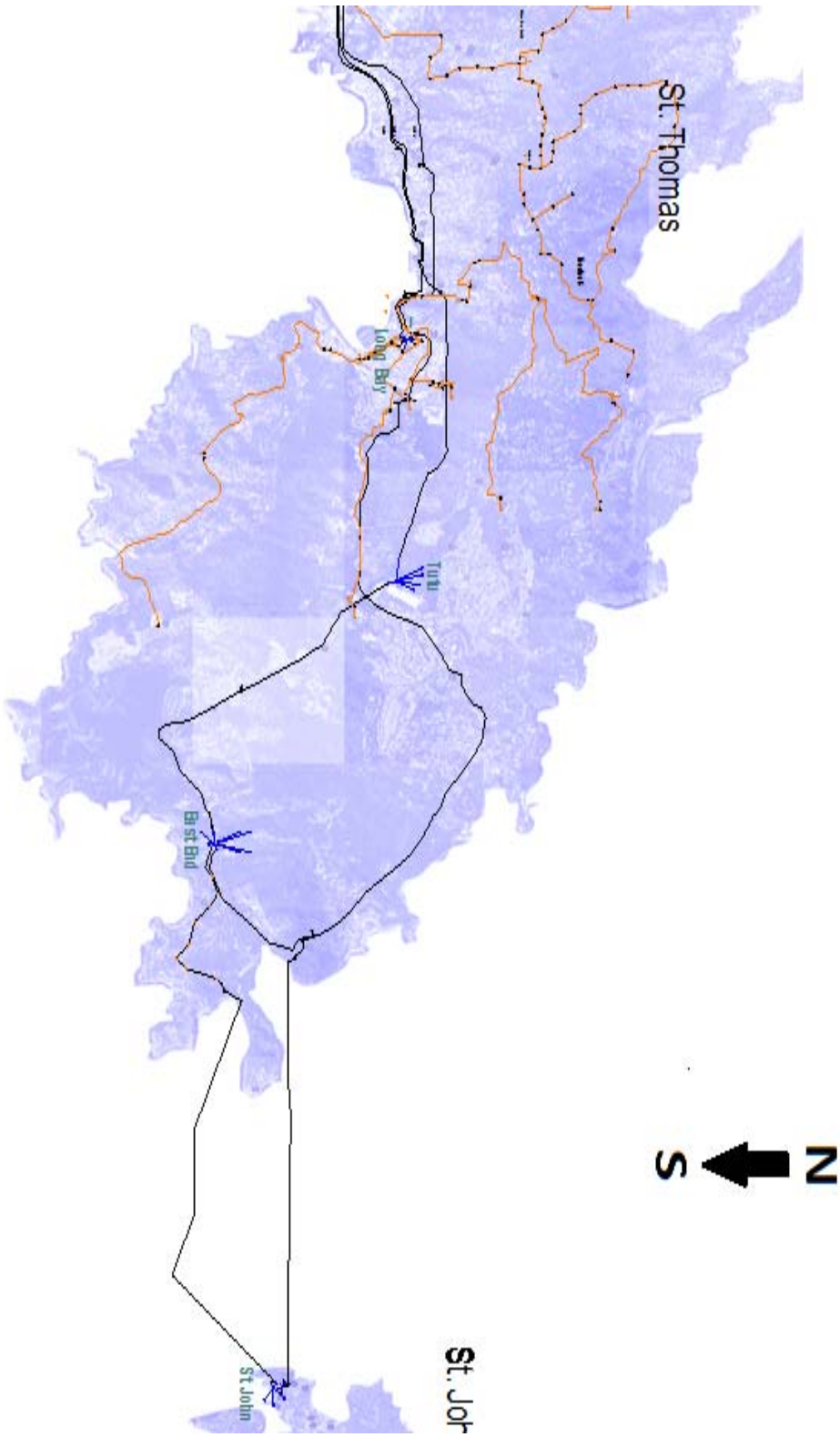

Figure A.6. Single line diagram of the St. Thomas and St. John electric power system.

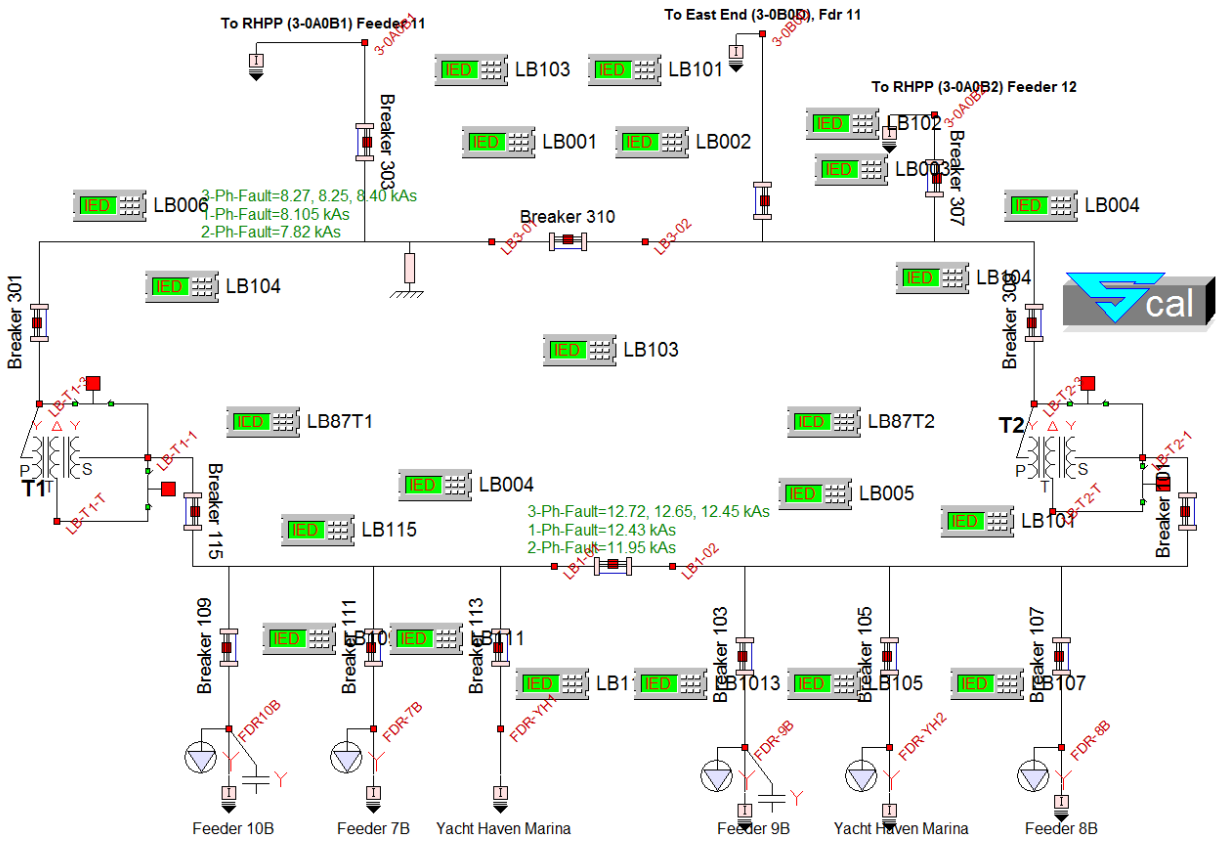

Figure A.7. Single line diagram of LongBay substation including relays.

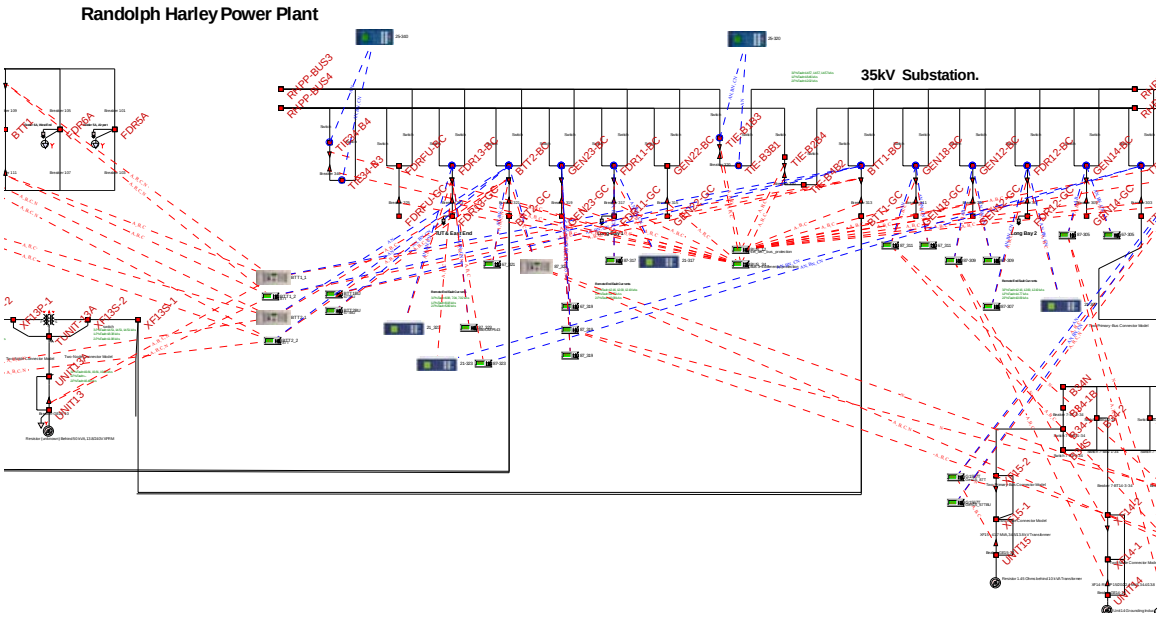

Figure A.8. Single line diagram of RHPP substation including relays.

REFERENCES

[1] U.S.-Canada Power System Outage Task Force, "Final Report on the August 14, 2003 Blackout in the United States and Canada: Causes and Recommendations," Apr. 2004.

[2] A. Monticelli, *State estimation in electric power systems: a generalized approach,* Kluwer Academic Publishers, Boston 1999.

[3] A. Abur and A. Gómez Expósito, *Power system state estimation: theory and implementation,* Marcel Dekker, New York, 2004.

[4] A. P. Meliopoulos and G. Stefopoulos, "Characterization of state estimation biases," *Probability in the Engineering and Informational Sciences, Cambridge University Press*, vol. 20, pp. 157-174, 2006.

[5] F. C. Schweppe and J. Wildes, "Power system static-state estimation, Part I: Exact Model" *IEEE Trans. Power App. Syst.*, vol. PAS-89, no.1, pp.120-125, Jan. 1970.

[6] F. C. Schweppe and D. B. Rom, "Power system static-state estimation, Part II: Approximate Model" *IEEE Trans. Power App. Syst.*, vol. PAS-89, no.1, pp.125-130, Jan. 1970.

[7] F. C. Schweppe, "Power system static-state estimation, Part III: Implementation" *IEEE Trans. Power App. Syst.*, vol. PAS-89, no.1, pp.130-135, Jan. 1970.

[8] K. A. Clements, O. J. Denison, and R. J. Ringlee, "The effects of measurement non-simultaneity, bias, and parameter uncertainty on power system state estimation," in *Proc. 1973 PICA Conference*, pp. 327-331, June 1973.

[9] M. C. de Almeida, E. N. Asada, A. V. Garcia, "Effects of load imbalance and system asymmetry on three-phase state estimation," *in Proceedings IEEE Power Engineering Society 2006 General Meeting*, June 2006.

[10] A. P. Sakis Meliopoulos, F. Zhang, and S. Zelingher, "Power System Harmonic State Estimation," *IEEE Trans. Power Systems*, vol. 9, no. 3, pp 1701-1709, July 1994.

[11] A. G. Phadke, J. S. Thorp, and K. J. Karimi, "State estimation with phasor measurements, " *IEEE Trans. Power Systems*, vol. PWRS-1, no.1, pp. 233-241, Feb. 1986.

[12] Sakis Meliopoulos, "State Estimation for Mega RTOs," in *Proceedings of the 2002 IEEE PES Winter Meeting*, New York, NY, Jan. 28-31, 2002.

[13] B. Fardanesh, S. Zelingher, A. P. Sakis Meliopoulos, G. Cokkinides, and Jim Ingleson, "Multifunctional Synchronized Measurement Network", *IEEE Computer Applications in Power*, vol. 11, no. 1, pp 26-30, Jan. 1998.

[14] J. S. Thorp, A. G. Phadke, K. J. Karimi, "Real-time voltage-phasor measurement for static state estimation," *IEEE Transactions Power Apparatus and Systems*, vol. PAS-104, No 11, pp. 3098-3106, Nov. 1985.

[15] S. Chakrabarti, E. Kyriakides, T. Bi, D. Cai, V. Terzija, "Measurements get together", *IEEE Power and Energy Magazine*, vol. 7, no. 1, pp.41-49, Jan./Feb. 2009.

[16] A. P. Meliopoulos, G. J. Cokkinides, and G. K. Stefopoulos, "Numerical experiments for three-phase state estimation performance and evaluation," *in Proc. IEEE PowerTech Conference*, pp 1 - 7, St. Petersburg, Russia, June 27-30, 2005.

[17] IEEE Standard for Synchrophasors for Power Systems, Std C37.118-2005, IEEE Power Engineering Society.

[18] M. Adamiak, W. Premerlani, B. Kasztenny, "Synchrophasors: Definition, Measurement and Application," *GE Multilin Publications*, pp. 1-13.

[19] Jun Zhu, Ali Abur, Mark Rice, G. T. Heydt, and Sakis Meliopoulos, "Enhanced state estimators," *Final project report for PSERC project S-22*, Nov. 2006.

[20] S. Chakrabarti, E. Kyriakides, G. Valverde, V. Terzija, "State estimation including synchronized measurements," in Proc. IEEE PowerTech, Bucharest, July 2009.

[21] Tao Yang, Hongbin Sun, A. Bose, "A Transition to a Two-Level Linear State Estimator—Part I: Architecture," *IEEE Trans. Power Systems*, vol. 26, no.1, pp. 46-53, Feb. 2011.

[22] Tao Yang, Hongbin Sun, A. Bose, "A Transition to a Two-Level Linear State Estimator—Part II: Algorithm," *IEEE Trans. Power Systems*, vol. 26, no.1, pp. 54-62, Feb. 2011.

[23] T. Van Cutsem, M. Ribbens-Pavella, "Critical survey of hierarchical methods for state estimation of electric power systems," *IEEE Transactions Power Apparatus and Systems*, vol. PAS-102, No 10, pp. 3415-3424, Oct. 1983.

[24] D. M. Falcao, F. F. Wu, and L. Murphy, "Parallel and distributed state estimation," *IEEE Trans. Power Systems*, vol 10, no 2, pp 724-730, May 1995.

[25] Zhao Liang and A. Abur, "Multi area state estimation using synchronized phasor measurements," *IEEE Trans. Power Systems*, vol 20, no 2, pp 611-617, May 2005.

[26] Yan Li, Xiaoxin Zhou, and Jingyang Zhou, "A new algorithm for distributed power system state estimation based on PMUs," in *Proc. 2006 International Conference on Power System Technology (PowerCon 2006)*, Oct. 2006.

[27] A. P. S. Meliopoulos, G. J. Cokkinides, F. Galvan, B. Fardanesh, and P. Myrda, "Delivering accurate and timely data to all," *IEEE Power and Energy Magazine*, vol. 5, no. 3, pp. 74-86, 2007.

[28] R. Ebrahimian and R. Baldick, "State estimation distributed processing [for power systems]," *IEEE Trans. Power Systems*, vol 15, no 4, pp 1240-1246, Nov. 2000.

[29] A. P. Meliopoulos, G. J. Cokkinides, F. Galvan, B. Fardanesh, and P. Myrda, "Advances in the SuperCalibrator Concept – Practical Implementations," *in Proc. 40st Annual Hawaii Int. Conf. System Sciences (HICSS)*, Waikoloa, Big Island, HI, USA, Jan. 3-6, 2007.

[30] A. P. Sakis Meliopoulos, George J. Cokkinides, Clinton Hedrington, and Terry L. Conrad, "The SuperCalibrator – A Fully Distributed State Estimator," *Proceedings of the IEEE-PES General Meeting, Minneapolis,* MN, July 25-29, 2010.

[31] S. Mohagheghi, R. H. Alaileh, G. J. Cokkinides, and A. P. Sakis Meliopoulos, "Distributed state estimation based on the SuperCalibrator concept – Laboratory

Implementation," *in Proc. IREP 2007 Symposium on Bulk Power System Dynamics and Control*, Charleston, SC, USA, Aug. 2007.

[32] A. P. Meliopoulos, G. J. Cokkinides, F. Galvan, and B. Fardanesh, "Distributed state estimator – Advances and demonstration," *in Proc. 41st Annual Hawaii Int. Conf. System Sciences (HICSS)*, Kona, HI, USA, Jan. 7-10, 2008.

[33] A. S. Debs and R. E. Larson, "A dynamic estimator for tracking the state of a power system," *presented at the IEEE Winter Power Meeting*, New York, N. Y., Jan. 25-30, 1970.

[34] I. M. Ferreira and F. P. Maciel Barbosa, "An algorithm for dynamic state estimation and bad data analysis using a square root filtering technique," *IEEE Athens PowerTech Conf.*, Athens, Greece, Sept. 5-8, 1993.

[35] K-R Shih and S.-J. Huang, "Application of a robust algorithm or dynamic state estimation of a power system," *IEEE Trans. Power Systems*, Vol. 17, no.1, pp. 141-147, Feb. 2002.

[36] G. Durgaprasad and S. S. Thakur, "Robust dynamic state estimation of power systems based on M-estimation and realistic modeling of system dynamics," *IEEE Trans. Power Systems*, Vol. 13, no.4, pp. 1331-1336, Nov. 1998.

[37] H. Zhenyu, K. Schneider, J. Nieplocha, "Feasibility studies of applying Kalman Filter techniques to power system dynamic state estimation", *Proceedings of International Power Engineering Conference, IPEC*, pp. 376-382, 2007.

[38] A.K. Sinha, L.K. Mondal, "Dynamic state estimator using ANN based bus load prediction," *IEEE Trans. Power Systems*, Vol. 14, no.4, pp. 1219-1225, Nov. 1999.

[39] S. Horowitz, D. Novosel, V. Madani, M. Adamiak, "System-Wide Protection," *IEEE Power & Energy Magazine*, vol. 6, no. 5, Sept./Oct. 2008.

[40] D. Novosel, V. Madani, B. Bhargava, K. Vu, J. Cole, "Dawn of Grid Synchronization," *IEEE Power & Energy Magazine*, vol. 6, no. 1, Jan./Feb. 2008.

[41] A. P. Meliopoulos, G. J. Cokkinides, O. Wasynczuk, E. Coyle, M. Bell, C. Hoffmann, C. Nita-Rotaru, T. Downar, L. Tsoukalas, and R. Gao, "PMU data

characterization and application to stability monitoring," *in Proc. IEEE 2006 PES General Meeting*, June 18-22, 2006.

[42] M. Zarghami, M.L. Crow, S. Jagannathan, "Nonlinear Control of FACTS Controllers for Damping Interarea Oscillations in Power Systems," *IEEE Trans. Power Delivery*, Vol. 25, no.4, pp. 3113-3121, Oct. 2010.

[43] Zhou Ning, D.J. Trudnowski, J.W. Pierre, W.A. Mittelstadt, "Electromechanical Mode Online Estimation Using Regularized Robust RLS Methods," *IEEE Trans. Power Systems*, Vol. 23, no.4, pp. 1670-1680, Nov. 2008.

[44] M. Glavic, T. Van Cutsem, "Adaptive wide-area closed-loop undervoltage load shedding using synchronized measurements," in *Proc. IEEE 2010 Power and Energy Society General Meeting,* pp. 1-8, July 2010.

[45] M. Glavic, T. Van Cutsem, "Wide-Area Detection of Voltage Instability From Synchronized Phasor Measurements. Part I: Principle," *IEEE Trans. Power Delivery*, Vol. 24, no.3, pp. 1408-1416, Aug. 2009.

[46] M. Glavic, T. Van Cutsem, "Wide-Area Detection of Voltage Instability From Synchronized Phasor Measurements. Part II: Simulation results," *IEEE Trans. Power Delivery*, vol. 24, no.3, pp. 1417-1425, Aug. 2009.

[47] Y. Haiping, F. Lingling, "PMU data-based fault location techniques," *in Proc. North American Power Symposium (NAPS)*, pp. 1-7, Sept. 2010.

[48] Ching-Shan Chen, Liu Chih-Wen; Joe-Air Jiang, "A new adaptive PMU based protection scheme for transposed/untransposed parallel transmission lines," *IEEE Trans. Power Delivery*, Vol. 17, no.2, pp. 395-404, Apr. 2002.

[49] Zhu Jun, A. Abur, "Identification of network parameter errors using phasor measurements," in *Proc. IEEE 2009 Power and Energy Society General Meeting,* July 2009.

[50] A. P. Sakis Meliopoulos and George J. Cokkinides, "Advanced Synchrophasor Applications," in *Proceedings of the IEEE-PES General Meeting*, Minneapolis, MN, July 25-29, 2010.

[51] M. Sherwood, Hu Dongchen, V. Venkatasubramanian, "Real-time detection of angle instability using synchrophasors and action principle," *in Proc. IREP 2007 Symposium on Bulk Power System Dynamics and Control*, Charleston, SC, USA, Aug. 2007.

[52] Hu Dongchen, V. Venkatasubramanian, "New Wide-Area Algorithms for Detection and Mitigation of Angle Instability using Synchrophasors," in *Proc. IEEE 2007 Power and Energy Society General Meeting,* July 2007.

[53] Edmund O. Schweitzer, D.E. Whitehead, A. Guzman, Y. Gong, M. Donolo, R. Moxley, "Applied synchrophasor solutions and advanced possibilities," in *Proc. 2010 Transmission and Distribution Conference and Exposition*, Apr. 2010.

[54] J. De La Ree, V. Centeno, J.S. Thorp, A.G Phadke, A.G. "Synchronized Phasor Measurement Applications in Power Systems," *IEEE Trans. Smart Grid*, Vol. 1, no.1, pp. 20-27, June 2010.

[55] North American Synchrophasor Initiative, www.naspi.org.

[56] M. A. Pai, *Power Systems Stability*, North Holland Publishing Co., New York, 1981.

[57] P. Kundur, *Power System Stability and Control*. New York: McGraw-Hill, 1994.

[58] P. W. Sauer, M. A. Pai, *Power System Dynamics and Stability*.

[59] P. M. Anderson, A. A. Fouad, *Power System Control and Stability*, IEEE Press, 2003.

[60] M. Pavella, P.G. Murthy, *Transient Stability of Power Systems, Theory and Practice*, John Wiley & Sons Publications.

[61] Mania Pavella, Damien Ernst, and Daniel Ruiz-Vega, *Transient Stability of Power Systems: A Unified Approach to Assessment and Control,* Kluwer's Power Electronics and Power Systems Series.

[62] P. C. Mangusson, "Transient energy method of calculating stability," *AIEE Trans.*, vol. 66, pp. 747-755, 1947.

[63] P. D. Aylett, "The energy-integral criterion of transient stability limits of power systems," *Proc. of the IEEE*, vol. 105C, 8, Sept. 1958, pp. 257-536.

[64] V. Vittal, S. Rajagopal, A. A. Fouad, M. A. El-Kady, E. Vaahedi and V. F. Carvalho, "Transient stability analysis of stressed power systems using the energy function method," *IEEE Trans. Power Systems*, vol. 3, pp. 400-412, May 1988.

[65] V. Vittal, N. Bhatia, A. A. Fouad, G. A. Maria and H. M. Z. El-Din "Incorporation of nonlinear load models in the transient energy function method," *IEEE Trans. Power Systems*, vol. 4, pp. 1031-1-36, Aug. 1989.

[66] M. A. El-Kady, C. K Tang, V. F. Carvalho, A. A. Fouad, V. Vittal "Dynamic Security Assessment Utilizing the Transient Energy Function Method," *IEEE Trans. Power Systems*, vol. 1, issue 3, pp. 284-291, Aug. 1986.

[67] A. A. Fouad, V. Vittal, S. Rajagopal, V. F. Carvalho, M. A. El-Kady, C. K. Tang, J. V. Mitsche, M. V. Pereira, "Direct Transient Stability Analysis Using Energy Functions Application to Large Power Networks," *IEEE Trans. Power Systems*, vol. 2, issue 1, pp. 37-43, Feb. 1987.

[68] A. Michel, A Fouad, V. Vittal, "Power system transient stability using individual machine energy functions," *IEEE Trans. Circuits and Systems*, vol. CAS-30, issue 5, pp. 266-276, May 1983.

[69] Y. Xue, T. Van Cutsem and M. Ribbens-Pavella, "A simple direct method for fast transient stability assessment of large power systems," *IEEE Trans. Power Systems*, vol. 3, pp. 400-412, May 1988.

[70] I. A. Hiskens and D. J. Hill, "Energy functions, transient stability and voltage behaviour in power systems with nonlinear loads," *IEEE Trans. Power Systems*, vol. 4, pp. 1525-1533, Nov. 1989.

[71] H.D. Chiang and J.S. Thorp, "The closest unstable equilibrium point method for power system dynamic security assessment," *IEEE Trans. Circuits and Systems*, vol. 36, pp. 1187-1200, Sept. 1989.

[72] T. S. Chung and D. Z. Fang, "Corrected transient energy function and transient stability limit assessment," in *Proc. 2000 IEEE Power Engineering Society Winter Meeting*, 23-27, vol. 1, pp. 72-77, Jan. 2000.

[73] F. A. Rahimi, M. G. Lauby, J. N. Wrubel and K. L. Lee, "Evaluation of the transient energy function method for on-line dynamic security analysis," *IEEE Trans. Power Systems*, vol. 8, pp. 497-507, May 1993.

[74] Y. Z. Sun, X. Li and Y. H. Song, "A new Lyapunov function for transient stability analysis of controlled power systems," in *Proc. 2000 IEEE Power Engineering Society Winter Meeting*, vol. 2, pp. 1325-1330, Jan. 2000.

[75] H. D. Chiang, *Direct Methods for Stability Analysis of Electric Power System,* Wiley Publications.

[76] Y. Xue, T. Van Cutsem, and M. Ribbens-Pavella, "Real-time analytic sensitivity method for transient security assessment and preventive control," *IEE Proc. Generation, Transmission and Distribution*, vol. 135, pp. 107-117, Mar. 1988.

[77] Y. Xue, T. Van Cutsem and M. Ribbens-Pavella, "Extended equal area criterion justifications, generalizations, applications," *IEEE Trans. Power Systems*, vol. 4, pp. 44-52, Feb. 1989.

[78] D. Ruiz-Vega, D. Ernst, C. M. Ferreira, M. Pavella, P. Hirsch and D. Sobajic, "A contingency filtering, ranking and assessment technique for on-line transient stability studies," in *Proc. 2000 Int. Conf. on Electric Utility Deregulation and Restructuring and Power Technologies (DRPT '2000)*, pp. 459-464, 4-7 Apr. 2000.

[79] R. A. Rosales, D. Ruiz-Vega, D. Ernst, M. Pavella and J. Giri, "On-line transient stability constrained ATC calculations," in *Proc. 2000 IEEE Power Engineering Society Summer Meeting*, vol. 2, pp. 1291-1296, July 2000.

[80] V. Vittal, G. M. Prabhu and Swee Lian Lim, "A parallel computer implementation of power system transient stability assessment using the transient energy function method," *IEEE Trans. Power Systems*, vol. 6, pp. 167-173, Feb. 1991.

[81] I. C. Decker, D. M. Falcao and E. Kaszkurewicz, "Parallel implementation of a power system dynamic simulation methodology using the conjugate gradient method," in *Proc. 1991 Power Industry Computer Application Conf.*, pp. 245-252, May 1991.

[82] I. C. Decker, D. M. Falcao and E. Kaszkurewicz, "Parallel implementation of a power system dynamic simulation methodology using the conjugate gradient method," *IEEE Trans. Power Systems*, vol. 7, pp. 458-465, Feb. 1992.

[83] Jun Qiang Wu, A. Bose, Jin An Huang, A. Valette and F. Lafrance, "Parallel implementation of power system transient stability analysis," *IEEE Trans. Power Systems*, vol. 10, pp. 1226-1233, Aug. 1995.

[84] Yalou Li, Xiaoxin Zhou, Zhongxi Wu, Jian Guo, "Parallel algorithms for transient stability simulation on PC cluster," in *Proc. 2002 Int. Conf. on Power System Technology (POWERCON '2002)*, pp. 1592-1596, vol. 3, Oct. 2002.

[85] L. Wekenkel, M. Pavella, E. Euxibie, B. Heilbronn, "Decision tree based transient stability method. A case study," in Proceedings IEEE PES Winter Meeting, 1993.

[86] L. Wekenkel, M. Pavella, "Decision tree approach to power systems security assessment," *International Journal of Electric Power and Energy Systems*, 1993.

[87] K. Sun, S. Likhate, V. Vittal, V.S. Kolluri and S. Mandal, "An online dynamic security assessment scheme using phasor measurements and decision trees," *IEEE Trans. Power Syst.*, vol. 22, no. 4, pp. 1935–1943, Nov. 2007.

[88] A. B. Ranjit Kumar, A. Ipakchi, V. Brandwajn, M. El-Sharkawi and G. Cauley, "Neural networks for dynamic security assessment of large-scale power systems: requirements overview," in *Proc. First Int. Forum on Applications of Neural Networks to Power Systems*, pp. 65-71, July 1991.

[89] K. L. Lo, R. J. Y Tsai, "Power system transient stability analysis by using modified Kohonen network," in *Proc. 1995 IEEE Int. Conf. on Neural Networks*, vol. 2, pp. 893-898, Dec. 1995.

[90] A. R. Edwards, K. W. Chan, R. W. Dunn and A. R. Daniels, "Transient stability screening using artificial neural networks within a dynamic security assessment system," *IEE Proc. Generation, Transmission and Distribution*, vol. 143, pp. 129-134, Mar. 1996.

[91] E. S. Karapidakis and N. D. Hatziargyriou, "Application of artificial neural networks for security assessment of medium size power systems," in *Proc. 10th Mediterranean Electrotechnical Conf. (MELECON '2000)*, vol. 3, pp. 1189-1192, May 2000,.

[92] K. W. Chan, A. R. Edwards, R. W. Dunn and A. R. Daniels, "On-line dynamic security contingency screening using artificial neural networks," *IEE Proc. Generation, Transmission and Distribution*, vol. 147, pp. 367-372, Nov. 2000.

[93] J.A. Imhof, J. Berdy, W.A. Elmore, L.E. Goff, W.C. New, G.C. Parr, A.H. Summers, C.L. Wagner, "Out-of-step relaying for generators working group report," *IEEE Trans. Power Apparatus and Systems*, vol. PAS-96, no. 5, pp. 1556-1564, Sept. 1977.

[94] Power System Relaying Committee WG6, "Power Swing and Out-of-Step Considerations on transmission lines", Report of PSRC to IEEE PES Society.

[95] D.A Tziouvaras, H. Daqing, "Out-of-step protection fundamentals and advancements," in *Proc. 57th Annual Conference for Protective Relay Engineers*, 2004.

[96] S.M Brahma, "Distance Relay With Out-of-Step Blocking Function Using Wavelet Transform," *IEEE Trans. Power Delivery*, vol. 22, issue 3, pp. 1360-1366, July 2007.

[97] W. Rebizant, "Fuzzy logic application to out-of-step protection of generators," *IEEE Power Engineering Society Summer Meeting*, vol. 2, pp. 927-932, 2001.

[98] A. Y. Abdelaziz, "Adaptive protection strategies for detecting power system out-of-step conditions using neural networks," in *IEE Proceedings of Generation, Transmission and Distribution*, vol. 145, pp. 387-394, 1998.

[99] E. Farantatos, G. K. Stefopoulos, G. J. Cokkinides, A. P. Meliopoulos, "PMU-Based Dynamic State Estimation for Electric Power Systems," *in Proc. 2009 PES General Meeting, Calgary*, Alberta, Canada, July 2009.

[100] A.P Meliopoulos, G. Cokkinides, R. Huang, E. Farantatos, S. Choi, Y. Lee , "Wide Area Dynamic Monitoring and Stability Controls," in *Proc. IREP Symposium 2010, Bulk Power System Dynamics and Control VIII*, Buzios, Brazil, Aug. 2010.

[101] A. P. Meliopoulos, G. J. Cokkinides, George K. Stefopoulos, "Quadratic Integration Method," *Proceedings of the 2005 International Power System Transients Conference (IPST 2005)*, Montreal, Canada, June 19-23, 2005.

[102] A. P. Meliopoulos, G. J. Cokkinides, and G. K. Stefopoulos, "Symbolic integration of dynamical systems by collocation methods," in *Proceedings of the 2006 IEEE PES Power Systems Conference and Exposition (PSCE 2006)*, Atlanta, GA, USA, Oct. 29-Nov. 1, 2006, pp. 362-367.

[103] A. P. Meliopoulos, G. J. Cokkinides, and G. K. Stefopoulos, "Improved numerical integration method for power/power electronic systems based on three-point collocation," presented at the *44th IEEE Conference on Decision and Control (CDC 2005)*, Seville, Spain, Dec. 2005.

[104] P. Sakis Meliopoulos, G. J. Cokkinides, and G. K. Stefopoulos, "Symbolic integration of dynamical systems by collocation methods," in *Proceedings of the 2005 IEEE-PES General Meeting*, San Francisco, CA, pp. 2387-2392, June 2005.

[105] G. K. Stefopoulos, G. J. Cokkinides, and A. P. Meliopoulos, "Expert symbolic transient simulator based on quadratic integration method," presented at the *13th International Conference on Intelligent System Application to Power Systems (ISAP 2005)*, Washington DC, Nov. 2005.

[106] R. Huang, E. Farantatos, G. Cokkinides, A. P. Meliopoulos, Bruce Fardanesh and George Stefopoulos, "Object-Oriented 3-Phase Distributed Dynamic State Estimator," in *Proc. 2011 PES General Meeting*, Detroit, MI, July 2011.

[107] E. Farantatos, R. Huang, G. Cokkinides, and A. P. Meliopoulos, "A Predictive Out-of-Step Protection Scheme based on PMU enabled Dynamic State Estimation," in *Proc. 2011 PES General Meeting*, Detroit, MI, July 2011.

[108] M.G. Adamiak, D. Novosel, B. Kasztenny, V. Madani, J. Sykes, A. G. Phadke, "Wide Area Protection and Control - Today and Tomorrow," *in Proceedings of the IEEE Transmission and Distribution Conference and Exhibition*, May 2006.

[109] A.P Sakis Meliopoulos, G. J. Cokkinides, "Power System Relaying, Theory and Applications," Georgia Institute of Technology Course Notes.

[110] A.P Sakis Meliopoulos "Power System Modeling Analysis and Control," Georgia Institute of Technology Course Notes.

[111] ABB – *Protective Relaying Theory and Applications* edited by W. A. Elmore, Marcel Dekker Inc., New York, 1994.

[112] A. P. Sakis Meliopoulos and George J. Cokkinides, "A virtual environment for protective relaying evaluation and testing," *IEEE Transactions of Power Systems*, Vol. 19, No. 1, pp. 104-111, Feb. 2004.

[113] R. Huang, E. Farantatos, G. Cokkinides, and A. P. Meliopoulos, "Substation Based Dynamic State Estimator - Numerical Experiment," *in Proc.2010 Transmission and Distribution Conference and Exposition*, New Orleans, Louisiana, Apr. 2010.

[114] G. J. Cokkinides, A. P. Meliopoulos, G. Stefopoulos, R. Alaileh, and A. Mohan, "Visualization and characterization of stability swings via GPS-Synchronized data," *in Proc. 40st Annual Hawaii Int. Conf. System Sciences (HICSS)*, Waikoloa, Big Island, HI, USA, Jan. 2007.

[115] A. P. Meliopoulos, E. Farantatos, G. Cokkinides, S. Mohagheghi, and G. K. Stefopoulos, "A new out-of-step protection scheme via GPS-Synchronized data," in *Proc. of the 2008 Power Systems Computation Conference (PSCC)*, Glasgow, Scotland, UK, July 2008.

[116] E. Farantatos, R. Huang, G. Cokkinides and A. P. Meliopoulos, "Implementation of a 3-Phase State Estimation Tool Suitable for Advanced Distribution

Management Systems," in *Proceedings of the 2011 Power Systems Conference & Exposition*, Phoenix, AZ, Mar. 2011.

[117] S. Choi, B. Kim, G. Cokkinides, and A. P. Sakis Meliopoulos, "Autonomous state estimation for the smart grid – laboratory implementation," in *Proceedings of the 2010 IEEE PES Transmission and Distribution Conference*, New Orleans, 2010.

[118] S. Choi, B. Kim, G. Cokkinides, and A. P. Sakis Meliopoulos, "Feasibility Study: Autonomous State Estimation in Distribution Systems," *IEEE Trans. Power Systems*, June 2011.

[119] T. K. Hamrita, B. S. Heck and A. P. Sakis Meliopoulos, "On-Line Correction of Errors Introduced By Instrument Transformers In Transmission-Level Power Waveform Steady-State Measurements," *IEEE Transactions on Power Delivery,* Vol. 15, No. 4, pp 1116-1120, Oct. 2000.

[120] A. P. Sakis Meliopoulos and George J. Cokkinides, "Virtual Power System Laboratories: Is the Technology Ready?," *in Proceedings of the 2000 IEEE/PES Summer Meeting*, Seattle, WA, July 2000.

[121] A. P. Meliopoulos, F. Zhang, S. Zelingher, G. Stillmam, G. J. Cokkinides, L. Coffeen, R. Burnett, J. McBride, "Transmission Level Instrument Transformers and Transient Event Recorders Characterization for Harmonic Measurements," *IEEE Transactions on Power Delivery*, Vol 8, No. 3, pp 1507-1517, July 1993.

[122] W. W. Kotiuga, M. Vidyasagar, "Bad data rejection properties of weighted least absolute value techniques applied to static state estimation," *IEEE Transactions Power Apparatus and Systems*, vol. PAS-101, No 4, pp. 844-853, Apr. 1982.

[123] K. I. Geisler, A. Bose, "State estimation based external network solution for on-line security analysis," *IEEE Transactions Power Apparatus and Systems,* vol. PAS-102, No 8, pp. 2447-2454, Aug. 1983.

[124] T. Van Cutsem, M. Ribbens-Pavella, "Critical survey of hierarchical methods for state estimation of electric power systems," *IEEE Transactions Power Apparatus and Systems,* vol. PAS-102, No 10, pp. 3415-3424, Oct. 1983.

[125] Th. Van Cutsem, M. Ribbens-Pavella, L. Mili, "Hypothesis testing identification: A new method for bad data analysis in power system state estimation," *IEEE Transactions Power Apparatus and Systems*, vol. PAS-103, No 11, pp. 3239-3252, Nov. 1984.

[126] A. Abur, "A bad data identification method for linear programming state estimation," *IEEE Transactions Power Systems*, vol. 5, No 3, pp. 894-901, Aug. 1990.

[127] G. N. Korres, G. C. Contaxis, "A reduced model for bad data processing in state estimation," *IEEE Transactions Power Systems*, vol. 6, No 2, pp. 550-557, May 1991.

[128] G. N. Korres, G. C. Contaxis, "Identification and updating of minimal dependent sets of measurements in state estimation," *IEEE Transactions Power Systems*, vol. 6, No 3, pp. 999-1005, Aug. 1991.

[129] K. Sun, S. Lee, P. Zhang, "An Adaptive Power System Equivalent for Real-Time Estimation of Stability Margin using Phase-Plane Trajectories," *IEEE Trans. Power Syst.*, vol. 26, no. 2, pp. 915–925, May 2011.

[130] Sakis Meliopoulos, Fan Zhang, "Multiphase power flow and state estimation for power distribution systems," *IEEE Transactions on Power Systems*, vol 11, No 2, pp 939-946, May 1996.

[131] G. N. Korres, "A robust method for equality constrained state estimation," *IEEE Transactions on Power Systems*, vol 17, No 2, pp 305-314, May 2002.

[132] E. Paulsen, "State estimation based real-time markets - PJM's state estimation based real-time markets," in *Proceedings IEEE Power Engineering Society 2005 General Meeting*, vol. 1, pp. 1968-1968, June 2005.

[133] M. Rothleder, "Evolution of use of state estimation and real-time markets at CAISO," in *Proceedings IEEE Power Engineering Society 2005 General Meeting*, pp. 1969-1970, June 2005.

[134] V. Brandwajn, X. Jiang, G. Liu, M. L. Johansson, G. E. Fahmy, "State estimation for Ontario market system," *in Proceedings IEEE Power Engineering Society 2006 General Meeting*, June 2006.

[135] J. Chen, A. Abur, "Placement of PMUs to enable bad data detection in state estimation," *IEEE Transactions on Power Systems*, vol 21, No 4, pp 1608-1615, Nov. 2006.

[136] Weiqing Jiang, Vijay Vittal, "Optimal placement of phasor measurements for enhancement of state estimation," in *Proceeding of the 2006 IEEE PES Power Systems Conference and Exposition (PSCE '06)*, pp. 1550-1555, Oct. 2006.

[137] Tom Overbye, Pete Sauer, Chris DeMarco, Bernie Lesieutre, Mani Venkatasubramanian, "Using PMU Data to Increase Situational Awareness," *Final project report for PSERC project S-36*, Sept. 2010. Available at www.pserc.org.

[138] V. Vittal, G. Heydt, S. Meliopoulos, "A Tool for Online Stability Determination and Control for Coordinated Operations between Regional Entities using PMUs," *Final project report for PSERC project S-27*, Jan. 2008. Available at www.pserc.org.

[139] Anjan Bose, Ali Abur, Kai Yin Kenny Poon, Roozbeh Emami, "Implementation Issues for Hiererchical State Estimators," *Final project report for PSERC project S-33*, Aug. 2010. Available at www.pserc.org.

[140] Mani Venkatasubramanian, Michael Sherwood, Venkataramana Ajjarapu, Bruno Leonardi, "Real-Time Security Assessment of Angle Stability and Voltage Stability using Synchrophasors," *Final project report for PSERC project S-31*, May 2010. Available at www.pserc.org.

[141] Vijay Vital, Feng Ma, Guanji Hou, "Next Generation On-Line Dynamic Security Assessment," *Final project report for PSERC project S-38*, Nov. 2011. Available at www.pserc.org.

[142] V. Madani, M. Parashar, J. Giri, S. Durbha, F. Rahmatian, D. Day, M. Adamiak, G. Sheble, "PMU placement considerations — A roadmap for optimal PMU

placement," in *Proceedings of 2011 IEEE Power Systems Conference and Exposition (PSCE)*, Mar. 2011.

[143] North American Electric Reliability Corporation, "Real-Time Application of Synchrophasors for Improving Reliability," Aug. 2010, available in www.nerc.com.

VITA

Evangelos Farantatos was born in Athens, Greece in 1983. He received the Diploma in Electrical and Computer Engineering from the National Technical University of Athens, Greece, in 2006, with specialization in power systems engineering. Upon his graduation he joined E.E.N Hellas S.A Renewable Energy, working as an electrical engineer supervising the operation of the company's wind farms. In Fall 2007 he enrolled as a graduate student at Georgia Institute of Technology, School of Electrical and Computer Engineering, and he obtained the M.S. degree in E.C.E. in 2009. He is currently a Ph.D. candidate at the same department working under the supervision of Professor Sakis Meliopoulos, as a Graduate Research Assistant. In Summer 2009, he was an intern in Midwest ISO, in the market operations department and especially in the FTR group. His research interests include power systems state estimation, synchrophasor applications, stability, protection, control and smart grid technologies.

Evangelos is a student member of IEEE. During his time at Georgia Tech, he has also served as a board member of the Energy Club at Georgia Tech and the Hellenic Society at Georgia Tech.